NEW ELECTROCHEMICAL SENSORS FOR DECENTRALIZED ANALYSIS

Marc Parrilla Pons

New Electrochemical Sensors for Decentralized Analysis

Doctoral Thesis

Marc Parrilla Pons

Tarragona, 2016

UNIVERSITAT ROVIRA i VIRGILI

Departament de
Química Analítica i
Quimica Orgànica

UNIVERSITAT ROVIRA I VIRGILI
NEW ELECTROCHEMICAL SENSORS FOR DECENTRALIZED ANALYSIS
Marc Parrilla Pons

MARC PARRILLA PONS

New Electrochemical Sensors for Decentralized Analysis

DOCTORAL THESIS

supervised by

Dr. FRANCISCO J. ANDRADE

UNIVERSITAT ROVIRA I VIRGILI

Department of Analytical Chemistry and Organic Chemistry

Tarragona, September 2016

UNIVERSITAT ROVIRA I VIRGILI
NEW ELECTROCHEMICAL SENSORS FOR DECENTRALIZED ANALYSIS
Marc Parrilla Pons

MARC PARRILLA PONS

New Electrochemical Sensors for Decentralized Analysis

Tribunal members:

Prof. Luis Fermín Capitán Vallvey - Universidad de Granada

Prof. Francesc Xavier Rius Ferrús - Universitat Rovira i Virgili

Dr. Gastón Adrián Crespo - Université de Genève

External examiners:

Prof. Joseph Wang - University of Califronia San Diego

Dr. Devin Daems - Katholieke Universiteit Leuven

UNIVERSITAT ROVIRA I VIRGILI

Department of Analytical Chemistry and Organic Chemistry

Tarragona, September 2016

UNIVERSITAT ROVIRA I VIRGILI
NEW ELECTROCHEMICAL SENSORS FOR DECENTRALIZED ANALYSIS
Marc Parrilla Pons

UNIVERSITAT ROVIRA I VIRGILI

DEPARTAMENT DE QUÍMICA ANALÍTICA I QUÍMICA ORGÀNICA

Campus Sescelades, Marcel·lí Domingo, 1, 43007, Tarragona

Tel.: +34 977 55 95 62

E-mail: *franciscojavier.andrade@urv.cat*

Francisco J. Andrade, Ramón y Cajal researcher at the Department of Analytical Chemistry and Organic Chemistry at the University Rovira i Virgili (URV).

I STATE that the present study, entitled "**New Electrochemical Sensors for Decentralized Analysis**", presented by *Marc Parrilla Pons* for the award of the degree of Doctor, has been carried out under my supervision at the Department of Analytical Chemistry and Organic Chemistry of this university.

Tarragona, 2 September 2016

Doctoral Thesis Supervisor

Dr. Francisco Javier Andrade

UNIVERSITAT ROVIRA I VIRGILI
NEW ELECTROCHEMICAL SENSORS FOR DECENTRALIZED ANALYSIS
Marc Parrilla Pons

ACKNOWLEDGEMENTS

Firstly, I would like to deeply thank my supervisor *Dr. Francisco Andrade* for giving me the opportunity to enroll the Nanosensors group and thus the outstanding and value-oriented projects. Also, I greatly appreciate him to advise me to undertake my PhD study in the field of electrochemical sensors. His scientific and innovative teachings have been really important in my growth as a researcher as well as in my professional career. I extremely value the training I received during the years about innovation in the Innovation Hub of the URV.

Secondly, I would like to thank all my family for pushing me to start my scientific career. Specially, my parents *Dolors* i *Carles*, and also my grandparents for making me happy along the way. And also, my partner's family for the enriched discussions during my PhD.

Thirdly, I would like to thank:

Dr. Gastón Crespo for being the first person that introduced me in the field of electrochemistry. He had made possible for me to stay in the Nanosenor group even a few years before I started my PhD. Without his contribution, I would not have met *Dr. Andrade* and probably did not accomplish this thesis.

Professor Francesc Xavier Rius for igniting my curiosity about sensors, for allowing me to undertake my PhD studies in his research group and thanks for all his scientific and personal support.

Professor Joseph Wang for allowing me to do my PhD stage in his group at the University of California, San Diego (UCSD). He introduced me in the advanced materials field as well as I gained interesting insights about wearable electrochemical sensors.

All Nanosensor group members, especially the future *Dr. Azizur Rahman Khan* who is going to finish the PhD at the same time of me and he has been a fantastic colleague along the PhD battlefield. I also specially thank *Adrià Maceira* for being my first student, *Jordi Ferré* for being so enthusiastic with the group work, as well as all the other colleagues who have played their role in the group. My credits also go to the Univeristy Rovira i Virgili (URV) for supporting this thesis.

All my friends that I met along my Bachelor degree in Tarragona, without their friendship this way would not have been as enjoyable as it has been. We have delighted many moments in these past few years together as well as sharing different scientific point of view. I would like to make a special thank you to *Albert Almasqué* and *Clara García* who passed away

before starting my PhD, but they have helped me to be stronger and to pursue high professional development through my PhD and complementary education.

All the friends I met as a visiting scholar in the UCSD, especially to *Dr. Jorge Delezuk* and *Dr. Berta Fernandez* for their scientific discussions and graduate meetings out of the laboratory.

Finally, I would like to state my deep and sincere gratitude to my partner and colleague, *Rocío Cánovas* who has supported me in each moment in and out of the lab during the thesis. Thank you very much for encouraging me in all the actions and decisions, either good or bad situations, and specially, for making me feeling important and happy to be at your side. Without *Rocío*, this thesis would not have been started and finished successfully through all these fantastic years.

TABLE OF CONTENTS

SUMMARY AND CHAPTER OVERVIEW

What is it like the computer-based world connected to the “real” (physical) world that surrounds the human being? How will the analytical tools help to face the new challenges of the daily life? These are the type of questions whose answers are going to be explored along this thesis. As a brief disclosure, this thesis explores simple, robust and cost-effective analytical sensors based on electrochemical techniques for the determination of relevant molecules as a path to collect and connect information. Potentiometry is mostly used as a simple to operate, low-power consumption and versatile technique to generate and open up new affordable platforms in the wearable and point-of-care fields for a wide range of applications such as healthcare and fitness, environment and homeland security tasks, among others.

Today, the increasing number and aging of the human population have raised big challenges for keeping the social wellbeing. Healthcare expenditure, pollution and security are some of the main issues that concern society. Moreover, the growth of the knowledge-based economy has brought huge opportunities to the world. Hence, new opportunities are emerging in order to solve the issues presented to people. The development of cost-effective tools and low-cost manufacturing processes to manage and solve these problems are crucial objectives for research and innovation. For this reason, analytical chemistry has a major role to play through the creation of new devices to determine and monitor fundamental markers than can provide an accurate feedback to society. Because of this need, the change of the analytical procedures from centralized, laboratory-based to more available decentralized systems where data is generated and directly transmitted is leading this new era in chemical analysis.

Advances in potentiometry such as the solid-state technology offer the possibility to develop robust sensors with ability to interact with the chemical information of our environment (biological fluids, environmental wastes, etc.) in a convenient way. This interaction allows producing large amount of data that can be transferred and processed via global network connections. Accordingly, this meaningful information will solve some of the present societal issues by taking the right actions in real-time. Therefore, the use of low-cost materials such as commercial carbon fibers, commodity textiles and paper or even commercial balloons to build electrochemical sensors has been addressed along the thesis. The technology already developed by the Nanosensors group at URV allows the fabrication

of a full potentiometric cell using different substrates for a complete decentralization of the chemical analysis. Ion-selective electrodes are mostly used to build robust solid-state sensors that provide an outstanding contribution in the wearable chemical sensors area. Furthermore, a new approach to develop enzyme-based potentiometric electrodes on paper substrate for the monitoring of biomolecules is successfully presented.

This thesis has been focused mostly on two directions: first, the development of new sensors through the use of tailored inks and hybrid materials to build affordable solid-contact ion-selective sensors with wireless data-transmission capabilities. One of the most attractive features of this research is the development of novel enzyme-based potentiometric tools with high sensitivity, which takes advantage of the unique features of the Nafion polymer. Second, considerations in the design of seamless platforms for application to the end-user is reflected by the use of wearable approaches such as textile-based sensors that mimic conventional cloth or even patches integrated directly on the skin. The main goal is the use of these electrochemical sensors to acquire reliable data without compromising the integrity of the wearer. Interestingly, both the analytical performance of the sensor and the design of the sampling cell are of similar significance in the successful development of a sensing device. All in all, the development of sensors and considerations about the design have been taken into account along the whole work in order to improve the applicability of the research in real scenarios.

Therefore, the thesis is structured in three different parts: The first part deals with the broad introduction to the whole landscape of the topic and more detailed technical information about the electrochemical sensors used in this thesis. In the second part, a detailed description of wearable electrochemical sensors for fitness applications is presented. Finally, in the third part, novel strategies for the determination of clinically relevant biomolecules are showed. Each one of these parts are distributed in different chapters, which start from a brief introduction, fundamentals of the technique, characterization techniques, the development of the sensors and, last but not least, conclusions and future prospects derived from the thesis. A more detailed description about each chapter is provided below:

- Chapter 1 is focused in the brief explanation about the information age, together with a deeper discussion regarding sensors. This chapter provides an overview of the main elements involved in this system: interfaces/sensors, internet of things, big data and information economy. It makes emphasis in the field of sensors, especially in the

affordable and wearable chemical sensors; some insights in the material aspect of this field are also presented.

- Chapter 2 illustrates briefly the fundamentals of electrochemistry and explains more in detail the potentiometric technique. It also describes the working principles of the most used type of sensor in this thesis, the solid-contact ion-selective electrodes, together with the parameters involved in the analytical characterization.
- Chapter 3 provides information about the characterization techniques, fundamentals, procedures and instrumentation commonly used over the chapters.
- Chapter 4 & 5 correspond to the development of wearable potentiometric sensors in commercial carbon fiber substrates and commodity textiles using solid-state ion-selective membranes and solid-state reference membranes.
- Chapter 6 follows the wearable approach, but it has been focused in a chemiresistor sensor to determine the amount of water-based solutions and designed mainly for monitoring sweat loss. First, the mechanism is explained by a phenomenological approach. Second, a full characterization of the sensor is performed. Finally, on-body tests with wireless integration is presented in more detail.
- Chapter 7 & 8 present a novel approach to develop enzyme-based potentiometric electrodes. First, chapter 7 focuses on the understanding of the mechanism of detection of hydrogen peroxide using a platinum electrode coated with a Nafion membrane. Second, chapter 8 describes the details for development of a paper-based enzymatic electrode for determination of glucose in biological samples.
- Chapter 9 describes a new methodology to study the resiliency of conductive nanocomposite inks used to fabricate electrochemical sensors in a conventional rubber balloon. Moreover, a demonstration of the sensor performance to monitor explosive compounds is also presented.
- Chapter 10 points out main conclusions derived from the experimental work and suggests future prospects.

Finally, some appendices have been added with additional information:

- Appendix 1 presents the list of abbreviations
- Appendix 2 shows the list of tables and figures
- Appendix 3 describes a short CV of the author

UNIVERSITAT ROVIRA I VIRGILI
NEW ELECTROCHEMICAL SENSORS FOR DECENTRALIZED ANALYSIS
Marc Parrilla Pons

Part 1

Introduction and Fundamentals

UNIVERSITAT ROVIRA I VIRGILI
NEW ELECTROCHEMICAL SENSORS FOR DECENTRALIZED ANALYSIS
Marc Parrilla Pons

Chapter 1

Plugging the Chemical World into the Information Society

UNIVERSITAT ROVIRA I VIRGILI
NEW ELECTROCHEMICAL SENSORS FOR DECENTRALIZED ANALYSIS
Marc Parrilla Pons

Plugging the Chemical World into the Information Society

Under the current high level of competition, producing value through scientific research is of utmost importance for the world's economy. Most of the scientific research is produced in universities and research institutes with public funding. This scientific research is extremely expensive, so it needs high amounts of resources to be productive. Indeed, during the last years, maintaining the whole research system in universities has started to increase the need of economic resources. Therefore, some efforts to orient research to the end-user application -thus maximizing the interests from the industry- are increasingly needed. This implies that innovation -as a concept aimed to introduce value to society- should be integrated in the goals of universities. One opportunity is to bring closer the research made at the university to the industries with ability to exploit the technology. This distance between high academic achievements and poor application of the scientific knowledge is called the innovation gap, and is having devastating effects for society. Hence, during the last decade, there have been considerable efforts to reduce this innovation gap by increasing the chances that the research produced in the universities becomes more attractive to the industry and to society. All in all, a research oriented to the end-user application and a step closer to the industrial applications will help to increase the ability of society to re-capture part of the resources invested in research, and thus improving the learning and knowledge of the educational system.

In this thesis, the development of tools for the connection of the chemical environment with one of the most revolutionary inventions of the last century, the global connectivity network, is being addressed. This goal is achieved through the development of different types of chemical sensors that will be connected to the cloud, opening a huge range of opportunities for generating short and long term value for society. In this chapter, the introduction to the information technology and its relation with the chemical sensors are described. First, a brief description of the information age and the components involved in this concept (big data, internet of things and interfaces) is provided. Second, a detailed description of the chemical sensors, interfaces that connect the chemical environment to the cloud system, is outlined. The final goal is to demonstrate that the electrochemical sensors developed along this doctoral thesis can be used as a gateway of chemical information from the environment to the economy of knowledge.

1.1. The Information Age

The evolution of technology has led to the "*Information Age*", a period in human history that is characterized by the shift from traditional industry-based economic models that the Industrial Revolution brought through industrialization, to an economy based on information

computerization.[1] The advances in information and communication technology (ICT) as well as the globally widespread communication network (internet, mobile networks, etc.), together with the availability of electronic devices, lead to the creation of an economy based on information. The digital revolution -considered the onset of the Information Age- was followed by the introduction of the global connectivity network, which has allowed the shift from the traditional industry to the knowledge-based economy. Moreover, the cloud storage technology has enabled the unlimited storage of digital data in logical pools. Cloud storage makes data available and accessible everywhere while the physical environment (servers) is capable of protecting the information. Also, cloud computing allows the remote processing, making the system incredibly efficient. Hence, cloud computing -as the centerpiece of the operation of the whole information exchange- is a kind of Internet-based computing that provides shared storing, processing and retrieving of resources and data to computers and other devices on demand. The introduction of this information age in our daily life and in social organizations has led to a world where the modernization of information and communication tools and processes has become a major driving force for social evolution.

This new industry -the information industry- is able to process this huge amount of data in an efficient and convenient way and extract valuable information for economic exploitation. Mining this massive amounts of data -a field now called “Big Data”- allows individuals to explore their own needs, improve medical outcomes, create better products, make shopping more enjoyable or optimize energy generation and consumption, among many other possibilities. Thus, the decision-making process and transactions are simplified and costs for both, the producers and buyers, are significantly lowered. For instance, Google’s self-driving cars average about 10.000 autonomous miles per week without crashing.[2] Having a connected kitchen could save the food and beverage industry as much as 15% annually.[3] Furthermore, real-time data from manufacturing plants allows system automation in different places at the same time making easier to decentralize the whole economy. The knowledge industry opens a wide range of opportunities based on a productive data processing approach all over the world.[4] Conventional objects, now endowed with the ability to generate information of the surroundings, become smart objects that allow improving the decision-makings processes. And when smart objects can be networked, the result is the generation of intelligent systems. We are witnessing the emergence of a smart planet, a system where information across the globe will be used to make systems more efficient while minimizing the human impact on nature.

Plugging the Chemical World into the Information Society

Information economy is structured in different elements. Hence, Figure 1.1 shows how the information-based economy is segmented. Firstly, the interfaces are able to get/read the information from the environment. Subsequently, this data is able to navigate through the "Internet of Things" (IoT) -connection between the sensors and the global connectivity network- and be stored as a vast amount of data in the cloud. Then, this complex data stored in cloud storage can be processed until get valuable information, Big Data. Finally, the knowledge, the whole set of relevant data, is used by society to develop a more efficient and wealthy world. The entire process pushes for a growing global economy based on information acquisition.

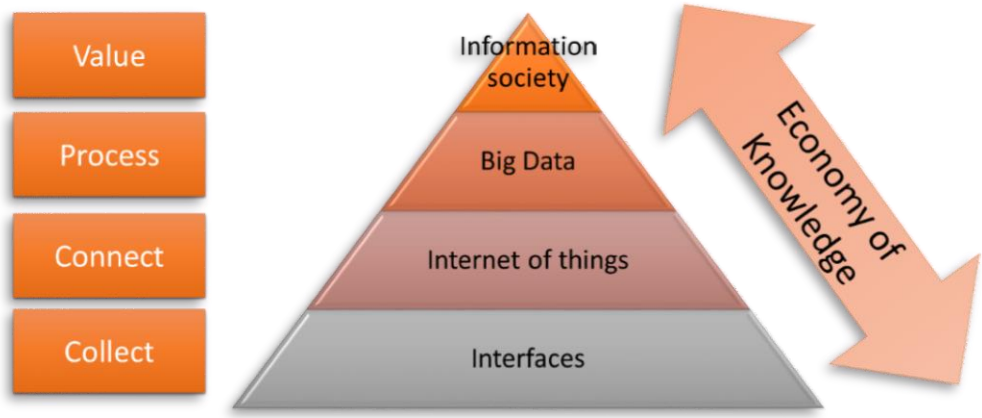

Figure 1.1. Simple schematic representation of the elements involved in the economy based on information.

Raw information has to be previously treated and wisely interpreted for the benefit of society. In the last century, data processing of complex amount of information used to be a limiting factor. However, advances in the way that information is treated resulted in the generation of big data,[5,6] an activity where large data sets undergo computational analysis (data mining) to reveal patterns, trends, and associations, especially related to human behavior and interactions. The use of high volume, high velocity, and/or high variety of information assets is crucial to enable enhanced decision making, insight discovery and process optimization. Integrating greater computer capabilities and using data analytics to extract meaningful information creates a huge advantage in order to take smart decisions. Hence, these decisions have the potential to transform our business, our lives, and our world in countless ways.

Today, data is easily transmitted from one place to the other almost immediately. This is allowed by the use of a global connectivity network, such as the mobile network (e.g. 4G, the fourth generation of mobile telecommunications technology). The whole system that can collect, connect and send data is recently called Internet of Things (IoT) and is considered as one of the Next Technological Revolutions.[7] IoT is an evolution of mobile, home and embedded sensors that are being connected to the Internet.[8] Billions of devices are connected to the Internet and hundreds of billions will be connected. Connecting devices through a decentralized network builds intelligent systems (Figure 1.2), and big possibilities arise from analyzing the data across these systems. According to some estimates, the IoT will add $10-$15 trillion to global gross domestic product (GDP) in the next 20 years. With the IoT, there are limitless opportunities for business and society all over the world.

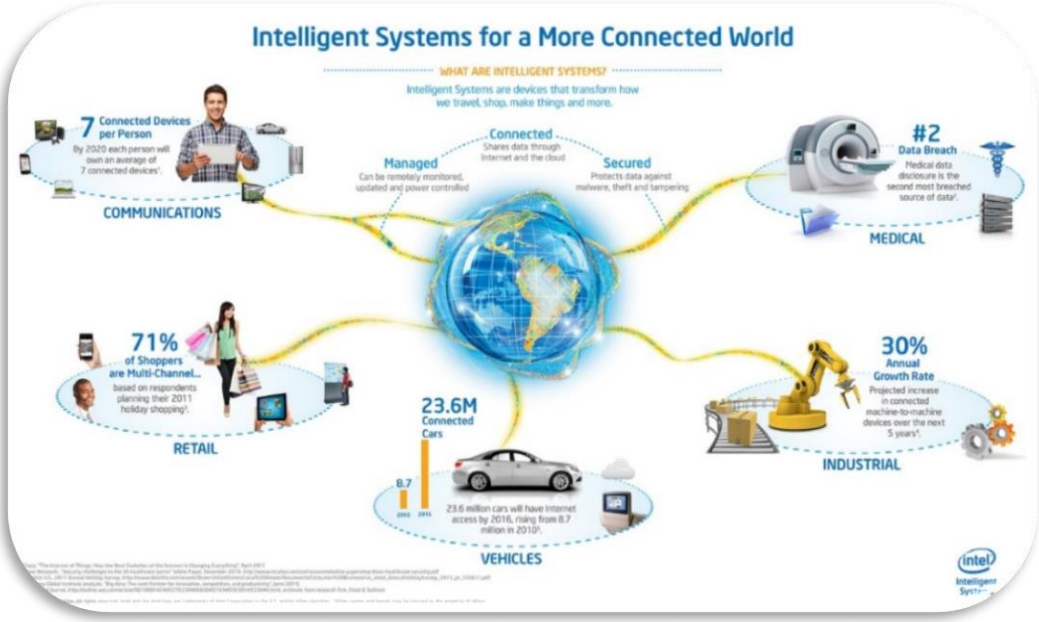

Figure 1.2. Schematic representation of an intelligent system. Picture obtained from Intel Corporation.[9]

Technological advances have made the evolution of the IoT possible.[10] Massive scaling, adequate architecture that allows easy connectivity, control, communications, and useful applications, generation of knowledge from Big Data, robustness of the system, interface technology availability from all over the world and solving security and privacy issues have enabled and consequently boosted the creation of IoT environment.[11,12] This evolution has widely diversify the number of opportunities in terms of companies to build and support an

entirely new information technology infrastructure. More and more new companies are being created for the development of products (software and hardware), network communication, product cloud services, data management services as well as identity and security tools. The product and services of all these companies are interconnected for a successful management of the information age.[13]

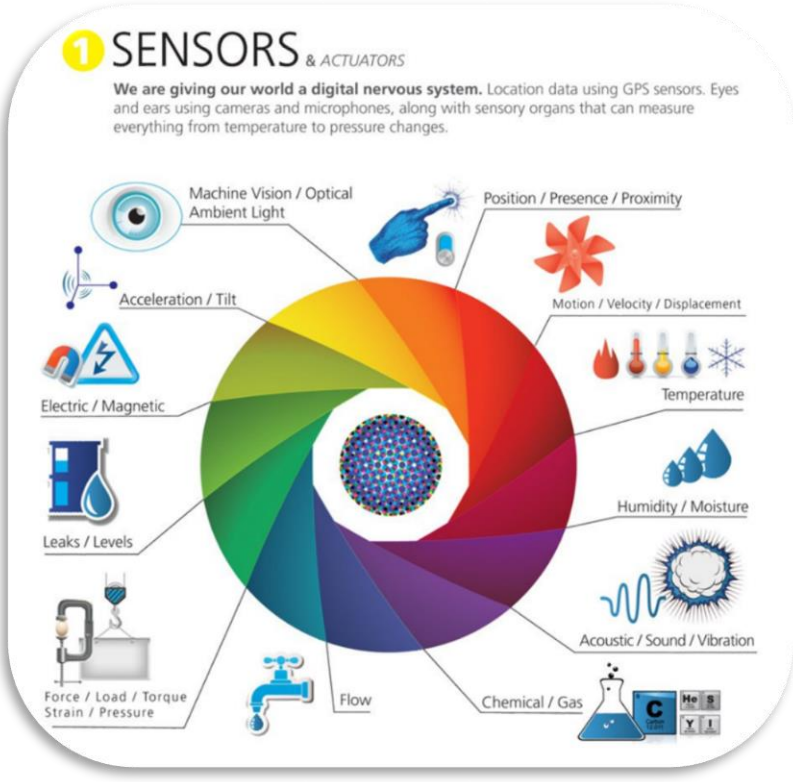

Figure 1.3. Schematic representation of different types of interfaces.[14]

The knowledge industry is largely nurtured by the raw data obtained from the environment. Millions of interactions can be detected and transmitted as raw information through physical or chemical information continually produced by the environment. Interface technology has evolved to allow this recognition and transmission. Therefore, specific interfaces have been created for reliable data capture. These interfaces are sensors or devices with ability to transduce this physicochemical information into electronic signals for further data transmission (Figure 1.3). Sensors act as a gateway of daily information collected from the environment. After the connection with the IoT system and a complex data processing (big data), the information can be used in the knowledge-based economy. All in all, the

environmental data will be captured by the system and thus provide value in a wide range of applications.

1.2. Sensors for Chemical Analysis

Sensors are interfaces whose purpose is to detect and quantify events or changes in its surroundings, and then provide a corresponding output. These tools produce high amount of data that after the right interpretation can offer information for taking smart decisions in different applications. Moreover, the sensor's ability to acquire reliable on-site signals without compromising the environment is becoming one of the crucial factors for the implementation of such interfaces in real scenarios.[15,16]

Since nowadays there is no limitations for the data distribution all over the world, the interface for data acquisition becomes the key success factor of the information system. Hence, the real challenge is to build a wide variety of sensors able to detect and quantify large amounts of information in an easy and convenient manner. In this way, the research and development activities in the sensors field are increasing the opportunities in the industry of sensor-based products as a gateway for data collection.

The field of sensor is thus experiencing a change from the laboratory-based measurements to the on-site measurements.[17] Opposed to the centralized measurements currently taken in the lab, this approach is called decentralization. Sensors are moving from centralized infrastructures where the analysis of the sample was treated and interpreted to a decentralized system where the whole analytical procedure takes place at the same point where the sample is obtained. Thus, with a proper network connection, new processes enable an easy distribution of the information at any point in the planet.

The field of sensors has a long history, so a broad range of sensors have been developed during the last decades. For our purposes, two main types of sensors can be found: sensors to detect physical parameters (e.g. all kind of motion and temperature[18,19]) and chemical sensors (e.g. detection of biomolecules, ions[20,21], etc.). All sensors have the ability to follow a property and transduce it into an electronic signal. However, today only sensors to measure physical parameters can be easily found in the market. For instance, today it is possible to buy a commercial wristband to monitor physiological parameters -such as counting footsteps, cardiac rhythm and location- and send it wirelessly to the cloud. In contrast, there is a lack of tools to electronically connect the chemical environment. For this reason, chemical sensors

are becoming the next big move of the sensor-based industry. These kind of sensors could be an invaluable tool for a wide range of fields such as healthcare, fitness, security, safety and pollution.

The ability to collect the chemical information and to connect it directly to the global network and cloud computing system is allowing to gather information in real-time for taking smart actions at the right moment. This widespread network is allowing a decentralization of chemical analysis, making information available almost instantly. In this way, chemical sensors may help to make social systems more efficient and effective. For instance, the use of point-of-care devices in telemedicine is decreasing the costs of the whole healthcare system. This novel chemical information will enhance the data value and open new opportunities in the knowledge-based society. All in all, much attention is focused today in the progress and characterization of chemical sensors.

The analysis of this growing demand shows two keys factors that will boost the creation of a whole decentralized system of chemical sensors. First, the cost of fabrication and deployment of the sensor. Second, the design of the device/sensor plays a decisive role in the end-user interface, which is crucial for the application in real scenarios. All in all, successful networks will be spread by developing cost-effective and user-friendly tools. In order to address these factors, a suitable approach that can address these needs using inexpensive materials while providing an attractive design is required. For our purpose, we believe that electrochemistry, and especially potentiometry, shows promise to satisfy all these requirements. Consequently, our efforts are focused on the construction of user-friendly and affordable electrochemical sensors for the detection of chemical compounds in real scenarios.

For this reason, in this thesis an emphasis on the essential key factors for the development of electrochemical sensors for a completely decentralized system is addressed. First, the affordability of chemical sensors is discussed. Afterwards, the seamless and user-friendly integration of the sensing platform is brought up by the section of *"Wearable Chemical Sensors"*. Finally, the chapter is closed by the discussion of materials that responds to the challenge of the decentralization of chemical analysis.

1.2.1. Affordable Chemical Sensors

Cost-effectiveness is essential to obtain a sufficiently widespread network of sensors with ability to record information. Indeed, affordable sensors are fundamental to reach all the regions of the planet.[22,23] Considering this approach, a great opportunity for the development

of cheap and decentralized analytical platforms, sensors that can provide meaningful medical (personalized health and wellbeing) and environmental (pollution, security, safety) information, is emerging.[24] Furthermore, the combination of affordable and sustainable devices is central to maintain a healthy environment. Additionally, sensors must display enough sensitivity, specificity, user-friendliness, speed and robustness. Not just the sensors, but the whole analytical platform must be affordable and deliverable to end users to truly capture large amount of chemical data from the environment. All in all, in order to build a full network of decentralized sensors, affordable electrochemical devices are required.

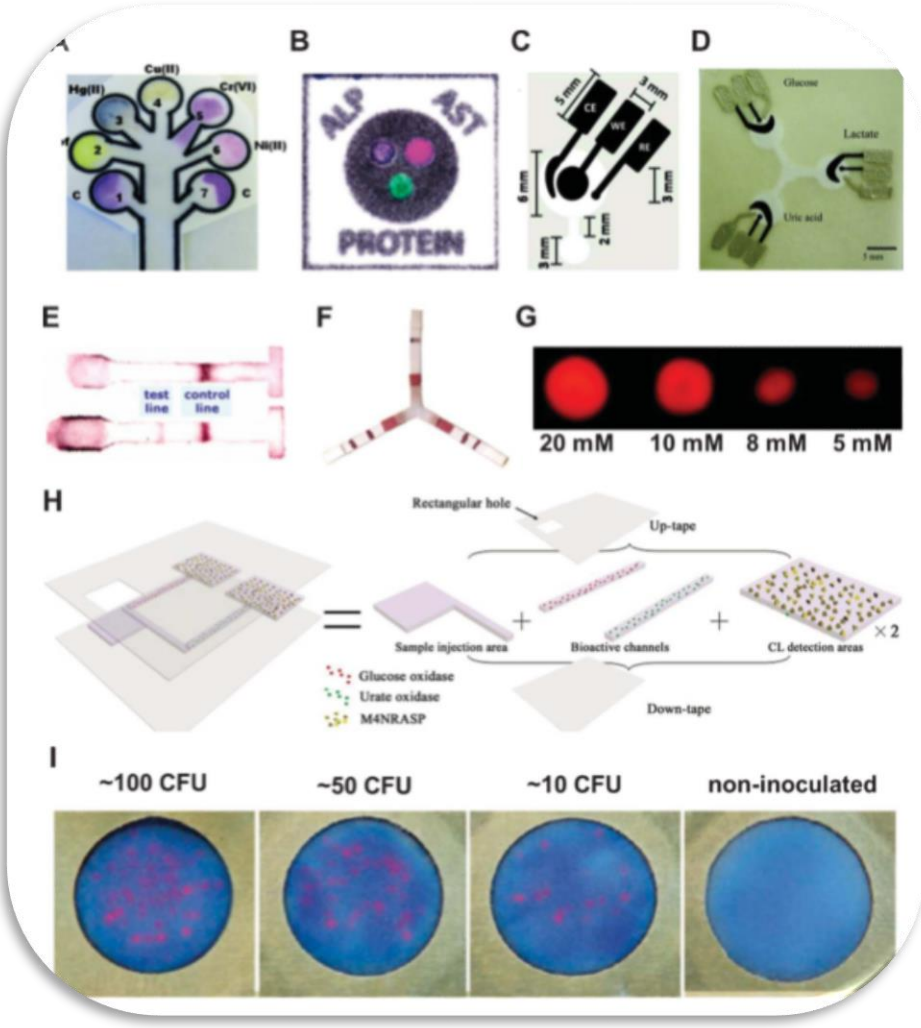

Figure 1.4. Examples of optical and electrochemical paper-based sensors. Image reproduced from Yetisen *et al*. [42]

In this way, new strategies to develop affordable sensors are nowadays being developed, especially through the use of low-cost materials to build the sophisticated sensing networks. Recently, the use of traditional or commodity materials such as paper or cotton to develop sensors has become a major trend in analytical chemistry.[25] Paper-based sensors have been widely used in the last years to build chemical sensors.[26–33] Paper is inexpensive and generally available. As it is made by cellulose fibers, it is easy to modify and compatible with biological samples in addition to its mechanical robustness (flexible and bendable). Sensors made out of paper are affordable, simple, portable and disposable.[34] Consequently, they become an ideal platform for intelligent data acquisition systems.

Nowadays, two main types of detection approaches in paper-based sensors are used in the chemical analysis for decentralized applications. Optical detection of paper-based sensors has been extensively used for their simplicity of operation.[35] Qualitative and semi-quantitative detection using paper strips has been around in analytical chemistry for many decades. More recently, bioactive paper has become an intense field of research and applications. Essentially, they take advantage of the microfluidics generated by the capillarity of the cellulose fibers to move and mix the reagents and provide a substantial change of color on the sensor.[36,37] The second approach is the electrochemical detection. This type of sensors has been recently gaining terrain in the area of paper-based chemical sensors. For instance, tailored-conductive inks are used to paint over the paper substrate thus becoming versatile electrodes.[38,39] This platform gives some advantages over the conventional electrochemical sensors such as a huge decrease in the cost as well as an easy of handling.[40,41] Paper-based sensors, either colorimetric or electrochemical, are receiving increasing attention to build information gateways for chemical analysis.

Electrochemical paper-based sensors offer some advantages over optical sensors such as a quantitative measurement, versatility in the techniques, miniaturization, imperviousness to light and sample color, etc. Moreover, the transduction, which is directly turned into an electrical signal, can be easily recorded and uploaded on the Internet. Hence, for our purpose, we prefer electrochemical sensors rather than colorimetric sensors that might need a transducer from optical to electrical signal. All in all, electrochemical paper-based sensor is a simple approach for a decentralization of chemical analysis.

One of the main challenges facing the decentralized electrochemical sensing is the development of methods of fabrication of platforms that can address the growing needs of producing rapid and cost-effective "*in situ*" analysis. As previously mentioned, painting could

be a technique for the scalability of the sensor manufacturing as it provides easy steps to fabricate the conductive part of the sensor as well as a fast adaptability to the present industry. Other techniques, such as screen-printing is also of interest for its easy scalability and automation, although at a higher cost. Screen-printed electrodes (SPEs) are devices that are produced by printing different inks on various types of substrates.[43] The use of designed patterns in line with the analytical purpose in mind provides a wide versatility in the process.[44] The composition of various inks and thus membranes used for painting or printing the electrodes determines the selectivity and sensitivity required for each analysis. Indeed, a wide variety of devices of this type are commercially available such as the glucometer strips.[45] All in all, merging affordable substrates with low-cost techniques for mass scaling of sensors production is a key factor to accomplish the sensor deployment over the day-by-day social environment.

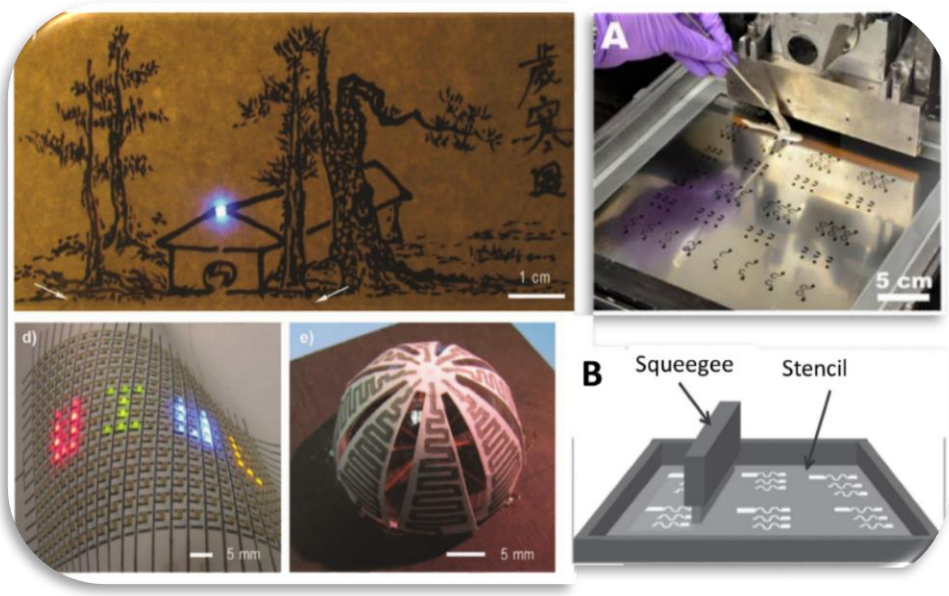

Figure 1.5. Example of painted papers (left) and screen-printing technique (right).[38,46,47]

1.2.2. Wearable Chemical Sensors

The second key factor is the simplicity and seamless integration with the sensing environment. Hence, chemical sensors must have a suitable design to become user-friendly as well as to obtain the analytically relevant information. The interaction between user and interface is the next big challenge that sensors must address. Today, there are different

approaches to electrochemical sensors depending on the applicability and function of the sensor. For instance, fingersticks, despite of being a somehow painful and invasive approach, help to assess a person pathophysiology. On the other hand, laboratory-based analytical instrumentation is robust but usually not amenable for field-based use. Thus, none of them have been capable of fulfilling the emerging user demands such as portability, miniaturization and automation. For this reason, advances in wearable sensors are gaining significant interests for the seamless integration of chemical analysis into human lives. The ability of wearable devices to withstand the rigors of field-based use is recently being applied in many IoT applications. In addition, wearable devices exhibit uncompromising resiliency to various forms of mechanical deformation that are typically encountered during routine use.[48,49] Therefore, wearable sensor systems with real-time feedback will enable a wide range of new preventive-health,[50] security[51] and fitness[32,52,53] data.

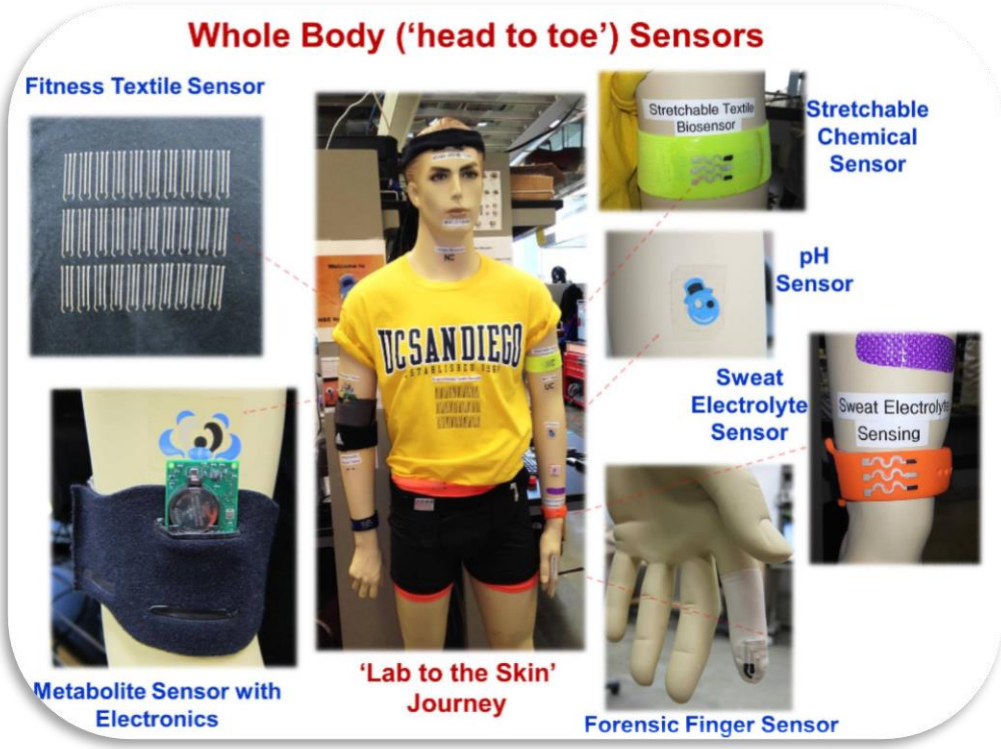

Figure 1.6. On-body printable sensors on textiles or directly on the skin. Embedded sensors are leading the generation of an autonomous "lab on a body". The whole system involving numerous interfaces can obtain real-time data of key physiological parameters from the wearer and send it wirelessly to the cloud. After data processing, the wearer or a third person (connected online) can decide to undertake the healthy action or prevent to choose the wrong choice. Source: Laboratory of Nanobioelectronics, University of California, San Diego.

Along the wearable technology evolution, wearable electrochemical sensors have been embedded onto both textile materials and directly onto the human epidermis for various monitoring applications, owing to their unique ability to process samples in a non-invasive and non-obtrusive fashion.[54] In this manner, multi-analyte detection can be easily performed, in real time, fast and robust way, in order to ascertain the overall physiological health of the wearer or to identify potential offenders in their environment.[55] A part from the typical use of textile,[51] tattoos[56] and epidermis patch[57,58] for an extensive range of applications, different wearable systems have been developed in recent times such as mouthguard[59] for health monitoring, gloves for forensic applications[60,61] or fingernails for environmental monitoring.[62] All in all, a wide range of wearable applications have been designed to meet the end-user needs of data acquisition without compromising the routine of the wearer.

Additionally, similar manufacturing processes for the fabrication of wearable sensors following a cost-effective approach have been performed. Screen-printing, painting and dipping by the use of tailored conductive inks are widely used.[63,64] In addition to cost-effectiveness, these techniques also provide manufactured electrodes able to withstand daily mechanical deformation, common wash procedures or even high temperature conditions such as autoclaving step for the sterilization of the sensors for the use in healthcare applications.[65–67] Finally, these techniques provide scalability to the fabrication of wearable chemical sensors.

Last but not least, the global wearable device market will produce a highly economic impact. With coverage of all of the prominent sensors and the most promising emerging options, there will be 3 billion wearable sensors by 2025, with over 30% of them being new types of sensors that are just beginning to emerge. Indeed, the market for wearable sensors is predicted to reach $6.1 billion by 2026.[68] Taking into consideration the forecast growth of the chemical sensors illustrated in Figure 1.8, a lot of attention must be paid to the field of research of wearable chemical sensors. All in all, the development of novel strategies for chemical sensing is driving a next generation of wearable devices.

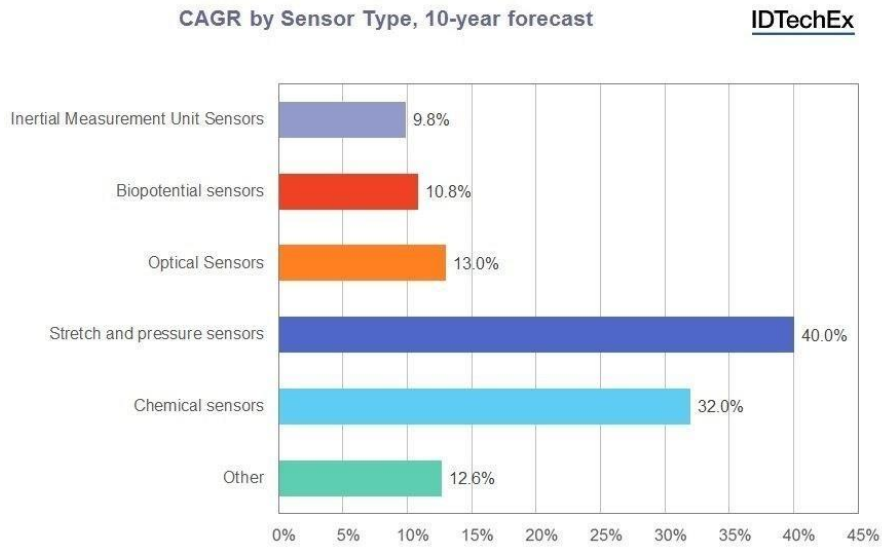

Figure 1.7. Growth rates for each sensor type. Image from IDTechEx.[68] *CAGR – Compound annual growth rate.

1.2.3. Advanced Materials for Chemical Sensing

During the last decades, advances in materials science have been providing novel substrates for the improvement of the features of the sensors. Moreover, as a result of this progress, advanced materials have been discovered, fabricated and thus boosted the generation of new products. Advanced materials refer to all materials that bring enhanced properties and compositions over the traditional materials that have been commonly used. All new materials and modifications to existing materials outperforming in one or more characteristics that are critical for the application under consideration are referred as advanced materials. Superior properties such as roughness, hardness, durability and elasticity -among others- are due to the use of advanced materials. The development of advanced materials leads the design of completely new products. In the case of this thesis, for instance, materials with outstanding electrochemical properties, including the fabrication of wearable electrochemical devices.

The use of convenient materials is of utmost importance in order to develop a reliable electrochemical sensor. New materials, including nanostructured elements, have been widely used in analytical chemistry. These nanostructures add a whole range of new functionalities to the sensor and improve the method of detection.[20,69,70] Major efforts have been focused on the improvement of the analytical performance of different electrochemical techniques and new methods of detection. Nevertheless, there is still a mismatch between

the research and the end-user application. Indeed, there is a need for improving the connection between the sensor and the end-user. Recently, applied research is starting to consider investing resources in platforms to enhance the design of the user interface. Technological progress in advanced materials is providing tools to improve the sensor performance as well as supplying wearable designs that truly fulfil the requirements of society.

The understanding of the end-user behavior is thus crucial to develop a successful sensor. Today, sensors are being integrated into garments and wearable devices as autonomous intelligent systems capable of recording valuable information. The ability to use advanced materials that withstand the daily life mechanical deformations to develop wearable electrochemical sensors opens a tremendous opportunity in research. Accordingly, the study of the mechanical properties of the sensorial platform in real scenarios is decisive to improve its resiliency and thus develop a useful application.

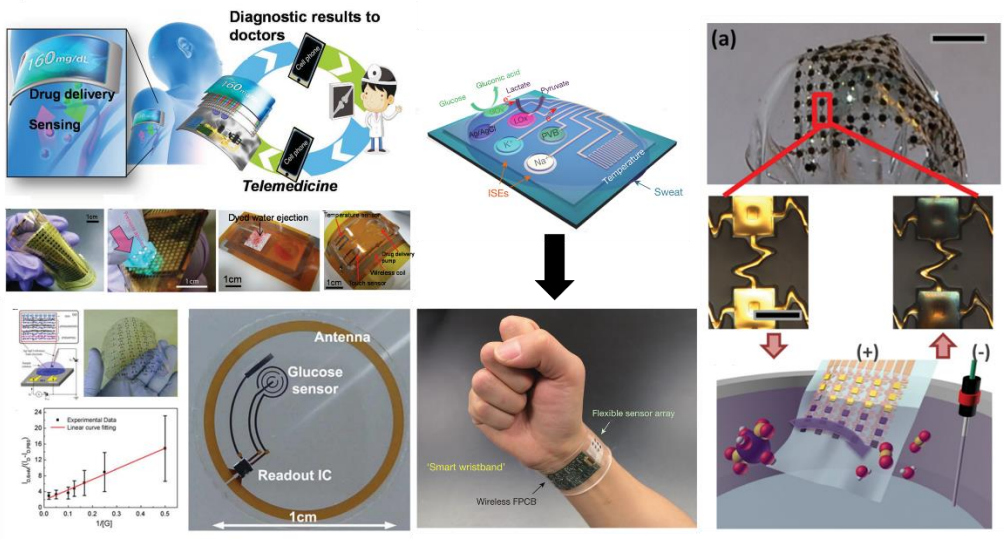

Figure 1.8. Advanced materials used for chemical sensing that can overcome usual biomechanical constrains.[50,57,81]

Recent progress in mechanics and materials science provide routes to wearable integrated circuits that can offer the electrochemical properties of conventional technologies but with the ability to be stretched, compressed, twisted, bent, and deformed into arbitrary shapes. Moreover, inorganic and organic electronic materials in micro-structured and nanostructured forms, intimately integrated with elastomeric substrates, offer particularly

attractive characteristics, with realistic pathways to sophisticated embodiments. The scope of research has expanded dramatically to include opportunities in soft, biointegrated electrochemical devices and in curved, bioinspired designs.[71–73] For this reason, a significant trend is moving towards the research on materials that could endure mechanical deformation during human routine as well as can be functionalized for the purpose of chemical analysis.[74,75]

Firstly, the development of hybrid nanocomposites is leading the fabrication of novel materials.[76,77] Subsequently, the use of tailored nanomposites conducts the sensor fabrication, although still mainly focused on strain sensors.[19,78] However, this fact is already changing. Nowadays, the tendency is moving towards the chemical sensing as it is gaining importance in the connection of the physiological, environmental and biological world to the intelligent data acquisition systems.[46] For instance, functionalization of advanced materials raise innovative applications for chemical molecules detection such as dopamine,[79] ethanol,[80] etc. in a more user-friendly manner. Giving complementary properties to common materials as well as developing new advanced materials become an interesting approach to create the next generation of electrochemical devices.

All in all, a huge opportunity has been opened for analytical chemistry to move closer to the end-user due to the growth of new resilient materials. The incorporation of advanced materials with already developed analytical techniques is increasing the number of smart and useful sensors for applications in the healthcare, environmental, security and fitness fields.[82,83] Merging high analytical requirements for the development of sensors with tailored materials brings a new level of complexity to scientific developments with high impact. In this way, highly stretchable materials are being utilized for analytical techniques to provide valuable insights into the decentralization of the chemical analysis.[47] Reinventing the traditional uses of conventional sensors by the use of advanced materials is a good opportunity that should not be missed. In this thesis, the combination of commodity materials and advanced materials are explored to create innovative sensing interfaces.

1.3. Objectives

The general objective of this doctoral thesis is the development of affordable and wearable sensors for the decentralization of chemical analysis, mainly in the fields of healthcare, fitness, security and surveillance.

This general objective is divided in the following specific objectives:

1. Explore the possibility to develop low-cost ion-selective electrodes using conventional substrates and advanced materials as well as evaluating their applicability using a wearable approach in real scenarios.
2. Explore new strategies for the development of enzymatic-based potentiometric biosensors and assess their analytical performance.
3. Explore different techniques to fabricate electrochemical sensors and evaluate their analytical performance during high mechanical deformations.

The main value of this thesis is to explore the development of affordable interfaces, by means of research in chemical sensors that meet the requirements for the present and especially the future of the decentralization of chemical analysis. This thesis evidences the availability of different substrates to become wearable and low-cost electrochemical sensors by customized fabrication and the use as potential interfaces for the transduction into valuable knowledge of chemical information obtained on real scenarios.

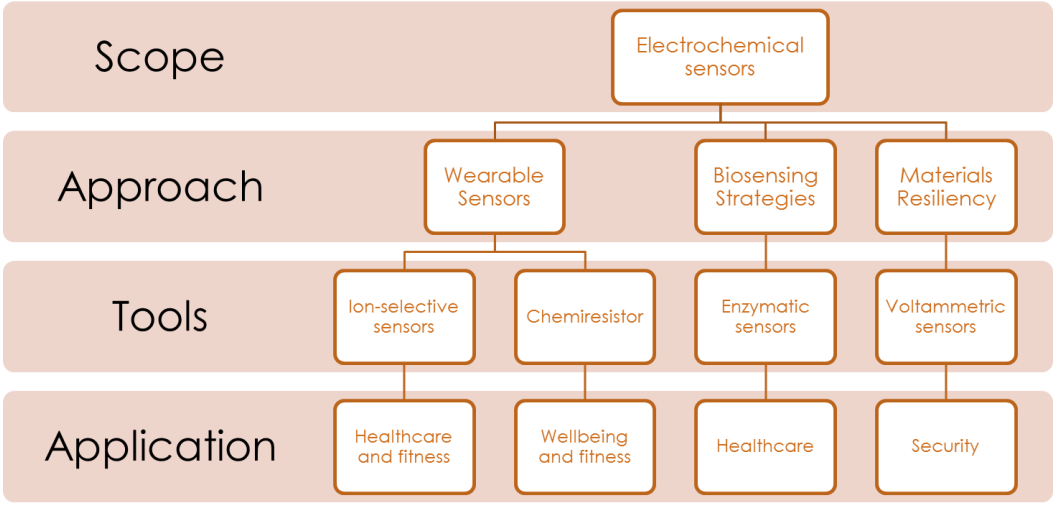

Figure 1.9. Diagram of the different parts of the work carried out during the thesis.

1.4. References

[1] M. Castells, The Rise of the Network Society: The Information Age, 2010, Wiley.

[2] J. Markoff, “Google Cars Drive Themselves, in Traffic,” The New York Times, 2010.

[3] D. Shanker, “The Kitchen of the Future Knows What’s in Your Fridge,” Bloomberg, 2016.

[4] M. Humbert, Technology and Workforce : Comparison between the Information Revolution and the Industrial Revolution, 2007. Report from University of California, Berkeley.

[5] H. Chen, R. H. L. Chiang, V. C. Storey, Mis Q. 2012, 36, 1165.

[6] McKinsey & Company, Big Data: The next Frontier for Innovation, Competition, and Productivity, 2011, McKinsey Global Institute.

[7] M. A. Feki, F. Kawsar, M. Boussard, L. Trappeniers, IEEE Comput. Soc. 2013, 35, 24.

[8] F. Wortmann, K. Flüchter, Bus. Inf. Syst. Eng. 2015, 57, 221.

[9] Intel, “The Internet of Thigs (IoT) Starts with Intel Inside,” 2016.

[10] R. Want, B. N. Schilit, S. Jenson, Computer. 2015, 28.

[11] J. A. Stankovic, Internet Things Journal, IEEE 2014, 1, 3.

[12] A. Whitmore, A. Agarwal, L. Da Xu, Inf. Syst. Front. 2015, 17, 261.

[13] M. E. Porter, J. E. Heppelmann, Harv. Bus. Rev. 2014.

[14] “What Exactly Is The ‘Internet of Things’? A graphic primer behind the term & technologies,” 2016, www.postcapes.com.

[15] R. Byrne, D. Diamond, Nat. Mater. 2006, 5, 421.

[16] D. Diamond, S. Coyle, S. Scarmagnani, J. Hayes, Chem. Rev. 2008, 108, 652.

[17] Y. Shuang-Hua, Wireless Sensor Networks: Principles, Design and Applications, 2014, Springer.

[18] R. Chambers, T. J. Gabbett, M. H. Cole, A. Beard, Sport. Med. 2015, 45, 1065.

[19] X. Liao, Q. Liao, X. Yan, Q. Liang, H. Si, M. Li, H. Wu, S. Cao, Y. Zhang, Adv. Funct. Mater. 2015, 25, 2395.

[20] T. Yin, W. Qin, TrAC Trends Anal. Chem. 2013, 51, 79.

[21] A. P. F. Turner, Chem. Soc. Rev. 2013, 42, 3184.

[22] D. Mabey, R. W. Peeling, A. Ustianowski, M. D. Perkins, Nat. Rev. Microbiol. 2004, 2, 231.

[23] A. Nemiroski, D. C. Christodouleas, J. W. Hennek, A. a Kumar, E. J. Maxwell, M. T. Fernández-abedul, G. M. Whitesides, Proc. Natl. Acad. Sci. 2014, 111, 1.

[24] A. a. Kumar, J. W. Hennek, B. S. Smith, S. Kumar, P. Beattie, S. Jain, J. P. Rolland, T. P. Stossel, C. Chunda-Liyoka, G. M. Whitesides, Angew. Chemie Int. Ed. 2015, n/a.

[25] T. Guinovart, M. Parrilla, G. a Crespo, F. X. Rius, F. J. Andrade, Analyst 2013, 138, 5208.

[26] J.-H. Kim, S. Mun, H.-U. Ko, G.-Y. Yun, J. Kim, Nanotechnology 2014, 25, 092001.

[27] E. J. Maxwell, A. D. Mazzeo, G. M. Whitesides, MRS Bull. 2013, 38, 309.

[28] C. Parolo, A. Merkoci, Chem. Soc. Rev. 2013, 42, 450.

[29] J. Hu, A. Stein, P. Bühlmann, Angew. Chemie Int. Ed. 2016, 1.

[30] W. Lan, X. U. Zou, M. M. Hamedi, J. Hu, C. Parolo, E. J. Maxwell, P. Buhlmann, G. M. Whitesides, 2014.

[31] J. Hu, K. T. Ho, X. U. Zou, W. H. Smyrl, A. Stein, P. Bühlmann, Anal. Chem. 2015, 87, 2981.

[32] G. Matzeu, C. O'Quigley, E. McNamara, C. Zuliani, C. Fay, T. Glennona, D. Diamond, Anal. Methods 2016, 8, 64.

[33] P. Sjöberg, A. Määttänen, U. Vanamo, M. Novell, P. Ihalainen, F. J. Andrade, J. Bobacka, J. Peltonen, Sens. Act. B Chem. 2016, 224, 325.

[34] D. D. Liana, B. Raguse, J. Justin Gooding, E. Chow, Sensors, 2012, 12, 11505.

[35] Q. Liu, J. Wang, B. Wang, Z. Li, H. Huang, C. Li, X. Yu, P. K. Chu, Biosens. Bioelectron. 2014, 54, 128.

[36] J. L. Delaney, C. F. Hogan, J. Tian, W. Shen, Anal. Chem. 2011, 83, 1300.

[37] A. W. Martinez, S. T. Phillips, E. Carrilho, S. W. Thomas, H. Sindi, G. M. Whitesides, Anal. Chem. 2008, 80, 3699.

[38] A. Russo, B. Y. Ahn, J. J. Adams, E. B. Duoss, J. T. Bernhard, J. A. Lewis, Adv. Mater. 2011, 23, 3426.

[39] M. Novell, M. Parrilla, G. Crespo A., F. X. Rius, F. J. Andrade, Anal. Chem. 2012, 84, 4695.

[40] J. Hu, S. Wang, L. Wang, F. Li, B. Pingguan-Murphy, T. J. Lu, F. Xu, Biosens. Bioelectron. 2014, 54, 585.

[41] M. Novell, T. Guinovart, P. Blondeau, F. X. Rius, F. J. Andrade, Lab Chip 2014, 14, 1308.

[42] A. K. Yetisen, M. S. Akram, C. R. Lowe, Lab Chip 2013, 13, 2210.

[43] J. Cai, K. Cizek, B. Long, K. McAferty, C. G. Campbell, D. R. Allee, B. D. Vogt, J. La Belle, J. Wang, Sens. Act. B Chem. 2009, 137, 379.

[44] J. P. Metters, R. O. Kadara, C. E. Banks, Analyst 2011, 136, 1067.

[45] O. D. Renedo, M. a. Alonso-Lomillo, M. J. A. Martínez, Talanta 2007, 73, 202.

[46] A. J. Bandodkar, R. Nuñez-Flores, W. Jia, J. Wang, Adv. Mater. 2015, 27, 3060.

[47] A. J. Bandodkar, I. Jeerapan, J.-M. You, R. Nuñez-Flores, J. Wang, Nano Lett. 2015, 16, 721.

[48] J. R. Windmiller, J. Wang, Electroanalysis 2013, 25, 29.

[49] L. Florea, D. Diamond, Sens. Act. B Chem. 2015, 211, 403.

[50] W. Gao, S. Emaminejad, H. Y. Y. Nyein, S. Challa, K. Chen, A. Peck, H. M. Fahad, H. Ota, H. Shiraki, D. Kiriya, D.-H. Lien, G. A. Brooks, R. W. Davis, A. Javey, Nature 2016, 529, 509.

[51] M. C. Chuang, J. R. Windmiller, P. Santhosh, G. V. Ramírez, M. Galik, T. Y. Chou, J. Wang, Electroanalysis 2010, 22, 2511.

[52] A. J. Bandodkar, D. Molinnus, O. Mirza, T. Guinovart, J. R. Windmiller, G. Valdés-Ramírez, F. J. Andrade, M. J. Schöning, J. Wang, Biosens. Bioelectron. 2014, 54, 603.

[53] T. Guinovart, A. J. Bandodkar, J. R. Windmiller, F. J. Andrade, J. Wang, Analyst 2013, 138, 7031.

[54] A. J. Bandodkar, J. Wang, Trends Biotechnol. 2014, 32, 363.

[55] A. J. Bandodkar, I. Jeerapan, J. Wang, ACS Sensors 2016, 1, 464.

[56] A. J. Bandodkar, W. Jia, J. Wang, Electroanalysis 2015, 27, 562.

[57] H. J. Chung, M. S. Sulkin, J. S. Kim, C. Goudeseune, H. Y. Chao, J. W. Song, S. Y. Yang, Y. Y. Hsu, R. Ghaffari, I. R. Efimov, J. A. Rogers, Adv. Healthc. Mater. 2014, 3, 59.

[58] D. Rose, M. Ratterman, D. Griffin, L. Hou, N. Kelley-Loughnane, R. Naik, J. Hagen, I. Papautsky, J. Heikenfeld, IEEE Trans. Biomed. Eng. 2014, 9294, 1.

[59] J. Kim, G. Valdés-Ramírez, A. J. Bandodkar, W. Jia, A. G. Martinez, J. Ramírez, P. Mercier, J. Wang, Analyst 2014, 139, 1632.

[60] A. J. Bandodkar, A. M. O'Mahony, J. Ramírez, I. a Samek, S. M. Anderson, J. R. Windmiller, J. Wang, Analyst 2013, 138, 5288.

[61] M. de Jong, N. Sleegers, J. Kim, F. Van Durme, N. Samyn, J. Wang, K. De Wael, Chem. Sci. 2016, 00, 1.

[62] J. Kim, T. N. Cho, G. Valdés-Ramírez, J. Wang, Talanta 2016, 150, 622.

[63] T. Guinovart, M. Parrilla, G. a Crespo, F. X. Rius, F. J. Andrade, Analyst 2013, 138, 5208.

[64] V. A. T. Dam, M. A. G. Zevenbergen, R. van Schaijk, Sens. Act. B Chem. 2015, DOI 10.1016/j.snb.2016.01.143.

[65] K. Yang, R. Torah, Y. Wei, S. Beeby, J. Tudor, Text. Res. J. 2013, 83, 2023.

[66] K. Malzahn, J. R. Windmiller, G. Valdés-Ramírez, M. J. Schöning, J. Wang, Analyst 2011, 136, 2912.

[67] T. Guinovart, G. Valdés-Ramírez, J. R. Windmiller, F. J. Andrade, J. Wang, Electroanalysis 2014, 26, 1345.

[68] J. Hayward, G. Chansin, Wearable Sensors 2016-2026 : Market Forecasts, Technologies, Players, 2016. Report from IdTechEx.

[69] H. Li, S. Liu, Z. Dai, J. Bao, X. Yang, Sensors 2009, 9, 8547.

[70] Z. L. Wang, Nat. Nanotechnol. 2009, 4, 407.

[71] X. Hu, P. Krull, B. de Graff, K. Dowling, J. A. Rogers, W. J. Arora, Adv. Mater. 2011, 23, 2933.

[72] J. A. Rogers, T. Someya, Y. Huang, Science. 2010, 327, 1603.

[73] J. A. Rogers, Mrs Bull. 2014, 39, 549.

[74] N. M. Farandos, A. K. Yetisen, M. J. Monteiro, C. R. Lowe, S. H. Yun, Adv. Healthc. Mater. 2015, 4, 792.

[75] A. Tamayol, M. Akbari, Y. Zilberman, M. Comotto, E. Lesha, L. Serex, S. Bagherifard, Y. Chen, G. Fu, S. K. Ameri, W. Ruan, E. L. Miller, M. R. Dokmeci, S. Sonkusale, A. Khademhosseini, Adv. Healthc. Mater. 2016, DOI: 10.1002/adhm.201500553.

[76] M. Park, J. Im, M. Shin, Y. Min, J. Park, H. Cho, S. Park, M.-B. Shim, S. Jeon, D.-Y. Chung, J. Bae, J. Park, U. Jeong, K. Kim, Nat. Nanotechnol. 2012, 7, 803.

[77] P. Lee, J. Ham, J. Lee, S. Hong, S. Han, Y. D. Suh, S. E. Lee, J. Yeo, S. S. Lee, D. Lee, S. H. Ko, Adv. Funct. Mater. 2014, 5671.

[78] Y. Wang, L. Wang, T. Yang, X. Li, X. Zang, M. Zhu, K. Wang, D. Wu, H. Zhu, Adv. Funct. Mater. 2014, 24, 4666.

[79] M. Zhang, C. Liao, Y. Yao, Z. Liu, F. Gong, F. Yan, Adv. Funct. Mater. 2014, 24, 978.

[80] G. Jiang, M. Goledzinowski, F. J. E. Comeau, H. Zarrin, G. Lui, J. Lenos, A. Veileux, G. Liu, J.

Zhang, S. Hemmati, J. Qiao, Z. Chen, Adv. Funct. Mater. 2016, 26, 1729.

[81] K. Takei, W. Honda, S. Harada, T. Arie, S. Akita, Adv. Healthc. Mater. 2015, 4, 487.

[82] H. Ota, S. Emaminejad, Y. Gao, A. Zhao, E. Wu, S. Challa, K. Chen, H. M. Fahad, A. K. Jha, D. Kiriya, W. Gao, H. Shiraki, K. Morioka, A. R. Ferguson, K. E. Healy, R. W. Davis, A. Javey, Adv. Mater. Technol. 2016, 1.

[83] D. J. Lipomi, Z. Bao, Energy Environ. Sci. 2011, 4, 3314.

Chapter 2

Fundamental Aspects of Electrochemistry and Potentiometry

UNIVERSITAT ROVIRA I VIRGILI
NEW ELECTROCHEMICAL SENSORS FOR DECENTRALIZED ANALYSIS
Marc Parrilla Pons

The drastic changes in the world during the last decades have created many new challenges that analytical chemistry must address in the field. Among these challenges, the democratization of the chemical analysis -making analytical tools available in every part of the world- and the simplification of the whole analytical process are paramount. Electrochemistry provides some of the solutions to these unsolved hurdles, because of the several advantages that have been widely recognized in the use of electrochemical sensors. Among them, versatility, cost-effectiveness, robustness, easy miniaturization and excellent limits of detection.[1] Moreover, the combination of advanced materials to build electrochemical tools can enhance the generation of new sensors with the ability to record valuable data from the surroundings. In spite of the significant number of developments, there are still some gaps that the electrochemical tools must fill. Hence, it is crucial to visualize the strengths and drawbacks of each electrochemical technique and use each method in the suitable application. In this chapter, the fundamentals in the electrochemical techniques used in this thesis are described.

2.1. Electrochemical Sensors

Over the past three decades we have witnessed a tremendous amount of activity in the area of electrochemical sensors.[2] This wave, which has its roots on the widespread implementation of the pH glass electrode (i.e., generalized use of potentiometry since the beginning of the last century) and, much more recently, on the glucose sensor (which generalized the use of amperometry during the last 30 years).[3,4] As a prelude to the electrochemical techniques, it seems appropriate to set some basic definitions about the elements of the sensor. An electrochemical sensor is a device that transforms chemical information, ranging from the concentration of a specific sample component to a total composition analysis, into an analytically useful signal. Electrochemical sensors contain usually two basic components connected in series: a chemical (molecular) recognition system (receptor) and a physicochemical transducer. The purpose of the transducer is to convert the chemical recognition event into a useful electrical signal. Moreover, there are several electrochemical techniques able to detect the electrical readout. Among them, the most used are amperometry and potentiometry. In potentiometric devices, the analytical information is obtained by converting the recognition process into a difference of electrical potential. Hence, in this approach many types of devices -such as ion-selective electrodes (ISEs) or redox sensitive probes- can be used. In contrast, amperometric sensors operate by applying a constant potential and monitoring the current associated with the reduction or

oxidation of electroactive species involved in the recognition process. A particularly relevant type of sensors are the biosensors, which are chemical sensors where the recognition event is based on a biochemical mechanism. Both sensors and biosensors can be used to monitor either biological or non-biological analytes.[5] All in all, the development of electrochemical tools for both, sensors and biosensors, has undergone a massive development over the last decades.

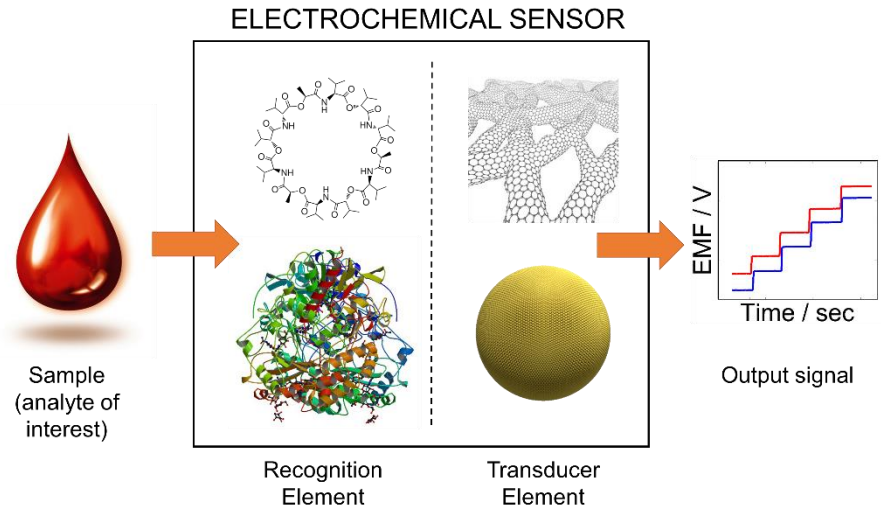

Figure 2.1. Schematic representation of the measuring process in a potentiometric sensor (a type of electrochemical sensor). In the recognition element, the upper drawing illustrates the elements involved in an ISEs and the lower drawing illustrates the elements involved in a potentiometric biosensor.

One of the areas where electrochemical sensors have made a major impact is the development of decentralized analytical tools. Indeed, the growth of electrochemical tools has facilitated the shift from the lab-based measurements (to the on-site testing (e.g., point-of-care device for measuring glucose in blood, glucometer).[6,7] Advances in specificity, ease of use, portability, and affordability of sensors and biosensors are offering new and exciting opportunities for numerous decentralized applications, ranging from 'alternative-site' testing (e.g., physician's office emergency-room screening, bedside monitoring, or home self-testing)[8] to a completely established intelligent data acquisition system (e.g., smart cities, smart homes, smart toilets, etc.). In this way, there is a massive opportunity to develop electrochemical sensors with the ability to collect and record data in decentralized settings.

Since most of the work of this thesis is based on potentiometric tools, this will be the technique herein described in detail.

2.2. Electrochemical Techniques

2.2.1. Voltammetry and Amperometry

Voltammetry refers to a number of techniques in which an applied potential causes an electrochemical oxidation or reduction of electroactive species (redox reaction) that produces a measurable current. The phenomenon is essentially an electrolysis of the species. There are different types of voltammetric methods that differ on the way how the applied potential is changing over the system to obtain a resulting current. For instance, cyclic voltammetry -performed by cycling the potential of a working electrode- and linear sweep voltammetry -where the potential is swept linearly in time- are among the most used methods.

Amperometry, one of the most used electrochemical technique, is performed by maintaining a constant applied potential -where the electrochemical reaction occurs- at a platinum, gold or carbon based working electrode or on array of electrodes (auxiliary or counter electrode where an electrical current is expected to flow) with respect to a reference electrode and measured the generated current.

In both methods, the resulting current is directly correlated to the bulk concentration of electroactive species or their production/consumption rate within the adjacent catalytic layer. The voltammetric and amperometric techniques utilize three electrodes. The three electrodes are the working electrode, the auxiliary electrode (also called the counter electrode), and a reference electrode. The current -that passes between the working and counter electrode- is recorded as a function of its potential measured against a reference electrode. A special electronic circuit -the potentiostat- for carefully controlling the voltage that the system receives is needed to perform these electrochemical methods.

2.2.2. Electrical Resistivity

Electrical resistivity quantifies the difficulty of a material to allow the flow of an electric current upon the application of a difference of potential. The unit is the ohm meter (Ω m). In analytical chemistry, the inverse of resistance –i.e. conductance- is normally used to monitor the presence of ions in a solution. In the field of sensors, however, the use of this property to determine an analyte in a sample leads to chemiresistors. Chemiresistors are chemical sensors where the recognition event is transduced into a change on the electrical resistance of a material. This type of sensors is composed by materials that changes its electrical resistance in response to changes in the nearby chemical environment. Moreover, the

modification of the chemical environment could be performed by chemical or biological reactions and thus be related to the concentration of the analyte in the sample.[9,10]

Recently, carbon nanotubes (CNTs) have been increasingly used as one of the key electronic materials for new classes of chemiresistors. Although there has been recent controversy whether the response in CNT chemiresistors are associated with a change in the resistance of the individual nanotubes or changes in the resistance of the junctions, huge efforts have been focused on the development of chemiresistors based on CNTs.[11,12]

2.2.3. Potentiometry

Potentiometry is a well-established analytical technique that was born at the beginning of the twentieth century. The exploration of this electrochemical technique was originated during Nernst experiments with metal electrodes.[13] Then, after the reports at the beginning of the 20th century showing that a glass electrode selectively responds to protons according to the formulation (the well-known Nernst equation), potentiometry was consolidated as an attractive electrochemical technique in analytical chemistry. Since then, potentiometry has experienced huge advances in technology. For this reason, it is still one of the workhorses in clinical laboratories and almost the universal approach to measure pH. Ion-selective electrodes have also become the standard procedure for measuring several ions. Furthermore, the development of solid contact ion-selective electrodes (SC-ISE) during the last few decades has produced a "*silent revolution*" that has led to drastic improvements of the limits of detection (LOD), increased range of applications, and simplification of the sensor construction, operation, and maintenance.[14–19] Recent works have also shown the advantages of miniaturization of the electrodes, and the development of the electrode arrays that could be remotely operated.[20–26]

Potentiometric measurements involve determination of the difference of electrochemical potential between a working and a reference electrode, or two reference electrodes separated by a permselective membrane. In all cases, measurement is performed in open-circuit conditions, i.e. when current flowing through the system is negligible. To do this, the potential must be recorded with a high-impedance voltmeter (a potentiometer) and this potential is referred in terms of electromotive force (EMF). The most common potentiometric devices are pH electrodes; several other ion (F^-, I^-, Na^+, K^+, Ca^{2+}, NH_4^+) or gas (NH_3) selective electrodes are also available.[27] The difference of potential between these working and reference electrodes are proportional to the logarithm of the ion activity as described by the

Nernst equation (Equation 2.1). Activities can be calculated using, for example, the Debye-Hückel approximation.[28]

$$E = E^0 + \frac{RT}{nF} log a_{i(aq)} \qquad \text{(Equation 2.1)}$$

Where E is the difference of electrical potential of the cell, E^0 is the standard electrochemical potential of the cell, n is the number of electrons involved in the reaction (or the charge of the ion), R is the universal gas constant (8.314 J (K mol)$^{-1}$), T the absolute temperature, F the Faraday constant (96485 C mol^{-1}) and $a_{i(aq)}$ is the activity of the uncomplexed primary ion in the aqueous phase.

A potentiometric measurement requires the following arrangement (Figure 2.2):

• A working electrode (also called an indicator electrode), which is sensitive to the activity of ions in solution (and thus related to analyte concentration)

• A reference electrode, which is necessary to complete the circuit, but it should neither be affected by the analyte concentration nor the matrix composition (or the environmental conditions)

• A high-impedance voltmeter that will produce the readout

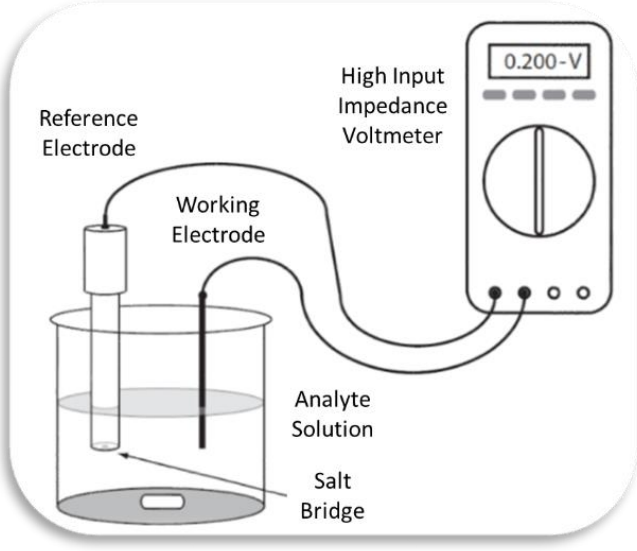

Figure 2.2. Electrochemical potential measurement with a metal working electrode and a glass reference electrode using a high-input impedance voltmeter.[27]

Potentiometry has a plethora of advantages over other electrochemical techniques, particularly when considering on-site methodologies. First, it displays an unrivalled roughness and simplicity of instrumentation. Subsequently, the response is relatively fast, has a wide dynamic range and is inexpensive and simple to operate. This inherent simplicity stems from the facts that is label free and almost current free, whereas other electroanalytical techniques usually require some label molecule and need current for performing the measurements. However, potentiometry has also some limitations, such as the more limited selectivity, the relatively poorer limits of detection -when compared against other electrochemical approaches- and the need for calibration of the electrodes (although this last one is a requirement common to all the techniques).[29–33] Despite of all limitations, potentiometry has presented many advantages to be a truly candidate for the development of the decentralization of the chemical analysis over other electrochemical techniques.

2.3. The Electrochemical Potential

By definition of the IUPAC, the electrochemical potential of a substance in a specified phase is the partial molar Gibbs free energy of the substance at the specified electric potential. Then, the electrochemical potential is the result of the combination of electrical and chemical potential: Electric potential, at a point, is the work required to bring a charge from infinity to that point in the electric field per unit of charge and the chemical potential of a substance B in a mixture of substances B, C, etc. is related to the Gibbs free energy (G) of the mixture. All in all, the electrochemical potential is a thermodynamic magnitude. Accordingly, all the chemical species have an electrochemical potential (J mol^{-1}) at a given point in space that is generated by the influenced of the electrical field of the system as well as the chemical gradient of the species.

2.3.1. Redox potential

Oxidation-reduction (or redox) reactions involve the energy transfer of an electron from a donor to an acceptor species. Because the difference of redox potential is measured under conditions of zero flux of current (the "reversible" conditions of classical thermodynamics, or the open circuit potential -OCP-), it is a direct measure of the free energy change of the reaction of the electrochemical cell. The tendency of these electrons is provided by the standard reduction potential of the chemical species, when the tendency is to acquire electrons (therefore be reduced), or release electrons (therefore be oxidized) (Equation 2.2). Any oxidation-reduction (redox) reaction can be divided into two half reactions: one in which

a chemical species undergoes oxidation and one in which another chemical species undergoes reduction. If a half-reaction is written as a reduction, the driving force is the reduction potential. If the half-reaction is written as oxidation, the driving force is the oxidation potential related to the reduction potential by a sign change. So the redox potential is the reduction/oxidation potential of a compound measured under standards conditions against a standard reference half-cell (Equation 2.3).

$$Ox + ne^- \leftrightarrow Red \qquad \text{(Equation 2.2)}$$

Example of two half-reactions.

$$M^0 \rightarrow M^{2+} + 2e^- \qquad \text{(Oxidation half cell)}$$

$$M^{2+} + 2e^- \rightarrow M^0 \qquad \text{(Reduction half cell)}$$

$$E = E^0 - \frac{RT}{nF} \ln \frac{[Red]}{[Ox]} \qquad \text{(Equation 2.3)}$$

2.3.2. Donnan potential

Donnan equilibrium is the equilibrium characterized by an unequal distribution of diffusible ions between two ionic solutions separated by a membrane or boundary which is impermeable to at least one of the ionic species present. Hence, the boundary layer acts as a selective barrier to diffusion of some ionic species. The measurement of the electrochemical potential risen between these two ionic solutions separated by a semipermeable membrane is called Donnan potential.

2.4. Generation of a Potentiometric Response in Ion Selective Electrodes

The generation of a measurable difference of electrochemical potential at the surface of an electrode is normally performed using of ion-selective electrodes (ISEs). In this thesis a type of ISEs -the solid-contact ion selective electrodes (SC-ISEs)- will be used instead of the internal solution ion selective electrodes (IS-ISEs). SC-ISEs, introduced more than two decades ago, are based on three main components. First, an ion selective membrane (ISM) that is the corresponding recognition layer and is composed by the selective receptor or ionophore, the ion exchanger, the plasticizer and the polymeric matrix. Second, the transducer element or layer responsible for transforming ionic into electronic signal. Third, the metallic conductor where the membrane and transducer are deposited (Figure 2.3).

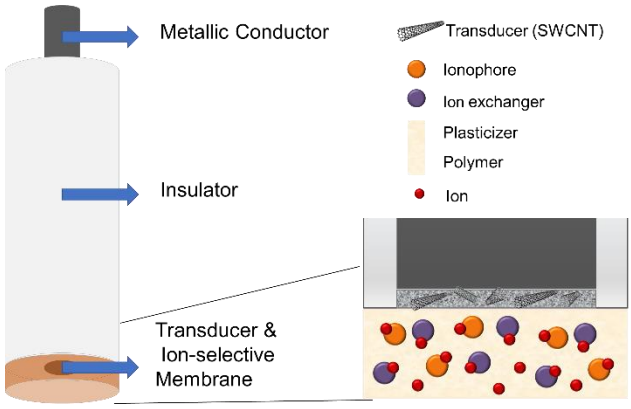

Figure 2.3. Schematic representation of a solid-state ion-selective electrode (SC-ISEs) and its corresponding units. The magnification displays the elements that conform an ion-selective membrane.

The potentiometric cell, involving the working and reference electrodes, is used to record a difference of potential generated across both electrodes. This difference of potential (EMF), measured under nearly zero-current conditions between working and reference electrodes, is the sum of potentials of the two electrodes (Figure 2.4) plus additional potentials that can be generated across the circuit, such as the liquid junction potential. First, EMF measured as a sum of the sample-membrane boundary potentials (E_M). Secondly, the liquid junction potential inside the reference electrode ($E_{D,Ref}$) (using a double junction reference electrode) (Equation 2.4). This potential can be calculated by the Henderson equation if the composition of the sample is known.[34,35] Finally, a constant potential generated at the internal interfaces from membrane-transducer and transducer-conductor (E_{Const}).

$$EMF = E_M + E_{D,Ref} + E_{Const} \qquad \text{(Equation 2.4)}$$

Although different models have been proposed since many years ago, similar considerations are used in order to address the membrane potential phenomena. One of the currently accepted models for the generation of the electrochemical potential in ion-selective electrodes is the phase-boundary potential.[36] In this model, the E_M is divided into different potentials. E_{PB}, the phase boundary potential between the inner solid contact and the membrane, E_D, the diffusion potential inside the membrane and, $E_{PB'}$, the phase boundary potential between the membrane and sample solution (Equation 2.5).

$$E_M = E_{PB} + E_D + E_{PB'} \qquad \text{(Equation 2.5)}$$

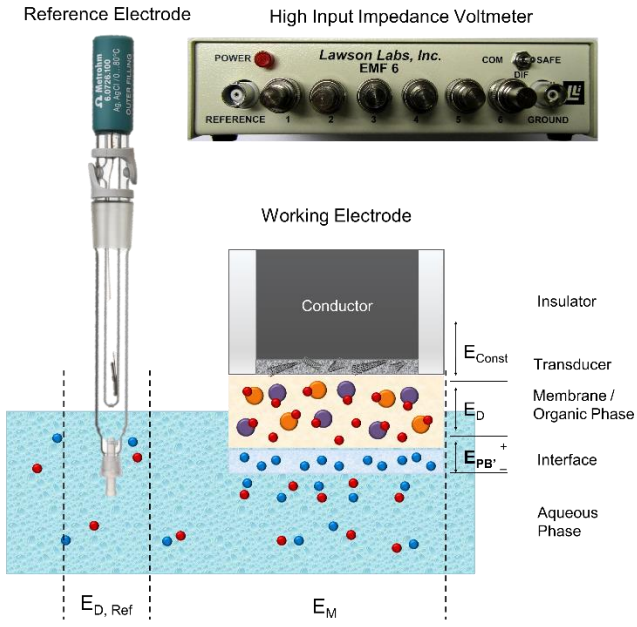

Figure 2.4. Potentiometric cell composed of a reference electrode (RE, left) and the representation of a solid-contact ion-selective electrode (SC-ISE, right) as a working electrode. Ideally, both electrodes are connected and the EMF generated is the sum of all the potentials involved in the cell ($E_{D,Ref}$ and E_M). The difference of potential is recorded by the use of a high input impedance voltmeter.

Some assumptions might be applied to simplify the calculation of the membrane potential. First, the contribution of the diffusion potential (E_D) is ignored, assuming thus the electroneutrality in the bulk of the membrane. Moreover, the internal phase boundary potential E_{PB} is considered constant. As a matter of fact, the control of this potential is what made possible the emergence of solid state technology. The coated-wire electrode, reported back in the '70s,[37] was a primitive form of the SC-ISE that did not use ion-to-electron transducer. Therefore, it had a highly variable E_{PB} that made impossible any practical application. With the use of conductive polymers -first- and nanomaterials -later- as transducers, this inner potential was stabilized and remains constant during measurements. Consequently, membrane potential depends only in the phase boundary in contact with the sample (aqueous-organic interface, $E_{PB'}$). Second, the electrochemical equilibrium is assumed at the sample (aqueous phase) and membrane (organic phase) (Equation 2.6).

$$E_M = E_{PB'} = \frac{\mu^0_{i(aq)} - \mu^0_{i(org)}}{n_i F} + \frac{RT}{n_i F} ln \frac{a_{i(aq)}}{a_{i(org)}} \qquad \text{(Equation 2.6)}$$

Where $\mu^{0}_{i(aq)}$ is the standard chemical potential in the aqueous phase, $\mu^{0}_{i(org)}$ is the standard chemical potential in the organic phase, n_i is the charge of the primary ion, R is the universal gas constant (8.314 J (K mol)$^{-1}$); T the absolute temperature, F the Faraday constant (96485 C mol^{-1}), $a_{i(aq)}$ the activity of the uncomplexed primary ion in the aqueous sample and $a_{i(org)}$ the activity of the primary ion in contact with the organic phase.

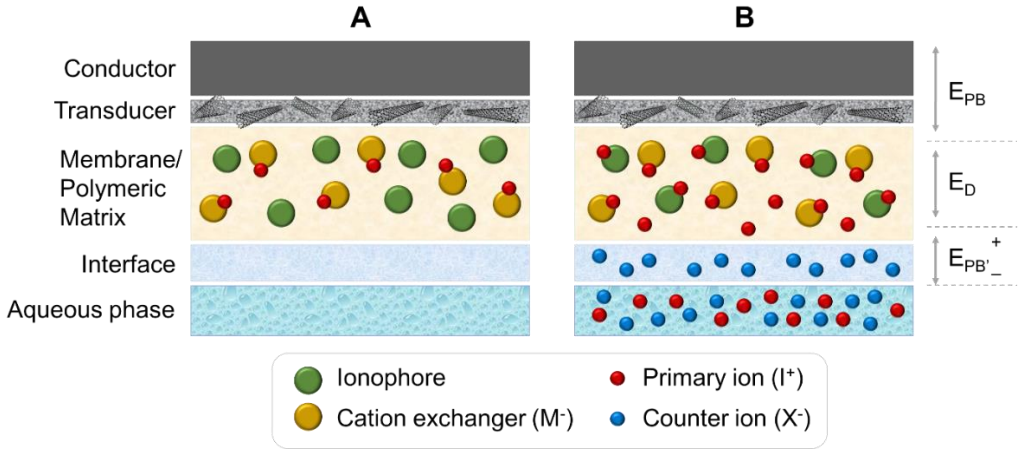

Figure 2.5. Diagram of the mechanism of the phase boundary potential. (A) Illustration of a SC-ISE in an aqueous solution without ions. (B) The membrane is placed in contact with an aqueous solution which has a primary ion and a counterion (I^+ and X^-). Then, the electrochemical equilibrium is assumed to happen between sample and membrane. Thus, the charge separations between cations and anions into the interface membrane/aqueous solution are generated due to the difference in the free energies of solvation presenting a change in potential.

The following mathematical expression explains the generation of the potential at the interface being $\Delta G_{tr}^{0,w\rightarrow m}$ the free standard energy of the distribution process of ion *i* between two phases and k_i correspond to the "single ion distribution coefficient" (Equation 2.7). Indeed, k_i is function of the relative free energies of solvation in both the sample and the membrane phase.

$$\mu_{i(aq)}^{0} - \mu_{i(org)}^{0} = \Delta G_{tr}^{0,w\rightarrow m} = RTlnk_i \qquad \text{(Equation 2.7)}$$

In the classical potentiometric arrangement, electrochemical potential arises from the chemical work (Equation 2.8):

$$W_{Chem} = (\mu - \mu_0) = RTln\frac{a_{i(aq)}}{a_{i(org)}} \qquad \text{(Equation 2.8)}$$

as a consequence of the generation of a chemical gradient (charge separations due to partition of cations and anions between the organic membrane and aqueous sample) and the electrical work (Equation 2.9) performed with the electrical field generated by the charges.

$$W_{El} = QV = n_i FV \quad \text{(Equation 2.9)}$$

Then, obtaining Equation 2.10 for the calculation of the membrane potential and consequently Equation 2.11.

$$nFV = RTln\frac{a_{i(aq)}}{a_{i(org)}} \quad \text{(Equation 2.10)}$$

$$(V - V_0) = \frac{RT}{n_i F} ln\frac{a_{i(aq)}}{a_{i(org)}} \quad \text{(Equation 2.11)}$$

Considering that the standard potential (V_0) is ideally constant (includes factors affecting the solvation of the ion in the membrane and solution phases) and the activity coefficients are constant in the organic phase (then included into the constant part of the equation), a simplistic mathematical representation can be obtained as the well-known Nernst equation (Equation 2.1).

The charge separations between cations and anions at the interface membrane-aqueous solution are generated due to the difference in the free Gibbs energies in each phase (thus hydration energies and ionophore affinity play a very important role in this phenomenon). Accordingly, the cation or anion ($I^{+/-}$) (depending on the membrane composition) has a greater tendency to pass into the membrane phase than the counterion ($X^{+/-}$) (due to the ion exchanger molecule and ionophore properties), generating an electrical double layer at the interface (charge separation) thus raising a difference of electrochemical potential. Under ideal conditions, the arrangement of the gradient of charges will lead to a magnitude of the electrical potential that is proportional to the logarithm of the concentration of the ions, as described by Equation 2.1.

2.5. Ion-Selective Membrane

In this section, a detailed description on the components shown in Figure 2.5, of a conventional potentiometric ISE membrane is provided. An Ion-Selective Membrane (ISM) is an essential part of the ISEs that is made by three main components:

- *Selective receptors, or Ionophores*: These molecules play a decisive role in terms of selectivity of the membrane. The primary ion must be bound to the ionophore more strongly than other interfering ions. Therefore, the ionophores are specifically designed and synthesized according to the nature of each analyte (charge and size) as well as considering the ability to form supramolecular interactions (host-guest) by hydrogen bonds, metal coordination and hydrophobic/lipophilic forces. Important

considerations in order to obtain a reliable ionophore are: (i) that should be flexible -in terms of binding to the analyte of interest-, (ii) the free energy from the activation of the complexation process, (iii) the hydration competition, and last but not least, (iv) the lipophilicity of the molecule. Adding ionophore into the ISM, the formation constant becomes the most relevant factor to determine a relevant selectivity coefficient of an ISM.

- *Lipophilic ion-exchangers*: The use of this element is crucial to obtain a Nernstian response and guarantee the permselectivity of the membrane (Donnan exclusion). This means that the co-extraction process (primary ion with their respective counter ions entering the membrane from the solution) is minimized as much as possible and only the exchange process of the primary ion is theoretically permitted. For instance, potassium tetrakis[p-chlorophenylborate] (KTpClPB) is broadly used as a cation exchanger (R^+).

- *Polymeric matrix*: provides mechanical stability and mechanical resiliency to the ISM. The polymeric matrix is usually composed by polymer and plasticizer. The polymer yields physical connection among the elements and the plasticizer is employed as a solvent facilitating the generation of a homogenous and flexible membrane. Poly(vinyl-chloride) (PVC) is one of the most used polymers for ISEs and bis(2-ethylhexyl sebacate (DOS) or o-nitrophenyl octyl ether (o-NPOE) are the commonest plasticizers used. These components will be used in this thesis.

2.6. Solid-Contact Ion-Selective Electrodes (SC-ISEs)

Advances in solid-contact ion-selective electrodes (SC-ISEs) allow the development of new robust electrochemical tools for the decentralization of chemical analysis. Although internal solution ion-selective electrodes (IS-ISEs) have demonstrated huge applicability in analytical chemistry, excellent stability and life time, being the glass electrode the most used ISEs (e.i. pH electrode), there are still many challenges to address. Some of the drawbacks such as the use of liquid, fragility, position of use and miniaturization are solved by the use of SC-ISEs. In contrast, the transduction mechanism, one of the significant limitations for the SC-ISEs, is nowadays solved by the introduction of conducting polymers and new nanomaterials, such as single walled carbon nanotubes (SWCNTs), acting as a transducing layer.[38–40] It is well-known the high stability provided by the liquid/solid transduction system of the IS-ISEs. In the inner solution electrodes, the transduction is established by coupling

ionic conductivity of the membrane and internal filling solution of chloride with the electronic conductivity of the internal reference half-cell (Ag/AgCl) via a reversible redox reaction (Ag/Ag^+). The incorporation of a solid transducer instead of the internal solution generates a wide range of new benefits (miniaturization, robustness, cost-effectiveness, dry storage and wearability among others) that can be translated into decentralized and on-site measurements.[41–44]

In the SC-ISEs, the membrane is in contact on one side with the solid transducer instead of the inner solution as in IS-ISEs, and on the other side with the aqueous phase of the test sample (Figure 2.5). In this way, all components in the SC-ISEs are "*solid*", making an all-solid-state sensor. This transduction layer is necessary to obtain high stability of the sensor signal. For this reason, a proper transduction mechanism strategy is essential to fulfil the ion-to-electron transducer challenge. For instance, a high redox capacitance transducer using conducting polymers have been widely used.[45–47]

Nowadays, there are several types of transducers used in potentiometry. Two of the most well-known and used solid-state transducers are the carbon nanotubes (CNTs) and the conducting polymers (CP), such as poly(3,4-ethylenedioxythiophene) (PEDOT). In the case of CNT the origin of the bulk capacitance is expected to be the large double layer capacitance[48] while in the case of PEDOT it is expected to be due to the faradaic process (redox capacitance) involving reversible oxidation (doping) of the conjugated polymer chains with simultaneous insertion/expulsion of charge-compensating ions.[38] However, still some drawbacks using conducting polymers as low stability due to the presence of acid-based groups, formation of a water layer and light sensitivity must be solved.

In this thesis, a network of carbon nanotubes (CNTs) is used as a transducing layer.[48] The extraordinary capacity of CNT to promote electron transduction between heterogeneous phases provides outstanding stability to the sensor.[49] Transduction through CNTs means that there are no redox reactions at the interface between the membrane and conductor. However, Nernstian response and stability is obtained. This phenomena might be attributed to the large bulk capacitance that is related to a large effective double layer at the SWCNT/ISM interface of the SWCNTs.[39] It can be described schematically as an asymmetric capacitor where one side is formed by electronic charge (electrons/ holes) in the SWCNT wall and the other side is formed by ions (anions/cations) in the ion-selective membrane. The high influence of the surrounding chemical environment on the conductance of carbon nanotubes makes them very sensitive to the phase-boundary potential changes

generated at the interface between the ion-selective membrane-test solution allowing to great analytical performance of the SC-ISEs.[50] Indeed, the characteristics of carbon nanotubes upon the electrochemical potential measurement were used in the development of paper-based ion-selective electrodes.[51,52] All in all, carbon nanotubes demonstrated their outstanding performance as a ion-to electron transducer in potentiometric measurements.

2.7. Analytical Performance

Different parameters have been extensively described to quantitatively determine the sensor analytical performance. Next points describe the most used parameters to fully validate the outstanding performance of potentiometric sensors:

- *Linear range*: is the range of concentrations -or ion activity- where the calibration curve presents Nernstian linearity (ideally $59.2/n_i$ mV/log a_i at 25ºC). This range determines the region where a sample of interest could be quantitatively measured.
- *Sensitivity*: is calculated from the slope of the calibration curve within the linear range. In potentiometry, the slope is well established by the Nernst equation and it depends on the number of charges. Hence, sensitivity gives us information about the proper functioning of the working electrode.
- *Limit of Detection (LOD)*: can be divided into lower and upper limit of detection. IUPAC defines the limits by the cross section of two extrapolated linear segments of the calibration curve.[53] The lower LOD is of great interests for the applications of ISEs. It is calculated as the activity/concentration of the analyte at the intersection point between the linear segments of linear range and the low concentration level segment of the calibration curve. One of the main issues that may affect the lower LOD is the presence of interfering species in the sample solution. In this thesis, the lower LOD will be utilized to determine this analytical parameter.
- *Selectivity*: is the ability of a sensor to detect a particular analyte in a complex mixture without interference from other components in the mixture. The selectivity of the sensor has to be quantified individually for each particular interference and in potentiometry is expressed in terms of selectivity coefficients (K_{ij}^{pot}). Two main methods to determine the selectivity coefficient are widely used.[32] In the separate solution method (SSM), calibration curves with the interfering ions (*j*) are performed, followed by a calibration curve of the primary analyte (*i*) (Equation 2.12). Standard

potential of each interfering ion (E^0_j) and the primary analyte (E^0_i) are extrapolated from the obtained calibration curves. Unbiased selectivity coefficients are obtained only if the standard potential has been calculated with ISE exhibiting a Nernstian response for both ions.

$$K_{ij}^{pot} = e^{\frac{n_i F}{RT}(E_J^0 - E_I^0)} \qquad \text{(Equation 2.12)}$$

Where n_i is the charge of the primary ion, R is the universal gas constant (8.314 J (K mol)$^{-1}$); T the absolute temperature and F the Faraday constant (96485 C mol^{-1}).

Fix interference method (FIM) is another widespread methodology to calculate the selectivity coefficient. In this case, the concentration of the primary analyte is gradually increased in a solution with a fixed concentration of the interfering species. The activity of the primary analyte at the LOD, $a_i(DL)$, is calculated from the calibration curve obtained, and according to the activity of the interfering ion in the background solution, $a_j(BG)$, the coefficient can be determined as follows the Equation 2.13:

$$log K_{ij}^{pot} = \log \frac{a_i(DL)}{a_j(BG)^{n_i/n_j}} \qquad \text{(Equation 2.13)}$$

Where n_i and n_j are the charge of the primary ion and interference, respectively.

- *Stability*: The evaluation of the potentiometric signal along short and long time periods is an important parameter in order to characterize ion selective electrodes. The quality of the transducer is also reflected by the stability of the sensor. The stability is usually expressed as a drift in μV·h^{-1} or mV·h^{-1}. Interestingly, high stability is crucial for long real-time measurements and on-site applications, situations where a calibrated electrode is previously needed.

- *Response time*: is the time required for a sensor to change from its previous potential to a final stable potential, which is established according to the experimental conditions. Usually, the response time is measured as the time lapse between the electrodes reaches the new concentration until gets 90 % of the final value.

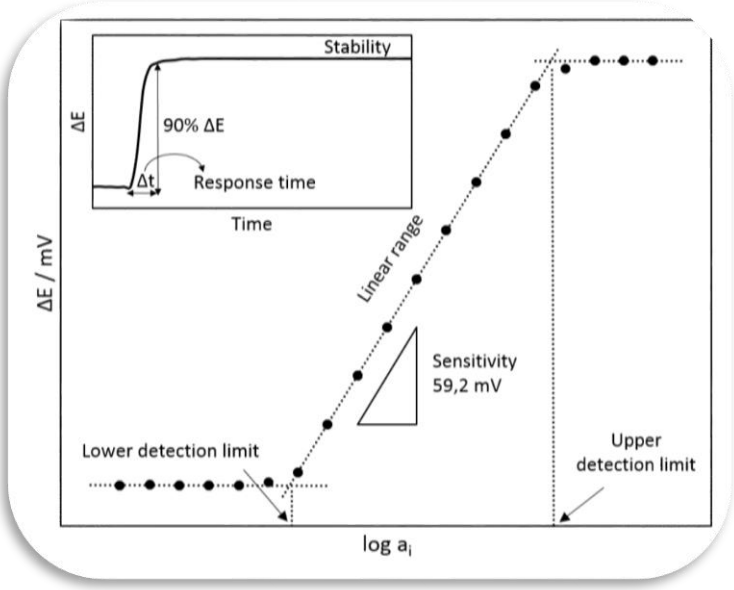

Figure 2.6. Graphical representation of some analytical parameters.[54]

2.8. References

[1] D. Grieshaber, R. MacKenzie, J. Vörös, E. Reimhult, Sensors, 2008, 8, 1400.

[2] J. Wang, Talanta 2002, 56, 223.

[3] B. Solnica, J. W. Naskalski, J. Sieradzki, Clin. Chim. Acta 2003, 331, 29.

[4] J. Wang, Chem. Rev. 2008, 108, 814.

[5] D. R. Thévenot, K. Toth, R. A. Durst, G. S. Wilson, Biosens. Bioelectron. 2001, 16, 121.

[6] J. Wang, Trends Anal. Chem. 2002, 21, 226.

[7] J. Hu, S. Wang, L. Wang, F. Li, B. Pingguan-Murphy, T. J. Lu, F. Xu, Biosens. Bioelectron. 2014, 54, 585.

[8] J. Wang, Biosens. Bioelectron. 2006, 21, 1887.

[9] M. Pozuelo, P. Blondeau, M. Novell, F. J. Andrade, F. Xavier Rius, J. Riu, Biosens. Bioelectron. 2013, 49, 462.

[10] A. Salehi-khojin, F. Khalili-araghi, M. A. Kuroda, Ḱ. K. Y. Lin, P. Leburton, R. I. Masel, ACS Nano 2011, 5, 153.

[11] F. Wang, T. M. Swager, J. Am. Chem. Soc. 2011, 133, 11181.

[12] J. W. Han, B. Kim, J. Li, M. Meyyappan, Appl. Phys. Lett. 2013, 102, 193104.

[13] M. D. Archer, in Electrochem. Past Present, 1989, pp. 115–126. ACS Symposium Series; American Chemical Society: Washington, DC.

[14] E. Khaled, H. N. a Hassan, G. G. Mohamed, F. a Ragab, A. E. a Seleim, Talanta 2010, 83, 357.

[15] M. Jańczyk, a. Kutyła-Olesiuk, X. Cetó, M. del Valle, P. Ciosek, W. Wróblewski, Sens. Act. B Chem. 2013, 189, 179.

[16] D. Yuan, A. H. C. Anthis, M. Ghahraman Afshar, N. Pankratova, M. Cuartero, G. A. Crespo, E.

Bakker, Anal. Chem. 2015, 87, 8640.

[17] E. Jaworska, K. Maksymiuk, A. Michalska, Chemosensors 2015, 3, 200.

[18] O. R. Shehab, A. M. Mansour, Biosens. Bioelectron. 2014, 57, 77.

[19] D. Tang, R. Yuan, Y. Chai, L. Zhang, X. Zhong, Y. Liu, J. Dai, Sens. Act. B Chem. 2005, 104, 199.

[20] W.-Y. Liao, C.-H. Weng, G.-B. Lee, T.-C. Chou, Lab Chip 2006, 6, 1362.

[21] A. Lynch, D. Diamond, M. Leader, Analyst 2000, 125, 2264.

[22] A. J. Bandodkar, D. Molinnus, O. Mirza, T. Guinovart, J. R. Windmiller, G. Valdés-Ramírez, F. J. Andrade, M. J. Schöning, J. Wang, Biosens. Bioelectron. 2014, 54, 603.

[23] M. Novell, T. Guinovart, I. M. Steinberg, M. Steinberg, F. X. Rius, F. J. Andrade, Analyst 2013, 138, 5250.

[24] M. D. Steinberg, P. Kassal, I. Kereković, I. M. Steinberg, Talanta 2015, 143, 178.

[25] M. D. Steinberg, P. Kassal, I. M. Steinberg, Electroanalysis 2016, 1.

[26] C. Zuliani, D. Diamond, Electrochim. Acta 2012, 84, 29.

[27] B. M. Tissue, Analytical Chemistry and Chemical Equilibria, 2013.

[28] P. C. Meier, Anal. Chim. Acta 1982, 136, 363.

[29] S. Yajima, K. Tohda, P. Bühlmann, Y. Umezawa, Anal. Chem. 1997, 69, 1919.

[30] E. Bakker, M. Nägele, U. Schaller, E. Pretsch, Electroanalysis 1995, 7, 817.

[31] J. Bobacka, A. Ivaska, A. Lewenstam, Chem. Rev. 2008, 108, 329.

[32] E. Bakker, E. Pretsch, P. Bühlmann, Anal. Chem. 2000, 72, 1127.

[33] E. Bakker, D. Diamond, A. Lewenstam, E. Pretsch, Anal. Chim. Acta 1999, 393, 11.

[34] G. T. Hefter, Anal. Chem. 1982, 54, 2518.

[35] H. W. Harper, J. Phys. Chem. 1985, 89, 1659.

[36] E. Bakker, P. Bühlmann, E. Pretsch, Talanta 2004, 63, 3.

[37] R. W. Cattral, H. Freiser, Anal. Chem. 1971, 43, 1905.

[38] J. Bobacka, Electroanalysis 2006, 18, 7.

[39] G. A. Crespo, S. Macho, J. Bobacka, F. X. Rius, Anal. Chem. 2009, 81, 676.

[40] T. Yin, W. Qin, TrAC Trends Anal. Chem. 2013, 51, 79.

[41] S. Anastasova-Ivanova, U. Mattinen, A. Radu, J. Bobacka, A. Lewenstam, J. Migdalski, M. Danielewski, D. Diamond, Sens. Act. B Chem. 2010, 146, 199.

[42] G. A. Crespo, D. Gugsa, S. Macho, F. X. Rius, Anal. Bioanal. Chem. 2009, 395, 2371.

[43] A. J. Bandodkar, V. W. S. Hung, W. Jia, G. Valdés-Ramírez, J. R. Windmiller, A. G. Martinez, J. Ramírez, G. Chan, K. Kerman, J. Wang, Analyst 2013, 138, 123.

[44] G. Lisak, T. Arnebrant, T. Ruzgas, J. Bobacka, Anal. Chim. Acta 2015, 877, 71.

[45] J. Bobacka, A. Ivaska, Electroanalysis 2003, 15, 366.

[46] U. Lange, N. V. Roznyatovskaya, V. M. Mirsky, Anal. Chim. Acta 2008, 614, 1.

[47] Z. Mousavi, J. Bobacka, A. Ivaska, Electroanalysis 2005, 17, 1609.

[48] G. A. Crespo, S. Macho, F. X. Rius, Anal. Chem. 2008, 80, 1316.

[49] H. Dai, Acc. Chem. Res. 2002, 35, 1035.

[50] G. Crespo, Solid Contact Ion Selective Electrodes Based on Carbon Nanotubes, 2010, Doctoral Thesis.

[51] M. Novell, M. Parrilla, G. A. Crespo, F. X. Rius, F. J. Andrade, Anal. Chem. 2012, 84, 4695.

[52] M. Novell, T. Guinovart, P. Blondeau, F. X. Rius, F. J. Andrade, Lab Chip 2014, 14, 1308.

[53] G. G. Guilbault, Pure Appl. Chem. 1981, 53, 1907.

[54] M. Novell, Paper-Based Potentiometric Platforms for Decentralized Chemical Analysis, 2015. Doctoral Thesis.

Chapter 3

Experimental Section

UNIVERSITAT ROVIRA I VIRGILI
NEW ELECTROCHEMICAL SENSORS FOR DECENTRALIZED ANALYSIS
Marc Parrilla Pons

This chapter provides the supporting information regarding reagents, methodologies and procedures for the manufacturing and characterization of materials and sensors broadly used throughout this thesis. Briefly, two main characterization areas were used: First, the microscopic characterization to understand what is performed on the electrode surface; second, the electrochemical characterization that provides information about the electrochemical behavior of the sensing system, providing valuable information of the mechanism as well as the analytical performance.

3.1. Materials

Carbon Nanotubes

Single-wall carbon nanotubes (SWCNTs) of 95 % purity (1−2 nm outer diameter, 5−30 μm length) were purchased from Chengdu Organic Chemicals Co. (Chengdu, Sichuan, China). Multi-wall carbon nanotubes (MWCNTs) of 95 % purity (30–50 nm outer diameter, ~15 μm length) were also purchased from Chengdu Organic Chemicals Co. (Chengdu, Sichuan, China). Carboxylic acid functionalized multi-walled carbon nanotubes (MWCNTs) purity >95%, diameter = 10-20 nm, length = 10-30 μm were purchased from US Research Nanomaterial, Inc. Both SWCNTs and MWCNTs were used without further purification.

Commercial Conductive Inks

Ag/AgCl ink (113-09) was obtained from Creative Materials, Inc., Ayer, USA. Also, Ag/AgCl ink (E2414) was obtained from Ecron Inc., Wareham, USA. These inks are medical grade, electrically conductive ink and coating suitable for application by screen printing and dipping.

Elastomers

Polyurethane (PU) (Tecoflex SG-80A) was obtained from Lubrizol, USA. Also, platinum-catalyzed silicone elastomer, Ecoflex 0030 was obtained from Smooth-On, Inc., USA.

Ion-selective Membrane Components

Ionophores

Valynomicin (potassium ionophore I), sodium ionophore X, tridodecylamine (hydrogen ionophore) were purchased from Sigma-Aldrich.

Ion-exchangers

Potassium tetrakis (4-chlorophenyl)borate (KTClPB) with >98% purity and sodium tetrakis[3,5-bis-(trifluoromethyl)phenyl]borate (NaTFPB) were purchased from Sigma-Aldrich.

Polymeric Matrix

As a polymer, polyvinyl chloride (PVC) of high molecular weight was used. As plasticizers, bis(2-ethylhexyl)sebacate (DOS) with >97% purity and 2-nitrophenyl-octyl ether (o-NPOE) with >99% purity. Everything were purchased from Sigma-Aldrich.

Reference Membrane Components

Polyvinyl butyral (PVB) B-98 was obtained from Quimidroga S.A., Spain.

Other reagents

Whatman® qualitative filter paper, Grade 5, sodium dodecylbenzenesulfonate (SDBS), poly(ethylene-co-acrylic acid) (PEAA) with 15 wt % of acrylic acid, glucose oxidase with 228.253 U/g (GOx), Nafion 117 solution (ca. 5% in a mixture of lower aliphatic alcohols and water), 30% (w/w) hydrogen peroxide (H_2O_2) standard solution, mineral oil, potassium ferricyanide (III) with > 99.99 % purity and potassium ferrocyanide (II) hydrate with > 99.99 % purity were acquired from Sigma-Aldrich. Analytical-grade chloride salts of ammonium, calcium, magnesium, potassium, and sodium were purchased from Sigma-Aldrich. Sodium hydrogen carbonate, potassium hydrogen phosphate, glucose and urea were also purchased from Sigma-Aldrich.

All solutions were prepared using deionized water (18.2 MΩ cm^{-1} specific resistivity) obtained from Milli-Q PLUS (Millipore Corporation, Bedford, MA, USA).

3.2. Characterization

3.2.1. Microscopic Characterization

Microscopy is essential for the characterization of materials used in the fabrication of sensors as well as the surface of the electrodes under study. The ability to observe the distribution of nanomaterials and microstructures helps to understand how they are organized on the electrodes, how the nanomaterials and membranes are deposited thus helping to understand the electrode mechanisms and performance.[1] In this thesis, scanning electron microscopy was mostly used.

Scanning Electron Microscopy

Scanning electron microscopy (SEM) produces a finely focused electron beam which is scanned over a specimen, and the emerging signals from the beam specimen interaction can be monitored in the form of images, graphs, digital recordings, etc.[2,3] In this thesis, a type of SEM, the environmental scanning electron microscope (ESEM), is used. ESEM allows for the option of collecting electron micrographs of specimens that are "wet," uncoated, or both by allowing for a gaseous environment in the specimen chamber. The ESEM is therefore a SEM which can operate at the low pressure of a usual SEM through to, at least, the pressure required to observe liquid distilled water. Hence, ESEM can deal with difficult samples - including both wet and insulating ones- by enabling a gas, sometimes water vapor, to be present in the sample chamber whilst retaining the rather high resolution of the standard SEM. All in all, the main advantages of the ESEM are to study hydrated samples (including those of biological origin) without significant specimen preparation and the study of non-conductive materials.

Environmental Scanning Electron Microscopy (ESEM, FEI Quanta 600, USA) was used for the surface characterization of the commercial carbon fibers and Nafion membranes deposited on electrodes by drop-casting method. The electrodes (paper or carbon fiber-based) were attached to the support inside the ESEM chamber by a carbon-based sticker. Parameters (potential, pressure and working distance) were characterized in each case to obtain the maximum resolution possible of the images. Low-conductive substrates (such as Nafion membranes) were previously gold sputtered to allow the electron transfer and thus obtain high magnification images.

3.2.2. Electrochemical Characterization

Electrochemical characterization is crucial to obtain insights on the electrode performance as well as understand the mechanism involved in a complex system. Different techniques were used in this thesis to characterize the developed sensors.

Electrochemical Impedance Spectroscopy

Electrochemical impedance spectroscopy (EIS) is a powerful method of analyzing the complex electrical resistance of a system and is sensitive to surface phenomena and changes of bulk properties. It is widely used for characterization of materials, for instance, in biosensing strategies, for characterization of charge transport across membranes and membrane/solution interfaces.[4–8] Moreover, EIS presents huge potential as an analytical

tool. Briefly, the analysis of the surface resistance when the analyte is bound selectively to an electrode's membrane is the main principle of detection. Hence, many researchers use EIS to detect biomolecules such as proteins, or even a whole bacteria.[9–11] However, the limiting factor still is the requirement of high level of mathematical skills for an effective interpretation of EIS data.[12]

The impedance (*Z)* of a system is generally determined by applying a voltage perturbation with a small amplitude and detecting the current response. From this definition, the impedance *Z* is the quotient of the voltage–time function $V_{(t)}$ and the resulting current–time function $I_{(t)}$:

$$Z = \frac{V_{(t)}}{I_{(t)}} = \frac{V_0 \sin(2\pi f\, t)}{I_0 \sin(2\pi f\, t+\theta)} = \frac{1}{Y} \qquad \text{(Equation 3.1)}$$

where V_0 and I_0 are the maximum voltage and current signals, *f* is the frequency, *t* the time, θ the phase shift between the voltage–time and current–time functions, and *Y* is the complex conductance or admittance. The impedance is a complex value, since the current can differ not only in terms of the amplitude but it can also show a phase shift θ compared to the voltage–time function.

The impedance is generally determined at different frequencies and provides an impedance spectrum that characterizes the surface, membrane as well as exchange and diffusion processes using an equivalent circuit. This circuit, which commonly consists of resistances and capacitances, represents the different physicochemical properties of the system under investigation.

The expression for *Z* is composed of a real and an imaginary part. If the real part is plotted on the X-axis and the imaginary part is plotted on the Y-axis of a chart, the result is a Nyquist Plot, where each point corresponds to the impedance at one frequency. Low frequency data are on the right side of the plot and higher frequencies are on the left. Under this view, the notion of resistance becomes a particular case of the measurement of impedance (when the imaginary component equals zero).

In electrochemical impedance spectroscopy, where the electrolyte solution is one component of the system to be investigated, four elements are usually used to describe the impedance behavior: ohmic resistance, capacitance, constant-phase element and Warburg impedance.

For the situation of an electrode in contact with an electrolyte, the so-called Randles circuit is used comprising the solution resistance (R_s), the charge transfer resistance (R_{ct}), the double layer capacitance (C_{dl}) and the Warburg impedance (W) (Figure 3.1). The double-layer capacitance C_{dl} results from charge being stored in the double layer at the interface. The charge transfer resistance R_{Ct} refers to current flow produced by redox reactions at the interface, and the Warburg impedance results from the impedance of the current due to diffusion from the bulk solution to the interface. R_s is the solution resistance afforded by the ion concentration and the cell geometry.

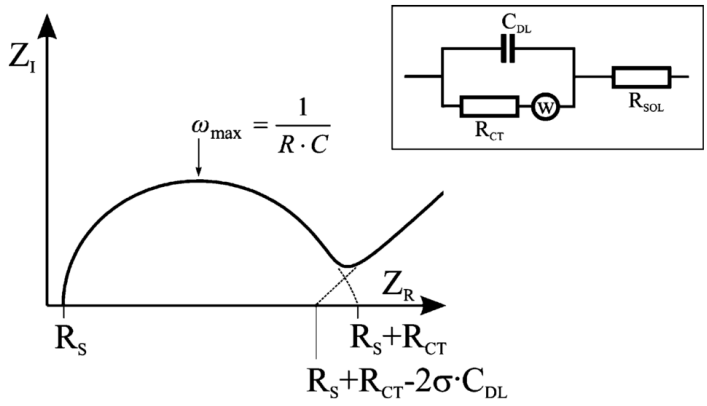

Figure 3.1. Randles equivalent circuit for an electrode in contact with an electrolyte.[6]

EIS measurements were performed using a potentiostat/galvanostat Autolab PGSTAT128N with a frequency response analyzer electrochemical impedance module (FRA2) (AUTOLAB, Eco Chemie, B.V., Utrecht, The Netherlands) fitted with a three electrode electrochemical cell and NOVA software (v.1.11, The Netherlands) as a measuring interface. The carbon fiber, paper-based or glassy carbon electrode was used as the working electrode, a glassy carbon rod with a diameter of 3 mm as the counter electrode, and a Ag/AgCl/KCl 3 M (type 6.0733.100, Metrohm AG) single junction electrode as the reference electrode. The impedance spectra were recorded within the frequency range 100 kHz to 10 mHz by using a sinusoidal excitation signal that was superimposed on a constant direct current potential, (Edc=0.2 V). The electrodes were studied using an excitation amplitude of 10 mV. The measurements were taken in a solution of 0.1 M KCl at room temperature (25ºC).

Cyclic Voltammetry

Cyclic voltammetry (CV) is a dynamic electrochemical method in which the potential applied to an electrochemical cell is scanned for monitoring redox events.[13,14] The

effectiveness of CV results from its ability for rapidly observing the redox behavior over a wide potential range. CV can be used to provide information about the electrochemical behavior of species diffusing to an electrode surface, interfacial phenomena at an electrode surface, and bulk properties of materials in or on electrodes.[15–17] Moreover, CV is perhaps the most versatile electroanalytical technique for the study of electroactive species. In this thesis is mainly used to provide information about the electrode surface and the electron-transfer process.

The potential scan is programmed to begin at an initial potential where no electrolysis occurs. The scan continues at the desired linear scan rate to the switching potential, then reverses direction and returns to the initial potential. The scan rate can be chosen over a wide range, typically from 0.001 to 200 or more V s^{-1}. The output of cyclic voltammetry is a plot of the current flowing in the electrochemical cell during the cyclic potential scan. Considering a solution containing electroactive species (*O)* in the cell with a metal working electrode, which also contains a large concentration (e.g. 0.01 to 1 M) of inert electrolyte to lower the cell resistance and minimize electrical migration. Assuming that *O* is reversibly and rapidly reduced. Then equation 1 occurs, where *n* is the number of electrons transferred from the electrode to *O.*

$$O + n\,e^{-} \rightarrow R \qquad \text{(Equation 3.2)}$$

This reaction is called diffusion controlled because the cell current is governed by the rate of diffusion of *O* to the electrode surface. In contrast, kinetic control may be active if the rate of the electrode reaction is slow with respect to the rate of potential scan.[18,19]

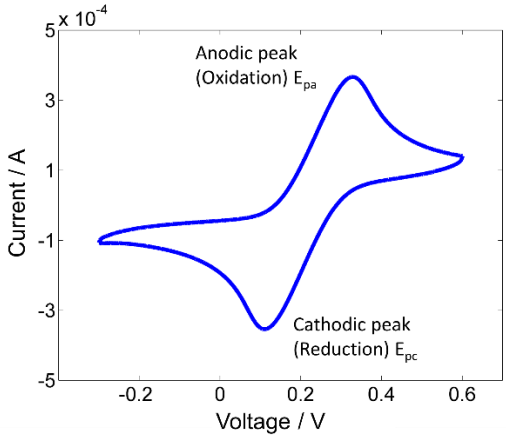

Figure 3.2. Typical CV spectra of a redox couple. E_{pa} and E_{pc} are the potential corresponding to the anodic and cathodic peaks respectively.

In cyclic voltammetry there is a function that relates the current peak intensity with other factors in the cell. Interestingly, the electroactive surface area can be calculated providing useful insights in order to characterize nanomaterials over a conductive surface.[20] This function is the Randles-Sevcik equation:

$$I_p = 2.69 \times 10^5 A D^{\frac{1}{2}} n^{\frac{3}{2}} \gamma^{\frac{1}{2}} C \qquad \text{(Equation 3.3)}$$

where *n* is the number of electrons participating in the redox reaction, *A* is the area of the electrode (cm^2), *D* is the diffusion coefficient of the molecule in solution ($cm^2\ s^{-1}$), *C* is the concentration of the probe molecule in the bulk solution ($mol\ cm^{-3}$), and *γ* is the scan rate of the potential perturbation ($V\ s^{-1}$).

For the experimental design, cyclic voltammograms were recorded using the same instrument and configuration than EIS spectra.

Adsorptive Stripping Voltammetry

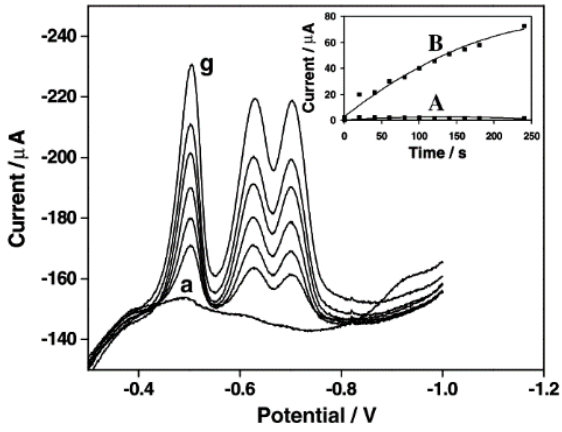

Figure 3.3. Typical reduction peaks obtained by adsorptive stripping voltammetry from increasing concentrations of organic molecules such as 2,4,6-trinitrotoluene (TNT).[22]

This technique is defined by applying a linear sweep potential in time after a preconcentration step between the working and reference electrode. Reduction of species is registered as a peak in the current signal. Preconcentration step is accomplished by adsorption of the electroactive species on the working electrode surface or by reactions with chemically modified electrodes. In this thesis, the ability of CNT to greatly enhance stripping voltammetry measurements in connection with strong interfacial accumulation allows a sensitive electrochemical detection of target organic compounds. For instance, the

adsorption properties of CNT, reflecting their huge surface area and graphene-sheet structure, were exploited for solid-phase extraction applications.[21] Furthermore, such ability of CNT to promote the adsorption of organic compounds is used for extending the scope of adsorptive stripping voltammetry (AdSV) towards important compounds that do not exhibit surface-active properties at conventional electrodes.

In this thesis, for electrochemical measurements, a three-electrode configuration was employed, consisting of two screen-printed MWCNTs-composite, serving as a working and counter electrodes, while a screen-printed Ag/AgCl served as a pseudo-reference electrode. The studies were executed using an AUTOLAB Type II (EcoChemie, B. V., Utrecht, The Netherlands) and NOVA software (v.1.11, The Netherlands) as a measuring interface.

Potentiometry

The fundamentals of potentiometry have been already discussed in Chapter 2.

Electromotive force (EMF) was measured with a high input impedance (10^{15} Ω) EMF16 multichannel data acquisition device (Lawson Laboratories, Inc. Malvern) and a Keithley high-input impedance (10^{15} Ω) voltmeter (Keithley Instruments, Inc., Ohio) at room temperature (22 °C) in a well stirred cell with distilled water solution without any ionic strength adjuster. A double junction Ag/AgCl/KCl 3 M reference electrode (type 6.0726.100, Metrohm AG) containing a 1 M LiAc electrode bridge was used. The substrate of the working electrode was a glassy carbon rod, carbon fiber or a paper electrode, depending on the application. The EMF values were corrected using the Henderson equation for the liquid-junction potential and the activity coefficients calculated by the Debye−Hückel approximation.

3.3. Procedures

Ion-selective Membrane

The ion-selective membrane used for potentiometric electrode were prepared as follows:

- Ionophore: between 15-30 mmol kg^{-1} (membrane) depending on the stoichiometric ratio between the ionophore and the primary analyte.
- Lipophilic anion or cation exchanger: 20-40% ratio of ionophore
- Polymeric matrix and plasticizer: 1:2 wt. ratio, respectively.

These membranes are usually prepared for a final weight ranging between 100-200 mg. Subsequently, the components are dissolved in tetrahydrofuran (THF) anhydrous 99.99%

and the mixture is vigorously shaken in a vortex and then placed in an ultrasonic bath for 20 minutes until a completely homogenous solution is obtained.

Reference Membrane

The reference membrane contains 39 wt % of sodium chloride, and 61 wt % of polyvinyl butyral (PVB). The membrane is prepared by dissolving the solid mixture in 1 ml of methanol. First, the mixture is vigorously shaken in a vortex and then placed in an ultrasonic bath for 20 minutes until a completely homogenous solution is obtained.

Platinum Sputtering

Sputtering of platinum was performed using an ATC Orion 8-HV (AJA International, Inc. MA, U.S.A.) at 200 W, 3 mTorr and magnetron DC sputtering onto a Whatman 5 filter paper. Platinum targets have a purity of 99.99 %.

Carbon Nanotubes Ink

The carbon nanotube ink (CNT-ink) was prepared by adding 3 mg ml^{-1} of SWCNTs to a 10 mg ml^{-1} sodium dodecylbenzenesulfonate (SDBS) aqueous solution.[23] The solution was sonicated using a bath sonicator (Fisherbrand Ultrasonic bath, FB11205, Fisher Scientific, Spain) for 30 minutes (100 % power, frequency of 37 kHz) and then in a tip sonicator (Ultrasonic processor UP200S, Hielscher Ultrasonics Gmbh, Teltow, Germany) for two hours (100 W, frequency of 24 kHz, 60 % of amplitude and a cycle of 0.5 s).

Stretchable CNT and Ag/AgCl Ink Preparation

Stretchable CNT ink was prepared by mixing CNTs with mineral oil (MO), proportion (1 mg CNT:0.7 mg MO). MWCNT were previously heated and ground to remove moisture. This composition (190 mg MWCNTs and 133 mg MO) was mixed in THF (2 ml) and placed for 1 h in the shaker. After that step, the ink was homogenized using ultrasonic bath for 30 minutes. The mixture was kept in the shaker overnight. Thereafter, 40% of polyurethane (PU) was added (previous mixture = 60%) and the resulting mixture was shaken overnight. A solid-to-solvent ratio (1 mg:9 µL) was maintained for printing purpose. The stretchable Ag/AgCl ink was prepared by thoroughly mixing 90% of Ag/AgCl ink (E2414, Ecron Inc., Wareham, MA) with 10% of Ecoflex (A+B). These stretchable inks were used in Chapter 5 and 9.

Conductive Carbon Nanotube Paper

A conventional qualitative filter paper -Whatman 5- (10 cm diameter, 0.01 cm thick paper disk, 10-20 µm fiber thickness) purchased from Sigma-Aldrich was used as initial substrate.

The conductive paper is made by painting it with the CNT-ink using a conventional paintbrush. Subsequently, the paper was dried, washed and dried again. This process is considered one cycle, and was repeated until the resistance of the dried paper reaches a stable value, usually around 200 Ω cm^{-2} -which usually takes 5 to 6 cycles-.

Membrane Deposition

In this thesis, mainly two different methods to apply the membrane over the surface of the electrode to develop a solid-contact potentiometric electrode, either working or reference electrodes have been performed:

Drop Casting

A desired aliquot of the membrane's cocktail is directly drop cast by pipetting onto the active area of the electrode. Depending on the fabrication of each type of electrode -substrate is directly involved- a specific amount of cocktail as well as the number of drops are optimized to achieve the suitable thickness and thus obtain the right analytical performance.

Dip Coating

The electrode is directly dipped into the membrane's cocktail and removed to dry. The process of dip coating is repeated several times until the suitable thickness and thus the right analytical performance is obtained.

Electrode Conditioning

In order to reach a suitable performance of the SC-ISEs, two basic steps were performed: First, the electrode after the deposition and drying of the membrane is placed in a relatively concentrated solution (10^{-2} M) of the primary ion for 24 h. Second, after the first step of conditioning, the electrodes have to be washed with MilliQ-water and placed in a diluted solution of the primary analyte (10^{-6} M) for 24 h.

3.4. References

[1] R. Liang, H. Peng, J. Qiu, J. Colloid Interface Sci. 2008, 320, 125.

[2] A. M. Donald, Nat. Mater. 2003, 2, 511.

[3] G. D. Danilatos, Foundations of Environmental Scanning Electron-Microscopy, Advances in Electronics and Electron Physics, 1988, Academic Press. Inc.

[4] V. Freger, S. Bason, J. Memb. Sci. 2007, 302, 1.

[5] E. Barsoukov, J. R. Macdonald, Impedance Spectroscopy, Wiley, 2005.

[6] F. Lisdat, D. Schäfer, Anal. Bioanal. Chem. 2008, 391, 1555.

[7] R. Tena-Zaera, J. Elias, C. Lévy-Clément, I. Mora-Seró, Y. Luo, J. Bisquert, Phys. Status Solidi 2008, 205, 2345.

[8] X. Sun, Y. Zhu, X. Wang, Sensors. 2011, 11, 11679.

[9] Y. Wang, J. Ping, Z. Ye, J. Wu, Y. Ying, Biosens. Bioelectron. 2013, 49, 492.

[10] A. Ahmed, J. V Rushworth, J. D. Wright, P. a Millner, Anal. Chem. 2013, 85, 12118.

[11] A. Periyakaruppan, R. P. Gandhiraman, M. Meyyappan, J. E. Koehne, Anal. Chem. 2013, 85, 8, 3858.

[12] D. D. MacDonald, Electrochim. Acta 2006, 51, 1376.

[13] R. G. Compton, C. E. Banks, Understanding Voltammetry, 2007, World Scientific.

[14] P. T. Kissinger, W. R. Heineman, J. Chem. Educ. 1983, 60, 702.

[15] I. Streeter, G. G. Wildgoose, L. Shao, R. G. Compton, Sens. Act. B Chem. 2008, 133, 462.

[16] J. Shan, P. G. Pickup, Electrochim. Acta 2000, 46, 119.

[17] Y. Fu, R. Yuan, D. Tang, Y. Chai, L. Xu, Colloids Surf. B. Biointerfaces 2005, 40, 61.

[18] G. a. Mabbott, J. Chem. Educ. 1983, 60, 697.

[19] J. F. Rusling, S. L. Suib, Adv. Mater. 1994, 6, 922.

[20] S. Hrapovic, Y. Liu, K. B. Male, J. H. T. Luong, Anal. Chem. 2004, 76, 1083.

[21] Y. Cai, G. Jiang, J. Liu, Q. Zhou, Anal. Chem. 2003, 75, 2517.

[22] J. Wang, S. B. Hocevar, B. Ogorevc, Electrochem. commun. 2004, 6, 176.

[23] L. Hu, H. Wu, Y. Cui, Appl. Phys. Lett. 2010, 96, 2008.

UNIVERSITAT ROVIRA I VIRGILI
NEW ELECTROCHEMICAL SENSORS FOR DECENTRALIZED ANALYSIS
Marc Parrilla Pons

Part 2

Wearable Chemical Sensors for Fitness Applications

UNIVERSITAT ROVIRA I VIRGILI
NEW ELECTROCHEMICAL SENSORS FOR DECENTRALIZED ANALYSIS
Marc Parrilla Pons

Chapter 4

Wearable Potentiometric Sensors based on Commercial Carbon Fibers

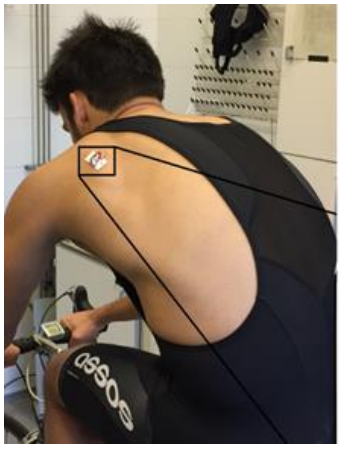

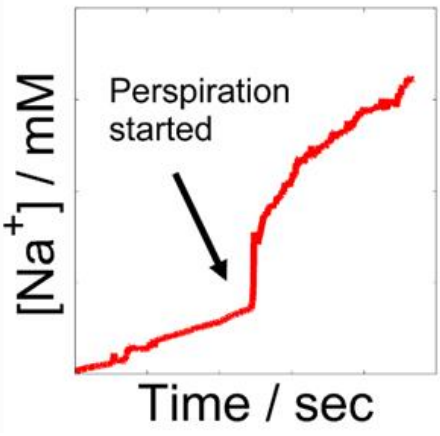

UNIVERSITAT ROVIRA I VIRGILI
NEW ELECTROCHEMICAL SENSORS FOR DECENTRALIZED ANALYSIS
Marc Parrilla Pons

Wearable Potentiometric Sensors based on Commercial Carbon Fibers

In this chapter the use of commercial carbon fibers (CCFs) to build wearable potentiometric sensors for the real-time monitoring of sodium levels in sweat during exercise is presented. CCFs are an attractive substrate for building wearable electrochemical sensors because of their good electrical conductivity, chemical inertness, flexibility and mechanical resilience. In the first part of this work, the analytical performance of these novel potentiometric ion-selective electrodes made with CCFs is presented. Then, through the incorporation of a solid-contact reference electrode, the development of a complete miniaturized potentiometric cell with a Nernstian response (59.2 ± 0.6 mV log[Na^+]$^{-1}$, N=4) is obtained. Finally, the cell is integrated into a wearable patch and attached onto the skin of an athlete. The analytical characterization of the wearable patch shows a near-Nernstian response (55.9 ± 0.8 mV log[Na^+]-1, N=3) for sodium levels from 10^{-3} M to 10^{-1} M in artificial sweat, well within the physiological range of interest. The device shows low noise levels and very good stability (-0.4 ± 0.3 mV·h^{-1}). To improve the usability of the sensor in real scenarios, a calibration-free approach is also explored. This platform opens new and attractive avenues for the generation of meaningful personalized physiological information that could be applied -among many other fields- in sports, nutrition and healthcare.

4.1. Introduction

The development of wearable sensors embedded into garments for monitoring exercise and improve sports performance is an increasingly growing trend.[1,2] Indeed, the seamless integration of sensors into clothes presents many attractive features for the end-user, such as the easy access to real-time personalized data, portability and simplicity of operation.[3,4] The information generated by these sensors may yield significant benefits, such as the improvement of the performance in athletes[5] and the minimization of the risks of injuries.[6] Hence, the generation of personalized physiological data can provide valuable insights to enhance the experience and early detect and prevent health issues.[7] For this reason, different approaches to integrate smart microsensors (i.e. heart rate, electromyography, accelerometers, gyroscopes and magnetometers) into sport garments have been intensively pursued. Today, a growing range of commercial products and applications are available.[8,9] Research activities for the development of watches, wristbands, adhesive patches and even epidermal tattoos are also being applied to monitor a broad range of movements and biometric parameters,[10] such as cardiac respiratory or skeletal muscle activity. “Wearability”, i.e., the ability to withstand mechanical stress and to embed these devices with minimal disruption for the user, is a key requirement. Thus, significant efforts in material science[11,12]

are currently being devoted to the development of stretchable and bendable electronics[13] that can serve as flexible substrates and adapt to different routines.[14] Remarkably, despite of all this progress, there is a relative lack of wearable sensors that can produce reliable (bio)chemical information. Indeed, while wearable sensors for physical parameters (temperature, heart rate, movement, etc.) have come a long way, the development of wearable sensors to produce relevant chemical and biochemical information has moved at a significantly lower pace.

The development of a wristband glucometer,[15] more than a decade ago, can be considered as one of the earliest wearable chemical sensors that reached the market. Although this device presented several practical issues and had to be recalled from the market, it stressed the advantages of electrochemical sensing in the field of wearable devices. Early contributions from Diamond *et al*. were also pioneers in this field, mostly by focusing on the improvement of the chemo-biosensing through body sensing networks (BSN).[16–18] Although they were truly visionaries, these early works faced two major challenges. First, that at the time many of those early platforms were proposed, most of the technology nowadays widely available (flexible substrates, miniaturized low-power consumption electronics, etc.) was not yet mature. Therefore, these prototypes were not fully portable and adaptable for monitoring properties in real scenarios. Second, the difficulty for building consistent chemical sensors, and the need of frequent recalibration was highlighted as “the chemical sensor paradox” and identified as a major barrier.[17,19]

Indeed, when dealing with wearable devices two major aspects need to be contemplated. One related to the electronic of detection, signal processing and transmission. The other regarding the sensor, signal generation and transduction, and sampling strategy. Fortunately, with the exponential progress in miniaturization, and the advances in material science that have led to bendable, stretchable and miniaturized electronics,[20] the wearability of the measuring instrument cannot be considered a major barrier anymore. Therefore, a major limitation on the development of wearable chemical sensors lies on the development of suitable sensing interfaces that can reproducibly sample and generate the signal in a simple and effective way. Our research group, for example, has recently introduced the use of commodity, flexible and disposable materials such as paper,[21] rubber[22] or cotton yarns,[23] modified with carbon nanotubes as substrates to build electrochemical platforms for wearable and decentralized sensors. Wang *et al.* developed screen-printed epidermal-based electrochemical sensors in the form of temporary tattoos.[24] These novel devices allow to

monitor a wide range of physiological biomarkers such as glucose, lactate, pH or ammonium from the human perspiration[25–28] using either voltammetric or potentiometric approaches. A potentiometric sensor in the form of an epidermal temporary-transfer tattoo for monitoring sodium in sweat was also reported.[29] More recently, Diamond *et al.* reported a miniaturized wearable cell for the monitoring of sodium in sweat.[30] All in all, because of the increasing social demand, and the explosive growth of wearable electronics,[31,32] wearable chemical sensors are becoming more required. For this reason, exploration of new platforms that show power of detection and simplicity of operation is essential.

Sodium is the primary cation located within the extracellular fluid space of the human body and accounts for 80 to 90% of plasma osmolality.[33] The loss of sodium through sweat has been linked to several homeostatic physiological imbalances such as hyponatremia, cognitive impairment or fatigue due to the potential development of muscle weakness or cramps.[34] Furthermore, sodium loss is reported to be highly variable due to individual factors such as age, gender, environment, diet or genetics.[35] Even though monitoring of sodium levels in sweat using potentiometric techniques has already been proposed,[36,37] there is still a wide space of opportunities to develop devices that can allow the seamless integration within sport garments.

Commercial carbon fibers (CCF) are an attractive substrate that holds the potential to build wearable devices. CCF are made using carbon fibers (*i.e.*, micron-sized carbon structures) extruded in the form of a thread using a polymeric matrix, typically an epoxide. CCF used in this work are produced by spinning carbon-based materials into the polymeric matrix to make “carbon fiber-reinforced plastics” in the form of threads. CCF are an ideal substrate for the development of wearable sensors since they show a good electrical conductivity (50 $\Omega \cdot cm^{-1}$), high stiffness and tensile strength, low weight, high temperature tolerance, both chemical and mechanical resistance[38] and -last but not least- their manufacturing cost is relatively low. CCFs have been used for building different types of electrochemical sensors.[39] For example, carbon nanofibers electrodes for the detection of cardiac troponin-I[40] and organic molecules such as dopamine[41] have been reported. Also, CCFs have been proposed for the amperometric determination of glucose.[42] However, to the best of our knowledge, these materials have not yet been tested as wearable potentiometric devices.

In this work, the advantages of using CCF as a substrate to build a fully integrated wearable potentiometric cell for the detection of sodium in sweat in real time are presented.

Details on the construction and the analytical performance of these wearable sensors are shown. Factors affecting sensitivity, selectivity, repeatability and stability are discussed. Also, an approach to minimize the hurdles of calibration of the sensors when working in real scenarios is explored.

4.2. Experimental Section

4.2.1. Materials

Commercial carbon fibers (CCFs) were acquired from a local supplier and used as a substrate for electrode fabrication. The material is purchased in the form of a cloth weaved with individual threads. Each thread is a bundle of single wires of approximately 6 µm of diameter each. A thread made with a CCFs bundle of approximately 1 mm diameter was used to build the electrodes (Figure 4.1A).

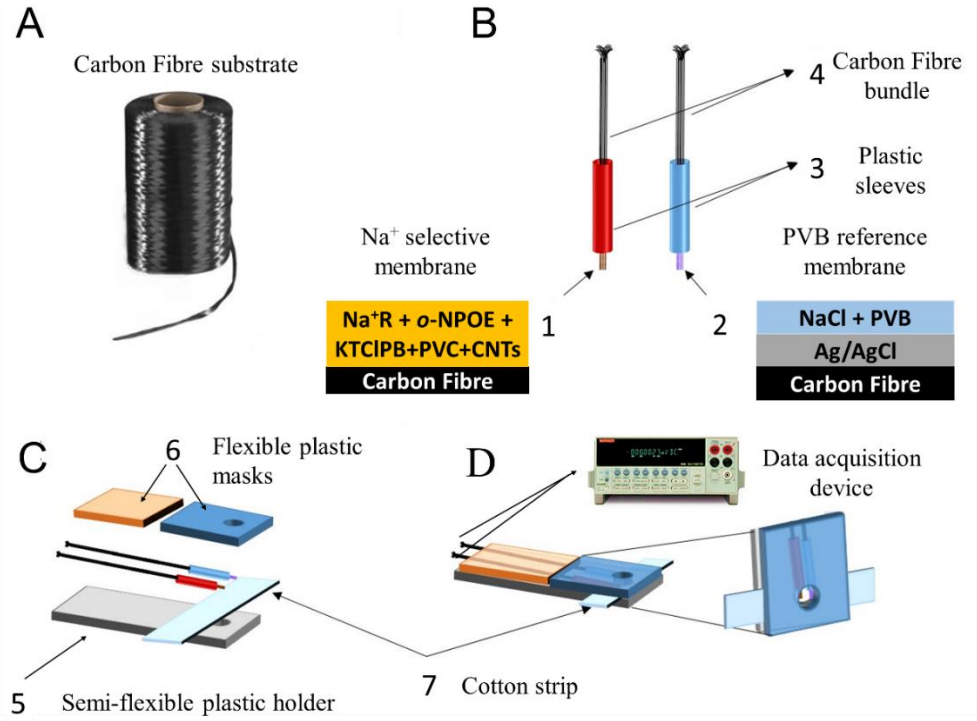

Figure 4.1. Schematic representation of the fabrication of a carbon fiber-based sodium sensor: (A) Commercial carbon fiber substrate (CCF), (B) (1) Working electrode with a sodium selective membrane, (2) PVB-based reference membrane, (3) plastics sleeves and (4) carbon fibers. (C) Electrodes integrated into a semi-flexible plastic holder and (D) Final CCF potentiometric cell incorporating a cotton cloth (5) for sampling.

A sodium selective membrane cocktail containing 0.7 wt.% sodium ionophore X, 0.2 wt.% KTClPB, 33 wt.% PVC and 66.1 wt.% NPOE in 1 ml of THF with 0.21 wt.% of MWCNT and 5.0 wt.% of PEAA was prepared.[43] A reference membrane cocktail was prepared by dissolving 78 mg of PVB and 50 mg NaCl in 1 ml of methanol, as it has been described elsewhere.[26] Artificial sweat matrix containing 6 mM KCl, 0.08 mM $MgCl_2$, 0.18 mM pyruvic acid, 0.17 mM glucose, 5 mM NH_4Cl and 10 mM Urea was also prepared.[44] Polyurethane semi-permeable film (Hydrofilm®, Hartmann, Barcelona, Spain) and silicone (RS Components®, 692-542, UK) were purchased in local stores.

4.2.2. Fabrication of Carbon Fibers Electrodes

A bundle of CCFs with a length of 3 cm and a diameter of approximately 1 mm was used for the development of both, the ion-selective and reference electrodes. The bundle was introduced through an electrically insulating plastic sleeve leaving exposed two opposite ends of the fiber of approximately 8 mm long each (Figure 4.1B). One of the ends acts as the sensing tip where the suitable polymeric membrane will be applied and the other is used for the electrical connection with the reading instrument. Thereafter, the sensing ends of the CCFs were dipped for 10 seconds in dichloromethane, then removed and let dry for 10 minutes. This cleaning step was aimed to remove all the impurities that could be deposited during the CCF manufacturing and manipulation process (Figure 4.2). Following this cleaning procedure, the edge of the bundle and plastic sleeve were sealed together with glue. After this preparation step, the CCFs were ready to build the potentiometric electrodes.

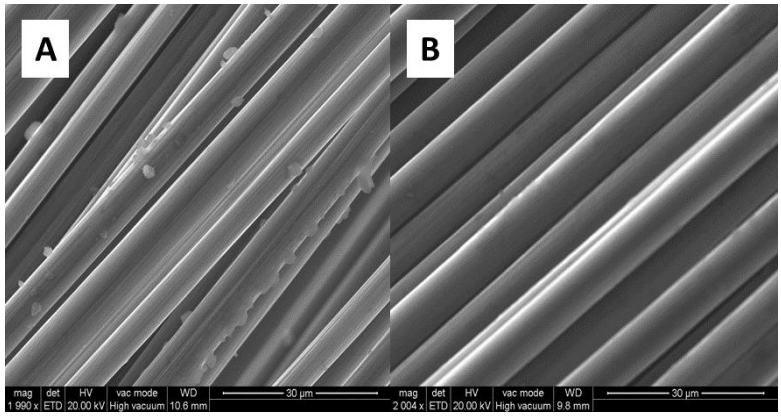

Figure 4.2. ESEM study of the CCF impurities: (A) CCF picture, (B) CCF cleaned with 2-chloromethane (10 seconds dip) picture.

For the ISE, the pre-cleaned exposed sensing end of the bundle was dipped into the ion-selective membrane cocktail. Experimentally, it was found that five dips were necessary to

obtain optimal results for K^+ISEs (Figure 4.3), with a drying time of 10 minutes between each dipping. It is important to remark that the dipping time has influence on the final results. Experimentally, it was found that a relatively fast dip (less than 2 seconds) into the cocktail solution was important to obtain optimum sensor performance, as it will be discussed later. Once the dipping is finished, these CCF electrodes were dried overnight. Later, Na^+ISEs were fabricated by dipping in the Na^+SM.

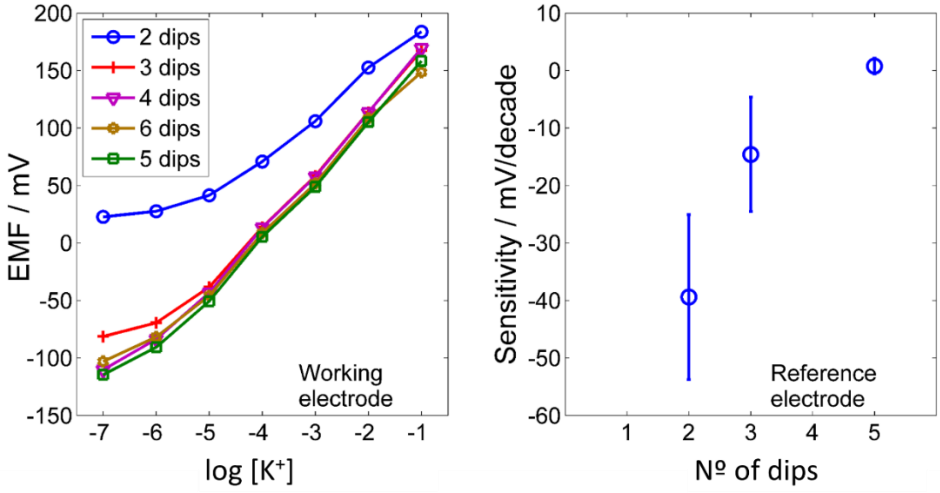

Figure 4.3. (A) Potentiometric potassium calibration curve for different number of dip coatings of the CCF working electrode. (B) Sensitivities obtained from 10^{-4} to 10^{-1} M for NaCl during reference electrode dip coating optimization procedure. The plot shows standard deviations of three different electrodes.

For building the reference electrodes, the sensing end of a CCFs bundle was first dipped into a Ag/AgCl ink and then cured at 90 ºC for 20 minutes. Once the ink was cured, the PVB-based reference membrane was applied by dip coating the electrodes. Optimization of the number of dip coating cycles was performed. Five dips and 10 minutes of drying time between each dip were necessary to obtain an optimum performance. The reference membrane provided a stable potential and remained almost insensitive to changes over a broad range of ion concentration, as it has been already reported.[26,45]

Overnight conditioning in 3M KCl (for the reference electrode) and 0.1M NaCl (for the working electrode) was carried out. Analytical performance of each CCF electrode was evaluated and optimized in a conventional two-electrode potentiometric cell arrangement. CCF electrodes were immersed into the solution and the potential was monitored as a

function of the changes of Na^+ concentration in either standard solutions or artificial sweat. Selectivity coefficients were calculated using the fix interference method (FIM).[46]

4.2.3. Integration of Carbon Fiber Electrodes into a Wearable Platform

Each CCF electrode was fitted with a planar connector and integrated into a suitable patch designed to improve the wearability of the sensing platform. To build the sensing patch, two planar (30x20x2 mm) semi-flexible plastic masks fitted with a 3 mm diameter orifice were used. Additionally, a 3 mm wide cotton cloth was placed as shown in Figure 4.1C. The main idea behind this arrangement is that the plastic masks sandwich the electrodes and keep them in a fix position, while the sensing and reference tips, located in the orifices of the mask, will be in contact with the solution. The function of the cotton cloth is two folded. From one side, to provide electrical contact between the electrodes once is wet. From the other, it aims to pump the sweat from the skin to the sensors by means of the capillary action of the cellulose fibers. The assembly of the cell was carried out in three steps (Figure 4.1C-D). First, the plastic masks were placed close to each other and the cotton strip was placed across them covering the orifices. Then, the electrodes were placed on top of one of the masks, with the sensing ends aligned on top of the orifice. Thereafter, the second plastic mask was flipped on top, sandwiching the whole system, and glued to the first mask with both orifices aligned. With this configuration, the cotton bedding surrounds and isolates the electrodes from any direct contact with the skin. Furthermore, by keeping the space between the electrodes wet, it helps to stabilize the signal by providing a continuous electrical connection between the electrodes. Last, but not least, a part of the cotton strip that sticks out of masks acts as a sample collector, helping to pump sweat by capillarity towards the electrodes.

To evaluate the analytical performance while the device was fixed on the skin, the cotton strips were first cleaned with deionized water several times to remove any traces of ions and avoid contaminations. To keep the sensors on a fix position of the body, an adhesive water-resistant film (Hydrofilm®, Hartmann) was used.

4.3. Results and Discussion

4.3.1. Characterization of the CCF Electrodes

The deposition of the membrane by dip coating was optimized by making electrodes with an increasing number of dips and evaluating the corresponding analytical performance. The results of this optimization can be seen in Figure 4.3. Experimentally it was found that 5 dips

are enough to reach an optimum performance for the working (Nernstian response) and reference electrodes (almost no response).

Thereafter, the analytical figures of merit of the CCF electrodes were evaluated. To do this, calibration plots for four CCF working electrodes were used. The results of these calibrations can be seen in Figure 4.4A, where the potentiometric time trace for each electrode is shown. The electrodes showed a Nernstian response, with slopes of 57.5 mV decade^{-1} (%RSD: 0.8, N=4) from 10^{-5} M to 10^{-1} M. This can be associated to the use of carbon nanotubes as ion-to-electron transducers.[47]

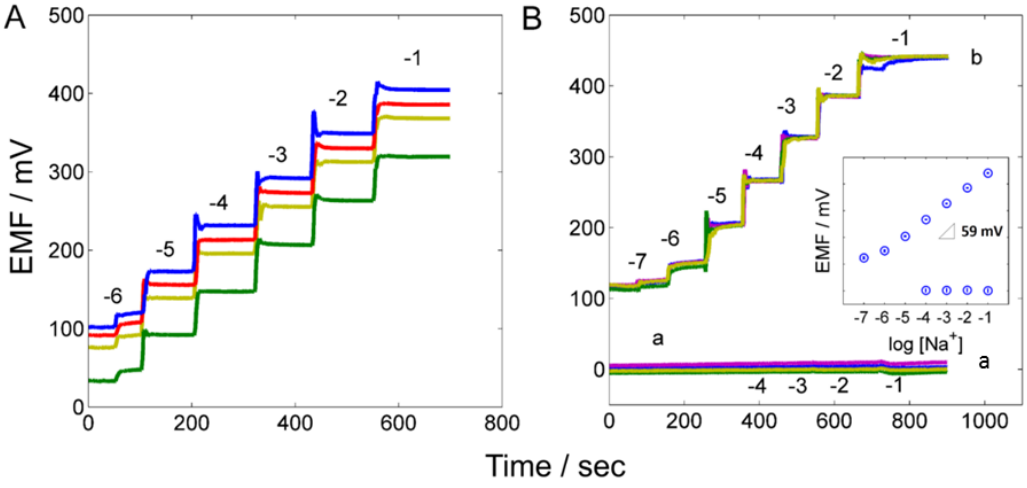

Figure 4.4. Calibration of CCF potentiometric electrodes: (A) Electrical potential time-trace for 4 different Na^+-CCF working electrodes. (B) Same calibration after the short-circuit approach. Calibrations were performed against a commercial reference electrode to show the enhanced reproducibility of (a) reference and (b) working electrodes. The inset shows the potentiometric response *vs.* the logarithmic concentration of Na^+ for both electrodes. The numbers on the time trace correspond to the logarithmic concentration of Na^+.

The constant and reproducible sensitivity is a unique feature that makes potentiometry very attractive in the field of wearable devices, where the calibration of the sensors represents a significant challenge. Indeed, while calibration procedures are routine in the lab, the adoption of wearable devices will critically depend on the simplicity of its operation in real scenarios. Clearly, minimization or -ideally- elimination of the calibration steps will certainly help to minimize the hurdles for the end user. Unfortunately, while the sensitivity remains constant for a given sensor (and among sensors), the variations in the intercept of the calibration plots makes necessary to use at least one point for calibration. Indeed, the intercepts of the calibration plots obtained had significant dispersion. For the CCFs shown here, an average value of 427.9 mV (%RSD: 8.8, N=4) has been found. This fluctuation in

the intercept among sensors is too high for most of the applications and forces to perform a calibration step for each sensor.

During the last few years significant efforts have been devoted to the development of methodologies to minimize this variation in order to produce calibration-free potentiometric sensors.[48,49] Among the many approaches, a method that is attractive because of its simplicity is based on short-circuiting both, the working and reference electrodes, before their use.[48] Thus, this approach was explored as a way to improve the reproducibility of the response and minimize the need for calibration. To do this, working CCF electrodes were short-circuited through their connecting ends to a reference electrode and immersed into the suitable conditioning solution overnight. Just before measuring, this connection between the two electrodes was removed and they were connected to the corresponding terminals of the reading instrument.

Using this approach, a significant enhancement was observed, as shown in Figure 4.4B. From one side, Nernstian response and high reproducibility of slopes between different electrodes is similar to the previous experiments, with slopes yielding an average value of 59.2 mV decade^{-1} (%RSD: 0.99, N=4). But the most remarkable improvement obtained is the reduction of the variability of the intercepts, which now presents an average value of 502.8 mV (%RSD: 0.29, N=4). Indeed, the original variance of the intercepts was in the order of 35 mV, and through this approach could be reduced down to 1.5 mV, a reduction of more than 20 times. Although this value is still not ideal -and it could in principle be reduced even more with other approaches- it presents an encouraging path towards the development of calibration-free wearable potentiometric sensors. For these electrodes a limit of detection (LOD) of $4.02 \cdot 10^{-7}$ M and linear range from 10^{-6} M to 10^{-1} M of Na^+ were obtained, which is in line with values already reported.

In order to build a truly calibration-free wearable system, the high reproducibility of the analytical parameters of the working electrodes needs also to be matched with a highly stable and reproducible reference electrode. In the case of the CCF reference electrodes, almost no variations of the potential with the total concentration of ions was obtained (the sensitivity was calculated as -0.19 mV decade^{-1} in a range from 10^{-4} M to 10^{-1} M of NaCl. Unfortunately, while the approach for the reduction of the variability for the working electrodes does not seem to have the same results for the reference systems. Thus, after integration of the complete cell, some variations on the electrical potential between wearable patches were observed. These changes are likely due to changes on the conditioning step of the reference

system, although it was not possible yet to fully address the problem. Additional work is now being conducted in this area to find suitable solutions.

The selectivity coefficients (Table 4.1) obtained with the Na^+-CCF was comparable to conventional membranes deposited by drop-casting on glassy carbon (GC) using separate solution method (SSM) [50]. Slight differences in the values obtained can be due to variations in the experimental methodology.[46]

Table 4.1. Selectivity values calculated with the FIM method for the sodium selective electrode (log K_{ij}^{pot} ± standard deviation (N = 6)) compared to the values reported in the literature using the SSM method.

Analyte	Log K_{Naj}[a]	Log K_{Naj} [50]
K^+	-2.25 ± 0.01	-2.3
Mg^{2+}	-2.64 ± 0.02	-2.3
Li^+	-2.25 ± 0.02	-2.5
Ca^{2+}	-2.71 ± 0.08	-2.6

[a] Results obtained in this work.

In order to further characterize the CCF electrodes, electrochemical impedance spectroscopy (EIS) was used. The impedance spectrum (complex plane impedance plots) of the CCF Na^+-ISE electrodes were recorded and the results can be seen in Figure 4.5. The shape of this plot shows the typical response obtained for the membrane-based potentiometric sensors,[47] with a well-defined high-frequency semicircle, which can be associated to the bulk resistance of the ion-selective membrane. Interestingly, the values obtained for this resistance are in the order of 80 kΩ, which is relatively low when compared with the conventional ISEs. To illustrate this point, a conventional ISE using a 3-mm diameter GC electrode as previously described[47] was built using the same membrane cocktail. Following a standard approach, 50 µL of the membrane cocktail were drop cast on the surface of the electrode and let dry. The impedance spectra, shown in the inset of Figure 4.5, yielded a value of approximately 2 MΩ, which is typical for conventional ISEs. It should be stressed that the sensing area of both systems (a 1 mm thick, 8 mm long bundle and a 3 mm diameter flat GC electrode) are very similar. Therefore, the difference in the impedance might be linked to the difference in thickness of the membranes generated by the two different approaches. Unfortunately, it was found experimentally that reductions in the volume of the membrane drop cast on the GC yield electrodes with a poor (sub-Nernstian) response.

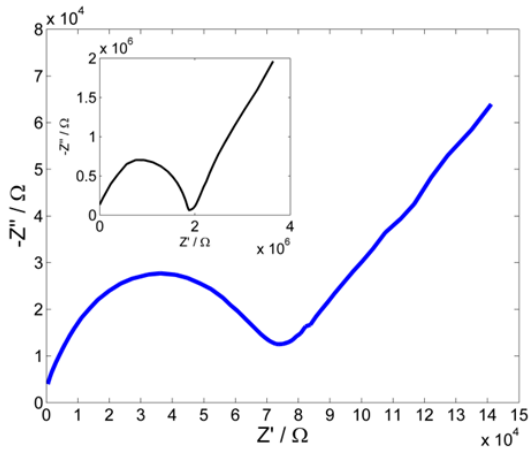

Figure 4.5. EIS spectra. The main plot shows results for a sodium selective membrane on a carbon fiber electrode. The inset shows the results for the same membrane drop cast on a glassy carbon substrate.

Evidently, considering the different approaches used to deposit the membrane, differences in thickness are not surprising. One additional aspect that cannot be ignored is the influence of the membrane-substrate interface to the overall resistance measured. Indeed, the CCF provides an organic polymeric matrix (the epoxide resin) that (because of the carbon fibers) shows good electrical conductivity. In the case of the conventional ISEs, the membrane-substrate interface is formed between the organic polymer and glassy carbon or other metallic conductors. Interestingly, as it was mentioned above, the time the CCF is dipped into the membrane cocktail has some influence on the performance of the sensor. Short dipping times (less than 2 seconds) yielded optimum results, but longer dipping times tend to yield electrodes with significantly higher resistance. A more careful study understanding the nature of this interface is required, but it is beyond the scope of this research. For the purpose of this work, it is important to stress that the use of CCF as a substrate allows the generation of miniaturized highly stable electrodes with a relatively low input impedance.

EIS measurements were also performed on CCF reference electrodes (data not shown). In this case, the resistance obtained was in the order of 10 KΩ. Interestingly, this value is also below the values previously reported for solid-contact reference electrodes on glassy carbon.[45]

4.3.2. Performance of the Integrated Cell in Artificial Sweat

After testing the performance of the individual electrodes, an integrated potentiometric cell was built by assembling a system as described in the experimental section and shown in

Figure 4.1D. In order to evaluate the analytical performance, three cells were placed in a beaker with stirred artificial sweat solution and calibration plots for sodium were performed. The results, shown in Figure 4.6, reveal a Nernstian response of 57.0 mV decade^{-1} (%RSD: 4.59, N=3) from 1 mM to 100 mM. Evidently, the high ionic concentration of the matrix affects the analytical parameters, reducing significantly the working ranges. Nevertheless, even though the linear dynamic range for sodium is reduced, the values obtained are well within the physiological range of interest for sodium in human sweat.[51]

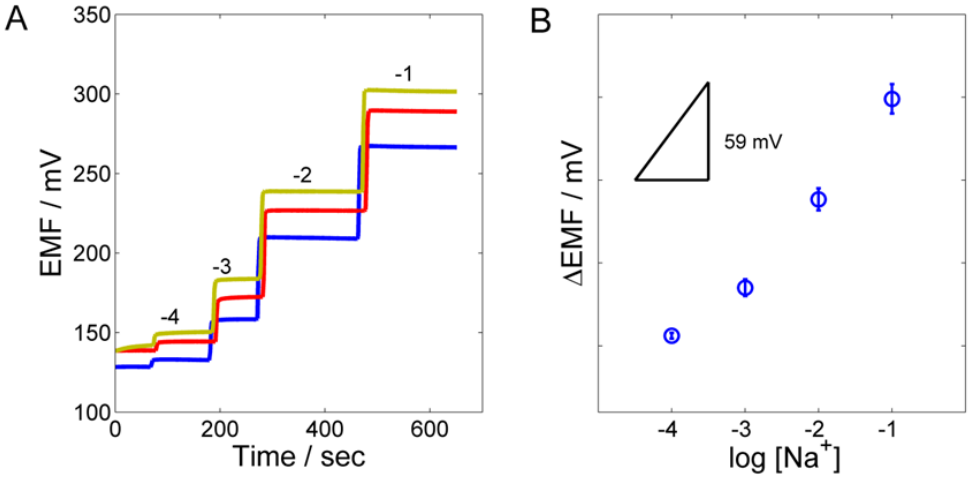

Figure 4.6. (A) Potentiometric time-trace and (B) calibration plot for three different Na^+-CCF sensors in artificial sweat.

A stability test in artificial sweat was also performed and the results are shown in Table 2, where the stability for different time windows is presented. Details on the potentiometric time-trace of three different sensors for mid-term stability test can be seen in Figure 4.7.

Table 4.2. Stability test results for three different CCF potentiometric sensors at different time frames.

Test	Time (h)	Drift (mV·h^{-1})
Short term	2	-1.3 ± 0.2
Mid term	4.5	-0.4 ± 0.3
Long term	13.5	-0.9 ± 0.1

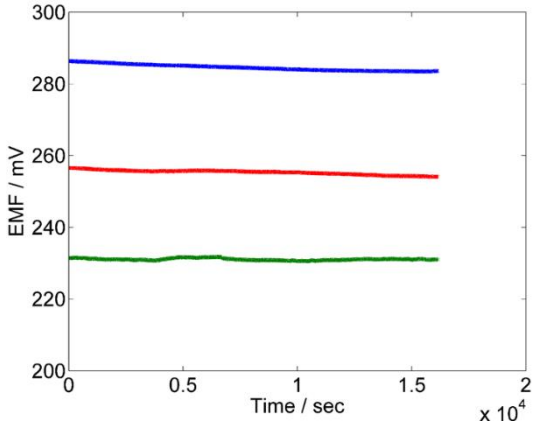

Figure 4.7. Potentiometric time-trace for the stability test during mid-term period of three different sodium sensors in artificial sweat at 25ºC.

Additional experiments were conducted in order to evaluate the repeatability of the measurements using the wearable platform. To do this, the response of the sensor to different Na^+ concentration in the range from 1 mM to 100 mM was performed. First, in line with the previous experiments, the integrated CCF potentiometric cell was tested in a beaker with stirred artificial sweat solution (Figure 4.8A). Increasing concentrations of Na^+ were added, then the system was rinsed with the artificial sweat matrix and the process was repeated 3 times. The results are shown in Table 3, where the average sensitivity of three measurements in a 4 ml beaker is presented (Experiment 1). Subsequently, the CCF cell was removed from the beaker, rinsed, and the solution was fed through the cotton strip, in an approach closer to the wearable applications, where the capillary action of the cotton strip acts as pumping system and electrical connection between the electrodes. The sodium standards in artificial sweat matrix were supplied through this cotton strip, emulating perspiration activity. Once again, three different standards of increasing concentration were added, then the cell was rinsed, and the process was repeated 3 times. The plots for these experiments are shown in Figure 4.8B. Table 3 shows the values of sensitivity obtained (Experiment 2).

Table 4.3. Sensitivity values obtained for three measurements on Na^+-CCF potentiometric sensors.

	Experiment 1		Experiment 2	
CCF	**Slope (mV decade^{-1})**	**%RSD**	**Slope (mV decade^{-1})**	**%RSD**
1	59.8	1.1	56.8	5.5
2	60.4	1.5	58.6	4.9
3	56.1	2.2	56.5	2.3

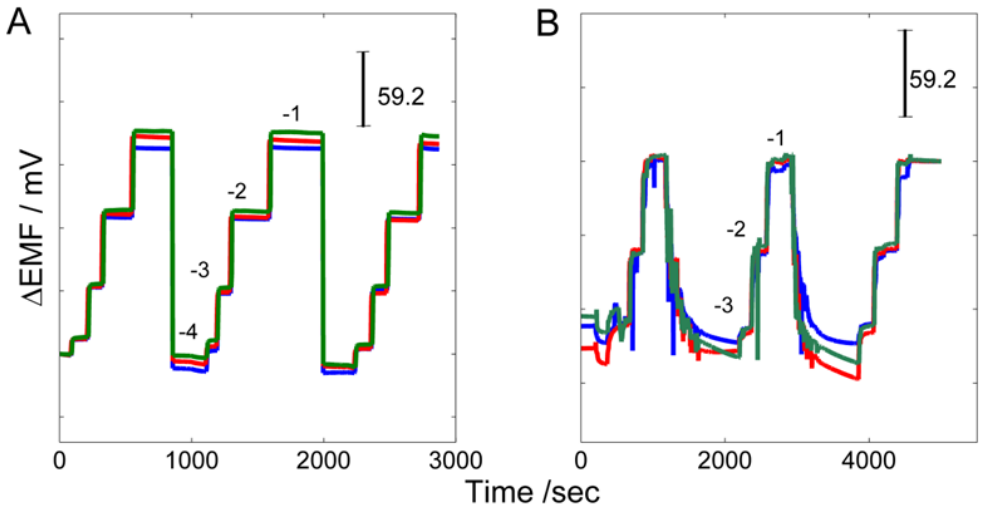

Figure 4.8. Repeatability test from 10^{-3} to 10^{-1} M range in artificial sweat with CCF potentiometric sensor. (A) Test with an integrated potentiometric cell (Experiment 1) and (B) test with the wearable platform (Experiment 2).

Evidently, when moving from the beaker to the more wearable approach (i.e., "cotton-sampling" cell), a higher level of noise and longer washing times of the system are observed. This is not surprising, as they are part of the challenge of developing truly wearable sensors. Regarding the noise, spikes (due to movements on the electrical connections) can be observed. Clearly, this noise can be minimized by further improving the prototype. Additionally, since the fluctuations expected in sweat occur in a different time scale, if some of this noise remains it could be easily filtered out. The main result from these experiments is the confirmation that the performance of the sensors is preserved and it is good enough for monitoring Na^+ in sweat in physiological ranges and that it remains constant through time when using the integrated cell with the cotton strip. Therefore, it encourages the test of the sensor in real settings.

4.3.3. On-body Measurements

As a further proof of concept, this wearable CCF-based platform was tested on the anatomical upper back region of several active male subjects. Before the sensor placement, the upper back regions were washed with deionized water and dried with clean sterile towels in order to avoid any contamination. In addition, a breathable and water resistant adhesive film was used to firmly fix the cell on the participant's skin surface with the aim to avoid any problem with electrical contacts. Once the cell was put in place, the cotton strip was wetted

with deionized water in order to overcome the lack of electrical contact between the electrodes. This eliminates the erratic fluctuations in the reading potential that otherwise will be obtained at the beginning and yields a stable baseline potential.

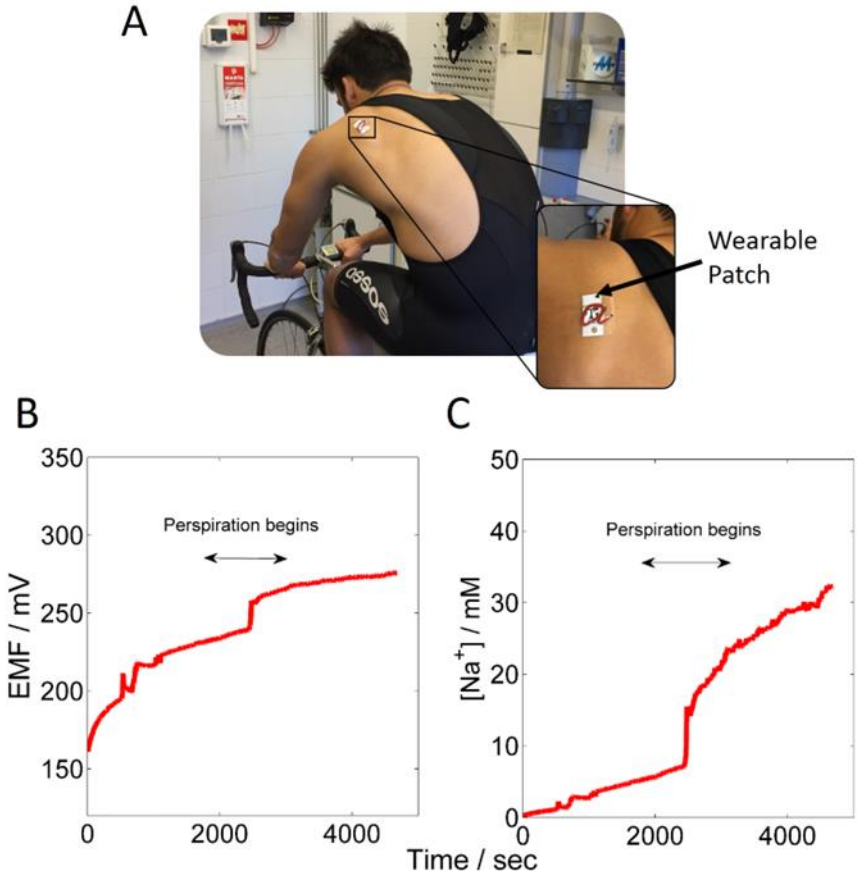

Figure 4.9. On-body sodium measurements. (A) Picture of the wearable patch worn in the athlete back. (B) Potentiometric time-trace of a wearable sensor and (C) real-time sodium concentration monitoring in human sweat. Real-time data obtained from a human participant during 80 minutes' steady-state cycling exercise.

Experimental measurements while individuals were making exercise were conducted following a stationary cycling protocol. A moderate steady state cycling exercise of 80 minutes (≈75 % of maximum heart rate, ≈90 rpm) in a moderate warm environment (25ºC, 50 % relative humidity) was selected to ensure sufficient volume generation of sweat.

Figure 4.9A illustrates the use of one sensor (cables have been removed for the sake of clarity) on the upper back region. Figure 4.9B displays the potentiometric time-trace curve obtained. Using the calibration plots, the real-time sodium concentration can be estimated, as shown in Figure 4.9C. The plots show first a smooth trend first, and then a sharp increase

in the concentration of Na^+. This pattern is likely due to the hydrodynamic characteristics of the cell, which determine how the sweat initially reaches and fills the space between the electrodes. The pattern then shows an increase of the sodium concentration in response to the progressive sweat loss of the participant.

As it was mentioned in the introduction, the elimination of sodium through perspiration during exercise depends on a wide range of factors. Therefore, an interpretation of the pattern found in Figure 4.9C falls beyond the scope of this study, which is focused on the development of a robust, suitable tool to monitor sweat composition. It is worth noticing, however, that the plot of Figure 4.9C shows a similar pattern to that reported by Diamond *et al*. for a similar type of experiment. These authors attributed the sharp increase of potential to the arrival of the sweat started into the cell.[30] It is also relevant to mention that the concentration found with the wearable CCF-sensor falls within the expected values of sodium for an athlete during a medium-intense exercise.[52] To further prove this point and validate the results, a sample of sweat was taken at the end of the exercise and analyzed under a conventional approach, i.e., using a beaker as a potentiometric cell. The results obtained were similar to those found with the wearable device.

All these results support the robustness of this wearable approach to monitor ions in sweat. The CCF-sensor displayed an excellent performance and remarkable stability for long term periods during exercise.

4.4. Conclusions

In this chapter, a new substrate to build a full wearable potentiometric cell has been presented. The use of CCFs for building ion-selective electrodes presents an attractive approach, since it provides a simple, flexible and rugged material that allows building sensors with good analytical performance, comparable to other conventional ion-selective electrodes. Also important is the development of a miniaturized solid-state reference electrode, which shows a performance similar to that already reported. Through the integration into a suitable cell, the real-time monitoring of sodium in sweat has been presented. It is evident that, from an analytical standpoint, the field of wearable devices has still many gaps to fill. Regarding the use of the sensors, development of strategies to simplify (either minimize or even eliminate) the calibration will be essential. In this work, preliminary steps in this direction using the “short-circuit” calibration-free approach have been followed. Although a calibration-free approach could not yet be fully developed, the results obtained are promising and encourage

further efforts in this direction. From a different perspective, sampling strategies that minimize the washing time of the cell in order to obtain faster response time will be ideal. The device presented in this work is simply a prototype, but it does not represent a limit to the possibilities of miniaturization of these CCFs sensors. As a future prospect, wireless amplifier and cloud data integration will be required to develop an entirely miniaturized, low-cost and autonomous system. The present device holds the potential to be seamless integrated into garments and textiles and provide novel individualized physiological insights across different fields such as sports, healthcare and nutrition.

4.5. References

[1] J. R. Windmiller, J. Wang, Electroanalysis 2013, 25, 29.
[2] A. J. Bandodkar, J. Wang, Trends Biotechnol., 2014, 32 (7), 363
[3] M. S. Patel, D. a Asch, K. G. Volpp, JAMA 2015, 313, 459
[4] S. Gorgutsa, V. Bélanger-Garnier, B. Ung, J. Viens, B. Gosselin, S. LaRochelle, Y. Messaddeq, Sensors 2014, 14, 19260
[5] R. J. Maughan, S. M. Shirreffs, J. Sports Sci. 1997, 15, 297
[6] E. F. Coyle, J. Sports Sci. 2004, 22, 39
[7] R. J. Maughan, S. M. Shirreffs, Int. J. Sport Nutr. Exerc. Metab. 2008, 18, 457
[8] B. a. MacRae, J. D. Cotter, R. M. Laing, Sport. Med. 2011, 41, 815
[9] M. Stoppa, A. Chiolerio, Sensors 2014, 14, 11957
[10] R. Chambers, T. J. Gabbett, M. H. Cole, A. Beard, Sport. Med. 2015, 45, 7, 1065
[11] K. Takei, W. Honda, S. Harada, T. Arie, S. Akita, Adv. Healthc. Mater. 2015, 4, 487
[12] W. Zeng, L. Shu, Q. Li, S. Chen, F. Wang, X. M. Tao, Adv. Mater. 2014, 36, 31, 5310
[13] A. J. Bandodkar, R. Nuñez-Flores, W. Jia, J. Wang, Adv. Mater. 2015, 27, 3060
[14] A. J. Bandodkar, V. Mohan, C. S. López, J. Ramírez, J. Wang, Adv. Electron. Mater. 2015, 1, 12, 1500289
[15] M. J. Tierney, H. L. Kim, M. D. Burns, J. a. Tamada, R. O. Potts, Electroanalysis 2000, 12, 666.
[16] R. Byrne and D. Diamond, Nat. Mater. 2006, 5, 421.
[17] D. Diamond, S. Coyle, S. Scarmagnani, J. Hayes, Chem. Rev. 2008, 108, 652.
[18] D. Morris, S. Coyle, Y. Wu, K. Tong, G. Wallace, D. Diamond, Chem. Rev. 2009, 139, 231.
[19] K. J. Fraser, V. F. Curto, S. Coyle, B. Schazmann, R. Byrne, R. M. Owens, G. G. Malliaras, D. Diamond, K. St, C. M. De Provence, et al., SPIE 8118 Org. Semicond. Sensors Bioelectron. IV 2011, 1.
[20] A. J. Bandodkar, I. Jeerapan, J.-M. You, R. Nuñez-Flores, J. Wang, Nano Lett. 2015, 16, 721.
[21] M. Novell, M. Parrilla, G. A. Crespo, F. X. Rius, F. J. Andrade, Anal. Chem. 2012, 84, 4695.
[22] M. Cuartero, J. S. del Río, P. Blondeau, J. A. Ortuño, F. X. Rius, F. J. Andrade, Anal. Chim. Acta 2014, 827, 95.
[23] T. Guinovart, M. Parrilla, G. A. Crespo, F. X. Rius, F. J. Andrade, Analyst 2013, 138, 5208.
[24] A. J. Bandodkar, W. Jia, J. Wang, Electroanalysis 2015, 27, 562.
[25] W. Jia, A. J. Bandodkar, G. Valdés-Ramírez, J. R. Windmiller, Z. Yang, J. Ramírez, G. Chan, J. Wang, Anal. Chem. 2013, 85, 6553.

[26] T. Guinovart, A. J. Bandodkar, J. R. Windmiller, F. J. Andrade, J. Wang, Analyst 2013, 138, 7031.

[27] A. J. Bandodkar, V. W. S. Hung, W. Jia, G. Valdés-Ramírez, J. R. Windmiller, A. G. Martinez, J. Ramírez, G. Chan, K. Kerman, J. Wang, Analyst 2013, 138, 123.

[28] A. J. Bandodkar, W. Jia, C. Yard, X. Wang, J. Ramirez, J. Wang, Anal. Chem. 2014, 87, 394.

[29] A. J. Bandodkar, D. Molinnus, O. Mirza, T. Guinovart, J. R. Windmiller, G. Valdés-Ramírez, F. J. Andrade, M. J. Schöning, J. Wang, Biosens. Bioelectron. 2014, 54, 603.

[30] G. Matzeu, C. O'Quigley, E. McNamara, C. Zuliani, C. Fay, T. Glennona, D. Diamond, Anal. Methods 2016, 8, 64.

[31] X. Hu, P. Krull, B. de Graff, K. Dowling, J. A. Rogers, W. J. Arora, Adv. Mater. 2011, 23, 2933.

[32] K. Cherenack, L. van Pieterson, J. Appl. Phys. 2012, 112, 091301 1.

[33] M. J. Luetkemeier, M. G. Coles, E. W. Askew, Sports Med. 1997, 23, 279.

[34] M. H. Rosner, J. Kirven, Clin. J. Am. Soc. Nephrol. 2006, 2, 151.

[35] R. J. Maughan, S. M. Shirreffs, Scand. J. Med. Sci. Sports 2010, 20, 40.

[36] A. Cazalé, W. Sant, F. Ginot, J.-C. Launay, G. Savourey, F. Revol-Cavalier, J. M. Lagarde, D. Heinry, J. Launay, P. Temple-Boyer, Sens. Act. B Chem. 2016, 225, 1.

[37] B. Schazmann, D. Morris, C. Slater, S. Beirne, C. Fay, R. Reuveny, N. Moyna, D. Diamond, Anal. Methods 2010, 2, 342.

[38] E. Frank, F. Hermanutz, M. R. Buchmeiser, Macromol. Mater. Eng. 2012, 297, 493.

[39] S. Poorahong, P. Santhosh, G. V. Ramírez, T.-F. Tseng, J. I. Wong, P. Kanatharana, P. Thavarungkul, J. Wang, Biosens. Bioelectron. 2011, 26, 3670.

[40] A. Periyakaruppan, R. P. Gandhiraman, M. Meyyappan, J. E. Koehne, Anal. Chem. 2013, 85, 3858.

[41] E. Rand, A. Periyakaruppan, Z. Tanaka, D. a Zhang, M. P. Marsh, R. J. Andrews, K. H. Lee, B. Chen, M. Meyyappan, J. E. Koehne, Biosens. Bioelectron. 2013, 42, 434.

[42] J. Fei, K. Wu, F. Wang, S. Hu, Talanta 2005, 65, 918.

[43] J. Zhu, Y. Qin, Y. Zhang, Electrochem. commun. 2009, 11, 1684.

[44] C. Callewaert, B. Buysschaert, E. Vossen, V. Fievez, T. Van de Wiele, N. Boon, J. Microbiol. Methods 2014, 103, 6.

[45] T. Guinovart, G. A. Crespo, F. X. Rius, F. J. Andrade, Anal. Chim. Acta 2014, 821, 72.

[46] E. Bakker, E. Pretsch, P. Bühlmann, Anal. Chem. 2000, 72, 1127.

[47] G. A. Crespo, S. Macho, F. X. Rius, Anal. Chem. 2008, 80, 1316.

[48] U. Vanamo, J. Bobacka, Anal. Chem. 2014, 86, 10540.

[49] X. U. Zou, X. V Zhen, J. H. Cheong, P. Bühlmann, Anal. Chem. 2014, 86, 8687.

[50] A. M. Cadogan, D. Diamond, M. R. Smyth, M. Deasy, M. A. Mckervey, S. J. Harris, Analyst 1989, 114, 1551.

[51] M. J. Buono, K. D. Ball, F. W. Kolkhorst, J. Appl. Physiol. 2007, 103, 990.

[52] L. B. Baker, J. R. Stofan, A. a Hamilton, C. a Horswill, J. Appl. Physiol. 2009, 107, 887.

Chapter 5

A Textile-Based Stretchable Multi-Ion Potentiometric Sensor

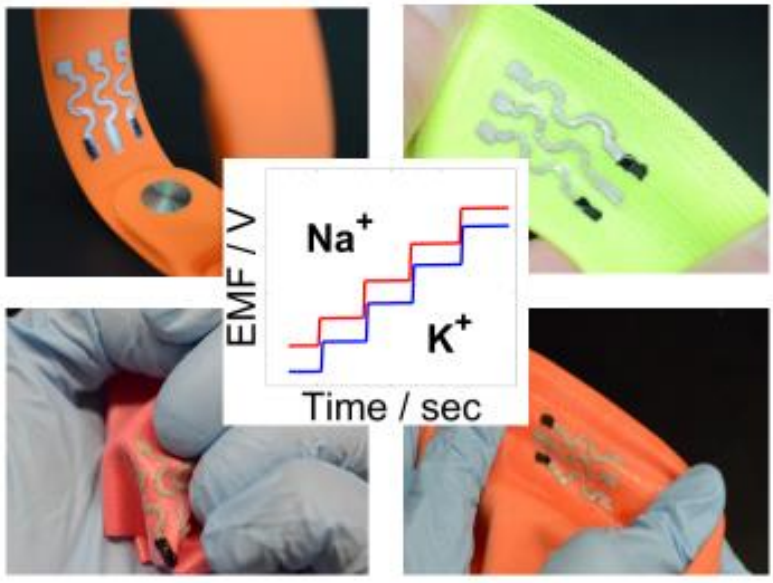

UNIVERSITAT ROVIRA I VIRGILI
NEW ELECTROCHEMICAL SENSORS FOR DECENTRALIZED ANALYSIS
Marc Parrilla Pons

This chapter is aimed to demonstrate the versatility of the screen-printing technique over different textile substrates to build wearable chemical sensors. The use of elastomeric materials (polyurethane and Ecoflex) in combination with conductive inks (Ag/AgCl and CNTs) gives the opportunity to develop wearable sensors in conventional textile materials. Hence, a highly stretchable and printable textile-based potentiometric sensor array for simultaneous multi-ion sweat analysis using variety of fabric materials that can be used in diverse healthcare and fitness applications is presented. The device withstands considerable mechanical deformation (stretching, crumpling, twisting, washing) without losing analytical performance. Moreover, the integration of the multi-ion sensor with a Bluetooth wireless device can give real-time data of the wearer physiological status and then the ability to gain insight, for example, on the dehydration status of a person (athlete or patient).

5.1. Introduction

Recent trends in personalized healthcare have led to growing demands for real-time monitoring of the physiological status of human subjects. Detecting disorders in electrolyte levels, such as hyperkalemia, hypernatremia, hypokalemia or hyponatremia is very important and challenging.[1,2] Electrolyte imbalance represents a potential risk of fatal abnormal heart rhythms.[3,4] Electrolyte loss is a major concern in disorders such as Cystic Fibrosis[5] and hyperhidrosis.[6] Monitoring key electrolytes may also alert to latent cardiac problems[7] and diagnose apparent life-threatening events.[8,9] Overall, real-time measurements of electrolyte concentrations could indicate the patient, doctor, coach or athlete to potential electrolyte loss,[10] dehydration status[11] and the associated need for electrolytes replenishment.[12] Cumbersome methods to measure the sodium and potassium imbalance, such as electrocardiogram and sweat patch, have been reported.[13,14] Recent activity have led to wearable electrochemical (potentiometric) devices for non-invasive electrolyte monitoring.[15,16] However, the success of wearable sensing devices for health monitoring requires proper attention to key challenges concerning their mechanical resilience and large-scale manufacturing. Recent efforts to address these issues have relied on stretchable printable electrochemical devices.[17]

5.2. Experimental Section

5.2.1. Materials

Dimethylformamide (DMF) was purchased from Fisher Chemical (Fair Lawn, NJ). Methanol (99.8% anhydrous) was purchased from Aldrich Chemical Co. Inc. (Milwaukee,

WI). Artificial sweat matrix containing 6 mM KCl, 80 mM NaCl, 0.08 mM $MgCl_2$, and 5 mM NH_4Cl was prepared.[18] Ecoflex® 00-30 was prepared in-house by mixing equal volumes of pre-polymer A with pre-polymer B provided by the supplier. A polyester textile laminated with polyurethane, polyester nylon reinforced reflective band, silicone watch straps and polyester-based underwear were used as a fabric to build the sensors. Other reagents and materials are detailed in Chapter 3.

5.2.2. Instrumentation

Electromotive force (EMF) was recorded using a high-input impedance data acquisition device (AUTOLAB Type II – EcoChemie, B. V., Utrecht, The Netherlands) and NOVA software (v.1.11, The Netherlands) as a measuring interface, at room temperature (22 ºC) without any ionic strength adjuster. EMF wireless measurements were recorded using Go Wireless® Electrode Amplifier (Vernier Software & Technology, Beaverton, USA).

5.2.3. Ion-selective Membranes and Reference Membrane

Polyurethane (PU) polymer was used to build the ion-selective membrane (ISM) instead of the typical polyvinyl chloride (PVC) membranes. Hence, the use of PU for the ISM made possible to build flexible and stretchable membranes. Sodium-selective membrane (Na^+SM). The Na^+SM contained 0.7 wt% of Sodium ionophore X, 0.25 wt% of potassium tetrakis (4-chlorophenyl) borate, 66.05 wt% of 2-nitrophenyl octyl ether (o-NPOE) and 33 wt% of PU. Potassium-selective membrane (K^+SM). The K^+SM contained 2 wt% Valinomycin (Potassium ionophore I), 0.5 wt% of potassium tetrakis (4-chlorophenyl) borate, 64.7 wt% of bis (2-ethylhexyl) sebacate (DOS) and 32.8 wt% of PU. Both membranes compositions were obtained as described elsewhere.[19] The membranes were prepared by dissolving each mixture (100 mg) in THF (1mL). The cocktails were vigorously shaken for 1 hour. Once membranes were deposited, cocktails were kept in the fridge at 4 ºC, and remained stable for 2 weeks. A solid-state reference membrane was prepared as described elsewhere.[20]

5.2.4. Fabrication of the Textile Sensor

Fabrication of the electrodes. The process employed an MPM-SPM semi-automatic screen printer (Speedline Technologies, Franklin, MA). Sensor patterns were designed in AutoCAD (Autodesk, San Rafael, CA) and outsourced for fabrication on stainless steel through-hole 12” x 12” framed stencils of 125µm thickness (Metal Etch Services, San Marcos, CA). For the analytical performance studies of the textile sensor, a common stretchable textile was used based on polyester fabric laminated with polyurethane. A sequence of

stretchable Ag/AgCl ink, stretchable CNT ink and Ecoflex layer was printed to realize the complete electrochemical device array. The printed stretchable Ag/AgCl and CNT patterns were cured (90ºC for 10min and 85ºC for 10 min) in a convection oven, respectively. The final Ecoflex layer, used to define the electrode area and contact pads, was cured at room temperature for 2h (Figure 5.1A). The device array was subsequently modified with specific reagents for achieving ion-selective sensors (Figure 5.1B).

For the other different substrates (such as bands and underwear) a previous treatment was necessary to develop a smooth layer where the ink could be well-attached. The printing process comprised of first screen printing a thick layer (100 µm) of Ecoflex on each supporting substrate. Precaution was taken to avoid entrapment of air bubbles while placing the Ecoflex layer onto the supporting surface. Subsequently, a thick layer (75 µm) of a 15 wt% PU in DMF solution was deposited onto each supporting surface and was cured (50ºC for 10 minutes). After that, the substrates were ready for printing the electrodes as discussed earlier (Figure 5.1C).

Fabrication of stretchable sodium and potassium ion-selective sensors. To fabricate the stretchable potentiometric ion-selective sensor, the reference membrane cocktail (2 µL) was drop-casted twice onto the Ag/AgCl reference electrode (10 minutes drying time between drops), and the sodium and potassium working electrodes were modified by dropping of the Na^+-selective membrane (2 µL) and K^+-selective membrane cocktail (2 µL) 7 times (3 min drying time between drops) onto CNT working electrode, respectively. Membrane deposition was optimized in order to get a stable and reproducible performance by drop-casting different amounts of the ion-selective membrane cocktail. It is important to note that low amount of cocktail drop-casted was needed to avoid dissolving the CNT ink. Then, the sensor was allowed to dry overnight before use; an important step for the reference electrode.[21] Subsequently, a hydrophilic polyurethane aqueous solution (1 µL) was dropped onto the reference membrane and let it dry for 3h. Finally, an overnight conditioning step was applied. The step consisted on drop cast 0.1 M NaCl solution onto sodium-selective electrode, 0.01 M KCl solution onto potassium-selective electrode and 3 M KCl solution onto the reference membrane. The sensor was kept at room temperature until use (Figure 5.1B).

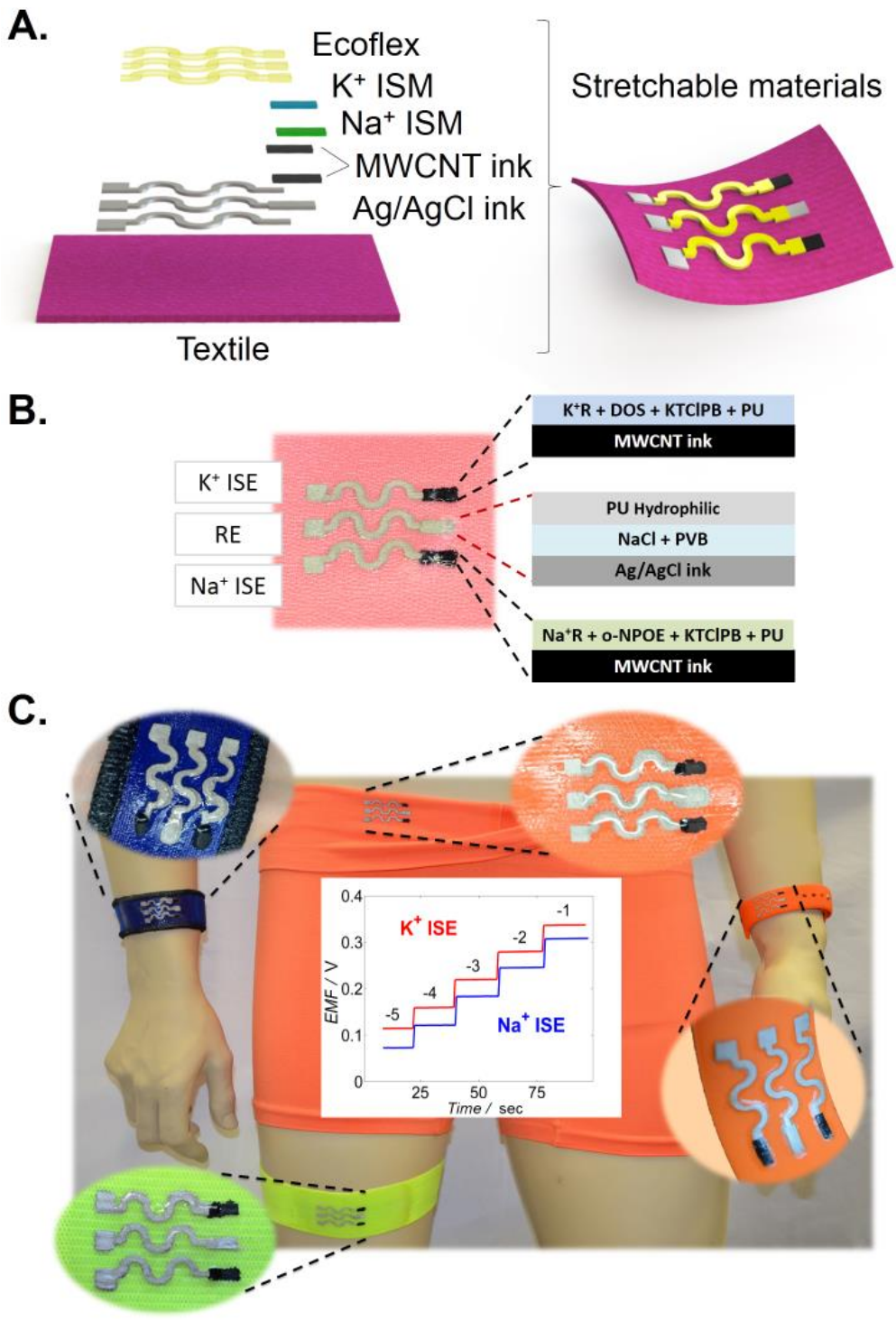

Figure 5.1. (A) Schematic representation of the tailor-made stretchable materials and manufacturing process. (B) Image depicting the wearable sensor based on textile and ion-selective membranes (ISM) composition. (C) Image of the stretchable printed sensors on different common textiles and typical time trace plots for potassium and sodium.

5.3. Results and Discussion

5.3.1. Analytical Performance

A slope value of 60.3±4 mV log[Na^+]$^{-1}$ (6.6 %RSD, N=5) and an intercept of 263.3±67.6 mV (25.7 %RSD, N=5) from 10^{-4} M to 10^{-1} M for Na^+ ISE and a slope value of 60.6±3.9 mV log[K^+]$^{-1}$ (6.4 %RSD, N=5) and an intercept of 316.6±56.3 mV (17.8 %RSD, N=5) from 10^{-4} M to 10^{-1} M for K^+ ISE were obtained. High %RSD values in the intercept values could be attributed to the use of sensors produced in different batches. Moreover, some of the electrodes were previously exposed to mechanical stress to test their variability. In contrast, constant values in the slope were obtained giving highly reproducible sensors. In this way, the variability in the intercept remains an issue for the wearable potentiometric sensors that needs to be addressed by calibrating each electrode before or after the potentiometric measurement. The results showed that the textile sensor offered a relatively fast change of EMF upon changing the ion concentration for both ions, reaching the steady-state response in about 10 seconds.

Another important parameter to assess is the selectivity of the working electrodes. This critical evaluation is needed to corroborate the feasibility of the sodium and potassium monitoring within physiological range. Sweat, rich in sodium and potassium, can act as interference for the working electrodes. For this reason, selectivity coefficient values were calculated by separate solution method (SSM) for each of the working electrode against the interfering ion. The results can be seen in Table 1. Slightly differences were obtained in the selectivity coefficient values. Regularly, ion-selective membranes are prepared with PVC instead of PU used in this work.[26] Different impurities found in the polymers can cause this change in the values. Typical values of K^+ in sweat fall within the 0.2 to 8 mM range[31] and for Na^+ from 20 to 110 mM.[13] Selectivity coefficients obtained in this work indicate that interferences should not affect the potentiometric measurements.

Table 5.1. Selectivity values obtained experimentally and in literature for the sodium and potassium-based polymeric membrane.

Analyte	Log K_{Kj}a	Log K_{Naj}a	Log K_{Kj}b	Log K_{Naj}b
Na^+	-3.34	-	-4.1	-
K^+	-	-1.93	-	-1.9

a Results obtained in this work.
b Results found in literature.[32,33]

5.3.2. Mechanical Deformation Tests

This chapter reports for the first time on a highly stretchable and printable textile-based potentiometric sensor array for simultaneous multi-ion sweat analysis using variety of fabric materials towards diverse healthcare and fitness applications. Screen-printing has been applied recently for fabricating amperometric sensors[22] and biofuel cells[23] on common textiles, but not in connection to potentiometric sensors and stretchable textile devices.[24] Textiles are attractive components of wearable sensing devices and offer rich elastomeric properties towards achieving conformal contact between the sensor and the body. Integrating chemical sensors directly into fabrics offer major advantages for future healthcare monitoring systems. Yet, a key issue involving textile-based sensing devices is the ability to operate under extreme mechanical tensions (that reflect daily activity) without compromising their analytical performance. In this work, we realized highly stretchable textile-based potentiometric sensors by combining polyurethane (PU)-based ion-selective membranes and inks with a serpentine sensor pattern and recently developed stretch-enduring printed electrodes.[25] The compositions of the selective potentiometric membrane and of the printed inks have thus been tailored for ensuring selectivity, electrical conductivity, reproducible printing, and strong adherence to conventional textiles. To provide the necessary biocompatibility and further resistance to mechanical stress we relied on polyurethane as replacement to the common PVC matrix of ion-selective sensing membranes as well as the binder of the printed CNT trace. Polyurethanes have attractive mechanical and biocompatibility properties that make them suitable for many wearable devices. These materials are known to minimize unwanted inflammation, fouling and other adverse physiological effects,[19] while providing exceptional analytical performance using potentiometric technique.[26] As illustrated in Figures 5.1A and 5.1B, such PU-based membrane and CNT ink have been coupled to an Ecoflex-containing Ag/AgCl ink and combined with a solid-contact reference electrode, leading to highly stretchable textile-based potentiometric sensors that transduce their potential response under extreme mechanical stress. Such resiliency is crucial for realizing high-performance wearable potentiometric sensing devices.

The resilience and analytical performance of the novel dual-electrolyte textile-based printable wearable potentiometric sensor was examined using open-circuit potential measurements (Figure 5.1B). A calibration curve was executed by recording the electromotive force (EMF) versus the time and changing the concentration of NaCl and KCl. Sensor array in Figure 5.1C exhibited a Nernstian response of 59.4 mV $\log[Na^+]^{-1}$, linear

range from 10^{-4} M up to 10^{-1} M and limit of detection (LOD) of $10^{-4.9}$ M for its sodium selective electrode (Na^+ISE) and a Nernstian response of 56.5 mV $\log[K^+]^{-1}$ from 10^{-4} M up to 10^{-1} M and a LOD of $10^{-4.9}$ M for the potassium selective electrode (K^+ISE). Both results are comparable to the values reported previously using similar ion-selective membranes.[27] These dynamic ranges cover the physiological sodium and potassium levels in sweat before, during and after prolonged exercise.[28] Electrolyte concentrations progressively increase during such exercise activity to provide a useful indicator of the dehydration status.[29] Moreover, understanding the amount of ionic species loss during exercise could facilitate recovery of the ionic balance during and after exercise.[30]

Stretchability tests were performed initially employing different strain conditions (Figure 5.2A). The textile was anchored and moved away at a speed of 1 mm s^{-1}. This process was repeated 10 times at 0%, 25%, 50%, 75% and 100% strains. Subsequently, the stretchability was tested by using a fixed 75% linear strain during 60 minutes, emulating a prolonged strain force during exercise. A calibration curve of each electrode was recorded every 15 minutes (Figure 5.2B). Both tests indicated a robust analytical performance under the different strains. Larger (>100%) strains of the textile led to some damage in the reference membrane and hence to an inferior performance.

Bending represents another common mechanical stress expected during daily wear. Bending of the textile sensor was tested by twisting it back and forth for 0º, 45º, 90º and 180º 10 times in each angle. The subsequently recorded calibration curve indicates no apparent change in the sensitivity (Figure 5.2C). A crumpling test was also performed, consisting of wrinkling the textile with the hand for multiple times (Figure 5.2D). A calibration curve was recorded after 0, 5, 15 and 30 such wrinkling. No apparent variation in the performance was observed under these repeated textile manipulations.

Finally, as shown in Figure 5.2E, a simulation of a conventional washing procedure was performed. This test consisted on immersing the sensor in a beaker full of water under a vigorous agitation for periods of 10 and 40 minutes. A calibration plot of each electrode was recorded after complete drying of the sensor, leading to favorable analytical results. Such attractive behavior indicates strong surface adherence of the organic polymeric membranes with no apparent leaching of the membrane components. In addition, placing the hydrophilic polyurethane membrane on top of the reference membrane prevents leaching of NaCl from the porous PVB membrane and maintains the baseline potential even after a prolonged

mechanical agitation. Table 2 summarizes the analytical performance of the sensor under different mechanical deformations shown in Figure 5.2.

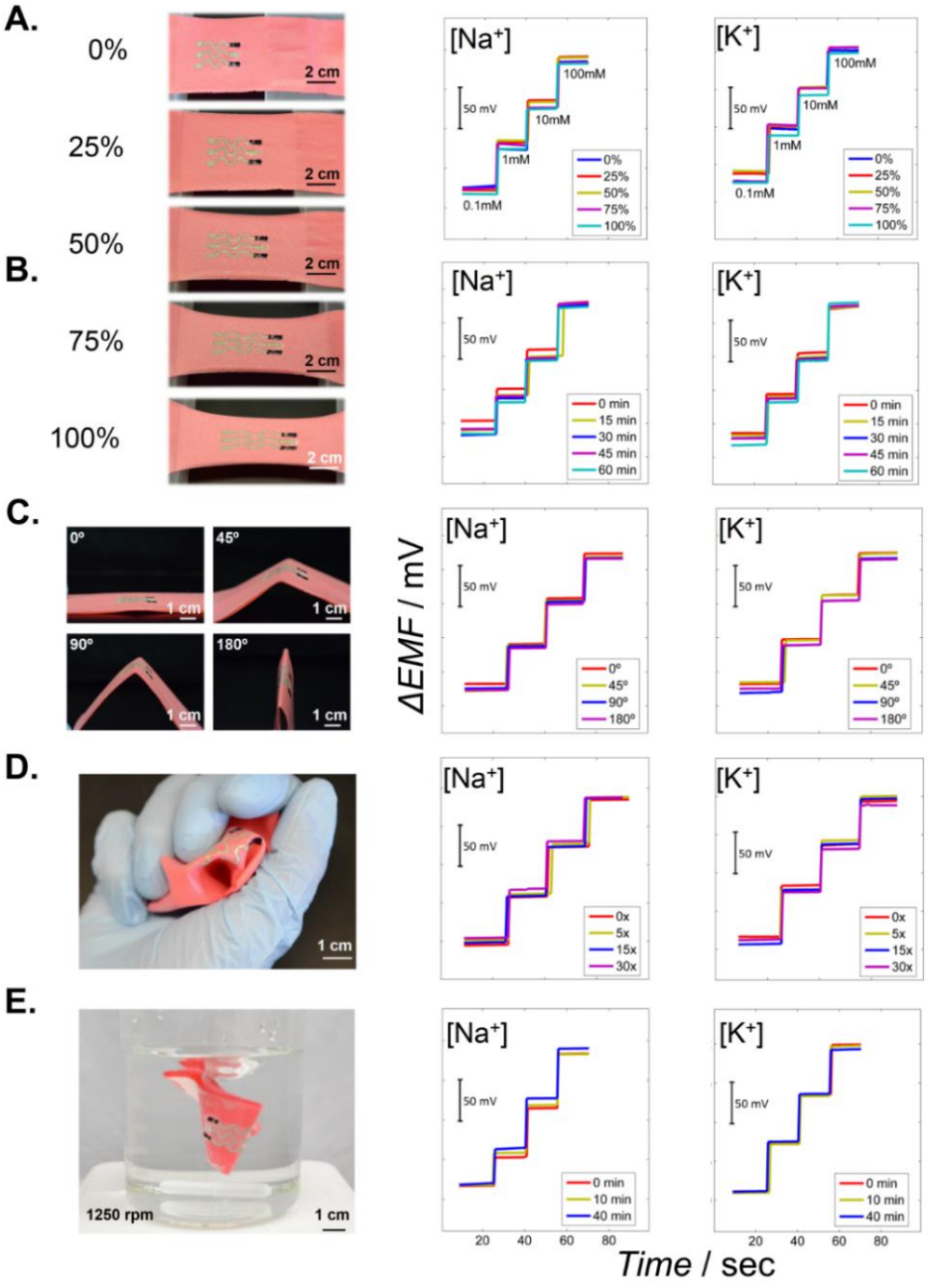

Figure 5.2. Images illustrating resilience studies involving exposing the printable textile potentiometric sensor to increasing levels of strain (left) along with the corresponding time trace calibration plots (right). (A) Linear stretchability test up to a total of 100% strain, 10 repetitions in each strain step. (B) Stretchability test, using a 75% linear strain for a total of 60 min (time trace recorded after every 15 min). (C) Bending assessment, up to a total of 180º, 10 repetitions in each angle. (D) Crumpling evaluation, up to 30 times wrinkling. (E) Washing step simulations (without soap) using short and long (10 and 40 minutes) periods.

Table 5.2. Average sensitivity values and intercept values obtained during several mechanical deformations of the textile ISE system.

Na^+ selective electrode				
Test	**Sensitivity [mV log$[Na^+]^{-1}$]**	**%RSD**	**Intercept [mV]**	**%RSD**
Stretching	54.1±1.5	2,7	239.5±6.3	2,6
Hold stretched	61.3±1.9	3,1	179.8±2.3	1,3
Bending	64.4±0.7	1,0	282.6±3.5	1,2
Crumpling	62.6±0.9	1,5	250.3±1	0,4
Washing	56.2±0.9	1,7	186±6.4	3,5
K^+ selective electrode				
Test	**Sensitivity [mV log$[K^+]^{-1}$]**	**%RSD**	**Intercept [mV]**	**%RSD**
Stretching	56.9±1.6	2,9	313.3±4.2	1,3
Hold stretched	64.9±2.8	4,3	235.4±4.1	1,7
Bending	64.1±1.1	1,7	335±4.4	1,3
Crumpling	60.6±2.6	4,2	307.5±8	2,6
Washing	61.8±1.1	1,8	258.3±2.8	1,1

Overall, the wearable textile potentiometric array displays an attractive analytical performance before and after exposures to severe mechanical stress. Such resilience can be explained by considering the behavior of the printed materials at the microscopic level. When an external force is applied to the stretchable sensor, the stress is absorbed mostly by the stretchable Ecoflex component in the Ag/AgCl ink and by the PU as a stretchable binder in the CNT ink. When the printed Ag/AgCl trace undergo high strain, its Ecoflex polymeric component stretches while maintaining the physical contact between randomly oriented multilayers of its conductive particles. Similarly, when the printed CNT trace is subject to extreme stress, its PU binder stretches while maintaining the electrical contact of the randomly distributed CNT. This ability to operate under high strain conditions meets the demands of using these printed textile potentiometric sensors in real-life scenarios involving extreme and repeated movements of the wearer.

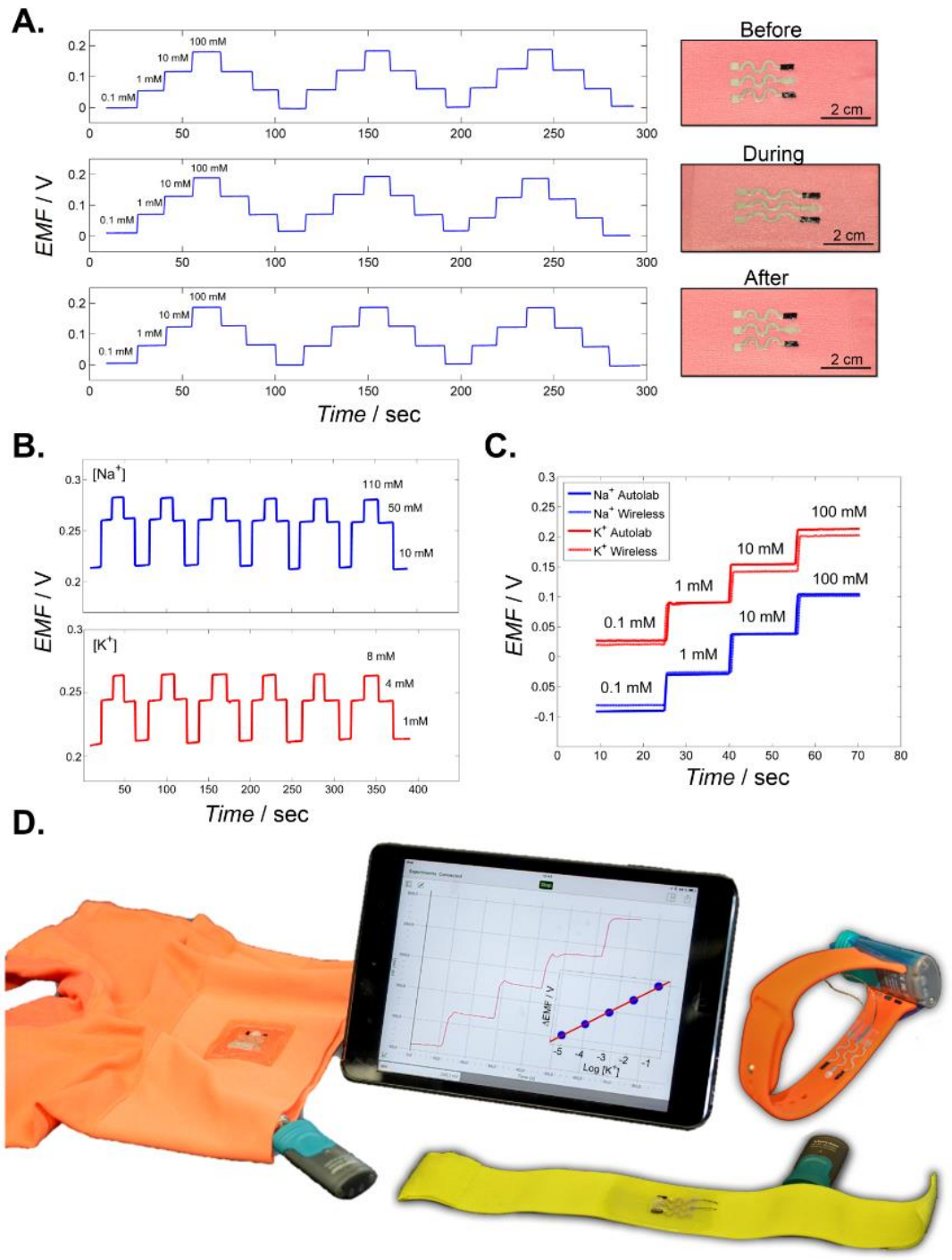

Figure 5.3. (A) Carry-over test of a textile-based sensor before, during (50% strain) and after such mechanical deformation. (B) Carry-over testing using artificial sweat test within the physiological range. (C) Correlation of calibration experiments carried out using a compact wireless high-input voltmeter and a conventional potentiostat. (D) Images depicting the versatility of the printable and stretchable sensor array on different common wearable substrates. The tablet displays a real-time trace of increasing potassium levels obtained wirelessly by the underwear printed sensor.

Repeatability represents another important feature of wearable biomedical sensors. It is crucial to obtain highly reproducible results for prolonged monitoring of fluctuating ions concentrations. Hence, the repeatability was evaluated through a carry-over test before, during and after the exposure to middle-high strain (50% stretched) (Figure 5.3A). The results from 10^{-4} M to 10^{-1} M showed a slope of 61.2±0.7 mV log$[Na^+]^{-1}$ and an intercept of 243.7±4 mV before mechanical stress, a slope of 59.2±1.4 mV log$[Na^+]^{-1}$ and an intercept of 247.6±4.4 mV during 50% strain and a slope of 61.5±0.9 mV log$[Na^+]^{-1}$ and an intercept of 247.1±2 mV after the resilience test. These carry-over tests demonstrate the ability to follow rapidly fluctuating ions levels. Finally, a carry-over test was performed in artificial sweat over the narrow physiological range of the target electrolytes (Figure 5.3B), using 10 - 110 mM NaCl (with 5 mM KCl) and the potassium sensor from 1 - 8 mM KCl (with 80 mM NaCl). The response of the array yielded a slope of 64.3±1.2 mV log$[Na^+]^{-1}$ with an intercept of 343.3±1.5 mV from 10^{-2} M to $10^{-0.96}$ M and a slope of 57.4±1.6 mV log$[K^+]^{-1}$ with an intercept of 383.4±3.8 mV from 10^{-3} M to $10^{-2.09}$ M. These data showed favorable reproducibility, stability and repeatability while varying the sodium and potassium concentrations within the physiological range, demonstrating the promise of the new potentiometric textile sensors in different real-life scenarios.

5.3.3. Wireless Data Reader Integration

Following the detailed characterization of the textile sensors, it was necessary to meet further the practical demands of their real-life wearable operation. Particular important is the integration of the textile sensors with wearable supporting electronics and wireless transmission devices. Hence, we addressed the miniaturization of the reader device and a real-time wireless data transmission to another portable device (*e.g.,* cell phone or a tablet). Complete integration and miniaturization of the textile sensor system was accomplished using a wireless high-input impedance voltmeter, with the potentiometric data being recorded with an iOS® application on an Ipad® tablet. Figure 5.3C compares calibration curves using the textile sensor array obtained with the compact wireless high-input voltmeter and with a benchtop Autolab potentiostat. The excellent agreement between the plots obtained using the two instruments support the integration of the wireless device with the textile-based potentiometric sensor. The response of the array from 10^{-4} M to 10^{-1} M yielded a slope of 63.1±2.7 mV log$[Na^+]^{-1}$ with an intercept of 164.8±5.3 mV and a slope of 61.1±1.8 mV log $[K^+]^{-1}$ with an intercept of 270.1±9.5 mV.

Wearable devices have large versatility in terms of the diverse types of substrate materials used. It is thus important to take advantage of existing commercial platforms to print the wearable electrolyte sensors. Accordingly, we printed the new potentiometric sensors onto conventional textiles such as underwear, watch straps and elastic band (Figure 5.3D). Coupling screen printing technology with commodity textiles could offer large-scale low-cost production of variety of electrochemical sensors and flexible electronics systems.[34] Nevertheless, in some cases, such as elastic band or underwear, the rough material surface might become a problem when external tensile load is applied, requiring pretreatment by printing of the stretchable ink. Firstly, an Ecoflex layer was deposited on top of the sensor zone, creating a smooth thin layer. Subsequently, a PU layer was deposited on top of the Ecoflex layer prior to printing the CNT and Ag/AgCl inks. This step was essential to maintain strong adherence of the potentiometric sensor onto the substrate, and hence a remarkable sensor stretchability and durability. The performance of the potentiometric sensor array printed in this way on different substrates was tested. The watch-straps based sensors yielded a sensitivity of 51.6 mV $\log[K^+]^{-1}$ and 51.8 mV $\log[Na^+]^{-1}$, compared to 50 mV $\log[K^+]^{-1}$ and 52.6 mV $\log[Na^+]^{-1}$ for the elastic-band sensors and 56.6 mV $\log[K^+]^{-1}$ and 52.5 mV $\log[Na^+]^{-1}$ using the underwear sensors. All the sensors performed favorably within a 10^{-3} M to 10^{-1} M linear range, yielding a near-Nernstian sensor response.

Finally, Figure 5.3D illustrates the proof of concept of creating a compact wearable sensor system by integrating the textile ISEs with a portable wireless data transmission device. Indeed, the time-trace plot obtained with the underwear textile sensor for increasing potassium levels was recorded wirelessly with the Bluetooth application. This resulted in a favorable Nernstian response, with a slope of 59.9 mV $\log[K^+]^{-1}$ over the 10^{-5} M to 10^{-1} M range.

5.4. Conclusions

In conclusion, we have demonstrated for the first time a stretchable textile-based potentiometric sensor that exhibits a Nernstian behavior under extreme conditions. Combining stretchable components as the PU, Ecoflex and stretch-enduring inks, along with a serpentine design, this printed textile sensor array can withstand high tensile stress without provoking major cracking common to previous electrochemical devices. Mechanical deformation studies revealed that stretching up to 100%, along with repeated bending, crumpling or prolonged washing have negligible effects on the potentiometric response. Moreover, the screen printing process offers large-scale mass production of low-cost

reproducible textile sensors. Further functionalization of the stretchable electrodes with other materials could enable a large arsenal of wearable textile sensors. Such integration of flexible chemical sensors with common textiles will lead to next-generation platform for personalized medicine, and will bring new opportunities for using wearable chemical sensing in the diagnostics, healthcare and sport fields.

5.5. References

[1] M. H. Rosner, J. Kirven, Clin. J. Am. Soc. Nephrol. 2006, 2, 151.

[2] A. Lehnhardt, M. J. Kemper, Pediatr. Nephrol. 2011, 26, 377.

[3] C. V Leier, L. Dei Cas, M. Metra, Am. Heart J. 1994, 128, 564.

[4] S. P. von Duvillard, W. A. Braun, M. Markofski, R. Beneke, R. Leithäuser, Nutrition 2004, 20, 651.

[5] E. Scurati-Manzoni, E. F. Fossali, C. Agostoni, E. Riva, G. D. Simonetti, M. Zanolari-Calderari, M. G. Bianchetti, S. a G. Lava, Pediatr. Nephrol. 2014, 29, 1015.

[6] E. Moraites, O. A. Vaughn, S. Hill, Dermatol. Clin. 2014, 32, 457.

[7] A. Bielecka-Dabrowa, D. P. Mikhailidis, L. Jones, J. Rysz, W. S. Aronow, M. Banach, Int. J. Cardiol. 2012, 158, 12.

[8] E. Tirosh, F. Haddad, A. Lanir, Y. Tal, A. Cohen, Acta Paediatr. 1994, 83, 1268.

[9] C. S. D. Almond, A. Y. Shin, E. B. Fortescue, R. C. Mannix, D. Wypij, B. A. Binstadt, C. N. Duncan, D. P. Olson, A. E. Salerno, J. W. Newburger, D. S. Greenes, N. Engl. J. Med. 2005, 352, 1550.

[10] R. J. Maughan, S. M. Shirreffs, J. Sports Sci. 1997, 15, 297.

[11] L. E. Armstrong, J. Am. Coll. Nutr. 2007, 26, 575S.

[12] R. J. Maughan, S. M. Shirreffs, Int. J. Sport Nutr. Exerc. Metab. 2008, 18, 457.

[13] C. E. Dziedzic, M. L. Ross, G. J. Slater, L. M. Burke, Int. J. Sport Physiol. Perform. 2014, 9, 832.

[14] D. B. Diercks, G. M. Shumaik, R. A. Harrigan, W. J. Brady, T. C. Chan, J. Emerg. Med. 2004, 27, 153.

[15] L. Florea, D. Diamond, Sens. Act. B Chem. 2015, 211, 403.

[16] A. J. Bandodkar, D. Molinnus, O. Mirza, T. Guinovart, J. R. Windmiller, G. Valdés-Ramírez, F. J. Andrade, M. J. Schöning, J. Wang, Biosens. Bioelectron. 2014, 54, 603.

[17] A. J. Bandodkar, R. Nuñez-Flores, W. Jia, J. Wang, Adv. Mater. 2015, 27, 3060.

[18] C. Callewaert, B. Buysschaert, E. Vossen, V. Fievez, T. Van de Wiele, N. Boon, J. Microbiol. Methods 2014, 103, 6.

[19] S. Y. Yun, Y. K. Hong, B. K. Oh, G. S. Cha, H. Nam, S. B. Lee, J. I. Jin, Anal. Chem. 1997, 69, 868.

[20] T. Guinovart, A. J. Bandodkar, J. R. Windmiller, F. J. Andrade, J. Wang, Analyst 2013, 138, 7031.

[21] T. Guinovart, G. A. Crespo, F. X. Rius, F. J. Andrade, Anal. Chim. Acta 2014, 821, 72.

[22] M. C. Chuang, J. R. Windmiller, P. Santhosh, G. V. Ramírez, M. Galik, T. Y. Chou, J. Wang, Electroanalysis 2010, 22, 2511.

[23] W. Jia, X. Wang, S. Imani, A. J. Bandodkar, J. Ramírez, P. P. Mercier, J. Wang, J. Mater. Chem. A 2014, 2, 18184.

[24] J. R. Windmiller, J. Wang, Electroanalysis 2013, 25, 29.

[25] A. J. Bandodkar, I. Jeerapan, J.-M. You, R. Nuñez-Flores, J. Wang, Nano Lett. 2015, 16, 721.

[26] V. V Cosofret, M. Erdosy, J. S. Raleigh, T. a Johnson, M. R. Neuman, R. P. Buck, Talanta 1996, 43, 143.

[27] T. Guinovart, M. Parrilla, G. a Crespo, F. X. Rius, F. J. Andrade, Analyst 2013, 138, 5208.

[28] L. B. Baker, J. R. Stofan, A. a Hamilton, C. a Horswill, J. Appl. Physiol. 2009, 107, 887.

[29] M. J. Buono, K. D. Ball, F. W. Kolkhorst, J. Appl. Physiol. 2007, 103, 990.

[30] E. F. Coyle, J. Sports Sci. 2004, 22, 39.

[31] M. J. Patterson, S. D. Galloway, M. a Nimmo, Exp. Physiol. 2000, 85, 869.

[32] A. M. Cadogan, D. Diamond, M. R. Smyth, M. Deasy, M. A. Mckervey, S. J. Harris, Analyst 1989, 114, 1551.

[33] E. Bakker, J. Electrochem. Soc. 1996, 143, L83.

[34] J. P. Metters, R. O. Kadara, C. E. Banks, Analyst 2011, 136, 1067.

Chapter 6

Wearable Paper-based Sweat Sensor: Towards Monitoring Human Dehydration Status

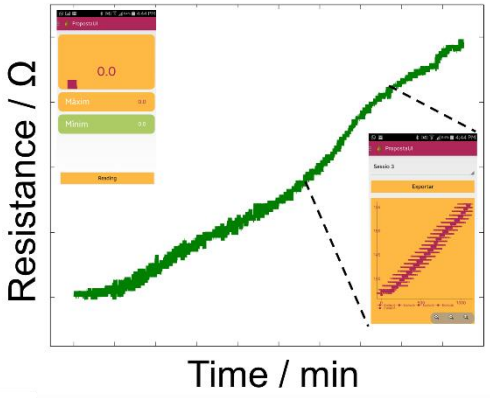

UNIVERSITAT ROVIRA I VIRGILI
NEW ELECTROCHEMICAL SENSORS FOR DECENTRALIZED ANALYSIS
Marc Parrilla Pons

Wearable Paper-based Sweat Sensor: Towards Monitoring Human Dehydration Status

This chapter presents the development of a wearable paper-based sensor for monitoring perspiration dynamics (sweat rate and sweat loss). It deals with a new approach to measure the amount of water by monitoring the change in resistance of a novel nanomaterial-based electrically conductive paper. This novel sensor is based on the use of a single walled carbon nanotubes and sodium dodecylbenzenesulfonate ink applied as a dye on the cellulose fibers of a conventional filter paper. The analytical performance of these sensors is presented and the sensing mechanism is discussed. Subsequently, a proof-of-concept of the quantification of sweat loss in human body is demonstrated. Finally, the integration of a wireless reader with the paper-based sensor for on-body tests is displayed by measuring in real-time the sweat pattern of different participants.

6.1 Introduction

The need to monitor physiological parameters in a wide range of fields such as personalized medicine, wellbeing, fitness and sport is nowadays increasingly required.[1] During the last few decades, scientist used to measure relevant physiological parameters in the laboratory and provide essential information after time-consuming assays, normally involving a long period of time. Beyond the cost and technical complexity of these studies, the results obtained only reveal insights of the human body in artificial conditions. However, when dealing with human physiology in real environments, factors such as terrain, climate factor, psychology, etc. may play an essential role. For this reason, there has been a constant need to monitor the human body in real-life scenarios. Recent advances in technology are enabling the measurement of the same parameters in real-time outside the lab, i.e., in a decentralized manner.[2–4] This growing trend has been possible due to the development of accurate, simple, robust and cost-effective manufacturing processes.[5] The combination of low-cost platforms and a suitable design is leading the new wave of decentralized systems in form of wearable devices.[6–9] This phenomenon has led to the production of massive numbers of portable and wearable sensors that help people to monitor in real-time key physiological parameters.[10] Moreover, suitable data treatment and interpretation help to control, understand and take the right actions in daily situations as well as prevent and diagnose diseases such as cardiovascular problems or diabetes.[11] Wearable technology is providing new miniaturized devices to manage diseases (for instance infectious diseases or obesity) and thus improve the health status of the people, especially old and young people.[12,13] The seamless integration and versatility of wearable platforms in decentralized

systems are driving the evolution of monitoring physiological parameters for personalized healthcare and wellbeing.

Recent developments in wearable sensors are focused on monitoring physical parameters such as temperature, movement and heart rate.[14,15] This information can be applied to monitoring cardiovascular diseases, control physical effort during sport practice, encourage people to be more active, and consequently, spur adherence to a healthy lifestyle.[16–18] This class of devices includes wristbands, chestbands and watches providing real-time information to the end-user, physician, patient or relatives. These integrated systems become almost invisible tools that are able to send real-time relevant information. These devices are being designed to increase the quality of life of people.[7,19] However, the need of remotely monitoring basic biochemical parameters of the human body, such as hydration, electrolytes, molecules and biomolecules, etc., is still an important challenge that can bring significant benefits in healthcare and high performance sports practice.[20] Fortunately, the introduction of new nanomaterials, such as carbon nanotubes, in the development of novel wearable sensors is helping to improve analytical parameters and create chemical sensors that can be embedded into clothes, garments or even directly onto the skin (e.g., tattoos or patches).[21–24] Consequently, the availability of new nanomaterials has opened the opportunity to develop wearable chemical sensors for monitoring fundamental (bio)chemical parameters in real time directly onto the body.

Advances in conductive inks for wearable electronics using carbon nanotubes (CNTs) is opening new and attractive avenues in this area. CNTs are well-known for their outstanding electrical and chemical properties, which have been extensively exploited in a plethora of different areas. During the past few years, dispersions of CNTs in aqueous solution have been used to generate conductive papers.[25] CNT-inks can be generated by functionalization of the CNTs (often through oxidation by acid treatment to generate carboxyl groups)[26,27] or by the use of surfactants.[28] Surfactant-based inks offer better electrical conductivity due to the higher weight fraction of CNTs that can be dispersed.[29,30] Furthermore, surfactants attach to the CNTs via non-covalent interactions, thus preserving the π conjugated system of the CNTs and their electrical properties.

Dehydration status is an essential physiological parameter for monitoring the health risk of a person.[31] Water is a vital resource for the proper functioning of the human body. Water content and distribution helps the body in the thermoregulation process as well as maintaining a synchronized cardiovascular rhythm.[32] Clearly, the amount of water

determines the concentration of substances, and therefore is a centerpiece for homeostasis. Nowadays, there are many different approaches for monitoring dehydration levels. Estimating the fluid loss (by weight loss), measuring the ions imbalance from the sweat,[33] monitoring urine color and composition,[34] etc. In all cases, the quantification of water and water loss is essential for generating reliable information. For this reason, there is an increasing interests for the development of new tools for measuring the amount of sweat loss from the human body.[35,36] Monitoring intense sweating during hard training or endurance competitions, for example, could be helpful to understand the body dehydration status thus avoid muscle crumps and even prevent heart failures.[37,38] Dehydration is the cause of major accidents in sports, since the loss of water leads first to impairment of the cognitive performance, and then -under severe dehydration- to organ damage and even death. Even for amateur sports, elderly and children, dehydration may lead severe short and long-term health risk. An accurate system to facilitate rehydration may significantly improve a healthy sport practice and keep optimum physiological performance.

There are several techniques that are used nowadays to estimate hydration in the field setting.[39] The methods to measure sweat loss, however, range from bulky devices such as bioimpedance monitoring,[40] inaccurate methods such as body weight changes or unpractical measurements such as urine-specific gravity, urine color, and urine osmolality by reactant strips while the athlete is practicing sport. Interestingly, the measurement of sweat-rate is also performed with the absorbent patch -by mass difference- technique.[41] This is in fact the gold standard used for the study of the regional sweat loss,[42] but it is still very difficult to accurately apply it on the field. Hence, there is a need to measure at real-time the amount of sweat lost during exercise and thus the sweat-rate of the regional parts of the body.

In this work, a flexible and electrically conductive material based on the use of single wall carbon nanotubes (SWCNTs) and sodium dodecylbenzenesulfonate (SDBS) ink entrapped in a commercial filter paper is presented. The conductive paper is aimed to determine water content when an aqueous solution contacts the surface of the sensor. The analytical determination is possible because of the increase in the electrical resistance of the conductive paper as a function of the amount of water absorbed. Hence, this system avoids the use of a reference system and provides an almost calibration-free approach. The analytical performance of the sensor is studied by recording the increment of resistance during absorption of aqueous solution into the paper-based sensor. This chemiresistor sensor is capable of changing up to 130% of its relative electrical resistance when an aqueous solution (such as any biological fluid) reaches the surface of the sensor. As a proof

of concept, the novel platform is embedded into a wearable patch to build low-cost sensors and tested on the body of a participant during cycling exercise. Furthermore, the sensor demonstrates the feasibility of the on-body measurement by a validation using standard methods (absorbent patch).[41] Finally, the wearable patch is integrated with a wireless data recorder able to transmit the information directly to a portable Android device (mobile phone). The resulting wearable device is opening the way to simple and cost-effective determination of real-time perspiration from the human body for monitoring dehydration status.

6.2. Experimental Section

6.2.1. Materials

To isolate the electrodes and conductive paper, a plastic tape (0.3 mm thick) coated with an acrylic adhesive on one side (Arcare 8565, Adhesives Research Inc., Limerick, Ireland) was used as a mask. A polycarbonate membrane (1 µm pore diameter) (Albet Labsciences) was obtained from Sigma-Aldrich. A conductive ink to weld the conductive paper to the copper wires (Electric paint, Bare conductive®) was purchased in Farnell components S.L., Spain. A polyurethane semi-permeable film (Hydrofilm®, Hartmann) was used for skin attachment and a polyamide-cotton tape (Omnitape®, Hartmann) were obtained from a local pharmacy.

The method to obtain SWCNTs-COOH is described elsewhere.[43] Briefly, purchased SWCNTs (100 mg) were oxidized in a silica furnace chamber in order to selectively remove any amorphous carbon impurity (T = 365 ºC, air flow-rate = 100 cm^3 min^{-1}, t = 90 min). Subsequently, the SWCNTs were refluxed in H_2SO_4/HNO_3 (3:1) for 30 min. The SWCNTs were then filtered on a Millipore membrane (Polycarbonate, 0.10 µm) and the solid on the filter was washed with Milli-Q water and dried as a black solid (60 mg of SWCNT-COOH).

Artificial sweat matrix containing 6 mM KCl, 0.08 mM $MgCl_2$, 0.17 mM glucose, 5 mM NH_4Cl and 50 mM NaCl was also prepared using Milli-Q water.[44] This matrix was used to emulate similar conditions to on-body tests.

6.2.2. CNT Ink Preparation

The carbon nanotube ink (CNT ink) was prepared as described elsewhere.[45,46] The CNT-ink, which shows a density of 0.99 g L^{-1}, was stored in a refrigerator at 4 °C to avoid destabilization. Under these conditions the CNT dispersion can be used for at least 3 months.

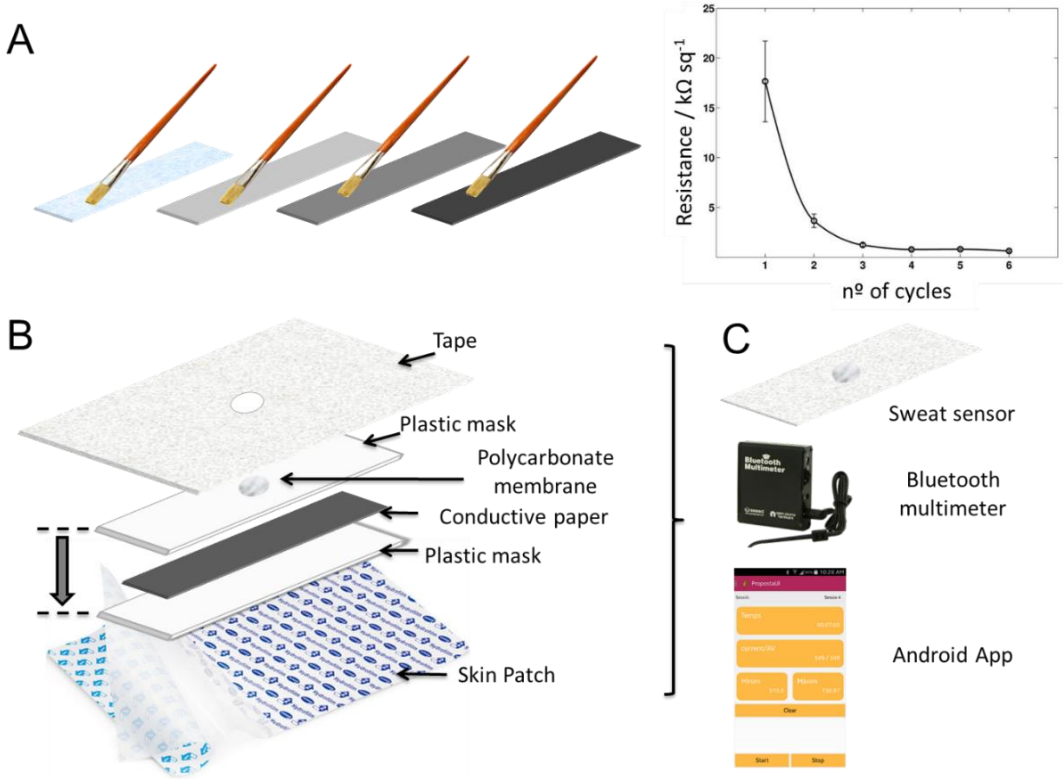

Figure 6.1. Illustration of the sensor fabrication within the whole wearable system. (A) Conductive paper fabrication by painting method. (B) Detailed scheme of the different elements involved in the construction of the wearable patch. The system contains a highly sensitive SWCNTs-SDBS cellulose composite paper for monitoring water inside the wearable patch (C) Illustration of the integrated system (wearable patch, Bluetooth data recorder and a screenshot of the interface from an Android mobile phone).

6.2.3. Conductive Paper

Highly conductive SWCNTs-SDBS conductive paper was made by consecutive painting with the SWCNTs-SDBS aqueous ink.[46] The conductive paper was made by painting a filter paper with the CNT-ink using a conventional paintbrush (Figure 6.1A). High percolation of the deposited CNTs was obtained when more painting repetitions were performed. After 6 paintings at both paper sides, the conductive paper reached a steady-state resistance value, usually around 200 Ω sq^{-1} (Figure 6.1A). Interestingly, it is important to avoid rinsing the paper during the last cycle. This step seems to leave more surfactant on the paper and improves the performance, as it will be discussed later.

6.2.4. Construction of the Paper-based Sensor as a Wearable Patch

The chemiresistor sensor was built with SWCNTs conductive paper sandwiched between two flexible polyester masks (Arcare® 8259, Adhesive Research Inc.). Details of the

electrode components (conductive paper, mask, and membrane) and assembly are schematically shown in Figure 6.1B. Briefly, the CNT conductive paper was cut into strips of 1 cm × 5 cm and partially covered with plastic masks of 2 cm × 6 cm on both sides. The sensing area was left in one of the plastic mask (0.28 cm^2 circle). Besides, the sensing part was covered with a polycarbonate membrane (1 µm porous diameter) (Albet Labsciences) to avoid any contact between the SWCNTs and the skin, and any potential risk of nanotubes leaching. All these components were entrapped in a polyamide-cotton tape (Omnitape®, Hartmann). Copper wires were previously weld to the conductive paper with a commercial conductive ink (Electric paint, Bare conductive®). Each sensor was integrated in a wearable patch using a polyurethane semi-permeable film (Hydrofilm®, Hartmann). Sensors were connected directly to a commercial Bluetooth® reader and experimental data was transferred to a mobile device (Figure 6.1C). For on-body tests, a layer of highly absorptive material was placed between the sensor and the human skin to avoid the sweat run-off and leaving just the sensing area in touch with the skin for a more accurate measurement (Figure 6.2).

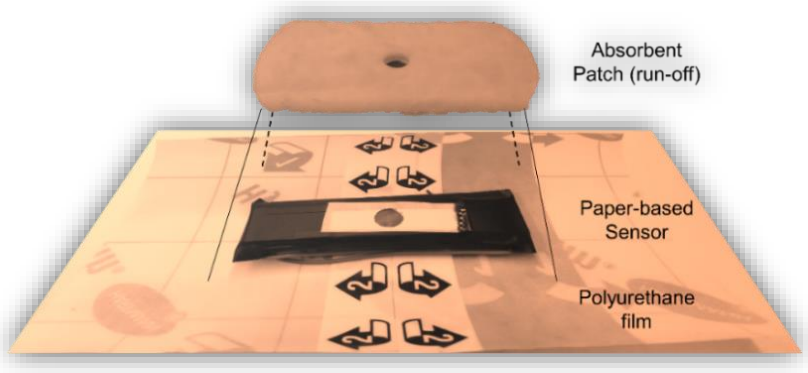

Figure 6.2. Schematic representation of the parts of the sweat patch before use. The paper-based sensor is between an absorbent patch (to avoid the sweat entrance from other parts of the body) and the polyurethane semi-permeable film that allows the sensor to be precisely stacked on the body.

6.2.5. Electrical Resistance Measurements

Resistance measurements were carried out using a Tenma 72-7720 digital multimeter (Tenma Corp.) and Keithley 6514 electrometer (Keithley Instruments, Inc., Ohio) as a measuring interface, at room temperature (22ºC). On-body tests were performed with a Bluetooth multimeter (Seeedstudio Co., China).

6.2.6. Liquid Sensing Tests

The measurements were carried out by adding drops of the suitable amount of liquid on the sensing area. Moreover, flow tests were performed with a conventional microfluidic pump (Gilson Minipuls 3). The Keithley electrometer was used to continuously monitor the electrical resistance of the paper-based sensor in both cases. During the experiments of optimization and characterization either distilled water or artificial sweat were used for calibration.

6.2.7. On body Measurements

On-body measurements were carried out with the sweat provided by the perspiration of a participant during cycling exercise. It is crucial to mention that before starting the on-body test, a highly absorbent pad was applied between the sensor and the skin. The pad had an orifice with the same electrode active area to allow just the sweat amount to flow through the sensing area. The function of the cotton pad was to absorb the sweat run-off coming from the surrounding areas and thus avoid over-estimation of sweat loss values (Figure 6.2).

6.3. Results and Discussion

6.3.1. Sensing Amount of Liquid: Mechanism

In all the experiments, the resistance is measured along the length of the paper. Preliminary experiments show that the addition of water or a dilute aqueous solution produces an increment of the electrical resistance of the paper (Figure 6.3A). Consecutive additions of liquid produce further increments in the electrical resistance (Figure 6.3B).

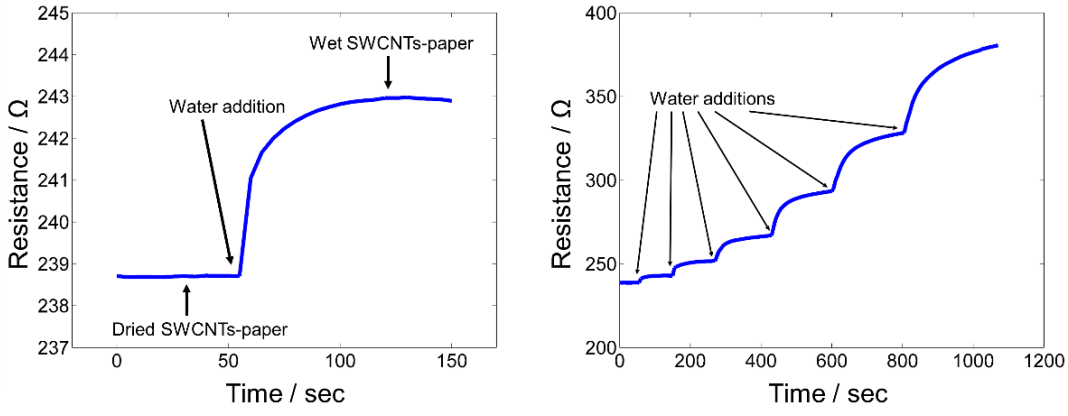

Figure 6.3. Response of the chemiresistor sensor producing an increment of the electrical resistance of the paper. (A) Plot displays the change in electrical resistance after the addition of 1 µL of distilled water. (B) Plot shows the increment of electrical resistance upon consecutive additions of distilled water.

At some point, a saturation is reached and no further increment on the resistance is observed. This point corresponds with a situation where the sensor can be seen completely wet. This feature is interesting, since it would allow measuring water content in the SWCNTs-SDBS filter paper by means of the relative change in its electrical resistance (ΔR %).

In an attempt to understand the phenomena involved, Figure 6.4 shows a diagram depicting the different steps of the fabrication of the conductive paper. First, the SWCNTs-cellulose interaction is allowed by the dispersion of SWCNTs into aqueous solution using sodium dodecylbenzene sulfonate as the surfactant (SDBS) (Figure 6.4A). In solution, SWCNTs are surrounded by the nonspecific physical adsorption of SDBS molecules allowing the dispersion of the hydrophobic SWCNTs in aqueous solution.[47,48] SDBS consists of a benzene ring moiety, a charged group, and an alkyl chains. It is suggested that the SWCNTs are stabilized by hemimicelles. Indeed, the alkyl chain part of adjoining surfactant molecules lies flat on the graphitic tube surface. Moreover, π-like stacking of the benzene rings onto the surface of graphite-like structures suggests to increase the binding and surface coverage of surfactant molecules to graphite significantly. When adsorbing onto a small-diameter nanotube surface, it is probably energetically favorable for the chains to lie along the length of the nanotubes rather than to bend around the circumference. Electrostatic repulsion of sulphonate groups (SO_3^-) leads to the charge stabilization of nanotubes via screened coulombic interactions that, by analogy with colloidal particle stabilization, may be significant for dispersion in water.[49]

Interestingly, similar nanotube stabilization was obtained using a sulphonate co-polymer such as Nafion indicating a crucial role in the dispersion stability of SO_3^- groups and a hydrophobic counterpart for a favorable dispersion of CNTs.[50]

Second, when the CNT-ink is spread over the cellulose fibers, the behavior of the SWCNTs-SDBS system on cellulose must be considered. The conductive paper suggests that there is a stronger interaction between SWCNTs and cellulose fibers than SWCNTs-SDBS (Figure 6.4B). The understanding of the microstructure of the substrate could provide some insights in the phenomena that involves the strong interaction between SWCNTs and cellulose thus providing a highly conductive paper. The cellulose fibers are comprised of multiple individual microfibrils. These microfibrils are made of poly-D glucose chains, usually arranged in crystalline, or partially crystalline, domains. This structure allows the fibers to absorb large amounts of water, or other polar solvents, which causes the fibers to swell when placed in such solutions. This phenomenon could explain the change in electrical resistance

that is discussed later. Moreover, Cui *et al* suggested that the electrical resistance of the system is influenced by the porous structure of paper, which leads to large capillary force for the ink.[30] The interaction of these polymeric fibers with SWCNTs thus can be described with two principles.[51] First, large van der Waals forces and hydrogen bonding exist between SWCNTs and the cellulose fibers.[52] Second, the flexibility of SWCNTs allows them to be conformably wrap around cellulose fibers which maximizes the surface contact area between SWCNTs and cellulose fibers.[53,54] Kotov *et al* suggested that SWCNTs have more flexibility than multi walled carbon nanotubes (MWCNTs) leading to stronger adherence to paper.[29] Upon contact, large van der Waals forces and hydrogen bonding occurs, which binds the SWCNTs very tightly to the cellulose thus allowing SWCNTs wrapping around cellulose fibers to create a highly conductive 3D porous structure. In addition, the cellulose is a straight chain polymer with multiple hydroxyl groups (OH^-).[55] Hence, residual chemical end groups -of some types of CNT- such as carboxyl and hydroxyl groups can form strong hydrogen bonds with the hydroxyl groups of the cellulose fibers, leading to the favorable CNT–cellulose inter-facial bonding.[56,57]

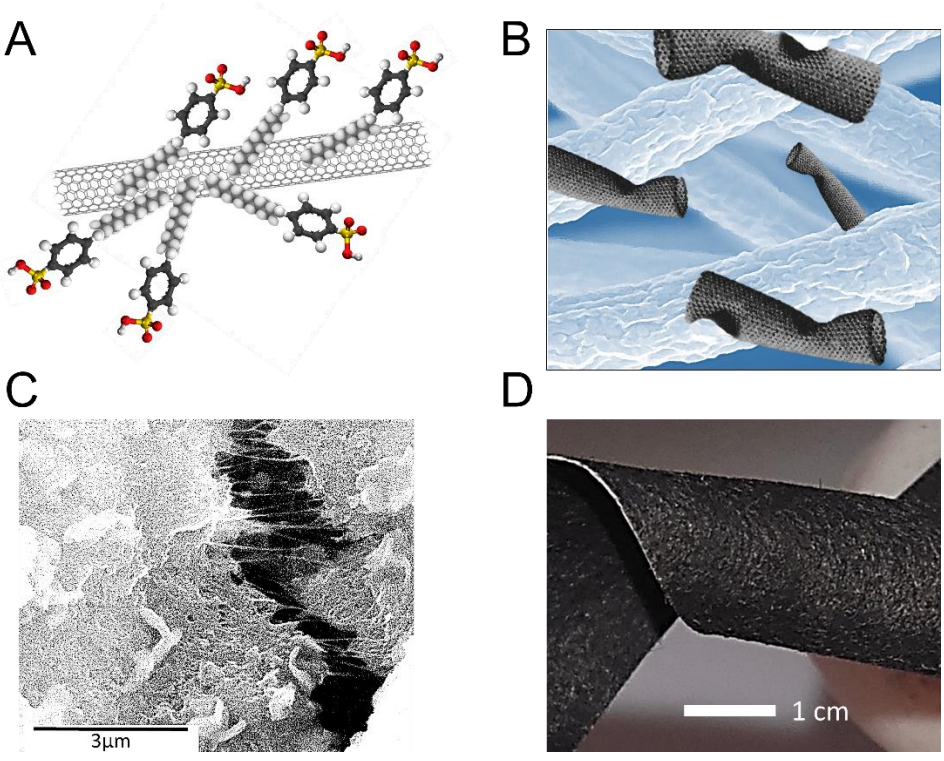

Figure 6.4. SWCNTs-SDBS cellulose paper fabrication scheme. (A) The schematic illustrates SDBS molecules surrounding the SWCNTs for the dispersion in aqueous solution. (B) The illustration represents the SWCNTs wrapping the cellulose microfibrils. (C) ESEM photograph displays the SWCNTs attached to the filter paper cellulose fibers. (D) Photograph showing a piece of filter paper after 6 coatings of SWCNTs-SDBS ink.

In our case, ESEM images confirm that SWCNTs are firmly attached to cellulose fibers of the paper after several painting cycles (Figure 6.4C). Finally, the black color observed after coating the conventional filter paper with CNT ink is a confirmation of the presence of the nanotubes (Figure 6.4D). It should be stressed that the CNTs are firmly attached to the cellulose fibers, since neither leaching of nanotubes nor changes on the electrical resistance of the paper are observed upon washing.

The analytical parameter used for evaluation of the performance of this sensor is the relative change of the electrical resistance (ΔR) of the conductive paper produced upon the addition of water. Some analogous systems have been described in the literature. Kim *et al* and Meyyappan *et al* developed a CNT-cellulose composite able to monitor moisture based on the change in the electrical resistance.[57,58] Similarly, Mäder *et al* and Liu *et al* developed a water sensor based on the CNTs-cellulose fibers composite where it was able to sharply increase the electrical resistance upon the immersion of the sensor in aqueous solution.[59,60] However, these authors did not report a linear relationship between water content and the increment of electrical resistance using conventional paper coated with a SWCNTs ink.

It has been claimed that the change of the electrical resistance of the SWCNTs-SDBS cellulose system depends on two phenomena (Figure 6.5): first, change of resistance due to adsorption; in this case, the water molecules adsorbed on the surface of CNTs change the charge carrier density concentration in the outer layer of graphite, which is responsible for electrical transport, leading to the increase of electrical resistance.[61] Second, the change in resistance due to swelling of the polymer matrix, which disrupts the electron transport between CNT network and causes the electrical resistance of materials to increase.[62] The second phenomenon plays a major role, which involves a fast and larger disconnection of conducting CNT networks induced by the swelling of the cellulose matrix in water.[59,60]

It has been suggested that the highly hygroscopic swelling of the cellulose matrix occurs at the initial contact with the liquid due to the hydrophilic parts of the SDBS molecules. Indeed, the SDBS attached to SWCNTs allows the transport of water molecules inside the system. It is well known that carbon nanotubes are highly hydrophobic. Therefore, in the absence of surfactant, a drop of water on top of a CNT paper will barely wet the surface, but will remain on top with a “spherical” shape. This is because the surface energy of the CNT interface will not be enough to compensate for the surface tension of the water droplet. Therefore, the role of the surfactant is to act as a tensioactive, decreasing the surface tension of water to facilitate the transport across the CNT network.[28] Hence, the surfactant is crucial because

the hydrophobic nature of bare SWCNTs would not allow a rapid swelling behavior of the sensor. The expansion of the cellulose matrix due to the swelling with water induces a large increase of the distance between neighbor nanotubes, thus increasing the tunneling or hopping distances, leading to the sharp increment of the resistance. During the continuous liquid deposition, the cellulose matrix is modified, with the resistivity of the CNT network increasing. Thermodynamic equilibrium (absorption–desorption of water) is expected to take place when relative resistance approaches a plateau after the sharp increase.

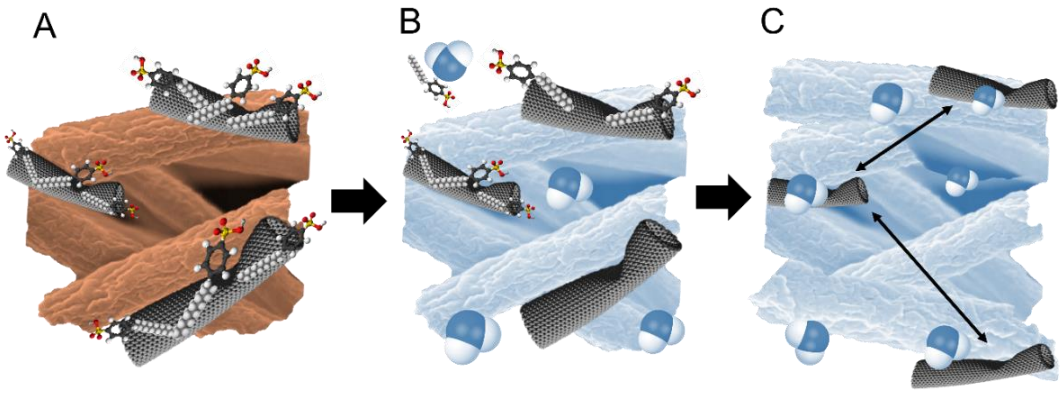

Figure 6.5. Illustration representing the proposed mechanism. (A) SWCNTs are wrapped along the cellulose microfibrils after the SWCNTs-SDBS ink coats by painting technique. (B) Water interacts with the SDBS molecules leaving the SWCNTs exposed to water adsorption as well as swelling between cellulose microfibrils. (C) Water is completely absorbed into the cellulose fibers leading to an increase of the electrical resistance of the whole conductive paper.

Following the work from Mäder *et al,* we can suggest that our sensing approach -monitor aqueous solution- is based on the interaction of water with the SWCNTs-SDBS cellulose system (consequently the sensitivity of the change in resistance, ΔR_T) and might depend on two main factors: First, the number of free hydroxyl groups in the free cellulose (amorphous region), not those linked with each other (crystalline region) or to SWCNTs, by letting the water molecules enter or leave the amorphous region and produce an increase of the percolation distance that leads to a disconnection of the SWCNTs network by swelling as well as a rearrangement of the cellulose microfibrils (ΔR_S); second, the SDBS molecules favor the water incorporation into the SWCNTs-cellulose structure by the dispersion of the SDBS thus removing it from the SWCNTs. Hence, water molecules are adsorbed directly onto the SWCNTs (by replacing the SDBS molecules) and thus perturbing the electron cloud (delocalized π band) along the SWCNTs (ΔR_A). The second factor indicates that the

interaction between SWCNTs and cellulose microfibrils is stronger than between SWCNTs-SDBS. Thus, we can conclude that the interaction between aqueous solution, SDBS, a network of SWCNTs and cellulose microfibrils yields to a global increase in electrical resistance (ΔR_T) provided by an increment of resistance from swelling (ΔR_S) and adsorption (ΔR_A) (Equation 6.1).

$$\Delta R_T = \Delta R_S + \Delta R_A \qquad \text{(Equation 6.1)}$$

Last but not least, the increase of resistance upon addition of aqueous solution is used to develop a chemiresistor sensor for healthcare and fitness applications such as monitoring the sweat loss of an athlete during exercise.

6.3.2. Mechanical Deformation

Withstanding common mechanical deformations without compromising the properties of the desired sensor is of high importance when dealing with use in real scenarios. Particularly, for wearable sensors, the ability of the sensor to conform over curvilinear surfaces is crucial. The flexibility of the CNTs allows them to be deposited efficiently onto the surface of the cellulose fibers as well as withstand common mechanical deformations. In this work, no significant changes in both electrical resistance and mechanical properties were observed after bending and twisting the conductive paper (Figure 6.6). Firstly, a bending process through different angle was applied to the composite. As the macroscopic bending did not affect the nanoscale CNT networks, the resistance change was negligible for various bending states (Figure 6.6A). Secondly, twisting several times was applied to see the effect of higher deformation degree in the resistance of the system. In this case, an increase in resistance value after each 10 times twist was obtained (Figure 6.6B). This phenomenon suggested that micro fractures along the cellulose paper could lead to SWCNTs separation, and then produced a slightly increment in resistance.

Regarding the mechanical properties of the system, the cellulose paper became slightly stiffer after being coated with SWCNTs. Nevertheless, the conductive paper was still very flexible, which is important for the wearability of the sensor and for the on-site real-time sweat monitoring purpose. All in all, a conductive paper with controllable electrical conductivities while preserving original physical properties was prepared through a simple process of painting.

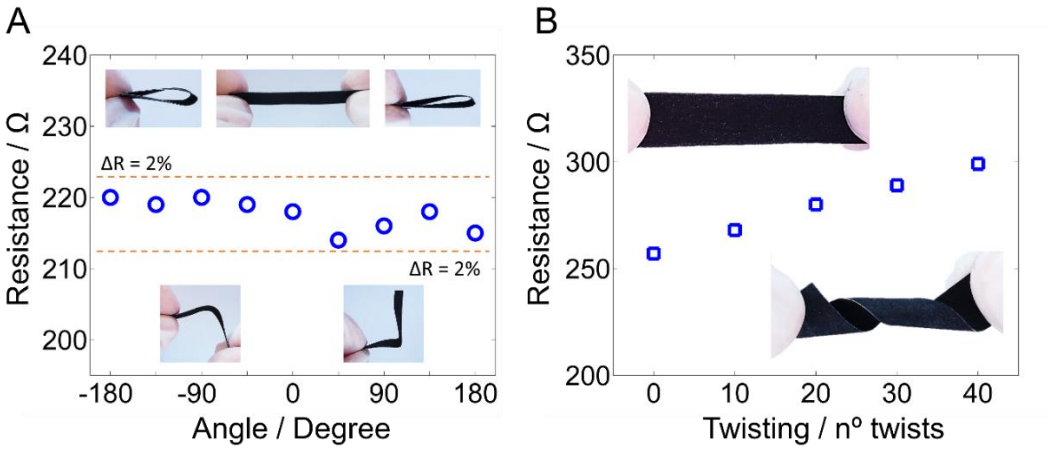

Figure 6.6. Mechanical deformation tests. (A) Bending test over a paper-based sensor during different degrees of freedom, from longitudinal inward to longitudinal outward bends by recording the resistance at each degree. (B) Twisting test over the conductive paper. Resistance obtained after each 10 cycles of twisting for a total of 40 repetitions.

6.3.3. Analytical Performance of the Sensor

In order to describe the sensitivity to water of the SWCNTs-cellulose system, the resistance of the conductive paper during addition of water as a function of time was recorded. For the corresponding calibration plots, the relative resistance (ΔR_{rel} %) as a function of liquid content (µL) was used (Equation 6.2).

$$\Delta R_{rel}\% = \frac{(R_f - R_0)}{R_0} * 100 \qquad \text{(Equation 6.2)}$$

Where R_f is the final resistance after the addition of liquid and R_0 is the original resistance of the system. First, the design of the paper-based sensor is crucial to optimize the response. Indeed, the width of the paper strip plays an important role in the sensor time of response during the experiments of water sensing. Narrower paper allows a faster and sharper change in resistance. In terms of the speed, for a given amount of liquid the water pass through the paper quicker in a thinner than in a wider paper strip. Indeed, the paper strip is acting as a pipe allowing the liquid flowing through a channel. In terms of the sharpness of the response, thinner papers force the liquid to move in the axial direction (i.e., the direction of the electrical field), thus increasing the number of equivalent serial resistors. In the wider papers, it can be considered that -being allowed to move perpendicular to the filed- the equivalent resistance added will be in parallel. Figure 6.7A displays the different response for conductive papers with different in widths (10 mm and 20 mm paper width). Narrower strips (10 mm) show faster, sharper and more sensitive response. Figure 6.7B shows the corresponding calibration

curves for both conditions (N=2). Therefore, the evidence suggests that the width of the system only influences the time of response of the sensor.

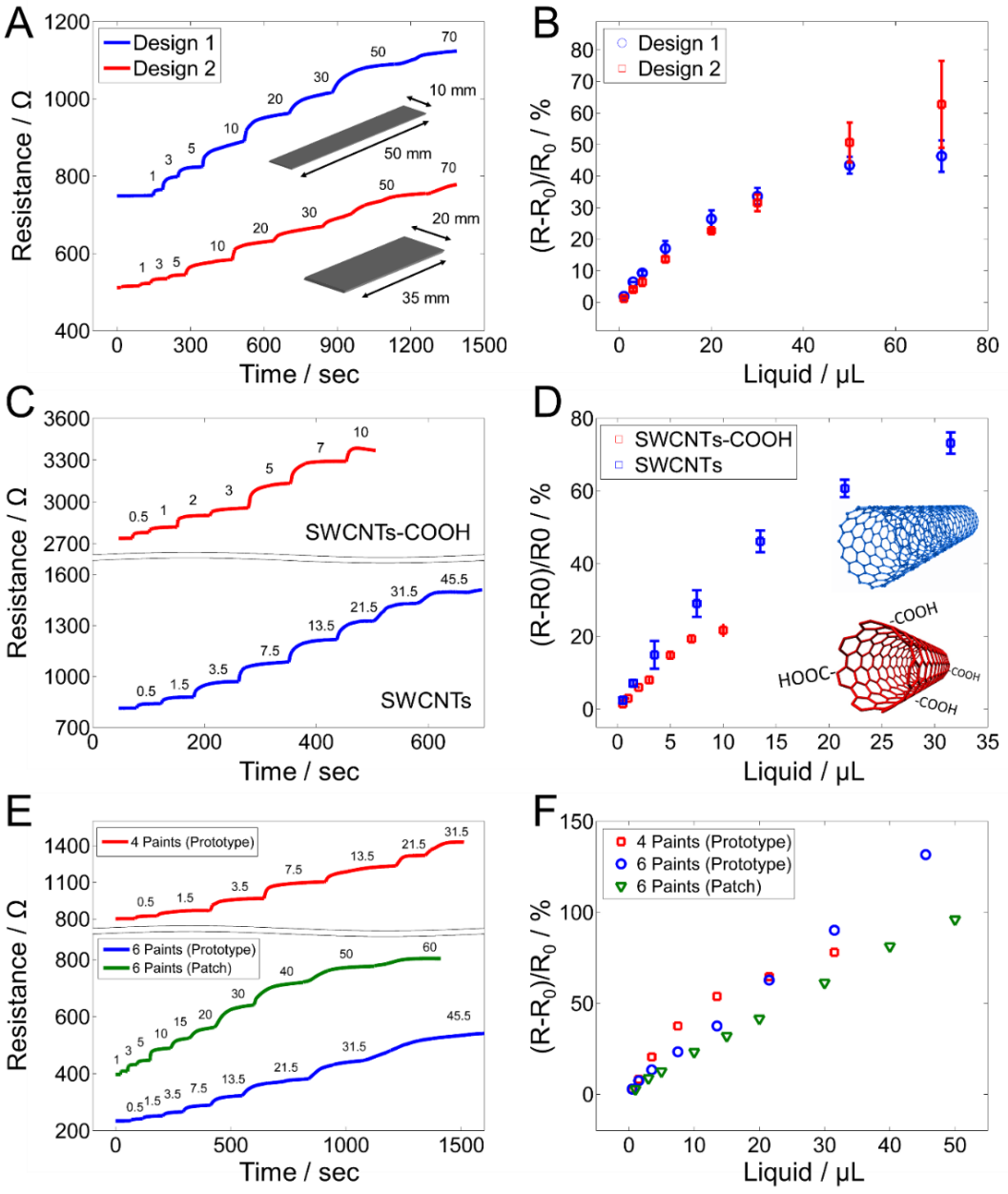

Figure 6.7. Optimization of the analytical performance of the sensor. Top, an evaluation of the width of the conductive paper by different paper size was carried out during water addition; (A) time-trace curves and (B) calibration curves (N=2) for each condition. Center, the effect of water addition to the functionalized SWCNTs by carboxylic group is presented; (C) time-trace curves and (D) calibration curve (N=3). Bottom, the effect of several SWCNTs-SDBS coatings during addition of water over the conductive paper; (E) time-trace curves and (F) calibration curves. The numbers on top of the time traces indicate the volume of liquid added each time.

Second, two different inks were tested in order to understand the interaction between SWCNTs and cellulose microfibrils. Hence, a filter paper was painted with the conventional SWCNTs ink and another with a carboxylated SWCNTs (SWCNTs-COOH) ink, both with the same methodology of preparation (see the experimental section) and number of paints (4 coatings). Interestingly, Figure 6.7C displays higher initial resistance for SWCNT-COOH than for non-functionalized SWCNTs conductive paper. It is suggested that COOH- group disrupt the SDBS-SWCNTs interaction producing a less homogenous ink, consequently high initial resistance value was reached after the paints.[63] Moreover, SWCNTs-COOH wrapped more strongly to the cellulose microfibrils due to the van der Waals forces interactions from OH- of cellulose groups and -COOH interfering with the change in conductivity of the system. Figure 6.7D presents the comparison of the calibration curve with conductive papers made with SWCNTs and functionalized SWCNTs-COOH. SWCNTs with carboxyl functional groups on the surfaces and in the ends, which can form strong hydrogen bonds with the hydroxyl groups in the cellulose fibers, lead to a narrower linear range upon aqueous solution interaction from 0.5 µL to 7 µL in comparison to 1.5 µL to 31.5 µL from SWNCTs (N=3). This phenomenon is in agreement with the mechanism previously described. As more functional group SWCNTs have, more strong interaction with cellulose exists decreasing the swelling capacity of the composite. It is suggested that only the resistance change from adsorption was performed using SWCNTs-COOH ink. All in all, non-functionalized SWCNTs ink was chosen for further applications, since it provides a broader linear range.

In order to improve the analytical performance of the paper-based sensor, an optimization of the number of layers painted over the paper was carried out. Figure 6.7E shows time- trace plots for 4 and 6 coatings using the prototype to perform studies of the analytical performance. Additionally, a comparison between the prototype and the final wearable patch was executed (showed in Figure 6.1). As it was expected, the initial resistance decreased as more layers of ink were applied. It is important to stress that, in order to increase the usability of the sweat sensor, the optimization of the linear range is paramount. Even if the sensitivity is good, a linear range that is too short will soon turn the sensor useless. As a matter of fact, this is problem found in many of the current option for sweat sensors. Skin galvanic conductance, for example, is highly sensitive to detect the onset of sweat, but the response quickly flattens out as a thin layer of liquid covers the skin. Therefore, the secret to create a truly useful sweat sensor is to maintain a high sensitivity while increasing as much as possible the linear range. Accordingly, Figure 6.7F compares the performance of two conductive

papers with different number of ink layers. First, a paper with 4 coatings, and second, one with 6 coatings. The performance of these two sensors can be seen in Table 6.1.

Table 6.1. Comparison of analytical parameters of paper-based sensors of 4 and 6 paints.

nº of coatings	Sensitivity / $\Delta R\%\ \mu L^{-1}$	Linear Range / µL
4 coatings	1.62	7.5 – 31.5
6 coatings	2.83	3.5 – 45.5
6 coatings / wearable patch	1.88	3 – 50

The comparison of performance was conducted with conductive papers of 4 and 6 coatings of ink because after the fourth coating the electrical resistance stabilizes and does not significantly change upon more coatings (see for example Figure 6.1A). The study shows good performance for both papers. However, the sensitivity and the linear range was improved for papers with 6 coatings. Thus, 6 coatings were chosen as the best condition to develop the sweat sensor because it shows wider linear range thus enabling the monitoring of higher perspiration activity.

These differences in sensitivity can be ascribed to a complete deployment of a network of CNT and SDBS over the cellulose fibers. In any case, it was considered that a paper with 6 layers of coating shows an optimum performance for this type of application. Therefore, this system was used to build a patch prototype as shown in Figure 6.2. The calibration plot of this wearable patch showed a slight decrease on the slope, although maintaining an excellent linearity (Figure 6.7F and Table 6.1). The decrease in the slope might be due to changes in the swelling behavior of the sensor due to a slightly different design (more compact) adjusted to ergonomic needs.

The stability of the conductive paper embedded into a wearable patch was assessed by a mid-term period measurement of the electrical resistance showing a value of 126.16±0.35 Ω. The dry conductive paper yielded a highly stable response with only a slightly drift (152.08 $\mu\Omega\ h^{-1}$) over 6 hours. The assay reflected a negligible increment (ΔR_{rel} = 0.7%) during the assay demonstrating the excellent stability of the SWCNTs-SDBS paper.

Reproducibility between Sensors

When thinking about producing a decentralized tool to be operated by an unexperienced end-user, simplicity of operation is essential. Calibration of the sensor is one of the typical

stages where expertise is required. Calibration is time and resource consuming, and can be complicated to perform outside the lab. This has been one of the major reasons why physical -but not chemical- sensors have been able to achieve quickly a mass market. The ability to produce calibration free sensors is a major goal for decentralized chemical systems. In this way, this work presents the development of a conductive paper with highly reproducible behavior within a batch production. Thus, only a calibration of a paper-based sensor from the manufactured conductive paper yields the same performance in all the paper-based sensors produced within the same batch.

The use of this approach to monitor liquid was demonstrated by a reproducibility test using a conductive paper of 6 coatings of ink using the prototype platform and the wearable patch platform). Figure 6.8A presents the calibration curve using the prototype platform performing a slope of 2.66±0.1 $\Delta R\%\ \mu L^{-1}$ (N=4) within a linear range from 3.5 µL to 45.5 µL. Finally, for the wearable patch platform a slope of 2.07±0.2 $\Delta R\%\ \mu L^{-1}$ (N=3) within a linear range from 3 µL to 50 µL (Figure 6.8B). Hence, the experimental work demonstrated high reproducibility between manufacturing batches. Indeed, only one calibration curve of each batch is necessary to have reliable information for the other already manufactured sensors. Hence, a calibration-free approach could be applied for on-site testing.

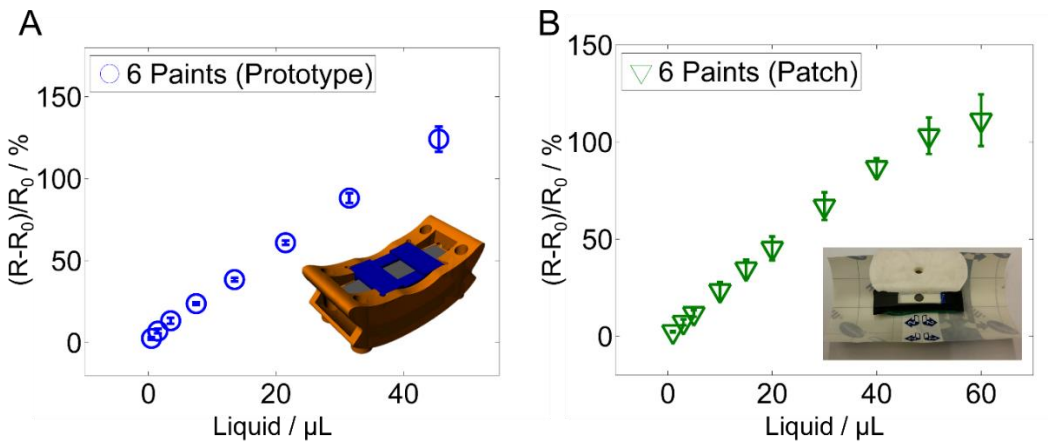

Figure 6.8. Reproducibility study. (A) Calibration curve from 6 coatings of SWCNTs ink paper (N=4). (B) Calibration curve using the wearable patch with 6 coats of ink conductive paper (N=3).

6.3.4. Dynamic Flowing Conditions

The aim of this sensor is to measure a flow of liquid over time to calculate the amount of liquid loaded for a sensor on a given area. Indeed, one of the future applications envisioned

for this sensor is to measure the dehydration status of a person by monitoring the sweat loss. Hence, before moving forward towards the end-user application (i.e., on-body measurements) a flow test was performed. In this experiment, an emulation of a constant sweat-rate (1.37±0.1 µL min^{-1}, N=3) was performed by a microfluidic pump that is continuously providing liquid to the sensing area. Figure 6.9A shows the pattern produced by the flow of liquid discharged directly onto the sensor surface. A constant increase of the resistance is observed. Figure 6.9B shows the calculated flow rate from the sensor taking into account the change in resistance, time and the parameters calculated by the previous calibration curve. This curve shows 3 well defined regions. The first points, where a slightly noisier pattern for flow rate is obtained, shows a somehow larger values of flow rates. This part, however, corresponds to the stabilization of the sensor and it is normally outside the linear range. Then, a constant flow rate can be predicted by the sensor during 30 minutes of the liquid flowing, according to the constant flow rate provided by the pump. An accuracy of 105% in the prediction of the final amount of liquid sensor and pump values was obtained. Finally, at the end, the variation resulted in a saturation of the paper-based sensor. All in all, the sensor exhibited excellent correlation for long-term monitoring of this small amounts of liquid flowing.

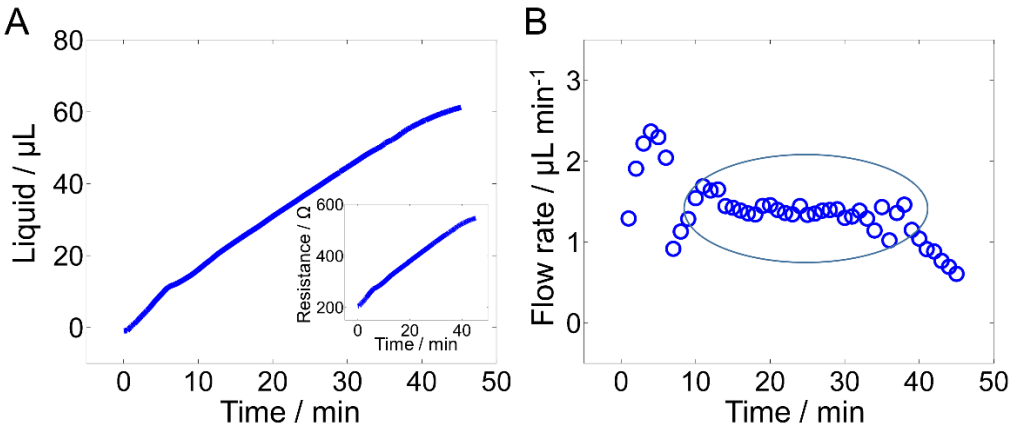

Figure 6.9. Dynamic flowing conditions test. (A) Continuous liquid monitoring provided by a flow pump using artificial sweat. Inset shows the corresponding increment in resistance without any interruptions. (B) Monitoring of flow-rate calculated from the paper-based sensor.

6.3.5. On-body Testing

This sensor is relevant in a large number of applications, ranging from healthcare, security, safety alarms or sport performance.[31,64] However, in this work, the use of the sensor

was focused on the field of physical fitness: the dehydration status of human body through monitoring the sweat loss. Knowing the amount of sweat loss in a specific body area let to an extrapolation of the whole body water loss thus to understand the dehydration status of a person.[65] By using the calculation of the whole body area, the regional factor (depending on the specific area of perspiration)[66] and corrected for fluid/food intake and urine output, the whole sweat loss can be estimated with the liquid sensor.[67] Therefore, the liquid or sweat sensor can provide real-time information of the dehydration status as the other factors are constant during the exercise. All in all, this meaningful data helps the person/athlete/coach to take actions in real-time avoiding unnecessary efforts or even preventing injuries.[68,69]

Preliminary studies with human subjects were carried out using the wearable patch platform. The disposable wearable patch was chosen to be the suitable platform for sweat loss monitoring as it was easy to stick on-body, thus to manipulate the sensor. Moreover, as a low-cost sensor, it can be discarded after use, and thus avoids contaminations between trials. Human subjects were recruited for evaluating the on-body performance of the new sweat sensor. During this study, the wearable patch was applied to the upper back of several participants during cycling exercise in a stationary bicycle (Figure 6.10A).

Figure 6.10B illustrates different designs for on-body testing platforms. A 3D printed wristband encompassed the SWCNTs paper-based sensor and allows to monitor the amount of liquid loss during perspiration in the wrist. This approach might create more value for entering the market as the use of wristbands are widespread on the market. In contrast, to study the sweat loss patterns along the regional parts of the body, a wearable patch approach is more comfortable for the wearer and allows to place extra sensors simultaneously (see the inset).

The ability of the sensor to monitor in real-time sweat loss was first examined by interfacing the wearable patch with a lab-based recorder. Figure 6.10C shows the sensor response to sweat during 45 minutes of high intensity cycling exercise. The inset presents the sensor change of resistance through time. In this case, the sensor was located in the upper back of a subject under high humidity conditions to assess the maximum rate of perspiration of the participant. The sensor showed ability to monitor the sweat loss from the subject in a specific skin area provided by the active window of the sensor.

According the sensor, sweat loss of this subject was almost 55 µL in that specific area. It is relevant to mention that the size of the window was 0.28 cm^2. Thus, knowing the regional factor and the whole body area, the sweat loss from the whole body can be extrapolated.

Interestingly, the window of the sensor can be modified accordingly to the application to fit the linear range of the sensor to the dehydration level of the athlete. During the on-body testing, the lack of sweat at the beginning of exercise led to a planar signal (high stability) until the subject started the perspiration and thus sensor resistance increased (approximately after 7 minutes). Hence, the sensor demonstrates the ability to show patterns of sweat loss. After 20 minutes cycling, there is a sharp increase due to an increment of the subject exercise intensity. The sensitivity of the sweating response on the regional parts of the body increased significantly only with changes to high intensity due to the thermoregulation and thus the cutaneous vasodilation of the body skin.[70,71] Subsequently, a mid-high intensity was maintained until 35 minutes where another high intensity exercise was performed. This is very interesting, since it is suggesting that the sensor can discriminate intensities between exercises. Several subjects presented similar sweat patterns, although there were significant differences in the amount of sweat loss. This indicates that each subject has different physiological performance and demands, thus adding value to the sweat sensor. Hence, this approach to individual monitoring of sweat loss opens an avenue towards the development of personalized hydration strategies for an improvement of the performance in the sports field.

Furthermore, a validation study was carried out using the comparison between the developed sensor and the existing standard methodology to monitor sweat loss values (difference of weight by regional absorbent-patch method).[41,72] Regional absorbent-patch method was performed by weighting the patch before and after the cycling exercise (by duplicates). These patches were stacked next to the wearable sensor to avoid regional sweat-rate differences. Moreover, the same area was exposed for both methodologies. Figure 6.10D presents the comparison between sensor and standard methodologies leading to a linear relationship among samples during one cycling exercise. Absorbent patch samples were removed and weighted at different time frames (indicated in Figure 6.10D) and compared to continuously data monitoring from the sensor. A linear relation of $y=0.89x-0.3$ was obtained indicating an outstanding relationship between methods. The recovery (chemiresistor/absorbent patch) of all data (5 points) was 113.2±31.2 %. It is important to remark that the wearable sensor was able to autonomously monitor the perspiration dynamics. Indeed, the wearable system correlates to the absorbent patch technique without the necessity to manipulate the samples.

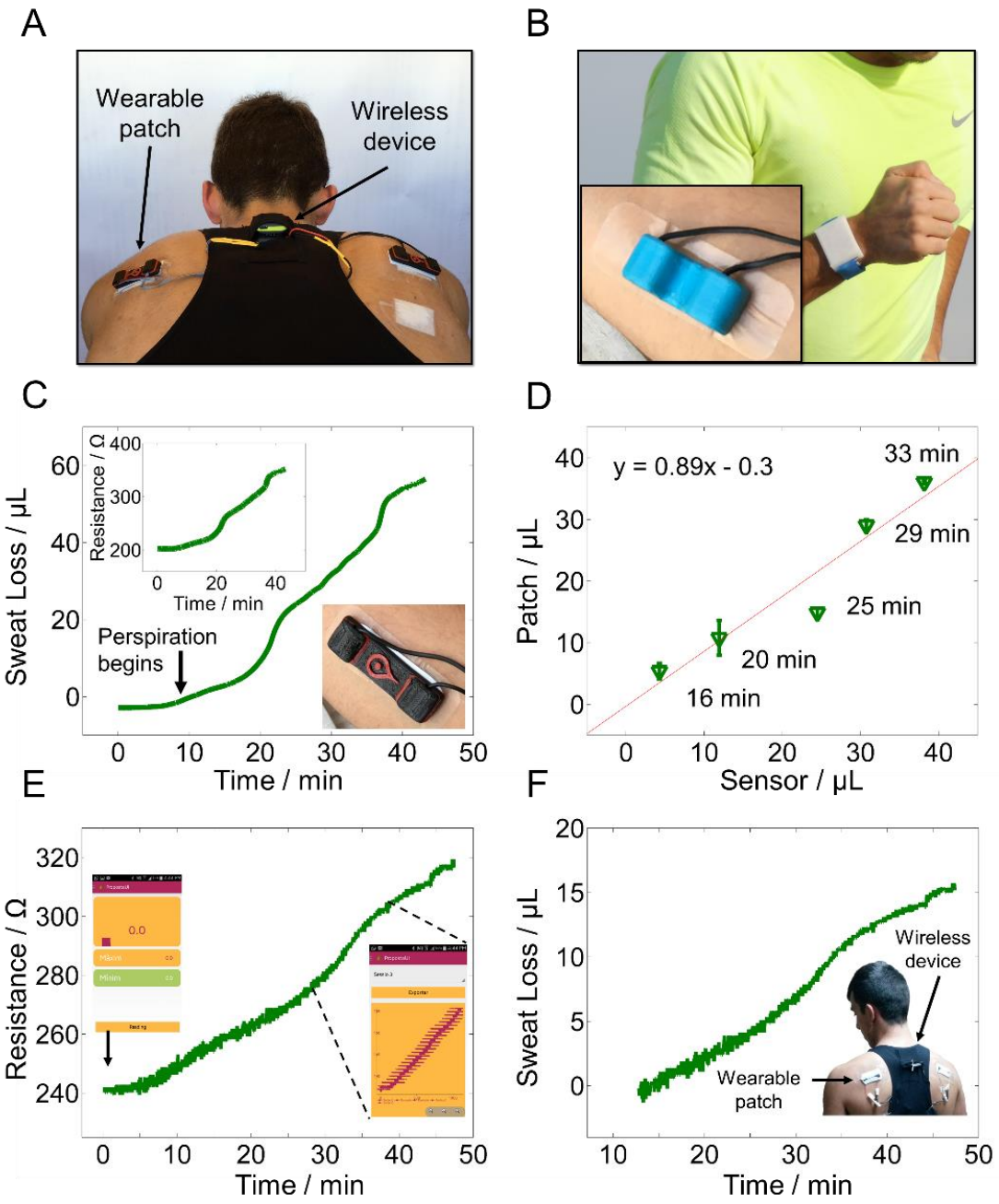

Figure 6.10. On body testing. (A) Photograph of the wearable patch on the upper back of a subject during cycling exercise. (B) Wristband design of the sweat sensor and wearable patch design magnification (inset). (C) On-body measurement at real-rime of the perspiration dynamics using the wearable sensor (inset shows the resistance increment). (D) Comparison of sweat loss values between wearable sensor and regional absorbent-patch method (N=3). (E) Monitoring of the real-time sweat by the use of a wireless reader and a mobile phone interface. Two screenshots from the cell phone app obtained during the on-body tests. (F) Sweat loss pattern of the subject. All the sweat loss plots were recorded during cycling exercises.

The subsequent phase of the on-body study involved implementing a commercial wireless multimeter to capture with a cellphone the data generated by the sweat sensor in real time. Particularly, the cell phone application (app) was designed for Android mobile operating system and can be used in all types of Android devices (tablets and cell phones) that have Bluetooth wireless module. During the on-body studies, the wireless device seamlessly transmitted the real-time analytical data over a maximum distance of 5 m (limitation of the Bluetooth technology) from the sweat sensor to the Android system. Figure 6.10E shows the increment in resistance during a cycling exercise provided by a sensor placed on the upper back of a male participant. This figure also illustrates the app interface between the user and the sensor at the initial step and during the exercise. The app was able to show the real-time increase of resistance thus the subject perspiration pattern. Finally, Figure 6.10F presents the corresponding sweat loss pattern providing valuable information regarding the real-time hydration status of the wearer. Despite an increase of the background noise due to the Bluetooth transceiver, a clear sweat loss increment was observed. The overall trend was comparable to the profile obtained with the lab-based recorder. The incorporation of a Bluetooth reader obviated the need for connectors and thus greatly facilitates moving from the lab-based measurement to the on-site monitoring. The autonomous, portable nature of the system makes the wearable device user-friendly without compromising the ability of the sensor to monitor at real-time the perspiration dynamics of the wearer during prolonged exercise.

6.4. Conclusions

Highly conductive paper based on SWCNTs-SDBS ink was successfully developed allowing accurate measurements of the total amount of aqueous solution by monitoring the change in electrical resistance. The paper-based sensor was easily prepared by a simple painting process. The randomly aligned SWCNTs networks were wrapped around the cellulose microfibrils leading to an electrically conductive paper. Indeed, the SWCNTs paper generated an electrical pathway reaching a resistance of 200 Ω sq^{-1}. The role of SDBS-SWCNTs and cellulose system in the mechanism of the increment in electrical resistance upon liquid addition is discussed. Moreover, the paper-based sensor has been demonstrated as a sensitive and highly reproducible device for monitoring liquid content with a change in the relative electrical resistance of up to 130%. This chapter also discuss a potential way to use the sensor for monitoring sweat loss as wearable technology. Easy manipulation, autonomy, robustness, simplicity and seamless integration make the sensor more

advantageous in front of other available techniques for the determination of the sweat loss of the human body during exercise. Finally, the integration of a Bluetooth multimeter with the sweat sensor demonstrates the ability to provide wirelessly data in real-time from the perspiration dynamics thus the dehydration status of the human body. In comparison to other established techniques, the sweat sensor is aimed to be leading the sweat monitoring in the field. This application shows outstanding promise to contribute with novel individualized physiological insights for the sport and wellbeing field. Moreover, such integration of flexible chemical sensors in wearable platforms will lead to the next-generation of wearable devices for personalized medicine, fitness and sport disciplines.

6.5. References

[1] A. Harvey, A. Brand, S. T. Holgate, L. V. Kristiansen, H. Lehrach, A. Palotie, B. Prainsack, N. Biotechnol. 2012, 29, 625.

[2] B. Solnica, J. W. Naskalski, J. Sieradzki, Clin. Chim. Acta 2003, 331, 29.

[3] A. P. F. Turner, Chem. Soc. Rev. 2013, 42, 3184.

[4] J. Wang, Chem. Rev. 2008, 108, 814.

[5] A. A. Kumar, J. W. Hennek, B. S. Smith, S. Kumar, P. Beattie, S. Jain, J. P. Rolland, T. P. Stossel, C. Chunda-Liyoka, G. M. Whitesides, Angew. Chemie Int. Ed. 2015, 54, 5836.

[6] M. S. Patel, D. a Asch, K. G. Volpp, JAMA 2015, 313, 459.

[7] W. Zeng, L. Shu, Q. Li, S. Chen, F. Wang, X. M. Tao, Adv. Mater. 2014, 26, 5310.

[8] K. Takei, W. Honda, S. Harada, T. Arie, S. Akita, Adv. Healthc. Mater. 2015, 4, 487.

[9] A. J. Bandodkar, J. Wang, Trends Biotechnol. 2014, 32, 363.

[10] D. Son, J. Lee, S. Qiao, R. Ghaffari, J. Kim, J. E. Lee, C. Song, S. J. Kim, D. J. Lee, S. W. Jun, S. Yang, M. Park, J. Shin, K. Do, M. Lee, K. Kang, C. S. Hwang, N. Lu, T. Hyeon, D.-H. Kim, Nat. Nanotechnol. 2014, 9, 397.

[11] A. J. Bandodkar, W. Jia, J. Wang, Electroanalysis 2015, 27, 562.

[12] R. Chambers, T. J. Gabbett, M. H. Cole, A. Beard, Sport. Med. 2015, 1065.

[13] W. Gao, S. Emaminejad, H. Y. Y. Nyein, S. Challa, K. Chen, A. Peck, H. M. Fahad, H. Ota, H. Shiraki, D. Kiriya, D.-H. Lien, G. A. Brooks, R. W. Davis, A. Javey, Nature 2016, 529, 509.

[14] Y. Wang, L. Wang, T. Yang, X. Li, X. Zang, M. Zhu, K. Wang, D. Wu, H. Zhu, Adv. Funct. Mater. 2014, 24, 4666.

[15] T. Q. Trung, S. Ramasundaram, B. U. Hwang, N. E. Lee, Adv. Mater. 2015, 28, 502.

[16] A. J. Bandodkar, D. Molinnus, O. Mirza, T. Guinovart, J. R. Windmiller, G. Valdés-Ramírez, F. J. Andrade, M. J. Schöning, J. Wang, Biosens. Bioelectron. 2014, 54, 603.

[17] T. Guinovart, A. J. Bandodkar, J. R. Windmiller, F. J. Andrade, J. Wang, Analyst 2013, 138, 7031.

[18] L. Florea, D. Diamond, Sens. Act. B Chem. 2015, 211, 403.

[19] T. Q. Trung, N. E. Lee, Adv. Mater. 2016, 1.

[20] A. J. Bandodkar, I. Jeerapan, J. Wang, ACS Sensors 2016, 1, 464.

[21] M. Parrilla, J. Ferré, T. Guinovart, F. J. Andrade, Electroanalysis 2016, 28, 1267.

[22] T. Guinovart, M. Parrilla, G. a Crespo, F. X. Rius, F. J. Andrade, Analyst 2013, 138, 5208.

[23] M. Parrilla, R. Cánovas, I. Jeerapan, F. J. Andrade, J. Wang, Adv. Healthc. Mater. 2016, 5, 996.

[24] A. J. Bandodkar, W. Jia, C. Yard, X. Wang, J. Ramirez, J. Wang, Anal. Chem. 2014, 87, 394.

[25] K. Kordás, T. Mustonen, G. Tóth, H. Jantunen, M. Lajunen, C. Soldano, S. Talapatra, S. Kar, R. Vajtai, P. M. Ajayan, Small 2006, 2, 1021.

[26] B. Zhao, H. Hu, A. Yu, D. Perea, R. C. Haddon, J. Am. Chem. Soc. 2005, 127, 8197.

[27] Y. Wang, Z. Iqbal, S. Mitra, J. Am. Chem. Soc. 2006, 128, 95.

[28] L. Vaisman, H. D. Wagner, G. Marom, Adv. Colloid Interface Sci. 2006, 128-130, 37.

[29] L. Wang, W. Chen, D. Xu, B. S. Shim, Y. Zhu, F. Sun, L. Liu, C. Peng, Z. Jin, C. Xu, N. a Kotov, Nano Lett. 2009, 9, 4147.

[30] L. Hu, J. W. Choi, Y. Yang, S. Jeong, F. La Mantia, L.-F. Cui, Y. Cui, Proc. Natl. Acad. Sci. U. S. A. 2009, 106, 21490.

[31] S. N. Cheuvront, R. W. Kenefick, Compr. Physiol. 2014, 4, 257.

[32] T. R. Ebert, D. T. Martin, N. Bullock, I. Mujika, M. J. Quod, L. a. Farthing, L. M. Burke, R. T. Withers, Med. Sci. Sports Exerc. 2007, 39, 323.

[33] N. A. Taylor, C. a Machado-Moreira, Extrem. Physiol. Med. 2013, 2, 4.

[34] L. E. Armstrong, Nutr. Rev. 2005, 63, S40.

[35] M. Beauchamp, L. C. Lands, Pediatr. Pulmonol. 2005, 39, 507.

[36] P. Salvo, F. Di Francesco, D. Costanzo, C. Ferrari, M. G. Trivella, D. De Rossi, A. Theory, IEEE Sens. J. 2010, 10, 1557.

[37] S. P. von Duvillard, W. A. Braun, M. Markofski, R. Beneke, R. Leithäuser, Nutrition 2004, 20, 651.

[38] A. E. Jeukendrup, J. Sports Sci. 2011, 29, S91.

[39] D. J. Casa, P. M. Clarkson, W. O. Roberts, Curr. Sports Med. Rep. 2005, 4, 115.

[40] H. Gatterer, K. Schenk, L. Laninschegg, P. Schlemmer, H. Lukaski, M. Burtscher, PLoS One 2014, 9, 1.

[41] C. E. Dziedzic, M. L. Ross, G. J. Slater, L. M. Burke, Int. J. Sport Physiol. Perform. 2014, 9, 832.

[42] G. Havenith, A. Fogarty, R. Bartlett, C. J. Smith, V. Ventenat, Eur. J. Appl. Physiol. 2008, 104, 245.

[43] E. J. Parra, P. Blondeau, G. A. Crespo, F. X. Rius, Chem. Commun. 2011, 47, 2438.

[44] C. Callewaert, B. Buysschaert, E. Vossen, V. Fievez, T. Van de Wiele, N. Boon, J. Microbiol. Methods 2014, 103, 6.

[45] L. Hu, H. Wu, Y. Cui, Appl. Phys. Lett. 2010, 96, 2008.

[46] M. Novell, M. Parrilla, G. Crespo A., F. X. Rius, F. J. Andrade, Anal. Chem. 2012, 84, 4695.

[47] K. B. Holt, C. Ziegler, J. Zang, J. Hu, J. S. Foord, J. Phys. Chem. C 2009, 113, 2761.

[48] J. W. Han, B. Kim, J. Li, M. Meyyappan, Appl. Phys. Lett. 2013, 102, 193104.

[49] M. F. Islam, E. Rojas, D. M. Bergey, A. T. Johnson, A. G. Yodh, Nano Lett. 2003, 3, 269.

[50] J. Wang, M. Musameh, Y. Lin, J. Am. Chem. Soc. 2003, 125, 2408.

[51] L. Hu, M. Pasta, F. La Mantia, L. Cui, S. Jeong, H. D. Deshazer, J. W. Choi, S. M. Han, Y. Cui, Nano Lett. 2010, 10, 708.

[52] T. Hertel, R. E. Walkup, P. Avouris, Phys. Rev. B 1998, 58, 13870.

[53] S. Iijima, C. Brabec, A. Maiti, J. Bernholc, J.Chem.Phys. 1996, 104, 2089.

[54] M. R. Falvo, G. J. Clary, R. M. Taylor, V. Chi, F. P. Brooks, S. Washburn, R. Superfine, Nature

1997, 389, 582.

[55] R. J. Moon, A. Martini, J. Nairn, J. Simonsen, J. Youngblood, Chem. Soc. Rev. 2011, 40, (7), 3941.

[56] R. E. Anderson, J. Guan, M. Ricard, G. Dubey, J. Su, G. Lopinski, G. Dorris, O. Bourne, B. Simard, J. Mater. Chem. 2010, 20, 2400.

[57] S. Yun, J. Kim, Sens. Act. B Chem. 2010, 150, 308.

[58] J.-W. Han, B. Kim, J. Li, M. Meyyappan, J. Phys. Chem. C 2012, 116, 22094.

[59] H. Qi, E. Mäder, J. Liu, Sens. Act. B Chem. 2013, 185, 225.

[60] H. Qi, J. Liu, Y. Deng, S. Gao, E. Mäder, J. Mater. Chem. A 2014, 2, 5541.

[61] D. R. Kauffman, A. Star, Angew. Chemie - Int. Ed. 2008, 47, 6550.

[62] T. Villmow, S. Pegel, A. John, R. Rentenberger, P. Pötschke, Mater. Today 2011, 14, 340.

[63] C. K. Najeeb, J.-H. Lee, J. Chang, J.-H. Kim, Nanotechnology 2010, 21, 385302.

[64] G. P. Bates, V. S. Miller, J. Occup. Med. Toxicol. 2008, 3, 4.

[65] C. J. Smith, G. Havenith, Med. Sci. Sports Exerc. 2012, 44, 2350.

[66] D. Fournet, L. Ross, T. Voelcker, B. Redortier, G. Havenith, J. Therm. Biol. 2013, 38, 339.

[67] L. B. Baker, K. A. Barnes, M. L. Anderson, D. H. Passe, J. R. Stofan, J. Sports Sci. 2016, 34, 358.

[68] R. M. Morgan, M. J. Patterson, M. a. Nimmo, Acta Physiol. Scand. 2004, 182, 37.

[69] R. J. Maughan, S. M. Shirreffs, Scand. J. Med. Sci. Sports 2010, 20, 40.

[70] N. Kondo, S. Takano, K. Aoki, M. Shibasaki, H. Tominaga, Y. Inoue, Acta Physiol. Scand. 1998, 164, 71.

[71] G. P. Kenny, J. Periard, W. S. Journeay, R. J. Sigal, F. D. Reardon, J. Appl. Physiol. 2003, 95, 2355.

[72] L. B. Baker, J. R. Stofan, A. a Hamilton, C. a Horswill, J. Appl. Physiol. 2009, 107, 887.

UNIVERSITAT ROVIRA I VIRGILI
NEW ELECTROCHEMICAL SENSORS FOR DECENTRALIZED ANALYSIS
Marc Parrilla Pons

Part 3

Beyond the Detection of Ions: Novel Strategies for the Determination of other Relevant targets

UNIVERSITAT ROVIRA I VIRGILI
NEW ELECTROCHEMICAL SENSORS FOR DECENTRALIZED ANALYSIS
Marc Parrilla Pons

Chapter 7

Enhanced Potentiometric Detection of Hydrogen Peroxide Using a Platinum Electrode Coated with Nafion

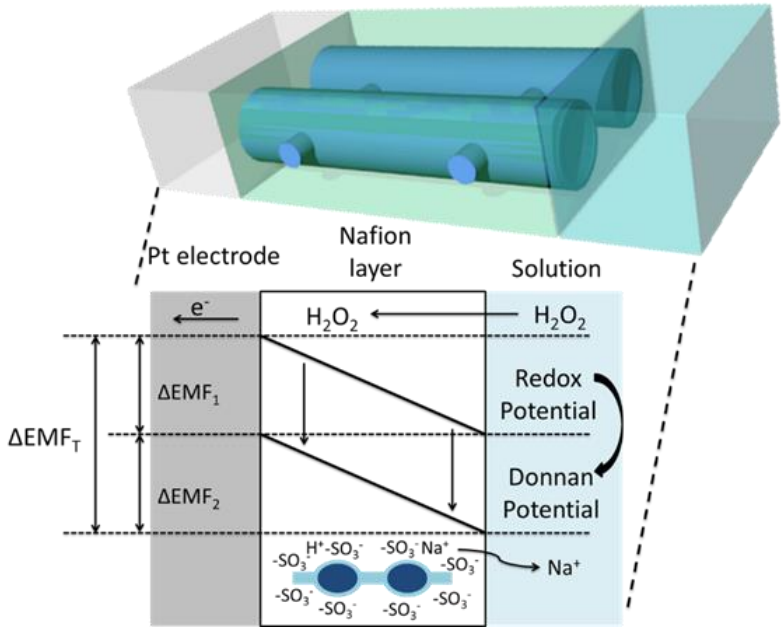

UNIVERSITAT ROVIRA I VIRGILI
NEW ELECTROCHEMICAL SENSORS FOR DECENTRALIZED ANALYSIS
Marc Parrilla Pons

This chapter presents the potentiometric redox response to hydrogen peroxide of a platinum electrode coated with a layer of Nafion®. The results show that the Nafion ion-exchange membrane acts as an effective permselective barrier against negative ions, thus significantly reducing the response to some redox active species, such as ascorbate. Even more interesting, though, these coated electrodes show a significant enhancement in sensitivity to H_2O_2 when the measurements are performed in solutions of high ionic strength. The influence of pH, ionic strength and supporting electrolyte on this enhancement are presented. Under optimized conditions these coated electrodes show a linear dependence with the logarithm of the concentration of H_2O_2, with sensitivities of -125.1±5.9 mV decade^{-1} (several times higher than the bare electrodes) and a linear range that spans from 10^{-5} to 10^{-3} M of H_2O_2. Preliminary studies suggest that the coupling between the redox equilibrium at the electrode and the Donnan potential of the membrane play a role on this enhancement. Considering this improved sensitivity, stability and linear ranges, this system shows promise as a platform to build enzyme-based potentiometric biosensors.

7.1 Introduction

The working principle of a large number of chemical and biochemical sensors is based on the use of an enzymatic reaction that generates hydrogen peroxide (H_2O_2), a substance that is then detected using a suitable analytical technique.[1–5] Therefore, finding alternative methods for the sensitive and selective detection of H_2O_2 may have significant impact in all those fields -such as clinical diagnostics,[6] food [7] and environmental analysis [8], etc.- where these biosensors play a central role.

Among the many different alternatives, the detection of H_2O_2 using electrochemical techniques is particularly attractive since it allows the integration of the enzyme-electrode system into a simple and compact arrangement. Voltammetric techniques have been traditionally preferred because they provide high sensitivity and low limits of detection. As a result, bioanalytical platforms[9,10] using enzyme-based amperometric sensors have become almost the norm, and because of this success the development of alternative solutions has been somehow hindered.[11,12] Nevertheless, with the growing interest on devices for point of care and decentralized measurements, new platforms that can offer additional advantages -such as simplicity of operation and cost- are increasingly required.[13,14] For this reason, potentiometric detection is re-gaining momentum. Potentiometry shows unrivalled simplicity of operation and instrumentation, low power consumption, easy of miniaturization and -with the recent trends, such as paper-based devices[15]- ability to produce ultra-low-cost

sensors.[16] Therefore, in many applications where extremely low limits of detection might not be a main issue, potentiometric tools may offer a simple and affordable alternative.[17]

A major limitation for the electrochemical detection of H_2O_2 is the interference produced by other redox-active species, such as ascorbic acid,[18,19] often present in biological media. To deal with this problem, the use of polyelectrolytes as permselective membranes has been successfully applied.[20] Nafion -for example- a negatively charged sulfonated tetra-fluoroethylene-based polymer, has been used as an effective barrier against electrode fouling and the interference produced by large negative ions.[21–23] Amperometric electrodes that are coated with this polymer have shown an improved stability and selectivity towards negatively charged redox species, such as ascorbate.[24,25] In the case of potentiometric methods, the direct detection of H_2O_2 can be easily performed using a platinum electrode. However, it is evident that this approach is also heavily interfered by the presence of redox active species.[26] Interestingly, to the best of our knowledge, the use of permselective membranes (such as Nafion) to coat platinum (Pt) electrodes for the potentiometric detection of H_2O_2 has not been yet reported.

It is worth noticing that the nature of the potentiometric response between H_2O_2 and bare Pt electrodes is not yet fully understood and has been the subject of many recent studies.[27–29] It has been shown that the H_2O_2-Pt system presents a non-Nernstian response, with the slopes that vary depending on the crystalline structure of the Pt, the surface of the electrode and its interaction with the solution pH and composition, as well as the several the reactions involved in the decomposition of H_2O_2. Additionally, the use of polyelectrolytes for coating the electrodes adds complexity to the system. The electrochemical response of electrodes coated with polymer films -and in particular with Nafion- has been reported several decades ago.[30,31] As a polyelectrolyte with ion-exchanging capabilities, Nafion membranes generate a Donnan potential at the solution interface. Naegeli *et al.* have demonstrated that magnitude of this potential is coupled to the different equilibriums (acid-base, redox) and the electrolyte composition of the solution.[32] All in all, the potentiometric response of a Nafion-coated Pt electrode to the addition of H_2O_2 is complex and cannot be easily predicted.

In this work, the potentiometric response to the addition of H_2O_2 of Pt electrodes coated with Nafion is studied. The results show that the Nafion not only prevents the interfering effect of negatively charged redox anions -such as ascorbate-, but that it also produces a significant enhancement of the potentiometric response that depends on the ionic strength of the solution. The data suggest that this enhancement is connected to an additional effect

resulting from the Donnan potential generated by the polyelectrolyte coating of the electrode. It is also shown that this enhanced sensitivity and selectivity show promise for the development of enzyme-based potentiometric biosensors.

7.2 Experimental Section

7.2.1 Reagents and Solutions

Initial measurements were performed in a 0.1 M phosphate buffer solution (PBS) at pH 7. Acetate, phosphate and borate buffer 0.1 M were used for the experiments involving the change of pH. Fresh solutions of hydrogen peroxide (H_2O_2) were prepared daily.

7.2.2 Materials

A 99.95 % purity Platinum wire of 1mm Ø diameter, (Goodfellow Cambridge Limited, England) was inserted into a Teflon® (polytetrafluoroethylene, PTFE) body to make a flat-disc electrode. The electrodes were polished with 1 µm and 0.3 µm alumina and then thoroughly rinsed with double-distilled water. After that, three steps of 10 minutes' bath sonication with acetone, then ethanol and finally with double-distilled water were performed. Thereafter, an electrochemical cleaning step was performed. The electrodes were immersed for 2 min in 0.5 M H_2SO_4 solution at a potential of +1.96 V vs. Ag/AgCl reference electrode. This process should eliminate organic residues and also anodically dissolves trace metals.[33] Finally, electrodes were rinsed with double-distilled water and dried at room temperature. The coating with Nafion was performed by drop casting 10 µL of Nafion solution on top of the platinum electrode. This electrode was left drying overnight at room temperature. For the enzyme-based potentiometric electrode, a similar construction was applied. After the first Nafion layer, a 10 µL drop (100 mg mL^{-1} glucose oxidase solution - GOx) was cast onto the Pt electrode and let it dry at 4ºC 24h. Subsequently, a second 10 µL Nafion layer was again drop cast. The enzymatic electrode was left drying overnight at 4ºC and keep it at the same temperature when not in use.

7.2.3 Electrochemical Measurements

Electromotive force measurements (EMF) were performed at room temperature (25 ºC) in well stirred solutions using a high input impedance (10^{15} Ω). The experiments were performed in a 20 mL beaker.

Cyclic voltammetry (CV) and electrochemical impedance spectroscopy (EIS) were performed by using an electrochemical analyzer/workstation. The measurements were taken

in a solution of 0.1 M KCl at room temperature (25ºC). For cyclic voltammetry (CV) experiments, a potassium hexacyanoferrate (III) and potassium hexacyanoferrate (II) ($Fe(CN)_6^{3-/4-}$) solution (5 mM $Fe(CN)_6^{3-/4-}$ and 100 mM NaCl as a supporting electrolyte) was used as redox couple. The working electrode was cycled from 0.4 V to -0.2 V at 50 mV s^{-1}. Both experiments were performed at room temperature (25ºC).

7.3 Results and Discussion

7.3.1 Potentiometric Detection Enhancement

Figure 7.1A shows the typical potentiometric response obtained for a bare and for a Nafion-coated Pt electrode upon the addition of H_2O_2 in 0.1M PBS at pH 7. For the bare electrodes a decrease of the potential as the concentration of H_2O_2 increases is observed. In general, this is in agreement with results already reported.[34–36] The Pt electrode is sensing the changes on the redox potential of the solution produced by the addition of peroxide. The redox half-reaction of H_2O_2 on the Pt surface can be expressed as:

$$H_2O_2 \rightarrow 2H^+ + O_2 + 2e^- \qquad \text{(Equation 7.1)}$$

and the half-cell potential (E) can be calculated according to the Nernst equation for this reaction (at 298 K):

$$E = E^0 - \frac{0.059}{2} log \frac{[H_2O_2]}{pO_2[H^+]^2} \qquad \text{(Equation 7.2)}$$

where the brackets represent the activities of the species, pO_2 is the partial pressure of oxygen, and E^0 (O_2/H_2O_2) is the standard potential for this reaction (0.695V). This equation predicts a linear decrease of the potential with the increase of the logarithm of the activity of peroxide (at a constant pH), as it is observed in Figure 7.1. The expected slope should be around 0.028V/decade. However, because of the many factors affecting the electrochemical behaviour of peroxide on Pt surfaces,[27,28] this equation is of limited use in quantitative terms. In fact, different values for this slope have been reported depending on the surface of Pt, crystalline structure, etc.

The first experimental evidence that shows the difference between bare and Nafion-coated electrodes is the initial potential (i.e., the potential before the addition of peroxide). Electrodes coated with Nafion show a significantly higher initial potential when compared to the bare Pt electrodes. These differences could be attributed to the accumulation of charges at the Nafion-solution interface. Nafion has significant ion-exchange capabilities[37,38] due to the

negatively charged sulfonate groups. Thus, a Donnan potential can be generated by the incorporation of cations from the solution.[32]

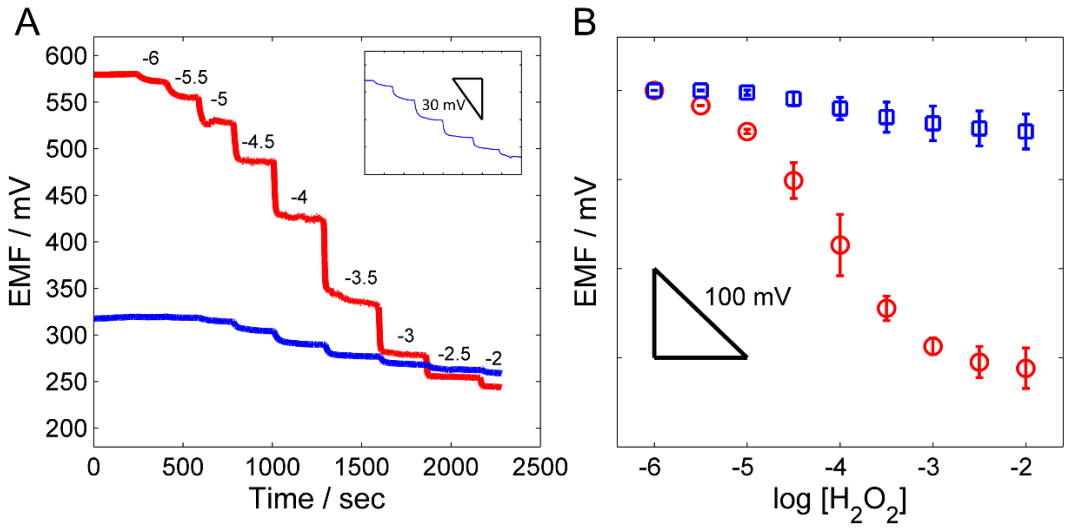

Figure 7.1. Potentiometric response curves. (A) Time-trace for bare (blue line) and Nafion-coated (red line) platinum electrode in PBS pH 7 at 25ºC (mean ± S.D., N=2). Inset shows a magnification of the calibration curve for bare platinum electrode. (B) Corresponding calibration plots for bare (blue, □) and coated (red, ○) electrodes. Initial potentials have been subtracted to better illustrate the differences between the two systems. Error bars correspond to the standard deviation (N=2).

Table 7.1. Comparison of analytical figures of merit for the determination of H_2O_2 with the two types of electrodes in 0.1 M PBS buffer (pH=7).

Parameters	Bare Pt	Nafion-coated Pt
Sensitivity (mV decade^{-1})	-18.5 ± 7.9	-125.1 ± 5.9
Linear Range (M)	$10^{-4.5}$ to 10^{-3}	10^{-5} to 10^{-3}
LOD (M)	$10^{-5.1}$	$10^{-5.4}$

Interestingly, these electrodes coated with Nafion show also a decrease on the potential with the addition of H_2O_2, but the magnitude of the change observed is much more pronounced. First, it has been shown that Nafion forms bi-continuous nanostructures[39] that allows the transport of small and neutral molecules. Previous studies have shown the permeability of this material to H_2O_2.[40] Therefore, it is not surprising that peroxide reaches the surface of the Pt electrode and produces a redox response. What is more interesting, however, is that this response is somehow modulated by the presence of Nafion. Figure 7.1B compares the response as a function of the logarithm of the concentration of H_2O_2 for both electrodes, and regression parameters from these plots are presented in Table 7.1.

Since both, coated and uncoated electrodes reach a similar potential at higher concentration of peroxide, the improvement in sensitivity observed can be ascribed to the higher initial potential displayed by the Nafion-coated electrodes, which -as it has been suggested- it is in direct relationship with the Donnan potential originated at the Nafion-solution interface.

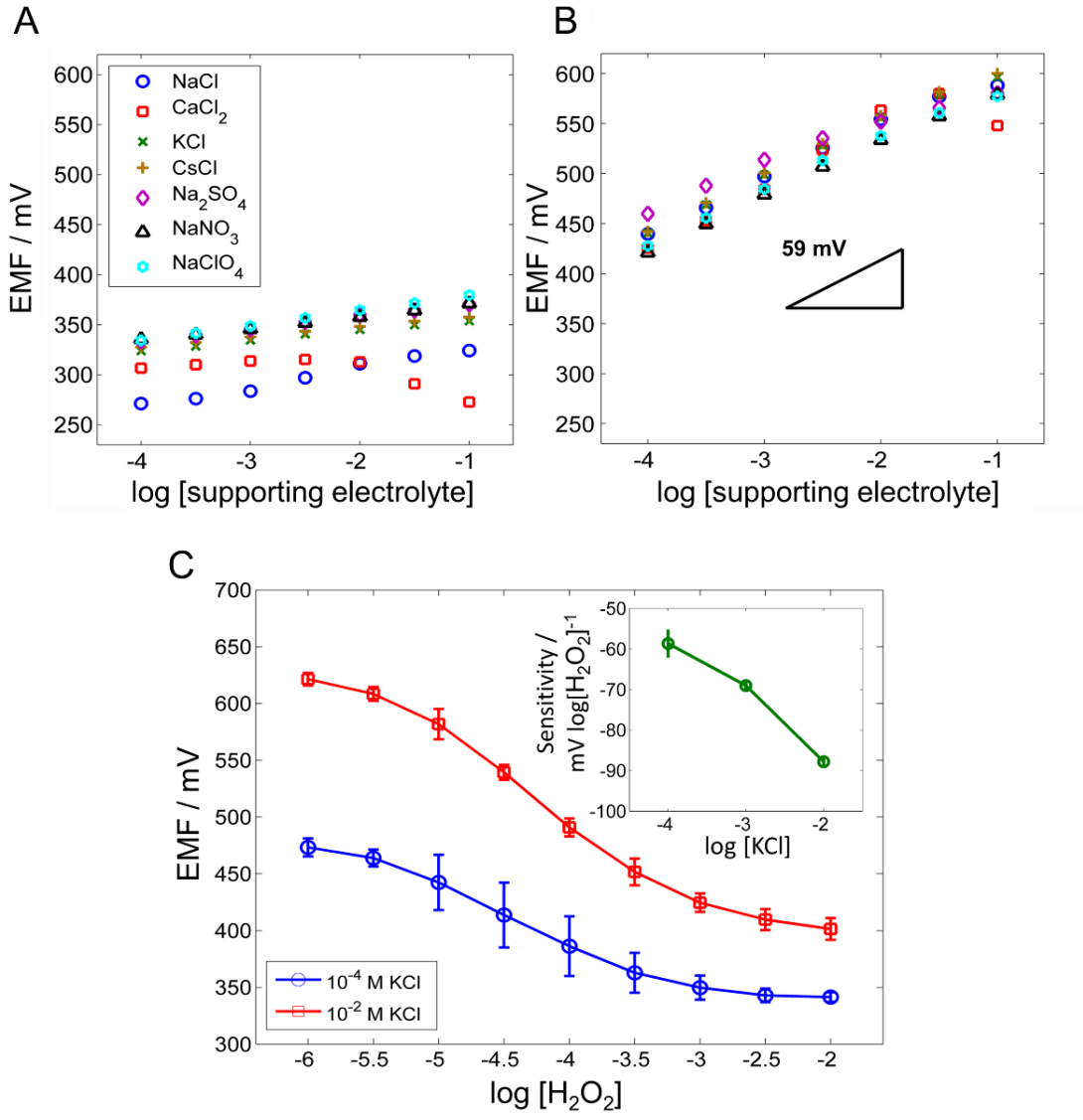

Figure 7.2. Comparison of the initial potential as a function of the total electrolyte concentration for (A) bare and (B) Nafion-coated platinum electrodes upon increasing concentration of different supporting electrolytes at 25ºC. (C) Comparison of the H_2O_2 calibration curves using coated electrodes at different concentrations of supporting electrolyte (KCl): 10^{-2} M (□) and 10^{-4} M (○) (mean ± S.D., N = 2). Inset displays H_2O_2 sensitivity versus supporting electrolyte (KCl) concentration.

To further explore this point, the dependence of this initial potential on the total concentration of the supporting electrolyte for bare (Figure 7.2A) and coated electrodes (Figure 7.2B) was evaluated. The results show a limited response for the bare Pt electrodes, while a marked linear increase with an almost Nernstian dependence is observed when the electrodes are coated with Nafion. This type of response has been already reported for analogous systems and strongly supports the idea of the Donnan contribution in the initial potential of the coated electrodes.[38]

For this reason, calibration plots for peroxide at different electrolyte concentrations were also performed and the results are displayed in Figure 7.2C. As the electrolyte concentration in the solution decreases, the slope also decreases and approaches that of bare Pt electrodes. In essence, the sensitivity to peroxide of the electrodes coated with Nafion is dependent on the total concentration of electrolyte. It is also worth noticing that the increase of the concentration of electrolyte improves the reproducibility of the response between electrodes.

The influence of pH on this phenomenon has been also evaluated. Figure 7.3 shows the response of bare (Figure 7.3A) and coated electrodes (Figure 7.3B) to the addition of H_2O_2 in a range of pH from 4 to 9. It is worth mentioning that the sensitivity for H_2O_2 on bare electrodes increases considerably as the pH increases. It has been suggested that this is in part due to a decrease on the stability of H_2O_2 at neutral and basic pH.[41] At the higher concentrations, the bare Pt electrodes yield an almost Nernstian dependence with the pH, as predicted by Equation 7.1. The coated electrodes, on the other hand, show also a range with a linear dependence with pH (for a given H_2O_2 concentration) but with slopes that are higher than the expected Nernstian value. These results, however, are hard to interpret. First, the changes in pH also imply a change in the total ionic concentration, which modulates the response of the electrode. Second, the changes in the pH of the bulk solution do not imply similar changes on the pH at the interface or at the bulk of the membrane. In other words, the modulation of the pH at the interface induced by the Donnan potential may have a significant effect on the redox response of the electrode. From the plots of Figure 7.3B it is evident that Nafion-coated electrodes display an enhanced sensitivity at all pH values. Nevertheless, the relative enhancement is more pronounced as the pH increases. As the sensitivity increases, the linear range is shifted towards lower concentrations, which results in an improvement of the limits of detection for H_2O_2 at higher pH.

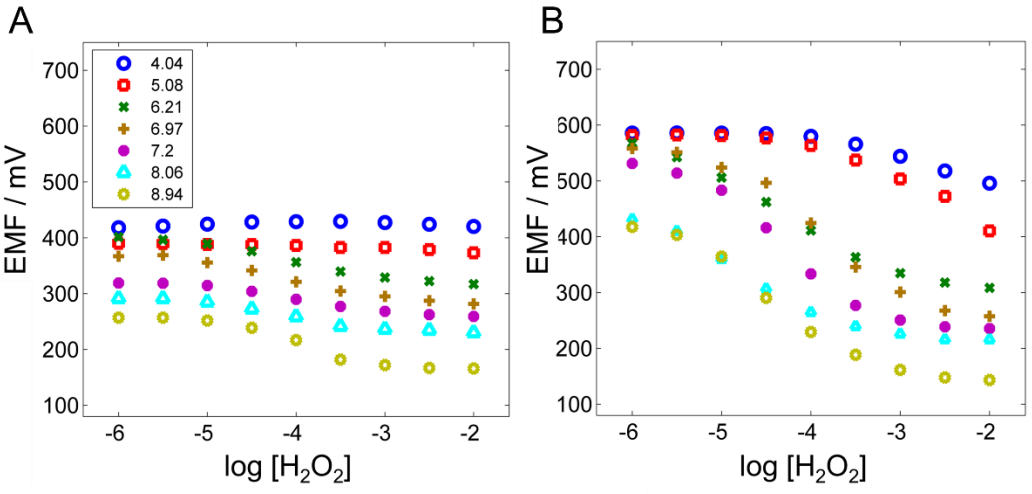

Figure 7.3. Calibration plots at several pH for (D) bare and (E) Nafion-coated electrodes in 0.1 M buffers of different pH at 25ºC.

As it was mentioned before, there are many factors that make difficult to elaborate an accurate description of the mechanism involved in the phenomena observed. First, the reactivity of H_2O_2 on Pt is complex and highly dependent on the experimental conditions. Second, many of the properties of Nafion are still under study.[37,42,43] Third, the combination of both systems (i.e., redox-sensitive electrodes coated with polyelectrolytes) adds another level of complexity, since it has been reported that in these types of systems the chemical equilibrium in solution (redox, acid-base) are strongly coupled with the ion-exchange properties of the membrane. Last, but not least, reactions between Nafion and H_2O_2 could also occur and they might -up to a certain degree- play a role on these results. This last point, however, is less likely, since the electrodes can be washed and re-used, obtaining reproducible results. All in all, a detailed study of the mechanism of generation of the potential in this system falls well beyond the scope of this work, and only some general observations can be elaborated.

Regarding the role of the Nafion membrane, it is important to remark that the coated electrodes are stabilized in a solution with high ionic strength (in general 0.1 M NaCl, unless stated otherwise) in neutral to slightly basic pH. Under these conditions, the membrane incorporates Na^+ from the solution (releasing H^+). This ion-exchange capacity of Nafion with singly charged electrolytes is well known.[32] The detection of H_2O_2 is performed after this stabilization has taken place. Beyond the permselective behaviour, the response obtained

with the coated electrodes seems to be an enhanced form of the response obtained with the bare electrodes. Thus, it could be assumed that the same underlying mechanism operates in both cases, (i.e., the reaction between Pt and H_2O_2), but that some amplification factor operates when Nafion membranes are present. From the previous evidence (see Figure 7.2B), this amplification is related to the Donnan potential as a result of the ionic concentration of the solution.

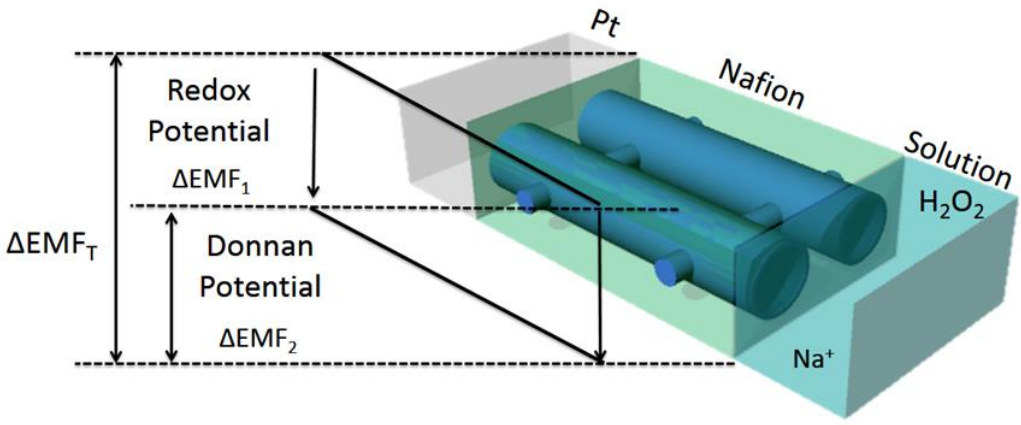

Figure 7.4. Schematic representation of the Nafion-coated electrodes mechanism studied in this work. The exchange capacity and the redox reaction performed the suggested mechanism.

The Nafion membrane is stabilized between two different interfaces: the Pt-membrane interface, from one side, where the membrane strongly interacts with the metal through the hydrophobic Nafion domains;[44] and the membrane-solution interface, from the other, where the ion-exchange process generates the Donnan potential. The gradient of electrochemical potential of the system Pt||membrane||solution is altered when H_2O_2 reaches the surface of the Pt. First, the metal-membrane interface registers a drop of the redox potential. As a result of this change, a rearrangement of the ionic species in the membrane and at the interface under the new equilibrium conditions may occur, which results in the amplification of the electrode response. If some oxidation of the H_2O_2 takes place inside Nafion membrane, the increase of the H^+ concentration might be leading to a leach of cations at the solution interface and a change on the internal pH of the membrane. Clearly, this is at this point speculation, and more work needs to be conducted to understand the conditions inside the membrane and the mechanisms involved. Figure 7.4 is an attempt to illustrate the suggested mechanism. Interestingly, there are many works devoted to the study of the interactions between platinum and H_2O_2, but there is not complete agreement on the mechanisms

involved. Similarly, the recent works on the structure and properties of Nafion membranes reveal the lack of models to fully understand the behaviour of this material.

7.3.2 Nafion as a Permselective Membrane.

The comparison of the impedance spectra between bare and Nafion-coated Pt electrodes (Figure 7.5) exhibits a typical capacitive mechanism for the coated electrode, with a single high-frequency semicircle related to the bulk resistance of the Nafion membrane. This resistance is smaller than what is observed in other conventional polymeric membranes electrodes,[45] due to the electrical and structural characteristics of Nafion. Furthermore, Nafion membranes exhibit different selectivity coefficients to different counterions and more uniform exchange site environment than conventional sulfonate ion-exchange resins.[22,46] The perfluorosulfonate ionomer morphology was suggested to follow an oriented ionic nanochannels embedded within a locally aligned polymer matrix where sulfonate groups ($-SO_3^-$) coated channels are invoked to account for intercluster ion hopping of positive charge species but rejection of negative ions.[40] However, there are several current models describing the Nafion morphology and membrane behaviour, and the evidence is not yet conclusive.[37] Figure 7.6A exhibits the rejection of negatively charge molecules thus performing a decrease in the oxidation and reduction peaks of the cyclic voltammogram. Besides, Figure 7.6B presents redox sensitivity for bare Pt electrode, as expected, and remains insensitive for Nafion-coated electrode.

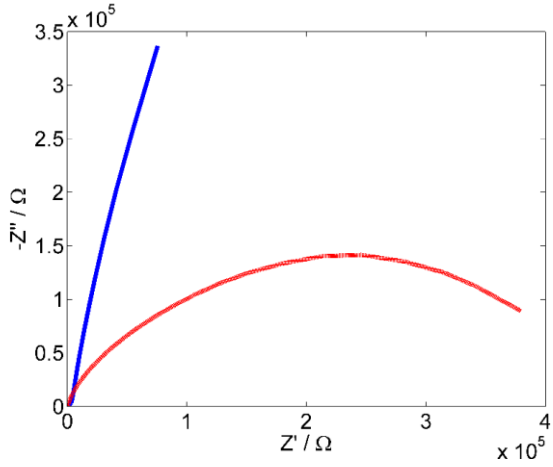

Figure 7.5. Electrochemical impedance spectroscopy results of bare (blue line) and Nafion-coated (red line) platinum electrode in 0.1 M KCl as a supporting electrolyte. The impedance spectra were recorded in the frequency range 100 kHz-10 mHz by using a constant direct current potential, (Edc) 0.2 V. The electrodes were studied using excitation amplitude of 10 mV at 25ºC.

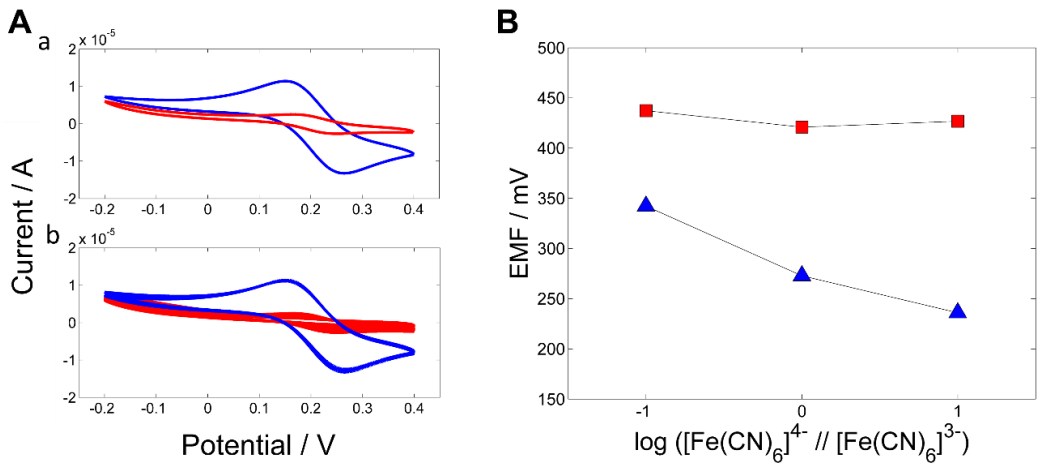

Figure 7.6. Cyclic voltammetry results. (Aa) Comparison between bare (blue line) and Nafion-coated (red line) electrodes and (Ab) comparison between bare (blue line) and Nafion-coated (red line) electrodes after 30 minutes in solution in 5 mM $Fe(CN)_6^{3-/4-}$ and 100 mM NaCl from -0.2 V to 0.4 V at 50 $mV \cdot s^{-1}$. Redox sensitivity assay. (B) Redox sensitivity of 1 mM $[Fe(CN)_6]^{4-}$ / $[Fe(CN)_6]^{3-}$ at different ratios (0.1, 1 and 10) for bare (▲) and Nafion-coated (□) platinum electrodes.

Even though mechanisms are still under debate, Nafion membranes have been extensively used in amperometric sensors as a permselective barrier against negatively charged redox species. Thus, the question remains on whether a similar effect could be used to improved potentiometric sensors. Figure 7.7A shows the results of the addition of ascorbic acid on the calibration plots for peroxide using coated and uncoated electrodes. Ascorbate is a reducing agent that is typically found as interference in biological fluids. Thus, when added to the solution at 100 µM level (normal upper range of the biological fluids) the bare Pt electrode becomes almost insensitive to the addition of peroxide (Figure 7.7A). Indeed, upon the addition of ascorbic the bare Pt electrodes register a drop of the initial potential, which remains almost constant until a higher concentration of peroxide is reached. The coated electrodes, on the other hand, show a significantly different behaviour (Figure 7.7A).

Table 7.2 compares the analytical parameters obtained for the coated electrodes before and after the addition of ascorbate. First, it can be seen that neither the sensitivity nor the limits of detection (LOD) show significant changes. The linear range shows a slight reduction, but it does not seem to be severely affected. The most significant change that can be observed is a decrease on the initial potential when ascorbate is added (Figure 7.7A). Evidently, an optimization of the Nafion layer could reduce these effects, and the development of suitable working protocols may help to further enhance the applicability of this approach. It has been suggested, for example, that a thickness of the Nafion membrane

could be modified to improve the permselectivity towards negatively charged molecules.[47] Clearly, further work is needed in order to optimize these aspects. However, as a preliminary conclusion, the results suggest that the interference of the potentiometric detection caused by negatively charged redox species can be overcome when using the Nafion coating.

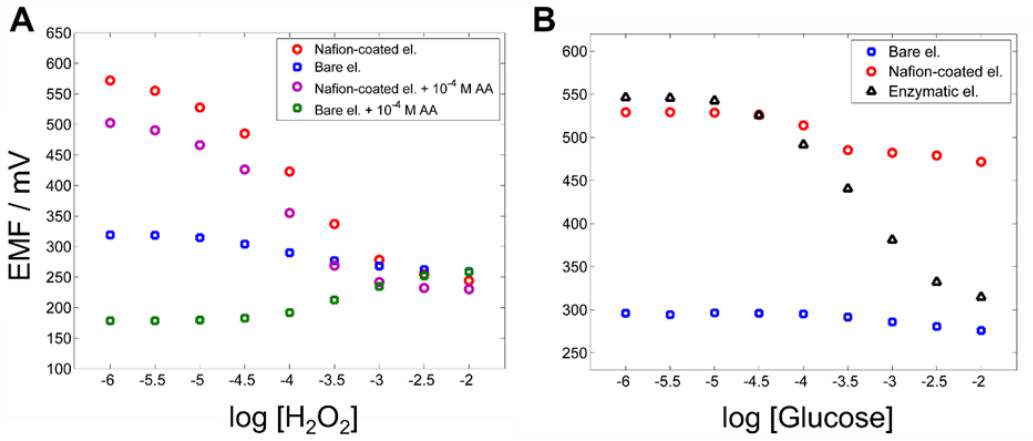

Figure 7.7. (A) Evaluation of the addition of ascorbic acid (AA) in the cell for bare and Nafion-coated electrodes in 0.1 M PBS pH 7.2 at 25ºC. (B) Calibration curve for increasing glucose concentration over time for bare, Nafion-coated and Nafion-coated enzymatic electrodes in 0.1 M PBS pH 7.4 at 25ºC.

Table 7.2. Comparison of analytical figures of merit for the determination of H_2O_2 with Nafion coated electrodes before and after the addition of ascorbic acid in 0.1M PBS.

Test	No Ascorbate	100 µM Ascorbate
Sensitivity (mV decade^{-1})	-129.1	-132.3
Linear Range (M)	10^{-5} to 10^{-3}	10^{-5} to $10^{-3.5}$
LOD (M)	$10^{-5.3}$	$10^{-5.4}$

The results shown so far are extremely relevant, since they present a way to alleviate two of the major limitations of the potentiometric detection of peroxide in biological fluids, namely: limited sensitivity and severe interference caused by redox species. Regarding the sensitivity, the Nafion provides a way to produce an enhancement due to the presence of electrolytes. While it could be argued that this modulation of the sensitivity by electrolytes might be a problem for some applications, many biological fluids -such as blood or serum- have a high and constant concentration of ions. Therefore, this should be advantageous for the detection of peroxide. The problem of the interferences, which is also a major issue, can be also successfully overcome as it has been previously shown. The experimental results also show some other practical advantages of the use of Nafion, such as a better reproducibility

between sensors and shorter stabilization times of the signal. It is well known that Pt surfaces can be easily contaminated, affecting the electrochemical response. Thus, Nafion might be acting as a barrier that limits this undesired effect.

There are significant implications of these findings in the field of biosensors. The use of oxidase enzymes, for example, that produce peroxide, could be used for the potentiometric detection of neutral molecules in a simple, sensitive and robust way. To prove this point, the enzyme glucose oxidase (GOx) was sandwiched between two layers of Nafion cast on a Pt electrode. The results of the addition of glucose to a bare Pt electrode, an electrode coated with Nafion, and an electrode coated with Nafion containing the GOx enzyme are presented in Figure 7.7B. As the concentration of glucose is increased, peroxide is generated and potentiometrically detected, as shown previously. The results exhibit a slope of approximately 110 mV decade^{-1} of glucose, with a linear range between 10^{-4} M to $10^{-2.5}$ M.

Clearly, these are just preliminary results, since a careful study and optimization of the enzymatic reaction must be performed. However, these initial results strongly encourage further research on this direction.

7.4 Conclusions

This chapter demonstrates that permselective membranes -such as Nafion- can be used as an efficient enhancer for the sensitive and selective potentiometric detection of H_2O_2. The approach presented allows the detection of H_2O_2 based on the change of the redox potential of the solution, as well as through the additional contribution of a Donnan potential generated at the membrane-solution interface. Because of this, a modulation of the sensitivity based on the ionic strength and pH of the solution is possible. The maximum sensitivities are thus obtained in high ionic strength, which can be advantageous when dealing with biological fluids.

As a proof of principle, the direct application of this simple H_2O_2 detection through the use of an enzymatic reaction is demonstrated. Thus, the proof of principle for the construction of a simple enzymatic electrode with an enhanced potentiometric response using Nafion permselective membranes is demonstrated for the first time. This device should provide significant advantages when facing the challenge of developing simple, low-cost decentralized platforms.

7.5 References

[1] Wang, J. Electroanalysis 2005, 17 (2), 7.

[2] Anh, D. T. V; Olthuis, W.; Bergveld, P. Sens. Act. B Chem. 2003, 91 (1-3), 1.

[3] Xiao, Y.; Ju, H. X.; Chen, H. Y. Anal. Chim. Acta 1999, 391 (1), 73.

[4] You, T.; Niwa, O.; Tomita, M.; Hirono, S.; Microsystem, N. T. T.; Laboratories, I.; Afty, N. T. T. Anal. Chem. 2003, 75 (9), 2080.

[5] Hrapovic, S.; Liu, Y.; Male, K. B.; Luong, J. H. T. Anal. Chem. 2004, 76 (4), 1083.

[6] Wang, J. Chem. Rev. 2008, 108 (2), 814.

[7] Prodromidis, M. I.; Karayannis, M. I. Electroanalysis 2002, 14 (4), 241.

[8] Vargas-Bernal, R.; Rodríguez-Miranda, E.; Herrera-Pérez, G. Pestic. Adv. Chem. Bot. Pestic. 2012, 329.

[9] Ahmad, R.; Tripathy, N.; Kim, J. H.; Hahn, Y. B. Sens. Act., B Chem. 2012, 174, 195.

[10] Kong, T.; Chen, Y.; Ye, Y.; Zhang, K.; Wang, Z.; Wang, X. Sens. Act. B Chem. 2009, 138 (1), 344.

[11] Yang, Z.; Zhang, C.; Zhang, J.; Bai, W. Biosens. Bioelectron. 2014, 51, 268.

[12] Shukla, S. K.; Deshpande, S. R.; Shukla, S. K.; Tiwari, A. Talanta 2012, 99, 283.

[13] Hu, J.; Wang, S.; Wang, L.; Li, F.; Pingguan-Murphy, B.; Lu, T. J.; Xu, F. Biosens. Bioelectron. 2014, 54, 585.

[14] Pai, N. P.; Vadnais, C.; Denkinger, C.; Engel, N.; Pai, M. PLoS Med. 2012, 9 (9), e1001306.

[15] Yetisen, A. K.; Akram, M. S.; Lowe, C. R. Lab Chip 2013, 13 (12), 2210.

[16] Novell, M.; Parrilla, M.; Crespo A., G.; Rius, F. X.; Andrade, F. J. Anal. Chem. 2012, 84 (11), 4695.

[17] Novell, M.; Guinovart, T.; Blondeau, P.; Rius, F. X.; Andrade, F. J. Lab Chip. 2014, 14, 1308.

[18] Martinello, F.; Luiz da Silva, E. Clin. Chim. Acta 2006, 373 (1-2), 108.

[19] Anzai, J.; Takeshita, H.; Kobayashi, Y.; Osa, T.; Hoshi, T. Anal. Chem. 1998, 70 (4), 811.

[20] Wynne, A.; Finnerty, N. Chemosensors 2015, 3 (2), 55.

[21] Vaidya, R.; Atanasov, P.; Wilkins, E. Med. Eng. Phys. 1995, 17 (6), 416.

[22] Szentirmay, M.; Martin, C. Anal. Chem. 1984, 1902 (52), 1898.

[23] Manowitz, P.; Stoecker, P. W.; Yacynych, A. M. Biosens. Bioelectron. 1995, 10, 359.

[24] Wang, J.; Musameh, M.; Lin, Y. J. Am. Chem. Soc. 2003, 125 (9), 2408.

[25] Karra, S.; Zhang, M.; Gorski, W. Anal. Chem. 2013, 85 (2), 1208.

[26] Adeloju, S. B.; Moline, A. N. Biosens. Bioelectron. 2001, 16, 133.

[27] Hall, S. B.; Khudaish, E. A.; Hart, A. L. Electrochim. Acta 1997, 43 (5-6), 579.

[28] Katsounaros, I.; Schneider, W. B.; Meier, J. C.; Benedikt, U.; Biedermann, P. U.; Auer, A. A.; Mayrhofer, K. J. J. Phys. Chem. Chem. Phys. 2012, 14, 7384.

[29] Burke, L. D.; Hurley, L. M. Electrochim. Acta 1999, 44, 3451.

[30] Dewulf, D.; Bard, A. J. J. Macromol. Sci. Part A - Chem. 1989, 26 (8), 1205.

[31] Lawson, D. R. J. Electrochem. Soc. 1988, 135 (9), 2247.

[32] Naegeli, R.; Redepenning, J.; Anson, F. C. J. Phys. Chem. 1986, 90, 6227.

[33] Goldstein, E. L.; Van de Mark, M. R. Electrochim. Acta 1982, 27 (8), 1079.

[34] Weiss, J. Trans. Faraday Soc. 1935, 31, 1547.

[35] Castner, J. F.; Wingard, L. B. Anal. Chem. 1984, 56 (14), 2891.

[36] Zheng, X.; Guo, Z. Talanta 2000, 50, 1157.

[37] Mauritz, K. A.; Moore, R. B. Chem. Rev. 2004, 104, 4535.

[38] Grygolowicz-Pawlak, E.; Crespo, G. A.; Ghahraman Afshar, M.; Mistlberger, G.; Bakker, E. Anal. Chem. 2013, 85, 6208.

[39] Michael A. Hickner; Hossein Ghassemi; Yu Seung Kim. Chem. Rev. 2004, 104, 4587.

[40] Schmidt-Rohr, K.; Chen, Q. Nat. Mater. 2008, 7 (1), 75.

[41] Watts, R. J.; Foget, M. K.; Kong, S.-H.; Teel, A. L. J. Hazard. Mater. 1999, 69 (2), 229.

[42] Kong, X.; Schmidt-Rohr, K. Polymer. 2011, 52, 1971.

[43] Diat, O.; Gebel, G. Nat. Mater. 2008, 7, 13.

[44] Wood, D. L.; Chlistunoff, J.; Majewski, J.; Borup, R. L. J. Am. Chem. Soc. 2009, 131, 18096.

[45] Crespo, G. A.; Macho, S.; Rius, F. X. Anal. Chem. 2008, 80, 1316.

[46] Yeager, H. L.; Steck, A. Water Pollut. Control 1979, 51 (7), 862.

[47] Bath, B. D.; White, H. S.; Scott, E. R. Anal. Chem. 2000, 72 (3), 433.

UNIVERSITAT ROVIRA I VIRGILI
NEW ELECTROCHEMICAL SENSORS FOR DECENTRALIZED ANALYSIS
Marc Parrilla Pons

Chapter 8

Paper-based Enzymatic Electrode with Enhanced Potentiometric Response for Monitoring Glucose in Biological Fluids

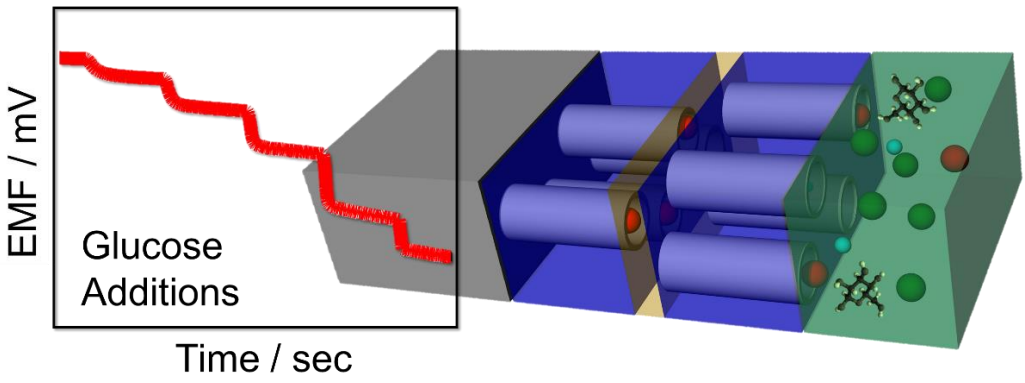

UNIVERSITAT ROVIRA I VIRGILI
NEW ELECTROCHEMICAL SENSORS FOR DECENTRALIZED ANALYSIS
Marc Parrilla Pons

In this chapter, a novel paper-based potentiometric sensor with an enhanced response for the detection of glucose in biological fluids is presented, using the findings and results reported in the previous chapter. The working electrode is built by sputtering platinum on a conventional filter paper in order to create a redox-sensitive surface. Glucose oxidase enzyme is immobilized between two layers of Nafion cast on top of this metallic surface. When this system is used in a conventional potentiometric arrangement a signal that is proportional to the logarithm of the concentration of glucose is obtained. The experimental evidence shows that this signal corresponds to the detection of the hydrogen peroxide generated due to the enzymatic reaction. The role of Nafion to increase the sensitivity of the technique as well as to help to minimize the interferences caused by redox active species, such as ascorbate, is studied. To validate this approach, the determination of glucose in human serum samples is performed. The results obtained show an excellent agreement when compared to standard methods. This approach could facilitate the implementation of new and simple devices for monitoring relevant biomolecules in body fluids in decentralized settings.

8.1. Introduction

Enzymatic biosensors have traditionally drawn significant attention because of their attractive analytical features. The specificity of the recognition obtained by the use of an enzyme allows the development of devices with exceptional selectivity. Additionally, these sensors display good reproducibility, stability and low limits of detection in complex matrices, such as biological fluids. Last -but not least-, a limited group of enzymes (oxidases, reductases, etc.) allows a wide range of molecules to be detected with a simplified detection approach.[1,2] For this reason, enzymatic biosensors are extensively used in different applications, such as clinical, environmental, forensic, food analysis, etc.[3–7]

As a general approach, the enzyme is used as a recognition element, catalyzing a specific reaction of the analyte, and then one of the reaction products is detected. Oxidase-type enzymes, for example, are widely used since they generate hydrogen peroxide (H_2O_2) as a byproduct.[4,8] Thus, there is a plethora of sensors for different molecules that are based on the detection of H_2O_2 using a suitable technique.[9–11] From the many different options, detection of peroxide using electrochemical-based techniques provide significant advantages, since they show outstanding analytical figures and a simple, compact setup.[12] Traditionally, electrochemical enzyme-based biosensors have relied on voltammetric techniques. Amperometric detection is by far the most used approach,[13] since it shows

outstanding sensitivity and robustness. In fact, one of the greatest achievements on the use of this technique for solving social needs was the successful development of devices to monitor glucose at home (glucometers), most of which are based on the use of glucose oxidase and amperometric detection.[13,14] Therefore, for many years, this technique has become almost the norm for many biosensors.

Despite of this undisputable success, emerging social needs are creating a growing demand for alternative detection schemes. As the need for new tools for decentralized chemical analysis -such as those required in point of care- is gaining momentum, new detection schemes that can combine good analytical performance with enhanced robustness, simplicity and lower costs are required. This is the case, for example, of wearable devices,[15] where power consumption, robustness and size are paramount, or the recent trend in the development of paper-based analytical platforms.[16] It is for this reason that approaches such as potentiometry are attracting a renewed interest, since they can offer an unrivalled simplicity of operation and instrumentation,[17–19] robustness and -with recent progress in the field- also ultra-low-cost devices.

Potentiometric biosensors using enzymatic reactions were proposed several decades ago. The first proposals made use of an enzyme immobilized on a glass electrode surface in order to detect the change in protons resulting from the reaction.[20] Following this seminal work, different types of devices where the enzymatic reaction generates a positively charge species -such as protons or ammonium ions- to be then detected by a suitable ion-selective electrode. For instance, a pH-based enzyme potentiometric sensor for glucose determination using glucose oxidase (GOx) was investigate.[21] In similar work, some discussions regarding the role of the changes on pH were also addressed.[22] Also, a coated-wire potentiometric enzyme sensor was also developed to detect urea and penicillin.[23] Nevertheless, most of these approaches never became widely adopted, possibly because they did not offer significant advantages over alternative schemes. Very recently, however, with the introduction of new materials, novel enzymatic biosensors with potentiometric detection have been reported. Willander *et al*. explored the use of ZnO nanostructures to immobilize cholesterol oxidase and glucose oxidase in order to build suitable biosensors.[24,25] Similarly, Adeloju *et al*, developed enzyme-based potentiometric sensors for glucose and phosphate.[26–28] The advantages of these type of devices, which have been recently studied present many attractive features for practical applications.[29,30] Nevertheless, most of them have not yet been validated with real samples. It is well known that interferences commonly found in biological fluids are major roadblocks for these sensors.

The search for alternative routes for the determination of glucose in biological fluids is still a very relevant topic of research. First, because it can be used as model to compare the performance with other systems. Second, because existing solutions only reach a fraction of the total population in need. It is estimated that 285 million adults were affected by diabetes in 2010, and it is expected that this number increases to 439 million by 2030. Most of this increment will be registered in developing countries, where conventional glucometers are still unaffordable[31] and public healthcare systems are crumbling under the increasing cost-cutting pressure. Hence, new detection approaches that can offer reduced cost and enhanced simplicity are needed. To reduce the cost of the sensors, new approaches to produce electrodes in large scale have been developed during the last years. Screen-printed techniques have partially addressed this problem.[32] More recently, breakthroughs in the area of nanomaterials and flexible electronics have helped to further reduce the cost of potentiometric sensors[33,34] by applying simple dyeing or direct printing approaches using paper as a substrate.[35] Last but not least, potentiometric sensors can be miniaturized (thus reducing even further the manufacturing cost) without affecting the analytical performance. Therefore, the development of a paper-based potentiometric biosensor for glucose may bring significant advantages in order to solve a growing social need.

Low-cost paper-based platforms to make affordable and portable analytical tools for poor and remote regions of the planet have been proposed many years ago.[36] Paper has been used in combination with new materials to fabricate sensors in a cost-effective manner.[37,38] However, the majority of paper-based enzymatic devices use the paper as a substrate for colorimetric assays, as in the traditional dipsticks, lateral flow systems and bioactive papers.[39,40] More recently, paper was proposed as a substrate to build enzymatic electrodes[41] using amperometric detection approach. Interestingly, paper sensors are based on a 3D network of cellulose fibers, which increases the active area where enzyme is immobilized and, consequently, improves the analytical performance. To the best of our knowledge, paper-based enzymatic biosensors with potentiometric detection that can be used in real samples have not yet been reported.

This work introduces a novel approach for the construction of a simple, robust and sensitive enzymatic paper-based biosensor for the potentiometric detection of glucose. The method is based on the detection of the hydrogen peroxide generated as a result of the oxidation of glucose catalyzed by glucose oxidase (GOx). A platinum-sputtered paper sensor is used as a redox sensitive substrate and, in order to eliminate interferences and increase the sensitivity of the technique, a recent approach where the enzyme is immobilized using a

Nafion layer is proposed. The results show that this device can accurately predict levels of glucose in body fluids such as serum. Furthermore, considering that the generation of peroxide is common to many enzymes, it is expected that this sensor can be applied for wide range of substances. Some limitations and potential future applications of these novel sensors in real life scenarios are discussed. For example, while platinum (Pt) was used in this first proof of principle, it is expected that the use of a redox-sensitizing material may help to further reduce costs. This study opens a new avenue for the development of electrochemical paper-based enzymatic sensors.

8.2. Experimental

8.2.1. Materials and Methods

Sodium urate, sodium ascorbate and D-Fructose were purchased from Sigma-Aldrich. Phosphate buffered saline (PBS) was prepared at 0.1 M with 0.135 M NaCl and used in all the experiments. An adhesive plastic mask (0.3 mm thick) coated with an acrylic adhesive on one side (Arcare 8565, Adhesives Research Inc., Limerick, Ireland) was used to expose a given area of a platinized paper and isolate the rest of the conductive surface.

For morphological analysis, all membranes were covered with a gold layer to improve the transduction and characterized using an environmental scanning electron microscope. For the chemical analysis of the surface, an attenuated total reflectance Fourier transform infrared spectrometer (Agilent 4100 ExoScan FT-IR) was used. A spectrum, collected as the average of 64 scans with a resolution of 4 cm^{-1}, was recorded from 4000 to 650 cm^{-1}.

8.2.2. Electrochemical Measurements

Laboratory measurements were made using a 4 ml cell in 0.1M PBS (pH 7.4) at 25ºC.

8.2.3. Fabrication of Glucose Biosensor

The first step of the fabrication of the biosensor is the generation of a conductive, redox-sensitive substrate. While there are many options, Pt was sputtered on one side of a conventional filter paper was chosen as proof of principle. Subsequently, 20 mm long X 5 mm wide rectangular pieces of this platinized paper were cut and sandwiched between to plastic masks. The top mask was a 15 mm X 10 mm rectangular piece fitted with a 3 mm diameter circular window in the center; the bottom mask was a slightly larger (20 mm X 10 mm) rectangular piece. Details illustrating the components and construction of the electrode are shown in Figure 8.1A. In essence, the role of the mask is to leave exposed only two parts

of the conductive paper: the top, where the electrode will be connected to the reading device, and the window, that will be used as the electrochemical active surface. These bare Pt electrodes are ready to be functionalized with the suitable membrane.

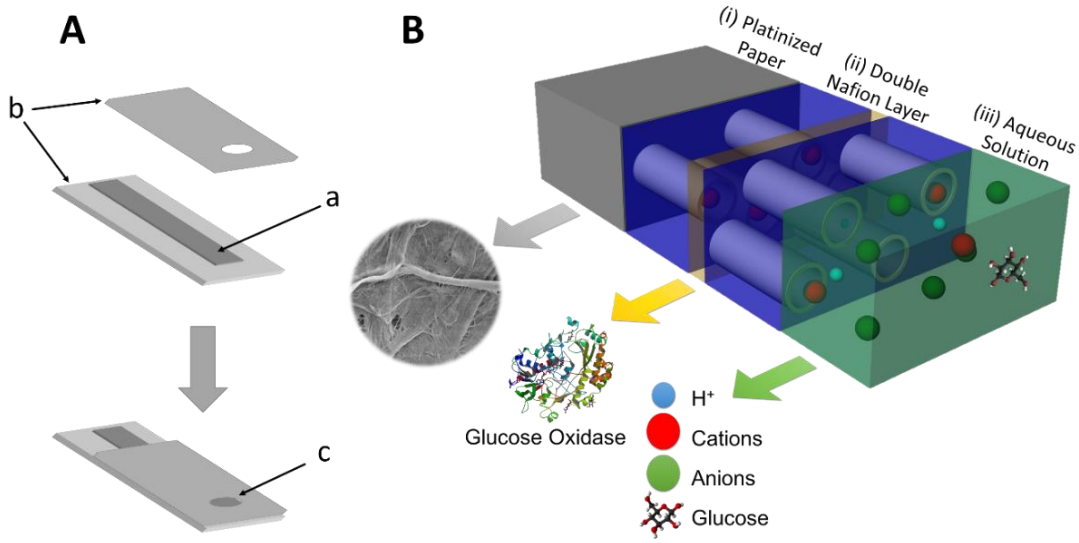

Figure 8.1. Schematic illustration of the biosensor. (A) Fabrication process of the paper-based electrode. A strip of platinized paper (a) is sandwiched between two plastic masks (b); the mask on top has an orifice to expose the electroactive surface (c). (B) Scheme of the structure of the enzymatic membrane deposited on the paper-based electrode: (i) Pt-Paper Substrate; (ii) enzyme (GOx) sandwiched between two layers of Nafion; one layer of Nafion is at Pt-interface and the other at the (iii) solution interface.

The biosensing membrane was made using Nafion as polymeric coating and glucose oxidase enzyme as the biological receptor. First, the electrochemical active window (i.e., the orifice left by the mask) of each electrode was thoroughly rinsed with double-distilled water and air-dried. Thereafter, a first layer of 4 µl of the 5% Nafion solution was drop cast and air-dried for 60 minutes at room temperature. Once the electrode is dried, 20 µL of a solution containing 20 mg mL^{-1} of glucose oxidase (GOx) in distilled water was drop cast on top of the Nafion membrane and the system was left drying overnight at 4ºC to avoid the denaturalization of the enzyme. Finally, 2.5 µl of the same solution of Nafion was applied as a second layer let dry overnight at 4ºC. This enzymatic electrode was kept at 4ºC after fabrication when not in use.

8.2.4. Analysis of Real Samples

Serum samples of patients were obtained by a local hospital (Hospital de Sant Pau i Santa Tecla). Values from serum samples were provided by the hospital using hexokinase/glucose-

6-phosphate dehydrogenase colorimetric test as a standard method for further validation of the paper-based potentiometric system.

8.3. Results and Discussion

8.3.1. Characterization of the Platinized Paper-based Electrodes

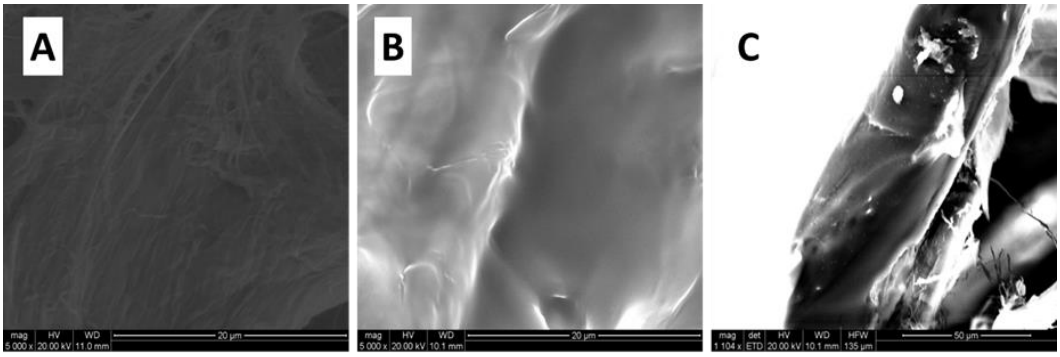

Figure 8.2. ESEM images of the paper-based electrode surface: (A) a bare platinized paper electrode, (B) a membrane (double layer of Nafion) on top of a platinized paper electrode and (C) transversal cut of the electrode membrane (ca. 40 µm thickness).

Environmental scanning electron microscopy (ESEM) was used to study the surface of the paper-based electrodes. The results reveal the cross-linked cellulose fibers completely covered by a thin layer of sputtered platinum (Figure 8.2A). Preliminary tests were conducted by adding a drop of water on top of the Pt layer to evaluate the wettability of this coated paper. The results show that the water does not percolate through the metallic layer. When the sputtering is performed over a flat surface -such as glass-, a layer of a thickness of approximately 100 nm is obtained. In the case of paper, because of roughness and 3D nature of the network created by the cellulose fibers, it is difficult to assess the actual thickness of the metal layer. In any case, the Pt-coated surface is waterproof and shows a homogenous and very low electrical resistance that corresponds to a metallic conductor. The tridimensional structure of the cellulose increases the electrochemically active surface of the electrode where the Nafion membrane and the enzyme are cast. When the Nafion is added, the surface of the metalized paper is completely covered by the polymer (Figure 8.2B). The membrane has an irregular morphology, as the Nafion layer follows the uneven cross-linked cellulose fibers. A transversal cut of the electrode reveals a membrane with approximately 40 µm thickness that is evenly spread over the platinized surface (Figure 8.2C).

8.3.2. Electrode Response and Principle of Detection

Preliminary experiments were conducted in order to verify the response of the enzymatic sensor. The results show that over certain concentration range the electrode potential decreases linearly with the logarithm of the concentration of glucose. To explore the nature of this response, "blank" measurements were performed. To do this, experiments where the enzymatic sensor was replaced either by a bare Pt electrode or by a Nafion coated electrode (i.e., without enzyme) were also conducted (Figure 8.3A). The results show that none of these electrodes respond to the addition of glucose (Figure 8.3B). Therefore, it is clear that the enzymatic sensor is responding to some byproduct of the enzymatic reaction. The reaction catalyzed by the GOx can expressed as:

$$H_2O + O_2 + Glucose \rightarrow Gluconolactone + H_2O_2 \qquad \text{(Equation 8.1)}$$

The gluconolactone quickly turns into gluconic acid. Therefore, for practical purposes, it can be considered that the reaction generates gluconic acid and hydrogen peroxide. To evaluate the influence of these products on the observed signal, the response of the sensor to each one of these substances was studied using a bare and Nafion-coated platinized electrode. The results show that none of the systems respond to the addition of gluconate (Figure 8.3C); however, the addition of peroxide produces a negative response that, in the case of the electrode coated with Nafion, is similar to the response obtained when adding glucose in the enzymatic sensor (Figure 8.3D). This evidence suggests that the response shown in Figure 8.3A is produced by the change on the redox potential due to the generation of hydrogen peroxide resulting from the enzymatic oxidation of glucose. The difference in response between the bare Pt and the coated electrode also suggests that the response to peroxide is modulated by the presence of the Nafion membrane, as it will be discussed later.

Although there are multiple models that have been proposed to describe the structure of Nafion[42] and its interactions with substrates such as carbon or platinum interfaces,[43] the topic is still a matter of debate. There is an agreement, though, on the presence of hydrophilic structures that allow the aqueous solutions to pass through the membrane. More recently, the Nafion structures have been described as randomly packed water channels surrounded by partially hydrophilic side branches, forming inverted-micelle cylinders.[44] These new model explains important features of Nafion, including fast diffusion of water and protons. It is important to stress that Nafion is a polyelectrolyte with negatively charged sulfonate groups ($-SO_3^-$), which provide strong ion-exchange capabilities. Because of this, a Donnan potential at the Nafion-solution interface is generated.[45]

In the previous chapter we have demonstrated that Pt electrodes coated with a layer of Nafion show an enhanced sensitivity and selectivity for the determination of H_2O_2. Indeed, bare Pt electrodes showed a limited sensitivity for peroxide and an unspecific response to any kind of redox-active species. However, when the Pt is coated with a layer of Nafion, the sensitivity increases significantly, while the effect of negatively charged species -such as ascorbate- can be significantly reduced. The improved selectivity can be explained in terms of the permselective behavior of the Nafion, a characteristic that has been already used in amperometric sensors. The enhanced sensitivity, on the other hand, is more difficult to explain, and has been ascribed to the effects produced by the Donnan potential on the physicochemical properties of the membrane. It is well known that due to the potential generated and the interface factors such as the pH may show local variations that significantly differ from the bulk properties of the solution.[46] As a result, complex coupling between the redox and acid-base equilibria at the bulk of the membrane show results that are different from what could be expected from the properties of the solution.[45] The nature of this coupling is still a matter of study.

To illustrate this point, experiments with bare platinized papers and Nafion-coated platinized papers were performed (Figure 8.3D). Figure 8.3E displays the significant increase in the sensitivity that was obtained when electrodes were coated with Nafion (-140.4±7.4 mV decade^{-1}, N=2) in comparison to bare platinized paper electrode (-53.6±6.2 mV decade^{-1}, N=2) in a linear range of 10^{-5} M to $10^{-3.5}$ M after additions of H_2O_2. These results are in general agreement with those previously reported. However, it is important to mention that the sensitivity for peroxide is highly dependent on the Pt surface. Indeed, while for a bare flat disk electrode we have found sensitivities in the order of 20-30 mV decade^{-1} of H_2O_2, these paper electrodes -with clean sputtered Pt- show higher sensitivities (in the order of 50 mV decade^{-1}).

All in all, this enzymatic sensor responds to a changes in the redox potential that are modulated by the Donnan potential created by the polyelectrolyte coating. To the best of our knowledge, this is the first time that this type of detection scheme is reported. Therefore, as it happens with more conventional amperometric sensors, the working principle of this sensor is based on the detection of H_2O_2. Thus, it should be different from the potentiometric sensors recently reported by Willander et al., which are claimed to be based on the local changes of pH resulting from the enzymatic reaction.[47] Therefore, the optimization of the detection of peroxide was considered as a first step prior the detection of glucose.

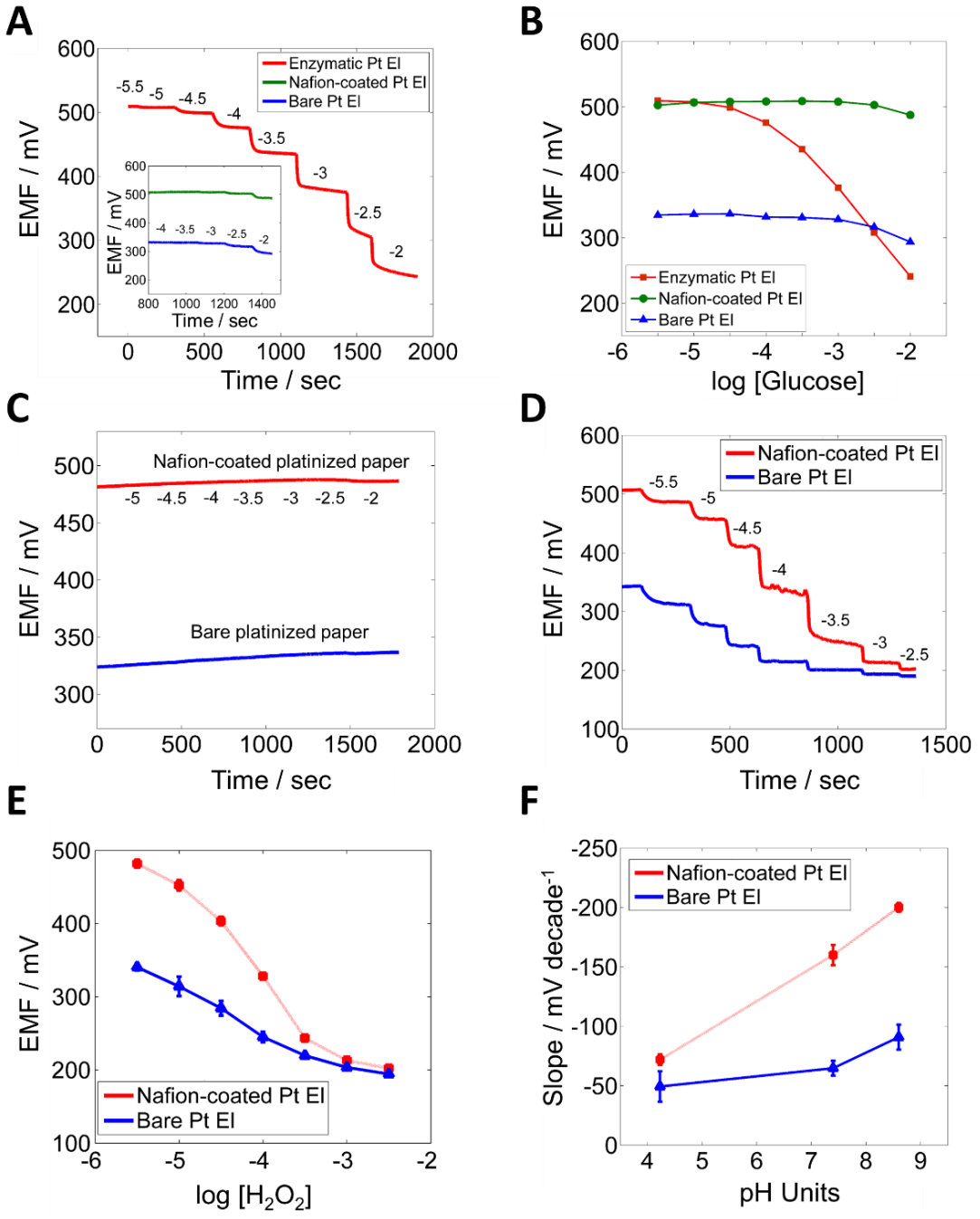

Figure 8.3. Response study of enzymatic paper-based electrode: (A) Potentiometric time-trace and (B) corresponding calibration curve of enzymatic, Nafion coated and bare platinized paper electrode upon additions of glucose; (C) potentiometric time-trace for gluconic acid for bare and Nafion-coated paper electrode; (D) H_2O_2 potentiometric time-trace and (E) corresponding calibration curve for H_2O_2 for bare and Nafion-coated platinized paper electrode (average ± S.D., N=2). (F) pH dependence of the sensitivity for H_2O_2 in the range from 10^{-5} M to $10^{-3.5}$ M (average ± S.D., N=2). All the measurements were performed in 0.1 M buffers, acetic buffer (pH 4.2), PBS (pH 7.4), borate buffer (pH 8.6) at 25ºC.

Because of the influence of the Donnan potential, the sensitivity for the detection of peroxide of these electrodes coated with Nafion is dependent on the total electrolyte concentration. Indeed, the initial potential (i.e., before the addition of peroxide) of the coated electrodes is strongly dependent on the Donnan potential at the Nafion-solution interface. High electrolyte concentrations show higher initial potentials, and this improves the sensitivity of the detection. Similarly, the enhancement of the sensitivity for peroxide is increased at higher pHs, as shown in Figure 8.3F. While bare Pt electrodes show a slight dependence of the sensitivity with the pH, the coated electrodes show a marked increase -almost three times- when the pH is changed from 4.2 to 8.9. Unfortunately, it not possible to withdraw conclusions regarding the mechanisms directly from this plot, since the pH of the bulk of the solution does not necessarily matches the pH inside the membrane. In fact, due to the strong accumulation of charge, variations of several pH units may take place on the vicinity of the membrane-solution interface. In any case, it is promising to observe that optimum conditions for detection of H_2O_2, such as high electrolyte concentrations and pHs slightly about 7, match the conditions usually found in many biological fluids.

8.3.3. Optimization of the Detection of Glucose

After the optimization of the detection of peroxide, the optimization of the detection of glucose is performed. In this case, conditions to immobilize the enzyme and to achieve optimum activity are explored. Preliminary experiments show that optimum results are obtained when the biosensor is built by sandwiching the enzyme between two layers of Nafion. The layer of Nafion cast on top of the Pt electrode plays 3 important roles. First, as it happens in other electrochemical sensors, it acts as a permselective barrier that minimizes the interference of negatively charged redox-active substances, such as ascorbic acid.[48] Second, as shown in the previous sections, the layer of Nafion produces an enhancement of the potentiometric detection of peroxide, due to the coupling of the redox and the Donnan potential. Third, the Nafion offers a better substrate for the stabilization and preservation of the enzymatic activity. Indeed, preliminary experiments (results not shown) show that when the enzyme is deposited directly onto the metallic surface, lower levels of activity are observed. Thus, a layer of Nafion on top of the Pt is beneficial before the enzyme is immobilized (a similar effect has been already described in the literature[49]). This immobilization is performed simply by direct drop casting of the enzyme solution on top of this first layer of Nafion. After the solution of the enzyme has dried, a second layer of Nafion is drop cast on top. This step is aimed to further improve the immobilization -avoiding any

leaching of the enzyme on the solution- as well as to isolate the generation of peroxide from the rest of the solution, avoiding the potential interferences.

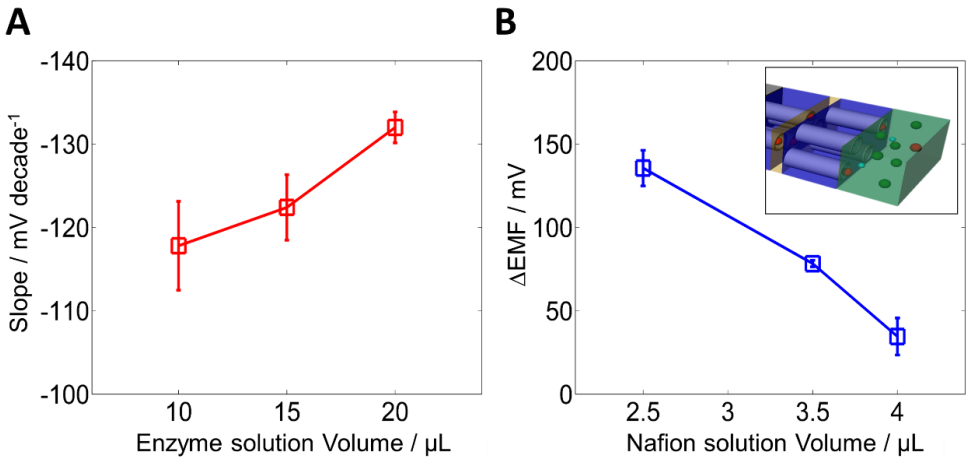

Figure 8.4. Optimization of the analytical conditions for the biosensor. (A) Sensitivity for glucose vs volume of solution of enzyme concentration (20 mg/mL) cast. (B) Change on the potentiometric signal after the addition of 10^{-4} M ascorbic acid as function of the increasing volume of Nafion membrane cast. In all cases, error bars correspond to the standard deviation of 3 different electrodes.

In order to optimize the analytical performance, the influence of the amount of enzyme was evaluated by adding a fix volume (15 µL) of solution with different concentrations of enzyme (0.2, 2, 20 mg/mL). Experimental evidence shows that none of these concentrations yield a difference on the final sensitivity obtained. Nevertheless, kinetic factors are improved at the highest concentration of enzyme. Under these conditions, faster production of H_2O_2 allows reaching steady state signal in less than 90 seconds. Alternatively, the amount of enzyme added was modified by adding different volumes (10, 15 and 20 µL) of the highest concentration (20 mg mL^{-1}) of the enzyme solution. In this case, an improvement in the sensitivity for glucose is observed (Figure 8.4A), suggesting a better distribution of the enzyme on the membrane during the drying process. Thus, optimum conditions for building the sensor were set at 20 µL of 20 mg/mL of enzyme.

Selectivity of the biosensor was assessed by monitoring the response in presence of redox interferences. Nafion ion-exchange membranes are negatively charge polyelectrolytes due to the sulfonic groups. Hence, Nafion is able to work as a cation exchange membrane, rejecting negatively charged species such as ascorbate and urate that are redox active molecules typically found in biological media. Experiments were carried out to evaluate the permselectivity of the first layer of Nafion, which separates the electrode from the solution.

Different volumes of the Nafion solution (2, 3.5 and 4 µL) were cast on the electroactive area, verifying that in all cases the whole Pt surface was covered. Therefore, the increase of the volume of solution cast produces an increase on the thickness of the membrane. To evaluate the performance of this membrane, the potentiometric response to a 100 µM ascorbate solution (upper concentration level typically found in body fluids) was tested. The difference in potential -before and after the addition of ascorbic acid- was used to characterize the selectivity of the system. The results are shown in Figure 8.4B. Clearly, the degree of interference is significantly reduced as the volume of solution cast (therefore, the membrane thickness) is increased. Nevertheless, it should be pointed out that the use of thicker Nafion membranes (5 µL) shows a poorer performance for the detection of glucose (Figure 8.5). Therefore, in a compromise between selectivity and sensitivity, a volume of 4 µl of Nafion solution was chosen as optimum drop-cast volume.

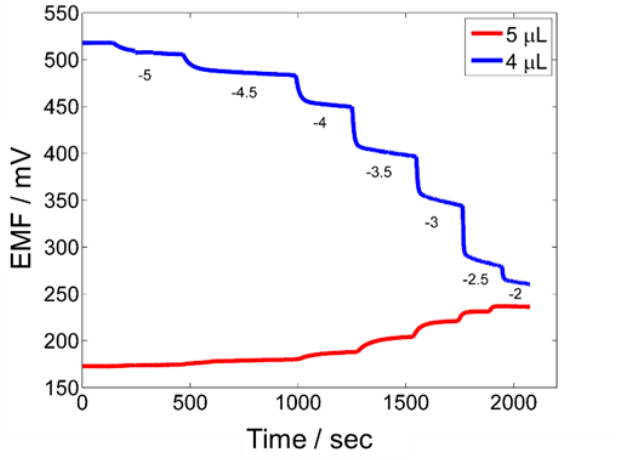

Figure 8.5. Time-trace curve for enzymatic paper-based sensors using different amount of Nafion solution in the platinized paper/enzymatic layer interface.

8.3.4. Analytical Performance

Enzymatic paper-based electrode was studied by monitoring change in electrochemical potential for increasing concentrations of glucose. Figure 8.6A shows the time-response curve of three different electrodes at different potentiometric cells in the concentration range from $10^{-5.5}$ M up to $10^{-1.5}$ M. A decrease in the potential was observed after addition of each glucose standard. Figure 8.6B presents the calibration curve on potential and glucose concentration with a linear response from 10^{-4} M to $10^{-2.5}$ M of glucose. The corresponding linear regression equation for the three calibration curves was: EMF (mV) = -118.6±7.6

log[Glucose] - 532.08±34.8, R^2 = 0.99, N=3. The limit of detection was found to be $10^{-4.5\pm0.08}$ M. This is the first time that such high sensitivity is obtained for a potentiometric paper-based enzymatic electrode.

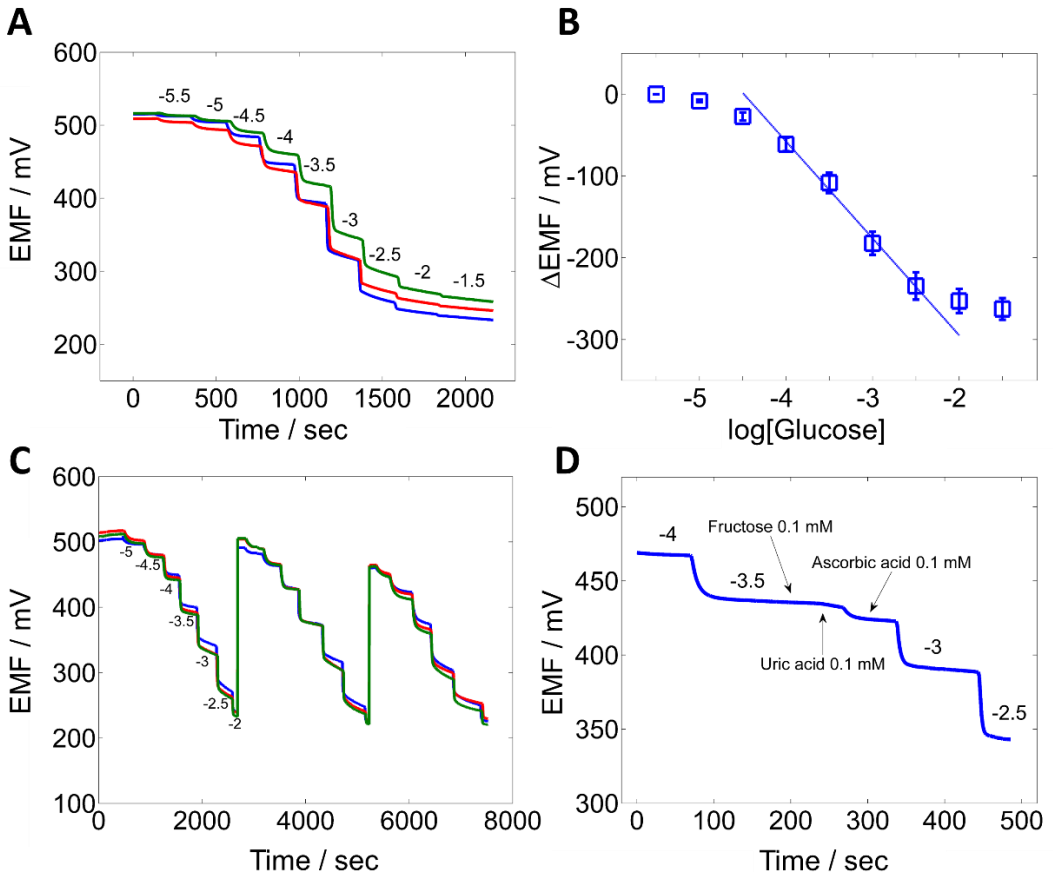

Figure 8.6. Analytical performance of the paper-based enzymatic electrode: (A) Time-trace plot of three different electrodes in three separated potentiometric cells, (B) the corresponding calibration curve of enzymatic electrodes showing the linear range (mean±S.D., N=3)). (C) Repeatability test for three different electrodes during consecutive calibration curves for glucose. (D) Enzyme-based electrode selectivity assessment to the main redox sensitive molecules (ascorbate and urate) and fructose. All the measurements were performed in 0.1M PBS (pH 7.4) at 25ºC.

Repeatability test was carried out by performing several consecutive calibration curves for three different electrodes from 10^{-5} M to 10^{-2} M (Figure 8.6C). The comparison between calibration curves (Table 8.1) yields an outstanding reproducibility among slopes (3.4% RSD, N=3). However, in the third calibration curve the linear range was narrowed on the upper end. In this last case, a decrease on the initial potential of the system was observed, possibly due to some rearrangement of the Nafion membrane. In any case, very reproducible potentiometric calibration curves between electrodes were obtained.

Table 8.1. Repeatability test. Analytical performance for 3 consecutive calibrations.

Sensors (N=3)	1st Curve	2nd Curve	3rd Curve
Sensitivity / mV decade-1	-118.7±1.9	-122.8±3.3	-114.8±1.5
Linear range	10^{-4} - $10^{-2.5}$ M	10^{-4} - $10^{-2.5}$ M	$10^{-4.5}$ - 10^{-3} M

The selectivity of the enzymatic sensors is associated with the specific enzymatic reaction between the enzyme and the target analyte. However, some redox sensitive interfering molecules found in real samples can induce to an error in the prediction. It is well-known that some molecules interfere in amperometric glucometers measurements such as uric acid and ascorbic acid. In this work, fructose, uric acid and ascorbic acid were tested at the high level of concentration found in blood (Figure 8.6D). For fructose and uric acid addition, the potentiometric response was almost negligible. However, for ascorbic acid addition (10^{-4} M) some small drop in potential was observed. Thus, despite of the permselectivity of Nafion, some residual electrochemical effect of the ascorbic was observed, possibly due to a slight diffusion of the ascorbic through the hydrophilic membrane. This effect, however, is observed at the highest concentration usually found in blood. Some further work is being currently performed to eliminate this residual effect.

8.3.5. Membrane Characterization

To gain insights on the changes during the enzymatic reaction, the membrane was characterized by ESEM to see possible electrode surface changes due to the hydration process. Besides, it is important to evaluate whether the surface is damaged by the action of the H_2O_2. Hence, Figure 8.7Aa shows the Nafion membrane over the platinized paper after the step of stabilization - hydration on PBS. In this case, a heterogeneous layer, showing some irregularities on the surface was observed. It has been reported that the interfacial area strongly increases with hydration,[50] thus producing different shapes along the surface. Figure 8.7Ab reveals similar behaviour as the previous image, with some orifices on the surface after a calibration curve for glucose has been performed. Finally, Figure 8.7Ac exhibits the minor effects on the electrode exposure to glucose (10^{-2} M), thus to consequently H_2O_2 generation in the membrane. The wrinkles that are observed on the surface could be attributed to the rearrangement of the Nafion polymer structure. First, some small degree of decomposition of the sulfonated tetrafluoroethylene based fluoropolymer-copolymer caused by oxidation with H_2O_2 may occur. Second, the ion-exchange process produced during the enzymatic reaction by-products (protons, gluconic, etc.).

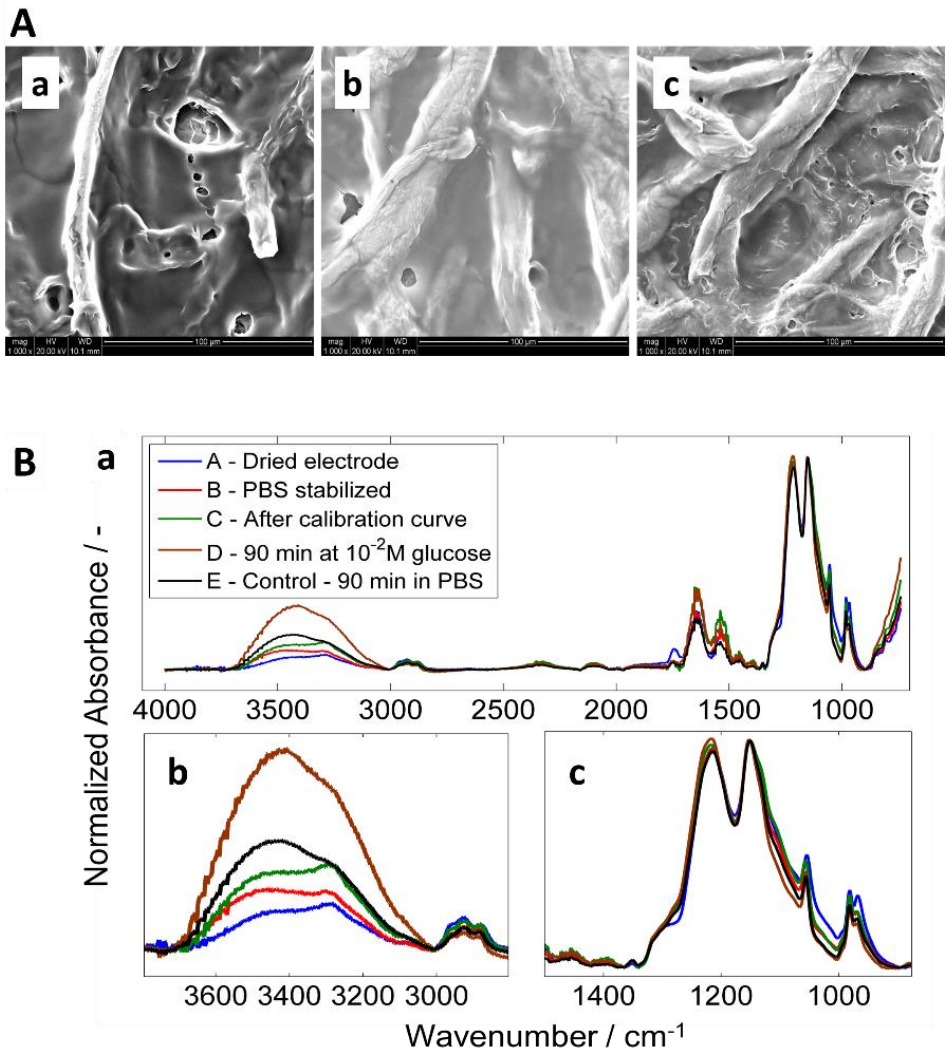

Figure 8.7. (A) ESEM images of the surface of the paper-based enzymatic electrode after hydration of the membrane: (Aa) PBS-solution-stabilized electrode, (Ab) after glucose calibration curve and (Ac) after 1.5 h 10^{-2} M glucose solution. Enzymatic reaction was performed in PBS pH 7.4 at 25 ºC. (B) FT-IR spectra of the paper-based enzymatic electrode in different conditions: (Ba) Whole overlap spectra, (Bb) magnification of peak at 3400 cm^{-1} of membrane swelling and (Bc) magnification from 900 to 1500 cm^{-1} showing Nafion backbone peaks. Potentiometric measurements were performed in PBS pH 7.4 at 25 ºC.

An infrared analysis of the enzymatic electrode surface was performed to study the distribution of the chemical species over the membrane. Figure 8.7B is consistent with the results of the FT-IR studies of Nafion performed by other authors[51,52] that reported at 1145 and 1200 cm^{-1} the C–F peaks and the C–C peak at 1300 cm^{-1}. These peaks represent the polytetrafluoroethylene (PTFE) backbone (main chain) of a Nafion membrane. Furthermore, the double peaks at 970 and 982 cm^{-1} assigned to the C–O–C bond, and the vibration at

1059 cm^{-1} assigned to the S–O bond are characteristic peaks of the pendant side chain and sulfonic groups of Nafion, respectively. A broad band at 3400 cm^{-1} was identified for water absorption from the membrane (OH stretching). Shown in Figure 8.7Ba, FT-IR spectra of the enzymatic electrode before and after potentiometric measurements. Figure 8.7Bb shows the water absorption peak. Increasing time of the electrode in aqueous solution allows the membrane swelling through the polymer ionic domains. Interestingly, the peroxide reaction may produce an alteration in the hydrophilic nanostrucutres causing an increment of the swelling by hydration. Figure 8.7Bc displays the Nafion characteristic peaks for the main and pendant side chains.

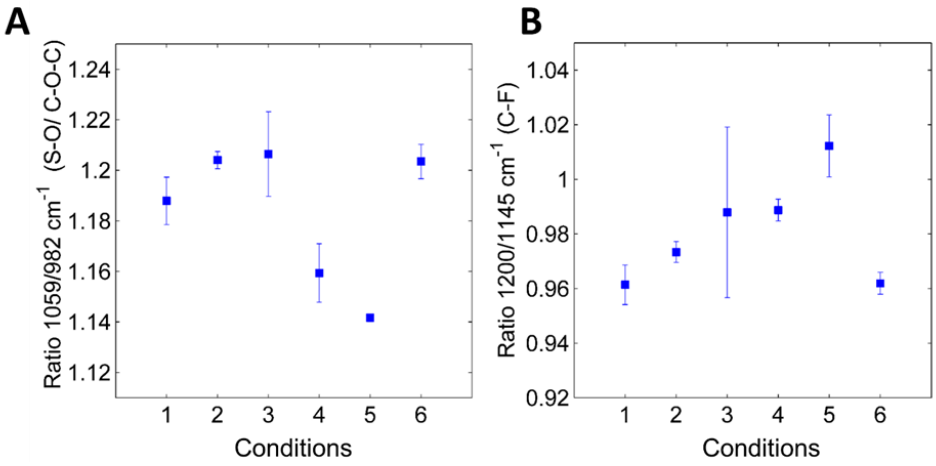

Figure 8.8. Ratio from FT-IR spectra between peaks (A) 1059/982 and (B) 1200/1145 in different conditions: (1) dried, (2) PBS stabilized, (3) after calibration curve, (4) 45 min at 10^{-2} M glucose, (5) 90 min at 10^{-2} M glucose and (6) control electrode, 90 min in PBS. Measurements were performed in PBS pH 7.4 at 25 ºC.

A comparison of the chemical study of the surface during glucose exposure onto the potentiometric cell was also carried out. The difference between peak ratios indicated that a chemical modification was performed on the Nafion membrane after the determination of glucose and during long-time exposures to glucose (conditions 4 and 5) and thus H_2O_2 (Figure 8.8). Figure 8.8A describes the ratio of groups on the side chain. As long time exposures to glucose, higher change in the ratio was generated. Moreover, Figure 8.8B shows the ratio between the chemical groups in the main chain. Also, a slightly variation was found after long exposure to glucose. In this case, the change in the ratios was lower indicating that the modification of the polymer started from the side chain. This variation may be attributed to a slightly degradation of the polymer by the long exposure to glucose, consequently to the oxidative activity of the H_2O_2.

All in all, it is suggested that the enzymatic electrodes undergo almost no degradation of the Nafion membrane after a calibration curve and only a hydration process is involved. For long time exposures, membrane experiences slightly degradation that may produce small difference in the formal potential of the system. However, a detailed study of the reactions involved in this system falls well beyond the scope of this work, and only some general observations can be elaborated.

8.3.6. Analysis of Real Samples

The feasibility of the paper-based enzymatic electrodes was evaluated through the determination of glucose concentration in real samples. In this work, serum samples from patients provided from a local hospital were used in order to proof the enzymatic paper-based electrode system. As the physiological range is higher than the current sensor linear range, a dilution (1:10) in PBS (0.1 M) was performed for the analysis of the serum samples. For the prediction of glucose, three different electrodes were used for each sample in order to have a reliable validation. Before the analysis, a calibration curve from 10^{-5} M to $10^{-2.5}$ M was performed. After that, the diluted serum sample was placed in the potentiometric cell. Potentiometric signal was recorded after a steady-state value of about 150 seconds.

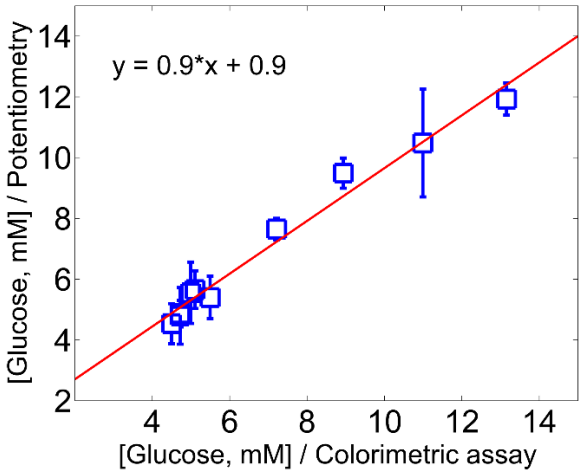

Figure 8.9. Comparison of glucose determination (mM) in real samples obtained by the potentiometric paper-based electrode (mean±S.D., N=3) and colorimetric assay (data provided by the local hospital) at 25ºC.

Results shown in Table 8.2 indicates an excellent recovery in agreement with the reference method results provided by the hospital (hexokinase/glucose-6-phosphate dehydrogenase colorimetric test). Moreover, Figure 8.9 presents a good linear correlation

between both methods. The recoveries for the assays from serum samples reached between 90.6-111.1 %, indicating that serum matrix had no significant effect on glucose determination. It should be mentioned that the same electrodes were used repeatedly for at least 6 predictions without losing their performance indicating high resistance to biofouling. Nevertheless, ideally the system is conceived to be used as a disposable sensor to make easy to handle and avoid contamination between biological samples.

Table 8.2. The recovery of glucose determination in serum samples (diluted 1:10).

Nº Sample	Potentiometry (mM)	Colorimetric assay (mM)	Recovery (%)
1	11.93±0.53	13.15	90.66
2	5.65±0.62	5.11	110.72
3	4.76±0.93	4.72	101.49
4	7.65±0.35	7.22	105.99
5	4.53±0.66	4.50	100.86
6	4.87±0.44	4.72	103.17
7	9.49±0.5	8.94	106.18
8	10.48±1.77	10.99	95.34
9	5.4±0.7	5.50	98.20
10	5.55±1.01	5.00	111.12

8.4. Conclusions

A new paper-based enzymatic electrode that shows high sensitivity for the determination of biomolecules such as glucose has been presented. Under the optimal conditions, this sensor exhibits excellent enzymatic activity and high reproducibility for the detection of glucose in a linear range from 10^{-4} M to $10^{-2.5}$ M with a limit of detection of $10^{-4.5}$ M. The use of the hydrophilic negatively charged Nafion membrane avoids minimizing interferences from negative redox active molecules such as ascorbate as well as the biofouling effect. The analytical parameters shown by the paper-based enzymatic electrode can be attributed to the elevated enzyme loading capacity and high stability provided by the Nafion membrane, which yield a favourable environment for glucose molecules oxidation. Furthermore, properties from thin Nafion membrane allowed this potentiometric enhancement as a result from a coupling of redox and Donnan potential. This principle opens a new strategy to develop highly sensitive paper-based enzymatic sensors for diseases monitoring. Other biomolecules monitoring could also be applied by only changing the biological receptor, the

enzyme. Future prospects involve a study of the storage properties and an integration with a reference electrode and wireless device to develop a full potentiometric cell for the decentralization of biochemical analysis.

8.5. References

[1] G. a. Evtugyn, H. C. Budnikov, E. B. Nikolskaya, Talanta 1998, 46, 465.

[2] J. Anzai, H. Takeshita, Y. Kobayashi, T. Osa, T. Hoshi, Anal. Chem. 1998, 70, 811.

[3] I. Karube, Y. Nomura, J. Mol. Catal. B Enzym. 2000, 10, 177.

[4] G. S. Wilson, Y. Hu, Chem. Rev. 2000, 100, 2693.

[5] L. Wang, W. Chen, D. Xu, B. S. Shim, Y. Zhu, F. Sun, L. Liu, C. Peng, Z. Jin, C. Xu, N. a Kotov, Nano Lett. 2009, 9, 4147.

[6] R. Khan, A. Kaushik, P. R. Solanki, A. Ansari, M. K. Pandey, B. D. Malhotra, Anal. Chim. Acta 2008, 616, 207.

[7] J. Wang, Biosens. Bioelectron. 2006, 21, 1887.

[8] S. A. Ansari, Q. Husain, Biotechnol. Adv. 2012, 30, 512.

[9] J.-M. You, Y. N. Jeong, M. S. Ahmed, S. K. Kim, H. C. Choi, S. Jeon, Biosens. Bioelectron. 2011, 26, 2287.

[10] D. T. V Anh, W. Olthuis, P. Bergveld, Sens. Act. B Chem. 2003, 91, 1.

[11] Y. Xiao, H. X. Ju, H. Y. Chen, Anal. Chim. Acta 1999, 391, 73.

[12] L. Li, Y. Wang, L. Pan, Y. Shi, W. Cheng, Y. Shi, G. Yu, Nano Lett. 2015, 15, 1146.

[13] J. Wang, Chem. Rev. 2008, 108, 814.

[14] M. A. Invernale, B. A. Tang, R. L. York, L. Le, D. Y. Hou, D. G. Anderson, Adv. Healthc. Mater. 2014, 3, 338.

[15] A. J. Bandodkar, I. Jeerapan, J. Wang, ACS Sensors 2016, 1, 464.

[16] E. J. Maxwell, A. D. Mazzeo, G. M. Whitesides, MRS Bull. 2013, 38, 309.

[17] Z. Yang, C. Zhang, J. Zhang, W. Bai, Biosens. Bioelectron. 2014, 51, 268.

[18] V. N. Psychoyios, G.-P. Nikoleli, N. Tzamtzis, D. P. Nikolelis, N. Psaroudakis, B. Danielsson, M. Q. Israr, M. Willander, Electroanalysis 2013, 25, 367.

[19] F. Ismail, S. B. Adeloju, Electroanalysis 2014, 26, 2701.

[20] D. J. Pasto, R. Meyer, S.-Z. Kang, J. Am. Chem. Soc. 1969, 91, 2164.

[21] S. D. Caras, J. Janata, Anal. Chem. 1985, 57, 1917.

[22] B. H. van der Schoot, P. Bergveld, Biosensors 1988, 3, 161.

[23] J. Anzai, T. Osa, Chem. Pharm. Bull. 1986, 34, 3522.

[24] S. M. Usman Ali, O. Nur, M. Willander, B. Danielsson, Sens. Act. B Chem. 2010, 145, 869.

[25] M. Q. Israr, J. R. Sadaf, M. H. Asif, O. Nur, M. Willander, B. Danielsson, Thin Solid Films 2010, 519, 1106.

[26] S. B. Adeloju, A. N. Moline, Biosens. Bioelectron. 2001, 16, 133.

[27] J. G. Ayenimo, S. B. Adeloju, Anal. Methods 2014, 6, 8996.

[28] A. T. Lawal, S. B. Adeloju, Biosens. Bioelectron. 2013, 40, 377.

[29] M. H. Asif, S. M. U. Ali, O. Nur, M. Willander, C. Brännmark, P. Strålfors, U. H. Englund, F. Elinder, B. Danielsson, Biosens. Bioelectron. 2010, 25, 2205.

[30] S. K. Shukla, S. R. Deshpande, S. K. Shukla, A. Tiwari, 2012, 99, 283.

[31] J. E. Shaw, R. a. Sicree, P. Z. Zimmet, Diabetes Res. Clin. Pract. 2010, 87, 4.

[32] O. D. Renedo, M. a. Alonso-Lomillo, M. J. A. Martínez, Talanta 2007, 73, 202.

[33] T. Guinovart, M. Parrilla, G. A. Crespo, F. X. Rius, F. J. Andrade, Analyst 2013, 138, 5208.

[34] M. Novell, M. Parrilla, G. A. Crespo, F. X. Rius, F. J. Andrade, Anal. Chem. 2012, 84, 4695.

[35] M. Novell, T. Guinovart, P. Blondeau, F. X. Rius, F. J. Andrade, Lab Chip 2014, 14, 1308.

[36] D. Mabey, R. W. Peeling, A. Ustianowski, M. D. Perkins, Nat. Rev. Microbiol. 2004, 2, 231.

[37] D. D. Liana, B. Raguse, J. Justin Gooding, E. Chow, Sensors 2012, 12, 11505.

[38] J.-H. Kim, S. Mun, H.-U. Ko, G.-Y. Yun, J. Kim, Nanotechnology 2014, 25, 092001.

[39] V. F. Curto, N. Lopez-Ruiz, L. F. Capitan-Vallvey, A. J. Palma, F. Benito-Lopez, D. Diamond, RSC Adv. 2013, 3, 18811.

[40] A. K. Yetisen, M. S. Akram, C. R. Lowe, Lab Chip 2013, 13, 2210.

[41] Z. Nie, C. a Nijhuis, J. Gong, X. Chen, A. Kumachev, A. W. Martinez, M. Narovlyansky, G. M. Whitesides, Lab Chip 2010, 10, 477.

[42] K. A. Mauritz, R. B. Moore, Chem. Rev. 2004, 104, 4535.

[43] D. L. Wood, J. Chlistunoff, J. Majewski, R. L. Borup, J. Am. Chem. Soc. 2009, 131, 18096.

[44] K. Schmidt-Rohr, Q. Chen, Nat. Mater. 2008, 7, 75.

[45] R. Naegeli, J. Redepenning, F. C. Anson, J. Phys. Chem. 1986, 90, 6227.

[46] R. B. M. Schasfoort, P. Bergveld, R. P. H. Kooyman, J. Greve, Anal. Chim. Acta 1990, 238, 323.

[47] S. M. Usman Ali, N. H. Alvi, Z. Ibupoto, O. Nur, M. Willander, B. Danielsson, Sens. Act. B Chem. 2011, 152, 241.

[48] A. Wynne, N. Finnerty, Chemosensors 2015, 3, 55.

[49] T. Klotzbach, M. Watt, Y. Ansari, S. D. Minteer, J. Memb. Sci. 2006, 282, 276.

[50] X. Kong, K. Schmidt-Rohr, Polymer. 2011, 52, 1971.

[51] M. Ludvigsson, J. Lindgren, J. Tegenfeldt, Electrochim. Acta 2000, 45, 2267.

[52] Z. Liang, W. Chen, J. Liu, S. Wang, Z. Zhou, W. Li, G. Sun, Q. Xin, J. Memb. Sci. 2004, 233, 39.

Chapter 9

Balloon-Embedded Sensors Withstanding Extreme Multiaxial Stretching and Global Bending Mechanical Stress

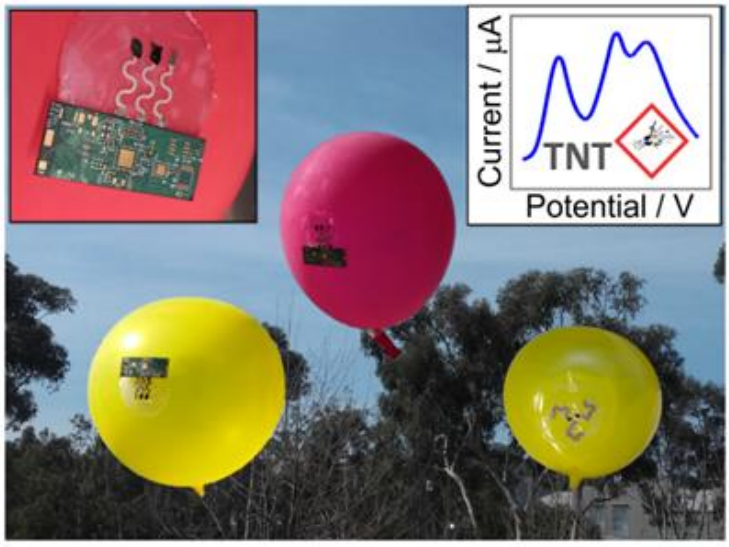

UNIVERSITAT ROVIRA I VIRGILI
NEW ELECTROCHEMICAL SENSORS FOR DECENTRALIZED ANALYSIS
Marc Parrilla Pons

Balloon-embedded Sensors Withstanding Extreme Multiaxial Stretching and Global Bending Mechanical Stress: Towards Environmental and Security Monitoring

In this chapter, balloon-embedded stretchable sensors, undergoing a simultaneous equal-multiaxial stretching along global bending motion, have been characterized and tested towards environmental and security monitoring missions. Stress-enduring inks are printed on the curvilinear surface of conventional rubber balloons and their resilience to extreme mechanical deformations, associated with repeated inflation and deflation cycles, is investigated. Unlike early studies of mechanically deformed electrochemical devices -performed with linear stretching or bending- the present balloon-embedded sensors undergo simultaneous multidimensional strains without any alteration of its electrochemical properties. The electrochemical detection of relevant military and homemade explosives in liquid and vapor phases is used to demonstrate the functionality and potential of the new balloon sensor system towards diverse environmental and defense missions. Negligible changes in the response to explosive compounds are observed following multiple repeated inflation and deflation cycles, involving over 400% increase of the balloon area.

9.1. Introduction

Wearable sensors have received a considerable recent attention due to their ability to record continuously valuable data regarding medical conditions, fitness level and air quality.[1] Most early applications of such devices have been devoted for on-body monitoring of the wearer physiological status,[2] and focused on monitoring of physical parameters and movement.[3,4] Recent efforts have led to the introduction of wearable chemical sensors and biosensors for biomedical and fitness applications.[5] However, wearable devices should not be limited to on-body measurements.[6] Indeed, these sensors hold considerable promise for diverse environmental and security monitoring applications when mounted on other surfaces, ranging from building walls to moving vehicles.

This work describes the development balloon-embedded sensors that withstand a simultaneous extreme multiaxial and global bending mechanical deformation, and demonstrates their potential towards environmental and security monitoring (Figure 9.1). The integration of flexible and expandable conductive components based on hybrid nanocomposites on a conventional rubber balloon is of considerable significance for two important reasons. First, it examines the fundamental role of the simultaneous multiaxial stretching and global bending motion upon the electrochemical behavior during repeated inflation and deflation cycles. Second, it offers considerable prospects for developing balloon-embedded sensors for in-situ security surveillance and

environmental monitoring, as will be illustrated below for the detection of different explosive compounds.

Conductive materials that can withstand high levels of mechanical deformation have been widely investigated.[7,8] Early studies of flexible printable electrodes examined the effect of their bending[9] or linear stretching deformations,[10] and led to stretchable electrochemical devices for potential wearable applications.[11–13] Nevertheless, materials that offer only flexibility or stretchability have limited potential for applications requiring bonding to or wrapping around non-planar substrates. Thus, there are considerable needs for enhancing the elastomeric properties of such materials to address new demanding applications.[14] Conformable and elastic electrochemical devices have the potential for seamless integration with variety of surfaces.[15,16] These devices are compliant with complex and dynamic surfaces while retaining their electrochemical properties. Such technology was used to develop a multifunctional balloon catheter with an expandable array of sensors for ablation therapy.[17] Other applications in which an expandable platform is needed are found in the wearable sensors field. Compressive garments, such as gloves, athletics suit and sport socks, might require to withstand extreme mechanical deformations and adapt to the muscle activity during rapid body movements. Accordingly, it is of considerable interest to study the mechanical stress produced by multiaxial stretchable spherical surfaces, as will be investigated here using electrochemical sensors embedded in conventional elasto-rubber curved balloon.

Inflatable technology has applicability in numerous fields, including mechanical and biomedical applications.[18–20] Over the past five decades several groups have worked on the static and dynamic inflation analysis and related deformation of different geometries and platforms.[21–23] Recent work has been focused on understanding the mechanics of inflation and applying it for the modelling of biomedical stents.[24,25] The present study represents the first example of modelling and testing such mechanical deformation using electrochemical devices on inflated platforms toward environmental and security monitoring.

Continuous terrorist threats greatly underscore the urgent needs for improved national security measures, in general, and vapor explosive detection, in particular.[26] Hence, there are growing demands for reliable field methods for detecting common nitroaromatic and peroxide explosives. The inherent redox activity of these explosives makes them ideal candidates for electrochemical (voltammetric) monitoring.[27] The advantages of electrochemical sensors for field measurements of explosives include remarkable sensitivity

and selectivity, a wide linear range, portability, minimal power requirements, and low-cost instrumentation.[28] The development of wearable electrochemical explosive-detection platforms thus represents a logical extension of recent activities in the areas of explosive detection and wearable sensors. Flying balloon platforms are particularly attractive for security surveillance applications aimed at detecting chemical threats. The successful realization of the new balloon-embedded sensor requires the understanding of the effect of extreme mechanical deformations upon the structure and performance of the corresponding printed hybrid nanocomposite electrodes. The printed carbon and silver inks, described here, have been tailored made with elastomers (Ecoflex and polyurethane) and dispersing agent (mineral oil) to withstand high degrees of mechanical stress associated with the inflation of the balloon substrate without compromising their electrochemical properties. Multiple inflation and deflation cycles, involving over 400% increase of the balloon surface area, thus result in negligible changes in the electrochemical behavior. The functionality of the new balloon-based printed sensor system is demonstrated using electrochemical detection of nitro-explosives and amperometric measurements of hydrogen peroxide in the liquid and vapor phases. While the new concept of balloon-embedded sensors is presented here toward explosive detection, such flying platform could serve a variety of defense and environmental monitoring missions.

9.2. Experimental section

9.2.1. Reagents and Materials

Permanent fabric adhesive (Aleene‘s, Inc., USA), Ag/AgCl ink (E2414, Ecron Inc., Wareham, MA). Mineral oil, agarose type I-A (low EEO), gelatin from porcine skin (type A) and 1-ethyl-3-methylimidazolium tetrafluoroborate ([EMIm][BF4]) were purchased from Sigma Aldrich (St. Louis, MO). Dimethylformamide (DMF) was purchased from Fisher Chemical (Fair Lawn, NJ). Ultra-pure deionized water was used in the preparation of the aqueous electrolyte solutions. Ecoflex® 00-30 was prepared in-house by mixing equal volumes of pre-polymer A with pre-polymer B provided by the supplier. Natural rubber latex balloons were employed to build the expandable sensors, purchased in a local store.

9.2.2. Electrochemical Measurements

Cyclic voltammograms were recorded in the -0.2 V to 0.6 V potential range with a scan rate of 0.1 V s^{-1}. The electrolyte redox probe consisted of ferricyanide (10 mM) in (0.1 M) phosphate buffer (PBS) (pH 7.4).

Resistivity studies were carried out using an Agilent 34411A digital multimeter (Agilent Technologies Inc., USA) and Keysight BenchVue software (Keysight Technologies Inc., USA) as a measuring interface, at room temperature (22ºC).

Chronoamperometric studies were executed using an AUTOLAB Type II (EcoChemie, B. V., Utrecht, The Netherlands) and NOVA software (v.1.11, The Netherlands) as a measuring interface, at room temperature (22 ºC) in PBS (0.1 M at pH 7.4). Current was sampled 60 seconds at potential -0.9 V for liquid and gas-phase assays. Adsorptive stripping voltammetry (AdSV) measurements of nitro explosives were carried out in a PBS solution (0.1 M) with the same reader arrangement as chronoamperometry. Following a 200 seconds accumulation step (at -0.4 V potential for DNT and at -0.1 V for TNT) and after a 15 seconds equilibration, the potential was scanned linearly at 0.1 V s^{-1}, usually from -0.4 V to -1.3 V for DNT and -0.1 V to -1.0 V for TNT. A cleaning step was not required between successive runs. Measurements employed a background subtraction protocol involving storing the response for the blank solution and subtracting it from the analytical signal.

The flexible printed circuit board (PCB) contained a commercial off-the-shelf (COTS) integrated circuits for instrumentation, control, and telemetry in a thin, wearable form-factor. Specifically, the PCB employs a Texas Instrument (TI) CC2541 Bluetooth Low Energy (BLE) System-on-Chip for communication.

9.2.3. Solid-state Electrolytes

Two types of solid-state electrolytes were explored towards the vapor explosive detection. Firstly, the agarose hydrogel (2% w/v) was prepared with NaCl (0.5 M) as a supporting electrolyte. A drop (150 µl) was casted over the sensing part and was quickly deployed. After 1h drying period, the sensor was ready to use. Secondly, a room temperature ionic liquid in the form of ionogel was used.[44] A gelator agent (gelatin from porcine skin) (40 mg ml^{-1} solution) was mixed with RTIL 1-ethyl-3-methyl imidazolium tetrafluoroborate ([EMIm][BF4]) at ratio (3:7) respectively. A thin layer (25 µl) was drop casted along the sensing area and let it dry overnight.

9.2.4. Mechanical Deformation Studies

The ability to sustain high levels of expandability was evaluated by measuring the resistance between each electrode of the serpentine. Firstly, increasing inflation levels (by air blowing) at constant speed (ca. 3 mm^2 s^{-1}) followed by holding it at each level state for 5 seconds was performed. Besides, the multiaxial stretching study consisted of inflating and

deflating the electrochemical device until more than 400% its initial area at constant speed (ca. 3 mm^2 s^{-1}). Subsequently, the study aims at assessing the electrochemical properties of the device when under continuous expandability load, comprised of multiaxial stretching the device during each of the inflation levels for a total of 5 levels at constant speed (ca. 3 mm^2 s^{-1}). Finally, CV plots were recorded before and after application of 4 inflation-deflation stress cycles for a total of 8 iterations.

9.2.5. Fabrication of the Expandable Sensor on the Balloon Surface

The process employed an MPM-SPM semi-automatic screen printer (Speedline Technologies, Franklin, MA). Sensor patterns were designed in AutoCAD (Autodesk, San Rafael, CA) and outsourced for fabrication on stainless steel through-hole 12” x 12” framed stencils (125 µm thickness) (Metal Etch Services, San Marcos, CA). Previously, the balloon was inflated and was kept stretched (30 minutes). Subsequently, the balloon was widespread into a planar surface and ready for the printing. Firstly, the planar surface was treated by applying and Ecoflex solidified thick layer (1 mm). Precaution was taken to avoid entrapment of air bubbles while placing the Ecoflex layer onto the supporting surface. Then, a thin layer (ca. 75 µm) of PU (15 wt%) in DMF solution was deposited on top of the balloon surface and was cured (50ºC for 20 minutes). The PU layer fixed the Ecoflex layer onto the balloon surface and served as a smooth material to stick the printed electrodes. Subsequently, the Ag/AgCl – Ecoflex (86 %wt – 14 %wt) ink was printed on the treated balloon surface, followed by curing (10 min at 95ºC). After printing this trace, the CNTs ink was used to print the working and counter electrodes (10 min curing at 85ºC). Finally, a layer of a permanent stretchable adhesive was used to isolate the sensor print by deploying a thin layer on top. Overnight drying step left the expandable sensor ready to use.

9.3. Results

9.3.1. Considerations for Practical Fabrication and Selection of Materials

Rapid inflation and deflation cycles of the sensor-embedded balloon platform result in extreme mechanical stress of the printed electrodes (Figure 9.1B). An elastomeric hybrid nanocomposite, tailored with multi-wall carbon nanotubes (MWCNTs) and materials with high viscoelasticity, is used to comply with the extreme multiaxial and global bending mechanical stress associated with the balloon inflation (Figure 9.2A). The nanocomposite electrode addresses current limitations in stretchable electronics by taking advantage of the high elastic properties of the elastomeric materials (polyurethane and Ecoflex silicone rubber) to

withstand extreme mechanical deformations without affecting the electronic properties and electrochemical activity of the MWCNTs. Elastomeric polymers provide remarkably complex and nonlinear macroscopic motions, due to their viscoelasticity feature, enabling large geometrical changes without compromising their physical properties.[29] A conductive backbone, the randomly aligned MWCNTs, is entrapped within the polyurethane matrix maintaining their outstanding electron transport properties during the mechanical deformation associated with the balloon inflation. Similar behavior is observed for the printed contacts and reference electrode with the silver/silver chloride and Ecoflex ink, where the long elastomeric chain is surrounded by Ag/AgCl particles and is able to reconfigure itself to distribute the applied deformation.

Successful sensor operation should be realized by addressing the stretchability of the materials tightly attached to the surface. After observing experimentally the expandable behavior of the balloon, an elastomeric layer (Ecoflex) has been placed below the printed sensor to absorb the tangential strain energy yielded associated with the inflation deformation and avoid potential fractures from the electrochemical device. The large Si-O-Si bond angles and bond lengths of the Ecoflex backbone confers high flexibility and stretchability to the polymer.

Crucial steps in the fabrication and assembly of the different layers are applied in the sensor manufacturing. These procedures add functionality to the balloon significantly enhancing their mechanical properties or the levels of expansion that they can accommodate. The printed conductive sensor traces can tolerate linear tensile strains of up to 500% without cracking through optimal composition and patterns guided by mechanics modelling. The strain distributions obtained through analytical modelling capture, quantitatively, the nature of these deformations.[30] After multiple repeated inflation and deflation cycles, involving over 400% increase of the balloon area, all devices and interconnects experienced negligible change in their performance.

To address the aforementioned requirements, we exploit two strategies in mechanics.[31] First the use of design patterns that stretch to accommodate the stress (Figure 9.1B and 9.1D). Second the use of materials that stretch, the intrinsic stretchability of the printed hybrid materials nanocomposite, imparted by combining CNT with elastomeric polyurethane (PU). PU is acting as the stretchable binder due to its ability to form hydrogen bonds with the carboxyl groups of the CNTs, thus leading to improved dispersion of CNTs within the PU binder.[32] Mineral oil further assists the CNT dispersion to create randomly distributed CNTs

branches along the stretchable polymer and providing multiscale electron path even during highly mechanical stress, thus retaining the electronic properties of the conductive material.

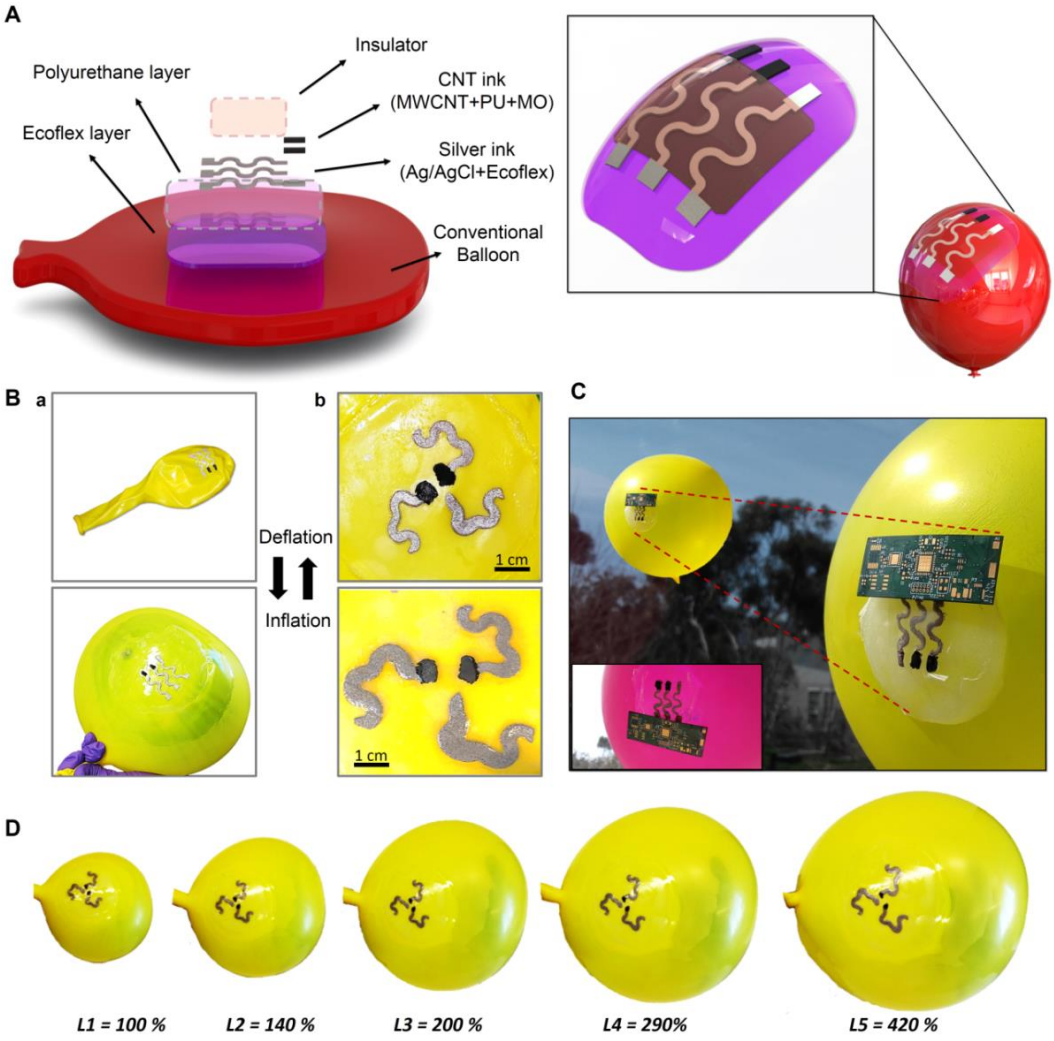

Figure 9.1. Expandable electrochemical device. (A) Schematic representation of the layers' composition for the expandable balloon device and the representation of its adaptability to curvilinear surfaces. Multiple layers consist of Ecoflex layer (inner), polyurethane (intermediate), printable sensor (Ag/AgCl with Ecoflex composite), the CNT hybrid nanocomposite layer (PU, MO and MWCNTs) and flexible insulator layer (upper). (B) Inflation and deflation status for both designs ((a) linear serpentine and (b) clover designs). (C) Integration of a flexible electronic/wireless circuitry with the expandable balloon device. (D) Different inflation levels (IL) used during the mechanical deformation study and the explosives monitoring.

The printed device conforms four different layers of elastic materials (Figure 9.1A). An inner silicone elastomer layer (Ecoflex) yields uniform distribution of the multiaxial deformation through the convex surface during the inflation and deflation cycle.

Subsequently, an intermediate PU layer is printed on top of the inner layer before printing the sensor trace. Improved adhesion between balloon and a stretchable ink by the use of a PU and Ecoflex layer increase the effective stretchability of the sensor by distributing strain uniformly. In a poorly adhered film, global tensile strains localize to delaminated regions and thus form cracks at much smaller strains than for systems with better adhesion.[15] Then, the sensor is printed using previously selected stretchable materials based on an analytical procedure. Ag/AgCl particles with the elastomeric Ecoflex material permit electrodes to sustain high degree of expandability as well as PU and CNT to stretch over the surface. Finally, an outer layer made by stretchable insulator is deposited on top of the sensor pattern leaving just the sensing area and the connector part.

Figure 9.1Ba displays the deflated and inflated balloons, the sensor pattern is expanded through the hemispherical surface producing bending and multiaxial stretching mechanical deformation. Materials start to accommodate mechanical stress energy during inflation until it reaches the point where the sensor starts its visual deformation. The effect of device design and stretchable inks provides the printed sensor with high tolerance toward inflation and deflation cycles). The images underscore the ability of the printed sensor to endure extreme and complex multidimensional strains with minimal effect on its structural integrity. Besides, different design patterns are tested in order to increase the sensor expandability (Figure 9.1Bb). Improvement in the curvatures of the sensor patterns (via a clover design) distributes the strain energy more equally during the inflation process, thus decreasing the deformation and fracture of the electrodes. The clover design displays higher compliance toward multidimensional mechanical deformation.

Finally, for the on-site explosives detection, wireless system integration is needed. Figure 9.1C shows a small flexible wireless circuit board able to record voltammetric signals upon an open area. The flexible electronic module can be coupled to the printed electrodes via magnetic connectors to enable real-time measurements and wireless data transmission. This flexible electronic board is compatible with the non-planarity of the balloon and offers resistance to mechanical stress. Automated systems are needed for the detection, and consequently warn of potential threats in public areas. The miniaturization and the ability of the wireless reader to withstand hard atmospheric conditions are key issues needed to validate the system in real scenarios. Hence, further improvements on these features will be necessary to test in the field.

9.3.2. Modelling

Before studying experimentally the mechanical deformation ability of the highly stretchable and flexible hybrid nanocomposite-based ink, a careful view to the inflation and deflation mechanism is needed to understand the expandability of the printed device. Figure 9.1D displays the inflation levels of the electrochemical device through the conventional balloon inflation. Hence, the geometric area could be calculated by having a look at the inflation technique as it will be carefully explained later.[33]

The novel expandability approach is studied by examining the rheological properties of the tailored printed ink on the curvature surface resulted from the balloon inflation and leads to multiaxial symmetric deformation. Several forms of the strain-energy function have been developed to describe these deformations of “rubber-like” materials. Hence, some mathematical expressions describing this deformation are documented in the literature. [21,22,34]

Figure 9.1D shows the evolution in the configuration of a multiaxial stretchable hemispherical surface associated with the use of a conventional elasto-rubber material such as a conventional curved balloon. The inflation and deflation cycles result in high strain levels (involving both multiaxial stretching with global bending motion, Figure 9.2A) over the sensor design, imparting expandability to the field of electrochemical sensors. Such curvatures produce the next level of mechanical deformation, resulting in an ideally equivalent multiaxial tensile strain, which many materials used in electrochemical devices cannot accommodate without crack or fracture. The mechanical properties of the new tailored ink allow the expandable sensor to maintain its electrochemical sensing behavior. Besides, the selected materials were required to stretch a planar layer over a hemispherical surface without generating wrinkles during the inflation and deflation cycles. The clearest application of expandable sensors is perhaps integration with components that deform regularly as part of their operation, or those that deform at randomly in response to their environment, such as the balloon in atmospheric conditions.

In the inflation technique test, the balloon is deposited with the circumference nozzle held in a clamp. Then, it is inflated to as spherical balloon using pressurized air. This method has long been used by many researchers for the characterization of synthetic polymers, especially rubbers and polymer melts.[18,19,23] Several attempts have been performed to simplify the study of the strain produced by the inflation test. An analysis that strives the non-uniformity in thickness of the studied element propose an analytical procedure for calculating

the stress and strain at the top of the balloon from the experimental data.[33] The analysis is based on the following assumptions: 1) the rubber is incompressible, 2) the balloon is spherical and 3) each rubber particle is shifted normally to itself during inflation. As the balloon inflates, the wall thickness reduces. However, due to the non-uniform deformation along the surface of the balloon, the thickness at the top is smaller than the thickness at the base of the balloon (close to the clamp) thus a thickness distribution arises. Therefore, an approach to calculate the thickness *t*, stress *σ,* planar strain *ε*, radius of curvature *R* and volume *V* at the top of the balloon can be executed with the following equations:

$$t = t_0 \left[\frac{a^4 + s^2h^2}{a^2(a^2+h^2)}\right]^2 \quad \text{(Equation 9.1)}$$

$$\sigma = \frac{PR}{2t_t} \quad \text{(Equation 9.2)}$$

$$\varepsilon = ln\left(1 + \frac{h^2}{a^2}\right) \quad \text{(Equation 9.3)}$$

$$R = \frac{a^2+h^2}{2h} \quad \text{(Equation 9.4)}$$

$$V = \frac{\pi}{6}h(3a^2 + h^2) \quad \text{(Equation 9.5)}$$

Where t_0 is the original sample thickness, t_t the thickness at the balloon top, *a* the original sample radius, *h* the height, *P* the pressure inside the balloon and *s* the distance from the center of the sample. Figure 9.2B illustrates the schematic representation related with the represented parameters in the equations.

On the other hand, we could assume the uniform balloon thickness. On this way, the thickness *t* and balloon surface area *S* could be calculated by the next equation:

$$t = \frac{\pi a^2 t_0}{S} \quad \text{(Equation 9.6)}$$

$$S = 2\pi R^2 \pm 2\pi R\sqrt{R^2 - a^2} \quad \text{(Equation 9.7)}$$

Finally, with this simplified approach, the expansion percentage could be calculated according to the surface area (Equation 9.7) of each inflation level from each radius of extension, R_x (Equation 9.4). Figure 9.1D displays the balloon inflation levels using the clover pattern with each calculated inflation percentage. Considerations during the printing are taken into account after the thickness assumptions regarding the position of the sensor in the balloon. To increase the inflation level, sensor should be printed in the lower part of the

balloon (as close to the nozzle as possible) to avoid high stretching stress from the material thickness.

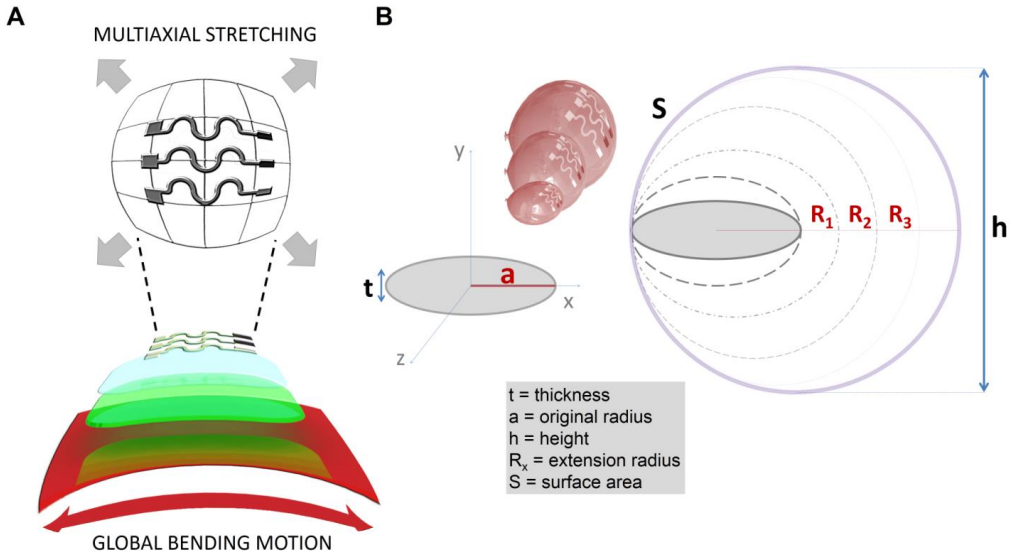

Figure 9.2. (A) Multiaxial stretching with bending motion schematics and (B) schematic representation related with the parameters in the equations.

9.3.3. Mechanical Deformation Studies

In order to test the inflation challenge and the corresponding mechanical stress that it occurs to the printed sensor, some mechanical tests were applied to the expandable device. The remarkable expandability and attractive performance of the new printable electrochemical sensor have been examined using conductivity measurements and cyclic voltammetry (CV) probing of changes in the electrochemical properties and in the electrode-electrolyte interface. Therefore, the expandable behavior of the sensor was assessed under static resistance measurements in each electrode during levels of inflation (Figure 9.3A). All the electrodes display low resistance values (<80 Ω) under these inflation-induced mechanical stress, with a slight resistance increase (from around 10 Ω) upon increasing the inflation level. Microscopic cracks on the conductive track and increased resistance have been observed after the 5th inflation level. While these still allowed electrochemical measurements, the stability and reproducibility are compromised. Further inflation of the balloon led to macroscopic fractures that did not allow sensing work.

The outstanding resiliency against mechanical deformation of the printed composite conductive traces can be explained by delving at the microscopic level of the printed traces

(Figure 9.3B). When an external expansion load is applied to the sensor, the stress generated within the printed pattern is absorbed by the stretchable elastomeric component that is able to deform and rebound to its original geometrical area without any distortion. For the Ag/AgCl ink under tensile stress, the interpenetrating Ecoflex long chains undergo stretching while maintaining the physical contact between the randomly printed conductive particles. Similarly, when the printed composite MWCNT working and counter electrodes are subject to extreme stress, their PU binder stretches while maintaining the electrical contact of the randomly distributed CNT. This hybrid nanocomposite is made by mixing functionalized MWCNTs with the PU elastomer to enhance the mechanical properties. The homogenous dispersion of the MWCNT reflects the hydrogen bonds between C=O groups and NCO groups of the PU chains with the -COOH of the MWCNT-COOH.[35] Moreover, the hybrid nanocomposite improves the tensile strength and modulus in compared to bare PU.[36] The elastomer cross-linkages ensure also that the polymer returns to its original position during deflation without affecting the electrical properties of the nanocomposite.

Interestingly, the electroactive area of the hybrid nanocomposited electrode is not changed during the balloon inflation and corresponding sensor stretching. As illustrated in Figure 9.3B, no alterations in the conducting carbon area take place upon inflating the balloon and expanding the printed nanocomposited MWCNT-PU electrodes. Although the geometrical area of the electrode increases dramatically due to the elastomeric behavior of polyurethane molecules, the same electrochemical active surface area (in direct contact with the solution) is maintained. This reflects the finite amount of the embedded MWCNTs. Therefore, the elongation of the chains from the elastomeric binder (PU) component is performed while maintaining the electrical connections of the composite electrode associated with the randomly aligned MWCNTs. Figure 9.3B illustrates the expansion of the elastomeric molecular chains while maintaining the same amount of MWCNTs, thus retaining the same electroactive area of the sensor. According to the Randles-Sevcik equation (Equation 9.8), the electroactive surface area maintained during the inflation over the electrode is ca. 0.19 cm^2.

$$A = \frac{I_p}{2.69x10^{-5}\, D^{1/2}\, n^{3/2}\, \gamma^{1/2}\, C} \qquad \text{(Equation 9.8)}$$

Where *A* is the surface area in cm^2, *D* is diffusion coefficient of the molecule in solution ($cm^2\ s^{-1}$), I_p is the peak current value, *n* is the number of electrons involved in the reaction, *C*

is the concentration of the probe molecule in the solution and γ is the potential scan rate (V s^{-1}).

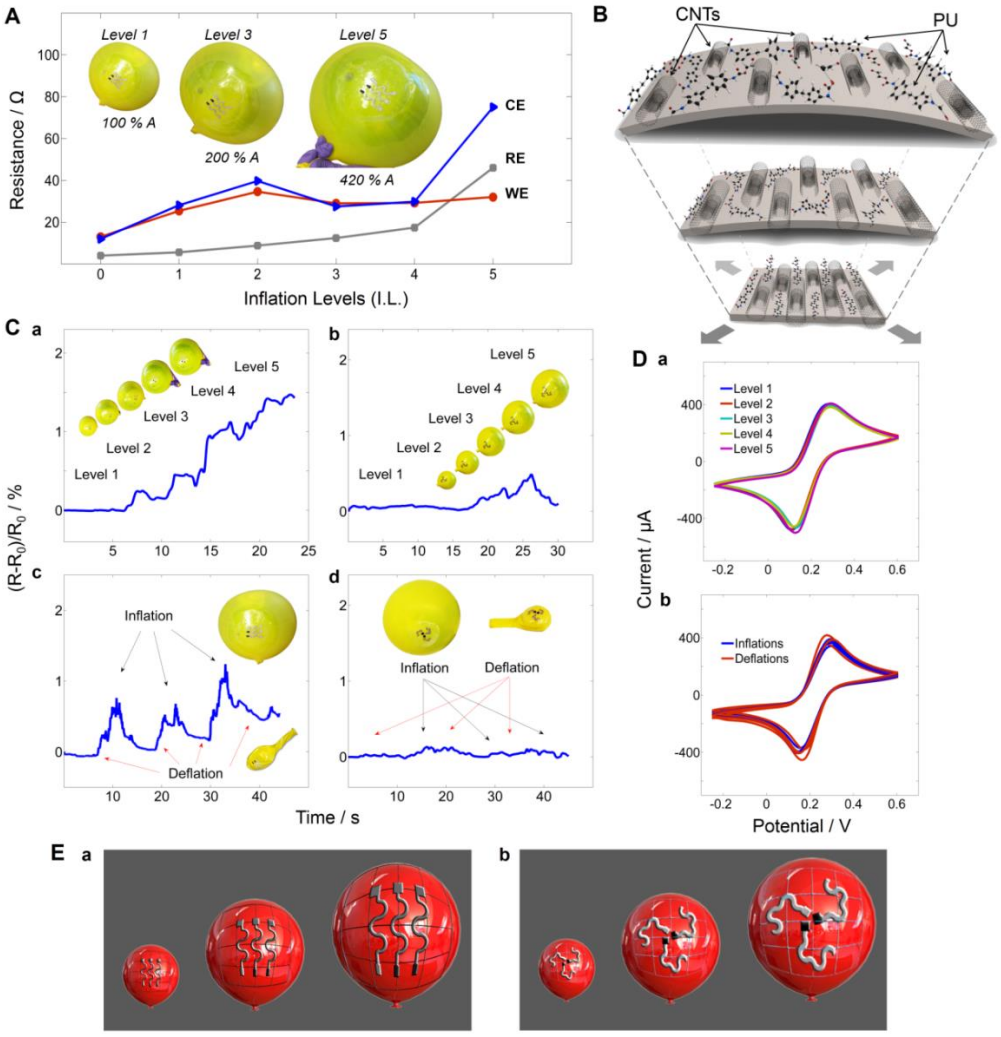

Figure 9.3. Mechanical deformation study and modelling of the expandable device. (A) Static resistance study during increasing inflation levels with the linear serpentine pattern for working, reference and counter electrodes. (B) Schematic representation of the expandable hybrid nanocomposite model of the carbon nanotubes (CNTs) and elastomeric stretchable polyurethane from deflation until inflation status. (C) Dynamic resistance study and comparison between different designs. (D) Cyclic voltammetry study for mechanical compliance assessment (Da) over all the inflation levels and (Db) during inflation and deflation cycles. (E) Schematics of the models between device patterns during the balloon inflation levels.

The assumption of unchanged electroactive area is supported further from the reproducible cyclic voltammograms of Figure 9.3Da, recorded for balloons inflated from level 1 to level 5. This is indicated from the reproducibility of the charging background current. Note also the similarity of the peak potentials that indicate that the small resistance changes

have minimal effect on the electrochemical behavior. In addition, no resistance changes are observed for the clover pattern for repeated balloon inflation/deflation cycles (Figure 9.3Cd). Similarly, the cyclic voltammograms of Figure 9.3Db show no apparent change in the electrochemical performance during such repeated cycles.

After understanding the behavior of the expanding sensor at the molecular level, a careful dynamic study for the resistance change was carried out during the balloon inflation status and upon repeated inflation/deflation cycles. Figure 9.3C illustrates the comparison between the linear serpentine and clover sensor designs by monitoring resistance change during different mechanical expansion tests. Figures 9.3Ca (linear pattern) and 3Cb (clover design) show the different behavior of the two designs upon the increasing inflation levels. Figure 9.3Cc (linear pattern) and 9.3Cd (clover design) show the resistance changes during inflation and deflation cycles. As indicated from Figure 9.3C (reference electrodes) and Figure 9.4 (working electrodes), the resistance study for both designs illustrates a higher signal stability using the clover design. Hence, more favorable outcomes are obtained for the clover pattern that offers a more uniform absorption of the tensile strain energy along the sensor trace.

A slight increase in the sensor resistance is observed during the balloon inflation. Such resistance change does not affect the explosive detection (described below). However, after certain inflation level, the resistance of the Ag/AgCl electrodes increases reflecting the limited density of Ag/AgCl particles (during the expansion of the Ecoflex material). Experimentally seen, the crack density is greatest at the non-curvilinear parts of the sensor pattern.

As shown in Figure 9.3D, the redox peak separation (ΔE_p) as well as the oxidation peak current (i_p) of the ferricyanide probe remain nearly identical even when the sensor undergoes high level of mechanical stress during inflation (RSD for i_p = 3%). Even during extremely stress cycles (continuous inflation and deflation cycles), the sensor displays an excellent peak heights stability (RSD for i_p = 5.9 %). These data indicate that the sensor can withstand high degree of multiaxial mechanical fatigue with minimal effect on the electrochemical properties.

9.3.5. Design Considerations

Following the detailed inflation model, we will proceed with discussion of the sensor pattern. Figure 9.3E illustrates the conceptual explanation of the balloon expandability containing the different sensor designs ((a) linear and (b) clover). These schematics and resistance tests suggest that the clover pattern should offer improved expandability of the

sensor by alleviating the stress applied during inflation (Figure 9.3Eb). Such clover design helps in the expandability and functionality of the sensor, instead of the linear one (Figure 9.3Ea) used earlier to sustain high amount of linear stretchability.[10] This assumption is supported by the resistance evaluation during different inflation levels shown in Figure 9.3C for the reference electrode and in Figure 9.4 for the working electrode. Figure 9.3C, Figure 9.4A and Figure 9.4B display resistance measurements using the balloon-embedded linear and clover serpentine patterns, respectively. The resistance increases gradually upon increasing the inflation level for the linear serpentine design (Figure 9.3Ca). In contrast, as shown in Figure 9.3Cb, the clover design is more resilient to resistance changes, with no apparent change up to the 3rd level. Similar advantages of the clover pattern are observed upon repeated inflation and deflation cycles (Figure 9.3Cd). Under this stress the linear design displays rapid increase of the resistance during the inflation step (Figure 9.3Cc), unlike the clover pattern that tends to accommodate more uniformly the energy stress associated with the inflation mechanical deformation.

Interestingly, Figure 9.4Ab and 9.4Ac as well as Figure 9.4Bb and 9.4Bc show that the working electrodes underscore less increment of resistance to allow a more stable signal. Such behavior reflects the difference in the binder characteristics. PU adhered to the CNT ink can absorb the energy coming from the mechanical stress more easily than Ecoflex found in Ag/AgCl ink. This ability to operate under extreme mechanical stress conditions meets the demands of using these balloon-embedded printed sensors for real-time atmospheric monitoring. Overall, the clover sensor pattern offers several advantages. Firstly, the elevated thickness is able to sustain more strain energy leading to a higher level of inflation. As discussed previously in the modelling, the balloon thickness decreases upon increasing the inflation level and high tensile strength is produced over the surface area of the sensor. Hence, high thickness in the sensor trace facilitates better distribution of the strain. Secondly, the curvilinear shape of the clover serpentine accommodates more mechanical stress than the linear one. Finally, a decrease of the geometrical sensing area is produced due to a circular shape instead of the linear shape allowing to a homogenous deposition of the solid-state electrolyte. The clover design thus leads higher multiaxial stretchability without compromising the integrity of the sensor. Previous work yielded to an inferior electrical resistance of linear serpentine pattern with higher angle, between the extremities of the circular shape, compared to lower angle toward external strain.[30,37] Therefore, decreasing the connecting angle as well as increasing the thickness of the clover serpentine leads to considerably higher resiliency and conductivity to strains associated with the balloon inflation.

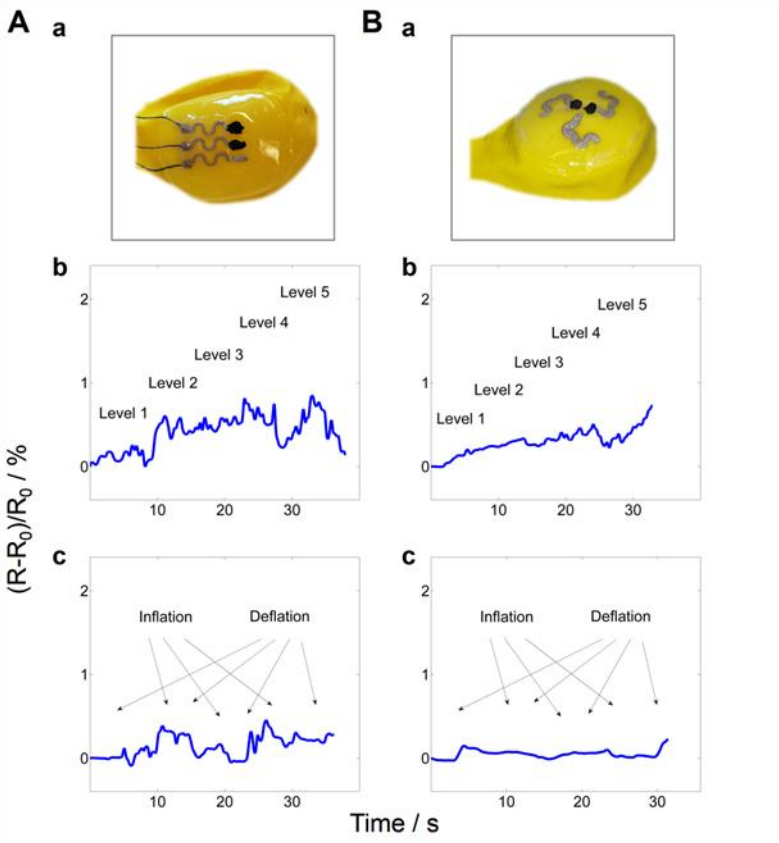

Figure 9.4. Dynamic resistance study and comparison between different designs: (A) linear serpentine pattern and (B) clover pattern, shown in (a). Figure (b) and (c) displays the change of resistance upon different mechanical expansion tests: increasing the inflation levels and inflation-deflation cycles, respectively, for working electrodes.

9.3.6. Liquid-phase Sensing

Electrochemical devices are advantageous for addressing the urgent needs for on-site detection of nitroaromatic explosives, such as 2,4,6-trinitrotoluene (TNT)[38] or 2,4-dinitrotoluene (DNT)[39] and of peroxide-based homemade explosives and their hydrogen peroxide (H_2O_2) precursor.[40] The ability of the balloon-embedded sensors to detect explosives has been evaluated first in the liquid-phase using variety of relevant mechanical strains associated with the balloon inflation. The strong accumulation of nitroaromatic compounds onto CNT can be used for effective pre-concentration step towards achieving highly sensitive explosive detection.[41] Figure 9.5A displays voltammetric signals for different TNT concentrations using highly sensitive adsorptive stripping measurements. The resulting stripping voltammograms reveal three well-defined redox processes, at -0.43 V, -0.65 V, and

-0.78 V (vs. the Ag/AgCl reference), characteristics of the stepwise TNT reduction to the corresponding hydroxylamine and amine.[41] The first signal (at -0.43 V), exhibiting the most favorable characteristics, was selected for subsequent analytical work. Figure 9.5Aa and 9.5Ab demonstrates the analytical performance of the sensor in the 1st and 4th levels of the balloon inflation, along with the corresponding calibration curve (inset). The peak currents increase proportionally with the TNT concentration from 20 to 100 µg ml^{-1} to yield a highly linear calibration plot, with a slope of 1.82 µA mL $µg^{-1}$ for the 1st level of inflation. Besides, the analytical performance of the 4th level of inflation sensor yields a slope of 2.09 µA mL $µg^{-1}$. To understand if the sensor can withstand different levels of inflation, the voltammetric signal using 60 µg ml^{-1} TNT was recorded at different levels of inflation (Figure 9.5Ac). Such investigation discloses its attractive performance even when subjected to increasing inflation levels (RSD for i_p = 7.7 %). Figure 9.5Ba and 9.5Bb display the sensor response for DNT (a TNT precursor) recorded during the 1st and 4th levels of inflation, respectively. The calibration plot (inset) yields a 3.31 µA mL $µg^{-1}$ and 3.72 µA mL $µg^{-1}$ for the 1st and 4th level of inflation (using -1.1 V DNT reduction peak) respectively. Figure 9.5Bc examines the sensor performance during different levels of deformation (L1-L5). These voltammetric data illustrate that the response for 60 µg ml^{-1} DNT is nearly independent of the inflation level of the balloon (RSD for i_p = 6.4 %).

Before applying the vapor-phase test, factors affecting the chronoamperometric detection of diluted peroxide aqueous solutions at the smart balloon were optimized. The signal increases slowly upon changing the potential from -0.6 V to -0.9 V where the reduction of the peroxide occurs. Hence, the analytical performance was examined by recording the current during 60 seconds at -0.9 V while varying the peroxide concentration from 0.5 mM to 3 mM. Figure 9.5Ca (1st level of inflation) and 9.5Cb (4th level of inflation), and corresponding calibration plots (insets), illustrate that the current increases linearly with the peroxide concentration. These plots lead to similar sensitivity (slope) between these 1st and 4th inflation levels (10.34 µA mM^{-1} and 10.54 µA mM^{-1}, respectively). Finally, Figure 9.5Cc shows a mechanical stress study recording chronoamperometric signals for 1.5 mM hydrogen peroxide (lower lines) during different levels of inflation (RSD for i = 1.1 %). Figure 9.5Cc also displays the corresponding background currents under these inflations (upper lines). Interestingly, only a negligible change in the current response is observed upon increasing the mechanical stress.

The results obtained from the voltammetric analysis of explosives compounds, TNT, DNT and hydrogen peroxide greatly support the ability of the expandable sensor to monitor these

compounds under extreme degree of mechanical strain. The system can thus be utilized for real-time security screening in real-scenarios.

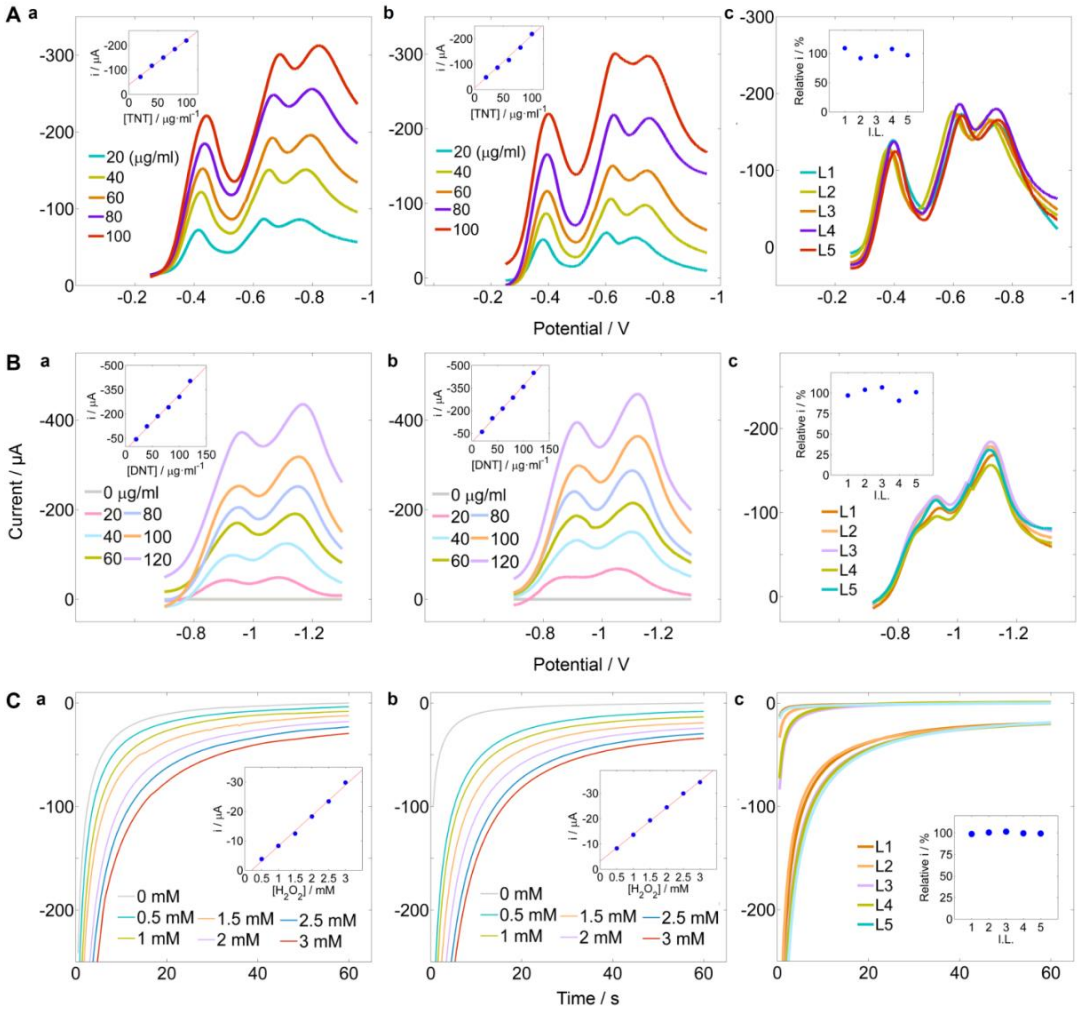

Figure 9.5. Explosive detection liquid-phase TNT, DNT and H_2O_2 using the balloon-embedded sensor. (A) TNT calibration curve in (Aa) the 1st, (Ab) the 4th level of inflation for the expandable device and (Ac) voltammetric signals during increasing inflation levels. (B) DNT calibration curve in (Ba) the 1st, (Bb) the 4th level of inflation for the expandable device and (Bc) voltammetric signals during increasing inflation levels. (C) H_2O_2 calibration curve in (Ca) the 1st, (Cb) the 4th level of inflation for the expandable device and (Cc) amperometric signals during increasing inflation levels.

9.3.7. Vapor-phase Sensing

Following the successful liquid-phase explosive detection, the balloon-embedded sensor system was tested for their ability to detect explosive vapor, toward future security surveillance applications. Essential considerations for the electrochemical gas sensing of such explosive compounds must be taken in order to perform an accurate measurement.

Firstly, a solid-state electrolyte with suitable transport properties is needed. Secondly, sensors must survive rapid atmospheric changes such as temperature and pressure. Preliminary gas-phase explosive sensing was carried out using the systems shown in the images of Figure 9.6, using vapors of DNT (A) and hydrogen peroxide (B). Such gas-phase DNT measurements have been facilitated by coating the printed electrodes with a thin layer of a solid-state electrolyte such as hydrogel (using agarose).[39] Figure 9.6Aa demonstrates the vapor-phase detection of DNT using the smart balloon. Plot exhibits the voltammetric DNT detection through different exposure times while blowing air to the sample (100 mg DNT powder) to accelerate the vapor diffusion through hydrogel layer. As expected, the DNT response increases upon using longer exposure times. Figure 9.6Ab displays the linearity of the voltammetric signal upon increasing the amount of DNT from 100 to 500 mg after 4 minutes' air blowing. Hence, a linear relationship of 0.3 μA mg^{-1} slope was obtained. Figure 9.6Ac shows the configuration of the system.

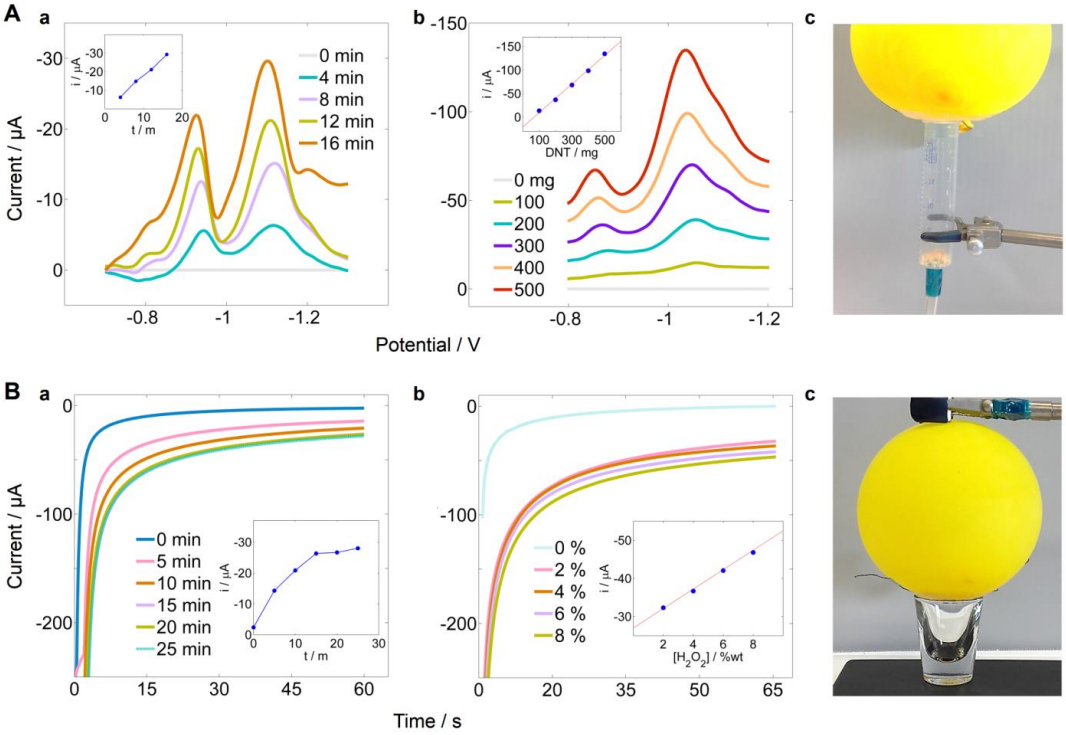

Figure 9.6. Explosive vapor detection: gas-phase measurements of DNT and H_2O_2. (A) Hydrogel solid-state electrolyte strategy for DNT vapor-phase detection (Aa) equilibration time voltammetric curve for 100 mg DNT, (Ab) voltammetric signal upon increasing the amount of DNT from 100-500 mg and (Ac) the corresponding experimental arrangement. (B) Ionogel solid-state electrolyte strategy for H_2O_2 vapor-phase detection, (Ba) equilibration time amperometric curve for 1% H_2O_2, (Bb) calibration curve for increasing amount of H_2O_2 and (Bc) corresponding configuration.

Room temperature ionic liquids (RTILs) are gaining growing interests for gas sensing due to their outstanding electrochemical stability.[42] The curvilinear shape of the balloon makes the viscosity and surface tension of the RTIL not sufficient for maintaining a thin layer onto the sensing area. For this reason, an ionogel approach, involving mixing the RTIL with gelatin, has been developed for its easy shaping to curvilinear surfaces while maintaining the RTIL properties.[43] Figure 9.6Ba shows the influence of the equilibration time upon chronoamperometric vapor peroxide measurements using 1 mL of 1% w/w H_2O_2 in a 35 mL beaker. Figure 9.6Bb displays current–time chronoamperometric recordings for H_2O_2 vapor generated during a 15 min equilibration with 1 mL droplets containing increasing levels of hydrogen peroxide in 2% increments. The system was evaluated from 2% to 8% following the configuration of Figure 9.6Bc. The current (sampled after 60 seconds) is proportional to the peroxide concentration. The resulting calibration plot (inset) yields a slope of 2.45 μA [% w/w H_2O_2]$^{-1}$.

9.4. Conclusions

We reported on the development of balloon-embedded sensors that withstand a simultaneous extreme multiaxial and global bending mechanical deformation, and demonstrated their potential for detecting different explosive compounds in gas and liquid phases. Such stress-enduring sensors rely on hybrid nanocomposited printable electrodes, combining the electronic properties of MWCNTs with the mechanical compliance of PU elastomer, on inflated balloon platforms. The electroactive area of the electrochemical device provided by the MWCNTs is maintained during the stretching of the elastomer providing high electronic compliance. The present study is of considerable significance for two important reasons. First, it examines the role of the nanocomposite upon the sensor performance during extreme multidimensional strains. The nanocomposite provides efficient electron transport path with the MWCNTs backbone and high degree of energy distribution even when high mechanical stress is applied. Mechanical deformation tests indicate remarkable performance of the hybrid nanocomposite electrochemical device without compromising the performance (even with >400% surface area increase). Such attention to the extreme demands of the inflated spherical dynamic balloon substrate reflects the elastomeric, electrical and electrochemical properties of the new expandable composite inks. Second, it offers great prospects for developing flying expandable sensor systems for in-situ security and environmental monitoring. The present work is thus opening up new possibilities in device engineering, with very important applications in different technological areas. The new

balloon sensor holds great promise for field-based screening operations, aimed at assisting security-surveillance and environmental missions. Finally, the integration with wireless electronics could facilitate real-time monitoring and warning capabilities. In addition to security surveillance applications, the new balloon sensing system should benefit other monitoring scenarios, ranging from tracking pollution to surveillance of industrial process controls.

9.5. References

[1] M. Amjadi, K.-U. Kyung, I. Park, M. Sitti, Adv. Funct. Mater. 2016, 26, 1678.

[2] W. Honda, S. Harada, T. Arie, S. Akita, K. Takei, Adv. Funct. Mater. 2014, 24, 3299.

[3] X. Liao, Q. Liao, X. Yan, Q. Liang, H. Si, M. Li, H. Wu, S. Cao, Y. Zhang, Adv. Funct. Mater. 2015, 25, 2395.

[4] T. Q. Trung, S. Ramasundaram, B. U. Hwang, N. E. Lee, Adv. Mater. 2015, 28, 502.

[5] W. Gao, S. Emaminejad, H. Y. Y. Nyein, S. Challa, K. Chen, A. Peck, H. M. Fahad, H. Ota, H. Shiraki, D. Kiriya, D.-H. Lien, G. A. Brooks, R. W. Davis, A. Javey, Nature 2016, 529, 509.

[6] D. Son, J. Lee, S. Qiao, R. Ghaffari, J. Kim, J. E. Lee, C. Song, S. J. Kim, D. J. Lee, S. W. Jun, S. Yang, M. Park, J. Shin, K. Do, M. Lee, K. Kang, C. S. Hwang, N. Lu, T. Hyeon, D.-H. Kim, Nat. Nanotechnol. 2014, 9, 397.

[7] J. A. Rogers, T. Someya, Y. Huang, Science. 2010, 327, 1603.

[8] D.-Y. Khang, H. Jiang, Y. Huang, J. A. Rogers, Science. 2006, 311, 208.

[9] J. Cai, K. Cizek, B. Long, K. McAferty, C. G. Campbell, D. R. Allee, B. D. Vogt, J. La Belle, J. Wang, Sens. Act. B Chem. 2009, 137, 379.

[10] A. J. Bandodkar, R. Nuñez-Flores, W. Jia, J. Wang, Adv. Mater. 2015, 27, 3060.

[11] N. Matsuhisa, M. Kaltenbrunner, T. Yokota, H. Jinno, K. Kuribara, T. Sekitani, T. Someya, Nat. Commun. 2015, 6, 7461.

[12] M. Parrilla, R. Cánovas, I. Jeerapan, F. J. Andrade, J. Wang, 2016, 1.

[13] A. J. Bandodkar, J. Wang, Trends Biotechnol. 2014, 32, 363.

[14] W. Zeng, L. Shu, Q. Li, S. Chen, F. Wang, X. M. Tao, Adv. Mater. 2014, 26, 5310.

[15] D. J. Lipomi, Z. Bao, Energy Environ. Sci. 2011, 4, 3314.

[16] H. J. Chung, M. S. Sulkin, J. S. Kim, C. Goudeseune, H. Y. Chao, J. W. Song, S. Y. Yang, Y. Y. Hsu, R. Ghaffari, I. R. Efimov, J. A. Rogers, Adv. Healthc. Mater. 2014, 3, 59.

[17] D.-H. Kim, N. Lu, R. Ghaffari, Y.-S. Kim, S. P. Lee, L. Xu, J. Wu, R.-H. Kim, J. Song, Z. Liu, J. Viventi, B. de Graff, B. Elolampi, M. Mansour, M. J. Slepian, S. Hwang, J. D. Moss, S.-M. Won, Y. Huang, B. Litt, J. A. Rogers, Nat. Mater. 2011, 10, 316.

[18] N. Reuge, F. M. Schmidt, Y. Le Maoult, M. Rachik, F. Abbé, Polym. Eng. Sci. 2001, 41, 522.

[19] A. Patil, A. Dasgupta, Eur. J. Mech. A/Solids 2013, 41, 28.

[20] M. De Beule, P. Mortier, S. G. Carlier, B. Verhegghe, R. Van Impe, P. Verdonck, J. Biomech. 2008, 41, 383.

[21] H. Takuda, K. Mori, N. Takakura, K. Yamaguchi, Int. J. Mech. Sci. 2000, 42, 785.

[22] L. J. Hart-Smith, J. D. C. Crisp, Int. J. Eng. Sci. 1967, 5, 1.

[23] J. E. Adkins, R. S. Rivlin, Philos. Trans. R. Soc. A Math. Phys. Eng. Sci. 1952, 244, 505.

[24] F. Gervaso, C. Capelli, L. Petrini, S. Lattanzio, L. Di Virgilio, F. Migliavacca, J. Biomech. 2008, 41, 1206.

[25] F. Ju, Z. Xia, K. Sasaki, J. Mech. Behav. Biomed. Mater. 2008, 1, 86.

[26] J. Yinon, TrAC - Trends Anal. Chem. 2002, 21, 292.

[27] J. Wang, F. Lu, D. MacDonald, J. Lu, M. E. S. Ozsoz, K. R. Rogers, Talanta 1998, 46, 1405.

[28] J. Wang, Electronalysis 2007, 19, 415.

[29] M. K. Shin, J. Oh, M. Lima, M. E. Kozlov, S. J. Kim, R. H. Baughman, Adv. Mater. 2010, 22, 2663.

[30] A. J. Bandodkar, I. Jeerapan, J.-M. You, R. Nuñez-Flores, J. Wang, Nano Lett. 2015, 16, 721.

[31] J. A. Rogers, Mrs Bull. 2014, 39, 549.

[32] N. G. Sahoo, Y. C. Jung, H. J. Yoo, J. W. Cho, Macromol. Chem. Phys. 2006, 207, 1773.

[33] M. N. Charalambides, L. Wanigasooriya, G. J. Williams, S. Chakrabarti, Rheol. Acta 2002, 41, 532.

[34] N. Reuge, F. M. Schmidt, M. Rachik, Engineering 2001, 41, 532.

[35] Z. Spitalsky, D. Tasis, K. Papagelis, C. Galiotis, Prog. Polym. Sci. 2010, 35, 357.

[36] N. G. Sahoo, S. Rana, J. W. Cho, L. Li, S. H. Chan, Prog. Polym. Sci. 2010, 35, 837.

[37] R. Carta, P. Jourand, B. Hermans, J. Thone, D. Brosteaux, T. Vervust, F. Bossuyt, F. Axisa, J. Vanfleteren, R. Puers, Sens. Act. A Phys. 2009, 156, 79.

[38] K. Cizek, C. Prior, C. Thammakhet, M. Galik, K. Linker, R. Tsui, A. Cagan, J. Wake, J. La Belle, J. Wang, Anal. Chim. Acta 2010, 661, 117.

[39] M. C. Chuang, J. R. Windmiller, P. Santhosh, G. V. Ramírez, M. Galik, T. Y. Chou, J. Wang, Electroanalysis 2010, 22, 2511.

[40] J. Benedet, D. Lu, K. Cizek, J. La Belle, J. Wang, Anal. Bioanal. Chem. 2009, 395, 371.

[41] J. Wang, S. B. Hocevar, B. Ogorevc, Electrochem. Commun. 2004, 6, 176.

[42] M. Armand, F. Endres, D. R. MacFarlane, H. Ohno, B. Scrosati, Nat. Mater. 2009, 8, 621.

[43] J. Le Bideau, L. Viau, A. Vioux, Chem. Soc. Rev. 2011, 40, 907.

[44] R. Yan, F. Zhao, J. Li, F. Xiao, S. Fan, B. Zeng, Electrochim. Acta 2007, 52, 7425.

Chapter 10

Conclusions and Future Prospects

UNIVERSITAT ROVIRA I VIRGILI
NEW ELECTROCHEMICAL SENSORS FOR DECENTRALIZED ANALYSIS
Marc Parrilla Pons

10.1. Conclusions

The successful development of low-cost electrochemical sensors has been accomplished along the thesis. In addition, the fabrication of robust devices for the use in decentralized settings has been exemplified. First, the development of wearable electrochemical sensors has been presented. Second, a new strategy for the progress in enzymatic-based potentiometric sensors has been described. Also, the study of resilient materials for the fabrication of electrochemical sensors has been performed. These new devices are ready to be used as interfaces or gateways for gathering chemical information for on-site applications. Hence, electrochemical sensors have an important role for building networks with highly valuable information thus leading to a high social impact and new businesses creation in the future.

In essence, in this thesis the development of whole electrochemical cells using different commodity substrates (filter paper, textiles, and rubber) has been accomplished. A complete wearable potentiometric cell has been developed in different substrates (commercial carbon fibers (Chapter 4) and textiles (Chapter 5)) for monitoring electrolytes in sweat. Moreover, an approach to tackle the issues of calibration of potentiometric sensors has been proposed and tested (Chapter 4). Indeed, sensors build in or with commodity materials allow to decrease the manufacturing costs thus enabling the development of disposable sensors. In this manner, sensors might undergo a previous calibration in the manufacturing facilities, and then, be ready to use by the final users in the field. Of course, further studies on the stability and storage must be conducted to drive the sensor as a final product.

The versatility of the printing technique over different substrates has also been tested, characterized and integrated into a wireless potentiometer for multi-ion monitoring (Chapter 5). Furthermore, tailored materials have been developed to endure daily mechanical stress conditions, such as stretching, bending or wrinkling without compromising the analytical performance of the system towards monitoring physiological parameters such as different electrolytes concentration in sweat.

In addition to determine the electrolyte concentration in biological fluids, the need of monitoring the liquid loss is interesting to define the physiological status of the human body. For this reason, a wearable patch for the quantification of the sweat loss has been developed (Chapter 6). The wearable patch is based on a paper-based sensor which provides high accurate sensitivity to water content by changing its electrical resistance. The sensor has been widely characterized for a suitable user application as well as it has been integrated

with a Bluetooth reader for an on-site use. Hence, the chemiresistor is relevant for monitoring the dehydration status in both health and fitness field. This type of sensor avoids the use of a reference electrode and allows a calibration free approach, two major advantages for wearable systems. Interestingly, the combination of both technologies (liquid quantification and electrolyte concentration) allows to measure the exact amount of electrolyte loss during the activity thus knowing the exact amount of salts that the human body must recover. This application is useful for healthcare, wellbeing and especially long-term fitness activities among others.

Huge efforts have been devoted to develop enzyme-based potentiometric sensors for determination of biomolecules. First, an outstanding potential sensitivity has been demonstrated by the use of Nafion ion-exchange membrane in addition to the redox sensitive ability of platinum substrate for hydrogen peroxide detection (byproduct of the enzymatic reaction involved by oxidases) (Chapter 7). This sensing mechanism has been conceptualized with the development of an enzymatic paper-based sensor where glucose oxidase is entrapped between Nafion layers in order to determine glucose concentration in biological fluids (Chapter 8).

Eventually, advanced materials that are able to overcome common mechanical deformation as well as provide a suitable platform for the development of an electrochemical cell have been developed (Chapter 9). Indeed, a new approach for the fabrication of screen-printed electrodes over a commercial rubber balloon has been realized. The study of stress-enduring inks over an expandable platform is crucial to overcome daily potential mechanical deformations without losing the electrochemical performance of the printed device. Last but not least, the applicability of the balloon-embedded sensor has been demonstrated towards the monitoring of explosive compounds.

It is also important to mention, that not all the work developed during this doctoral thesis have been included. Some approaches in relation to the development of potentiometric immunosensors have been performed. Further studies need to be carried out in order to study the mechanism involved and improve the analytical performance of the immunosensors. Moreover, the study of a phenylalanine-selective electrode for the monitoring of phenylketonuria (PKU) was conducted. Preliminary results concluded the need of a better receptor to increase the linear range within clinical relevant levels for PKU patients and improve the selectivity towards other ions.

This thesis has been a significant advance in the decentralization of chemical analysis for three main reasons. First, the development of wearable electrochemical sensors in the fitness field. Second, the development of new enzyme-based potentiometric sensors towards the monitoring of uncharged biomolecules with an enhanced sensitivity. Third, the use of a wide range of materials as well as the functionalization of commodity materials for a successful chemical analysis. The goal of this work is to provide tools to society for manage, diagnose or prevent actions in real scenarios by processing real-time data of the environment over a wide variety of fields (healthcare, pollution, food, security, and safety) for a better care and life quality. Moreover, the decentralization of the chemical analysis opens up new opportunities for businesses creation along the information-based economy by providing services such as data treatment, data storage, and data distribution as well as for fabrication of the electrochemical devices.

10.2. Future Prospects

This thesis has broadly demonstrated the ability to perform chemical analysis in a cost-effective manner by the use of simple and robust techniques. It has been focused in the research of low-cost detection methods for wearable and point-of-care (POC) applications. Nevertheless, having accurate tools that permit the scalability for a completely spreading of sensing networks is still a huge challenge that the industry must address.[1–5] Therefore, the development of full analytical systems is still an issue to work on. Moreover, sampling, sample treatment, data collection and data treatment are operations for further improvement in the already developed sensors.[6] The integration of all these operations into a robust and portable system will help to reach the market and the end-user approval.[3] Whether any of these operations is not well-designed, the chemical data cannot be delivered accurately for a valuable interpretation.

Accordingly, future work should be focused in the following three directions. Firstly, prototyping a wearable design towards the end-user that meets the analytical standards. A decrease in the sample amount to a just a few microliters of sample for an accurate real-time measurement of electrolytes in sweat should be performed.[7] Indeed, the design of a suitable sampling cell is as crucial as the design of an electrochemical cell. Furthermore, a well-designed sampling cell can provide sample treatment by the use of paper microfluidics and help to obtain more accurate measurements.[8] Secondly, data collection has to change from voluminous lab-based devices to miniaturized wireless devices to gather a fully decentralized platform for sample measurement “everywhere”.[9–11] Hence, the data transmission should be

integrated in the sampling and electrochemical cell to develop an easy-to-use system. Thirdly, the data treatment and interpretation is the way to validate the recorded information. Hence, the right tools/software to manage the data should be addressed. Later, handling and securing the big data generated by the wearable and POC devices will be a crucial issue to investigate. These include achieving high data transfer rates, efficient data mining, data security and user privacy to fulfill the demands of the decentralization of a worldwide sensing network.

This thesis has paved new ways to develop cost-effective sensors for present growing demands in society, but still needs the integration to miniaturized wireless devices and data mining systems for a successful social adoption. Furthermore, research efforts in extend biomolecules detection methods must continue. Each methodology has to be applied according to the suitable on-site analysis. Investigations to increase sensors stability, biocompatibility and avoid biofouling by the use of hydrophilic membranes must be also addressed to provide to society the useful tools for life quality improvement.

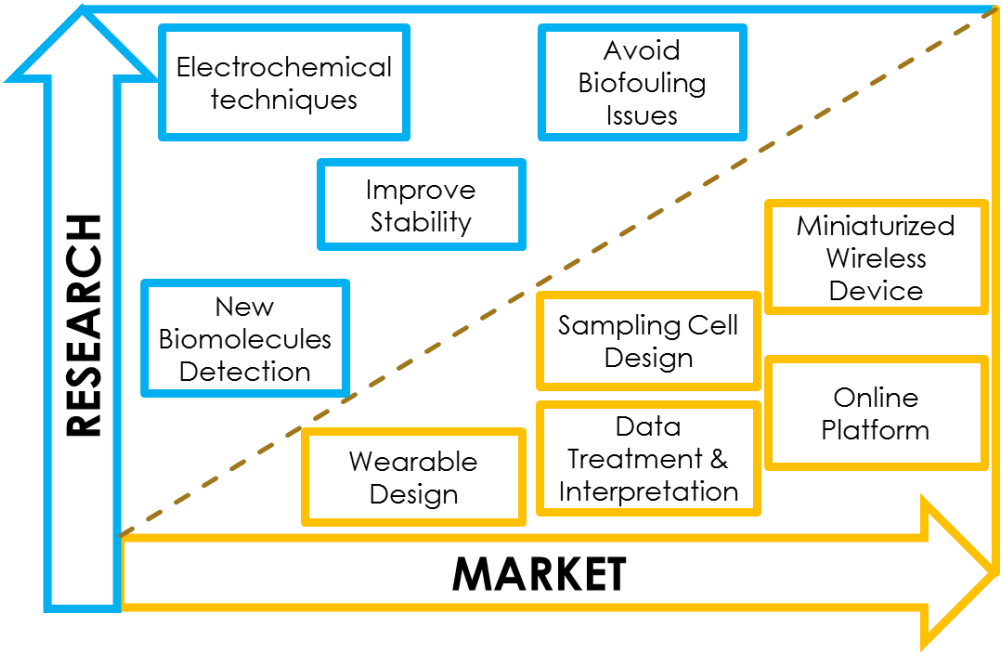

Figure 10.1. Diagram describing the future prospects.

10.3. References

[1] D. Diamond, S. Coyle, S. Scarmagnani, J. Hayes, Chem. Rev. 2008, 108, 652.

[2] A. Darwish, A. E. Hassanien, Sensors 2011, 11, 5561.

[3] M. R. Mahfouz, M. J. Kuhn, G. To, BioWireleSS 2013 - Proc. 2013 IEEE Top. Conf. Biomed. Wirel. Technol. Networks, Sens. Syst. - 2013 IEEE Radio Wirel. Week, RWW 2013 2013, 16.

[4] Y. Shuang-Hua, Wireless Sensor Networks: Principles, Design and Applications, 2014, Springer.

[5] R. Byrne, D. Diamond, Nat. Mater. 2006, 5, 421.

[6] J. Hu, S. Wang, L. Wang, F. Li, B. Pingguan-Murphy, T. J. Lu, F. Xu, Biosens. Bioelectron. 2014, 54, 585.

[7] A. K. Yetisen, M. S. Akram, C. R. Lowe, Lab Chip 2013, 13, 2210.

[8] T. Glennon, D. Diamond, Electroanalysis 2016, 28, 1.

[9] M. Novell, T. Guinovart, I. M. Steinberg, M. Steinberg, F. X. Rius, F. J. Andrade, Analyst 2013, 138, 5250.

[10] S. Armstrong, Br J Sport. Med 2007, 41, 285.

[11] M. D. Steinberg, P. Kassal, I. Kereković, I. M. Steinberg, Talanta 2015, 143, 178.

UNIVERSITAT ROVIRA I VIRGILI
NEW ELECTROCHEMICAL SENSORS FOR DECENTRALIZED ANALYSIS
Marc Parrilla Pons

Appendices

- **Abbreviations**
- **List of Tables and Figures**
- **Short CV**

UNIVERSITAT ROVIRA I VIRGILI
NEW ELECTROCHEMICAL SENSORS FOR DECENTRALIZED ANALYSIS
Marc Parrilla Pons

Appendix 1. Abbreviations

$\mu^{o}_{i(aq)}$ – Chemical standard potentials of the ion in the aqueous phase

$\mu^{o}_{i(org)}$ – Chemical standard potentials of the ion in the organic phase

µPAD – microfluidic paper-based analytical device

ΔE – Peak separation

ΔR_A – Resistance increment from adsorption

ΔR_{rel} – Relative resistance

ΔR_S – Resistance increment from swelling

σ – Stress

ε – Planar strain

γ – Potential scan rate

λ – Ratio of extension

A - Electrode area

a – original radius

$a_{i(aq)}$ – Activity of the primary ion in the aqueous sample

a_i (DL) – Activity of the primary ion in the limit of detection

$a_{i(org)}$ – Activity of the primary analyte in contact with the organic phase boundary

a_j (BG) – Activity of the interfering ion in the background solution

C – Capacitance

c – Concentration of analyte in solution

CAGR – Compound annual growth rate

CCF – Commercial carbon fibers

C_D – Bulk capacitance

CNT – Carbon nanotube

CP – Conductive polymer

CV – Cyclic voltammetry

D – Diffusion coefficient

DNT – Dinitrotoluene

DOS – Bis(2-ethylhexyl)sebacate

E^0_i – Potential of the primary ion at 1M concentration, also known as standard potential

E^0_j – Potential of the interfering ion at 1M concentration

E^0 – Standard potential

E_{Const} – Constant potential generated at the internal interfaces

E_D – Diffusion potential inside the membrane

EIS – Electrochemical impedance spectroscopy

EMF – Electromotive force

E_{pa} – Anodic peak potential

E_{PB} – Phase boundary potential between the sample-membrane interfaces

E_{pc} – Cathodic peak potential

ESEM – Environmental scanning electron microscopy

E_t – Potential at time t

F – Faraday constant (96485 C/mol)

FIM – Fixed interference method

GC – Glassy carbon

GDP – Gross Domestic Product

GOx – Glucose oxidase

h – height

HF – High frequency

Hz – Hertz (frequency unit)

H_2O_2 – Hydrogen peroxide

I – Current (Amperes)

I – Primary ion

I_0 – Amplitude

ICT – Information and Communication Technology

IoT – Internet of things

I_p – Peak current

i_{pa} – Anodic peak current

i_{pc} – Cathodic peak current

ISE – Ion-selective electrode

Abbreviations

ISM – Ion-selective membrane

I_t – Current at time t

J – Interfering ion

K_{ij}^{pot} – Selectivity coefficient of the *I*-ISE towards the ion *J*

k_i – Constant function of the relative free energies of solvation in both the sample and the membrane phase

KTClPB – Potassium tetrakis (4-chlorophenyl) borate

LOD – Limit of detection

MO – Mineral oil

MWCNT – Multi-walled carbon nanotube

n – Number of electrons transferred per molecule diffusing to the electrode surface

n_i – Charge of the primary ion

n_j – Charge of the interfering ion

N – Number of replicates

NaTFPB – Sodium tetrakis[3,5-bis(trifluoromethyl)phenyl]borate

o-NPOE – 2-nitrophenyl octyl ether

PEAA – Poly(ethylene-co-acrylic acid)

PEDOT – Poly(3,4-Ethylenedioxythiophene)

POC – Point-of-care

POCT – Point-of-care tests

Pt – Platinum

PU – Polyurethane

PVB – Polyvinyl butyral - Butvar B-98

PVC – Polyvinyl chloride

Q – Charge

R – Resistance

R– Universal gas constant (8.314 J/K·mol)

R_0 – Initial resistance

R_f – Final resistance

RE – Reference electrode

R_S – Solution resistance

RSD – Relative standard deviation

R_x – Extension radius

S – Surface area

SC – Solid contact

SDBS – Sodium dodecylbenzenesulfonate

SEM – Scanning electron microscopy

SPE – Screen printed electrodes

SSM – Separate solution method

SWCNT – Single-walled carbon nanotube

T – Absolute temperature (K)

t – Thickness

t_t – Thickness at the top

t_0 – Initial thickness

THF – Tetrahydrofuran

TNT - Trinitrotoluene

v - Scan rate

V – Voltage (volts)

W – Warburg impedance

WE – Working electrode

wt % – Weight percentage

Z_0 – Impedance magnitude

Appendix 2. List of Tables and Figures

Figures

Figure 4.3. (A) Potentiometric potassium calibration curve for different number of dip coatings of the CCF working electrode. (B) Sensitivities obtained from 10^{-4} to 10^{-1} M for NaCl during reference electrode dip coating optimization procedure. The plot shows standard deviations of three different electrodes.

Figure 4.4. Calibration of CCF potentiometric electrodes: (A) Electrical potential time-trace for 4 different Na^+-CCF working electrodes. (B) Same calibration after the short-circuit approach. Calibrations were performed against a commercial reference electrode to show the enhanced reproducibility of (a) reference and (b) working electrodes. The inset shows the potentiometric response *vs.* the logarithmic concentration of Na^+ for both electrodes. The numbers on the time trace correspond to the logarithmic concentration of Na^+.

Figure 4.5. EIS spectra. The main plot shows results for a sodium selective membrane on a carbon fiber electrode. The inset shows the results for the same membrane drop cast on a glassy carbon substrate.

Figure 4.6. (A) Potentiometric time-trace and (B) calibration plot for three different Na^+-CCF sensors in artificial sweat.

Figure 4.7. Potentiometric time-trace for the stability test during mid-term period of three different sodium sensors in artificial sweat at 25ºC.

Figure 4.8. Repeatability test from 10^{-3} to 10^{-1} M range in artificial sweat with CCF potentiometric sensor. (A) Test with a potentiometric complete cell (Experiment 1) and (B) test with the wearable platform (Experiment 2).

Figure 4.9. On-body sodium measurements. (A) Picture of the wearable patch worn in the athlete back. (B) Potentiometric time-trace of a wearable sensor and (C) real-time sodium concentration monitoring in human sweat. Real-time data obtained from a human participant during 80 minutes steady-state cycling exercise.

Figure 5.1. (A) Schematic representation of the tailor-made stretchable materials and manufacturing process. (B) Image depicting the wearable sensor based on textile and ion-selective membranes (ISM) composition. (C) Image of the stretchable printed sensors on different common textiles and typical time trace plots for potassium and sodium.

Figure 5.2. Images illustrating resilience studies involving exposing the printable textile potentiometric sensor to increasing levels of strain (left) along with the corresponding time trace calibration plots (right). (A) Linear stretchability test up to a total of 100% strain, 10 repetitions in each strain step. (B) Stretchability test, using a 75% linear strain for a total of 60 min (time trace recorded after every 15 min). (C) Bending assessment, up to a total of 180º, 10 repetitions in each angle. (D) Crumpling evaluation, up to 30 times wrinkling. (E) Washing step simulations (without soap) using short and long (10 and 40 minutes) periods.

Figure 5.3. (A) Carry-over test of a textile-based sensor before, during (50% strain) and after such mechanical deformation. (B) Carry-over testing using artificial sweat test within the physiological range. (C) Correlation of calibration experiments carried out using a compact wireless high-input voltmeter and a conventional potentiostat. (D) Images depicting the versatility of the printable and stretchable sensor array on different common wearable substrates. The tablet displays a real-time trace of increasing potassium levels obtained wirelessly by the underwear printed sensor.

Figure 6.1. The schematics illustrates the sensor fabrication within the whole wearable system. (A) Conductive paper fabrication by painting method. (B) Detailed scheme of the different elements involved in the construction of the wearable patch. The system contained a high sensitive SWCNTs-SDBS cellulose composite paper for monitoring water inside the wearable patch (C) Illustration of the integrated system (wearable patch, Bluetooth data recorder and a screenshot of the interface from an Android mobile phone).

Figure 6.2. Schematic representation of the parts of the sweat patch before use. The paper-based sensor is between an absorbent patch (to avoid the sweat entrance from other parts of the body) and the polyurethane semi-permeable film that allows the sensor to be precisely stacked on the body.

Figure 6.3. Response of the chemiresistor sensor producing an increment of the electrical resistance of the paper. (A) Plot displays the change in electrical resistance after the addition of 1 µL of distilled water. (B) Plot shows the increment of electrical resistance upon consecutive additions of distilled water.

Figure 6.4. SWCNTs-SDBS cellulose paper fabrication scheme. (A) The schematic illustrates SDBS molecules surrounding the SWCNTs for the solubilization in aqueous solution. (B) The illustration represents the SWCNTs wrapping the cellulose microfibrils. (C) ESEM photograph displays the SWCNTs attached to the filter paper cellulose fibers. (D) Photograph showing a piece of filter paper after 6 coats of SWCNTs-SDBS ink paints.

Figure 6.5. Illustration representing the proposed mechanism. (A) SWCNTs are wrapped along the cellulose microfibrils after the SWCNTs-SDBS ink coats by painting technique. (B) Water interacts with the SDBS molecules

leaving the SWCNTs expose to water adsorption as well as swelling between cellulose microfibrils. (C) Water is completely swelled into the cellulose fibers and yield to an electrical resistance increment of the whole conductive paper.

Figure 6.6. Mechanical deformation tests. (A) Bending test over a paper-based sensor during different degrees of freedom, from longitudinal inward to longitudinal outward bends by recording the resistance at each degree. (B) Twisting test over the conductive paper. Resistance obtained after each 10 cycles of twisting for a total of 40 repetitions.

Figure 6.7. Optimization of the analytical performance of the sensor. First, an evaluation of the width of the conductive paper by different paper size was carried out during water addition; (A) time-trace curves and (B) calibration curves (N=2) for each condition. Second, the effect of water addition to the functionalized SWCNTs by carboxylic group is presented; (C) time-trace curves and (D) calibration curve (N=3). Finally, the effect of several SWCNTs-SDBS coatings during water addition over the conductive paper is displayed; (E) time-trace curves and (F) calibration curves. The numbers on top of the time traces indicate the volume of liquid added each time.

Figure 6.8. Reproducibility study. (A) Calibration curve from 6 coats of ink SWCNTs paper (N=4). (B) Calibration curve using the wearable patch with 6 coats of ink conductive paper (N=3).

Figure 6.9. Liquid flow test. (A) Continuous liquid monitoring provided by a flow pump using artificial sweat. Inset shows the corresponding increment in resistance without any interruptions. (B) Monitoring of flow-rate calculated from the paper-based sensor.

Figure 6.10. On body testing. (A) Photograph of wearable patch on the upper back of a subject during cycling exercise. (B) Wristband design of the sweat sensor and wearable patch design magnification (inset). (C) On-body measurement at real-rime of the perspiration dynamics using the wearable sensor (inset shows the resistance increment). (D) Comparison of sweat loss values between wearable sensor and regional absorbent-patch method (N=3). (E) Monitoring of the real-time sweat by the use of a wireless reader and a mobile phone interface. Two screenshots from the cell phone app obtained during the on-body tests. (F) Sweat loss pattern of the subject. All the sweat loss plots were recorded during cycling exercises.

Figure 7.1. Potentiometric response curves. (A) Time-trace for bare (blue line) and Nafion-coated (red line) platinum electrode in PBS pH 7 at 25ºC (mean ± S.D., N=2). Inset shows a magnification of the calibration curve for bare platinum electrode. (B) Corresponding calibration plots for bare (blue, □) and coated (red, ○) electrodes. Initial potentials have been subtracted to better illustrate the differences between the two systems. Error bars correspond to the standard deviation (N=2).

Figure 7.2. Comparison of the initial potential as a function of the total electrolyte concentration for (A) bare and (B) Nafion-coated platinum electrodes upon increasing concentration of different supporting electrolytes at 25ºC. (C) Comparison of the H_2O_2 calibration curves using coated electrodes at different concentrations of supporting electrolyte (KCl): 10^{-2} M (□) and 10^{-4} M (○) (mean ± S.D., N = 2). Inset displays H_2O_2 sensitivity versus supporting electrolyte (KCl) concentration.

Figure 7.3. Calibration plots at several pH for (D) bare and (E) Nafion-coated electrodes in 0.1 M buffers of different pH at 25ºC.

Figure 7.4. Schematic representation of the Nafion-coated electrodes mechanism studied in this work. The exchange capacity and the redox reaction performed the suggested mechanism.

Figure 7.5. Electrochemical impedance spectroscopy results of bare (blue line) and Nafion-coated (red line) platinum electrode in 0.1 M KCl as a supporting electrolyte. The impedance spectra were recorded in the frequency range 100 kHz-10 mHz by using a constant direct current potential, (Edc) 0.2 V. The electrodes were studied using excitation amplitude of 10 mV at 25ºC.

Figure 7.6. Cyclic voltammetry results. (Aa) Comparison between bare (blue line) and Nafion-coated (red line) electrodes and (Ab) comparison between bare (blue line) and Nafion-coated (red line) electrodes after 30 minutes in solution in 5 mM $Fe(CN)_6^{3-/4-}$ and 100 mM NaCl from -0.2 V to 0.4 V at 50 $mV \cdot s^{-1}$. Redox sensitivity assay. (B) Redox sensitivity of 1 mM $[Fe(CN)_6]^{4-}$/ $[Fe(CN)_6]^{3-}$ at different ratios (0.1, 1 and 10) for bare (▲) and Nafion-coated (□) platinum electrodes.

Figure 7.7. (A) Evaluation of the addition of ascorbic acid (AA) in the cell for bare and Nafion-coated electrodes in 0.1 M PBS pH 7.2 at 25ºC. (B) Calibration curve for increasing glucose concentration over time for bare, Nafion-coated and Nafion-coated enzymatic electrodes in 0.1 M PBS pH 7.4 at 25ºC.

Figure 8.1. Schematic illustration of the biosensor. (A) Fabrication process of the paper-based electrode. A strip of platinized paper (a) is sandwiched between two plastic masks (b); the mask on top has an orifice to expose the electroactive surface(c). (B) Scheme of the structure of the enzymatic membrane deposited on the paper-based electrode: (i) Pt-Paper Substrate; (ii) enzyme (GOx) sandwiched between two layers of Nafion; one layer of Nafion is at Pt-interface and the other at the (iii) solution interface.

Figure 8.2. ESEM images of the paper-based electrode surface: (A) a bare platinized paper electrode, (B) a membrane (double layer of Nafion) on top of a platinized paper electrode and (C) transversal cut of the electrode membrane (ca. 40 µm thickness).

Figure 8.3. Response study of enzymatic paper-based electrode: (A) Potentiometric time-trace and (B) corresponding calibration curve of enzymatic, Nafion coated and bare platinized paper electrode upon additions of glucose; (C) potentiometric time-trace for gluconic acid for bare and Nafion-coated paper electrode; (D) H_2O_2 potentiometric time-trace and (E) corresponding calibration curve for H_2O_2 for bare and Nafion-coated platinized paper electrode (average ± S.D., N=2). (F) pH dependence of the sensitivity for H_2O_2 in the range from 10^{-5} M to $10^{-3.5}$ M (average ± S.D., N=2). All the measurements were performed in 0.1 M buffers, acetic buffer (pH 4.2), PBS (pH 7.4), borate buffer (pH 8.6) at 25ºC.

Figure 8.4. Optimization of the analytical conditions for the biosensor. (A) Sensitivity for glucose vs volume of solution of enzyme concentration (20 mg/mL) cast. (B) Change on the potentiometric signal after the addition of 10^{-4} M ascorbic acid as function of the increasing volume of Nafion membrane cast. In all cases, error bars correspond to the standard deviation of 3 different electrodes.

Figure 8.5. Time-trace curve for enzymatic paper-based sensors using different amount of Nafion solution in the platinized paper/enzymatic layer interface.

Figure 8.6. Analytical performance of the paper-based enzymatic electrode: (A) Time-trace plot of three different electrodes in three separated potentiometric cells, (B) the corresponding calibration curve of enzymatic electrodes showing the linear range (mean±S.D., N=3)). (C) Repeatability test for three different electrodes during consecutive calibration curves for glucose. (D) Enzyme-based electrode selectivity assessment to the main redox sensitive molecules (ascorbate and urate) and fructose. All the measurements were performed in 0.1M PBS (pH 7.4) at 25ºC.

Figure 8.7. (A) ESEM images of the surface of the paper-based enzymatic electrode after hydration of the membrane: (Aa) PBS-solution-stabilized electrode, (Ab) after glucose calibration curve and (Ac) after 1.5 h 10^{-2} M glucose solution. Enzymatic reaction was performed in PBS pH 7.4 at 25 ºC. (B) FT-IR spectra of the paper-based enzymatic electrode in different conditions: (Ba) Whole overlap spectra, (Bb) magnification of peak at 3400 cm^{-1} of membrane swelling and (Bc) magnification from 900 to 1500 cm^{-1} showing Nafion backbone peaks. Potentiometric measurements were performed in PBS pH 7.4 at 25 ºC.

Figure 8.8. Ratio from FT-IR spectra between peaks (A) 1059/982 and (B) 1200/1145 in different conditions: (1) dried, (2) PBS stabilized, (3) after calibration curve, (4) 45 min at 10^{-2} M glucose, (5) 90 min at 10^{-2} M glucose and (6) control electrode, 90 min in PBS. Measurements were performed in PBS pH 7.4 at 25 ºC.

Figure 8.9. Comparison of glucose determination (mM) in real samples obtained by the potentiometric paper-based electrode (mean±S.D., N=3) and colorimetric assay (data provided by the local hospital) at 25ºC.

Figure 9.1. Expandable electrochemical device. (A) Schematic representation of the layers' composition for the expandable balloon device and the representation of its adaptability to curvilinear surfaces. Multiple layers consist of Ecoflex layer (inner), polyurethane (intermediate), printable sensor (Ag/AgCl with Ecoflex composite), the CNT hybrid nanocomposite layer (PU, MO and MWCNTs) and flexible insulator layer (upper). (B) Inflation and deflation status for both designs ((a) linear serpentine and (b) clover designs). (C) Integration of a flexible electronic/wireless circuitry with the expandable balloon device. (D) Different inflation levels (IL) used during the mechanical deformation study and the explosives monitoring.

Figure 9.2. (A) Multiaxial stretching with bending motion schematics and (B) schematic representation related with the parameters in the equations.

Tables

Appendix 3. Short Curriculum Vitae

Journal Publications:

1. Parrilla, M., Ferré, J., Guinovart, T., Andrade, F.J., 2016. Wearable Potentiometric Sensors Based on Commercial Carbon Fibres for Monitoring Sodium in Sweat. Electroanalysis, 28, (6), 1267-1275. doi:10.1002/elan.201600070
2. Parrilla, M.*, Cánovas, R.*, Jeerapan, I., Andrade, F.J., Wang, J., 2016. A Textile-Based Stretchable Multi-Ion Potentiometric Sensor. Advanced Healthcare Materials. 5, 996–1001. doi:10.1002/adhm.201600092 (*Shared first author)
3. Cánovas, R.*, Parrilla, M.*, Andrade, F.J., Mercier, P., Wang, J., 2016. Balloon-Embedded Sensors Withstanding Extreme Multiaxial Stretching and Global Bending Mechanical Stress: Towards Environmental and Security Monitoring. Advanced Materials Technologies 1-11. Doi:10.1002/admt201600061 (*Shared first author)
4. Parrilla, M., Cánovas, R., Andrade, F.J., 2016. Enhanced Potentiometric Detection of Hydrogen Peroxide using a Nafion-coated Platinum Electrode. Accepted. doi:10.002/elan.201600403
5. Parrilla, M., Cánovas, R., Andrade, F.J., 2016. Paper-based enzymatic electrode with enhanced potentiometric response for glucose determination in biological fluids. Submitted.
6. Cánovas, R., Parrilla, M., Andrade, F.J., 2016. Wireless paper-based potentiometric cell for glucose monitoring in real samples. In preparation.
7. Guinovart, T., Parrilla, M., Crespo, G. a, Rius, F.X., Andrade, F.J., 2013. Potentiometric sensors using cotton yarns, carbon nanotubes and polymeric membranes. Analyst 138, 5208–15. doi:10.1039/c3an00710c
8. Novell, M., Parrilla, M., Crespo, G.A., Rius, F.X., Andrade, F.J., 2012. Paper-based ion-selective potentiometric sensors. Anal. Chem. 84, 4695–4702. doi:10.1021/ac202979j

Poster Presentations:

1. Biosensors 2016 Conference, Gothenburg, Sweden. Wearable Potentiometric Sensors Based on Commercial Carbon Fibres for Monitoring Sodium in Sweat.
2. Matrafüred 2014, Budapest, Hungary. Potentiometric tools for decentralized monitoring of phenylalanine levels.
3. VI Workshop Nanociencia y Nanotecnología analíticas 2013, Alcalá de Henares, Spain. Development of immunopotentiometric sensors based on nanomaterials.

UNIVERSITAT
ROVIRA i VIRGILI